ABSTRACT

Title of Dissertation: MOLECULAR INTERACTIONS OF UBIQUITIN AND POLYUBIQUITIN CHAINS WITH UBIQUITIN BINDING DOMAINS

Aydin Haririnia, Doctor of Philosophy, 2007

Directed By: Professor David Fushman
Department of Chemistry and Biochemistry

Ubiquitin is a small protein that is covalently attached to proteins, either as a single ubiquitin moiety or as polyubiquitin chains. A cascade of enzymatic reactions is required for the isopeptide linkage between the C-terminus of ubiquitin and a lysine residue on a substrate protein or another ubiquitin. Attachment of ubiquitin or polyubiquitin, termed ubiquitination, mediates numerous cellular processes by acting as a versatile signal. The signal transmitted by the tag depends on the nature of the modification, which defines the specificity of the tag for different cellular machinery. This versatility is conferred by the variations in polyubiquitin tags, both in terms of length and lysine-linkage. Polyubiquitin chains can adopt a variety of different conformations based on these variations. The conformational and dynamic properties of the tag may optimize its binding to specific ubiquitin binding domains, therefore committing the target protein to distinct cellular outcomes.

A combination of NMR methods are used to study the interaction of several ubiquitin binding domains with Lys48- and Lys63-linked di-ubiquitin, the simplest model

of a polyubiquitin chain, to gain insights into polyubiquitin recognition. The di-ubiquitin binding interface with ubiquitin-interacting motifs (UIMs) and ubiquitin-associated domains (UBAs) are mapped. Structural models of the complexes are also presented. The results provide the first direct evidence that UIM binding involves a conformational transition in Lys48-linked di-ubiquitin, which opens the hydrophobic interface. The results also show that the UBA domain of Ede1 preferentially binds to Lys63-linked di-ubiquitin. Structural models of the UBA in complex with Lys48- and Lys63-linked di-ubiquitin are shown.

Although ubiquitin is highly conserved in eukaryotes, it is promiscuous with regard to its binding partners, ranging from small molecules to UIM and UBA domains. This study examines the effects of point core leucine to serine mutations on UIM and UBA binding specificity. The results show that these mutations bestow ubiquitin with the ability to discriminate between ubiquitin-receptor proteins. Here, we solved the three-dimensional structure of the L69S Ub mutant in solution by NMR. These mutations have a profound effect on binding specificity while causing subtle changes in the protein's three-dimensional fold and reducing its stability.

Modification of a specific lysine located on Ub's hydrophobic surface has been reported to inhibit proteasomal degradation and endocytosis. Here, the effects of mutation to tryptophan at this position are investigated within the context of binding to a proteasomal receptor protein, hHR23A, and an endocytic receptor protein, Ede1.

MOLECULAR INTERACTIONS OF UBIQUITIN AND POLYUBIQUITIN CHAINS WITH UBIQUITIN BINDING DOMAINS

By

Aydin Haririnia

Dissertation submitted to the Faculty of the Graduate School of the
University of Maryland, College Park, in partial fulfillment
of the requirements for the degree of
Doctor of Philosophy
2007

Advisory Committee:
Professor David Fushman, Chair
Professor Dorothy Beckett
Professor George Lorimer
Professor Nicole Laronde-Leblanc
Professor Jonathan Dinman- Dean's representative

Acknowledgements

I would like to express my deepest appreciation and gratitude for the support and encouragement of my advisor, Prof. David Fushman. Without his guidance and persistent help this dissertation would not have been possible.

My thanks to all past and present members of the Fushman lab, especially Drs. Mariapina D'onofrio, Ranjani Varadan and Daoning Zhang for their assistance and contributions to this work. Special thanks to Nisha Purohit, Bryan Dickinson, and Shirley Lee for their countless hours of help with sample preparations and contributions.

I would also like to thank the collaborators who have made this work possible. Thanks to Prof. Ray Deshaies and Dr. Rati Verma at Caltech, and Prof. Dan Bolon at UMASS for truly insightful ideas. I would also like to thank Prof. Kylie Walters and Dr. Qinghua Wang at Univ. of Minnesota for permission to include their unpublished data in this dissertation and Prof. Robert Cohen and Joshua Sims at Johns Hopkins University for reagents and many helpful discussions. Moreover, I would like to thank Prof. Allen Taylor and Dr. Fu Shang at Tufts University for K6W and H68F Ub.

Also, many thanks to Prof. John O'Bryan at the University of Illinois for purified $S5a_{196-306}$ and Prof. Patrick Young at Stockholm University for S5a plasmids.

I also wish to thank Dr. and Mrs. Bailey and Dr. Herman Kraybill for fellowships during my graduate career. Their financial support is truly appreciated.

Thanks to Prof. Beckett and Saranga Naganathan for allowing me to explore ITC and Prof. Lorimer for the use of the preparative centrifuge.

Finally, I would like to thank my friends and family for their support, and my gratitude to Rebecca for all the help and sacrifice.

Table of Contents

List of Tables

List of Figures

Abbreviations

ATP	Adenosine tri-phosphate
CD	Circular dichroism
C-terminal	Carboxy-terminal
CUE	Coupling of ubiquitin conjugation to ER degradation
D_2O	Deuterium oxide
Ddi1	DNA-damage inducible-1
Dsk2	Dominant suppressor of kar1 mutant-2
DTT	Dithiothreitol
DUB	Deubiquitinating enzyme
E. coli	*Escherichia coli*
EDTA	Ethylenediaminetetraacetic acid
GST	Gluthathione-S-transferase
H/D	Hydrogen/Deuterium
HMQC	Heteronuclear multiple-quantum coherence
HSQC	Heteronuclear single-quantum coherence
IPAP	In-phase/ Anti-phase
IPTG	Isopropyl β-thiogalactoside
ITC	Isothermal calorimetry
kDa	kiloDalton
LB	Luria Bertani broth
MOPS	3-(N-morpholino)propanesulfonic acid
MTSL	1-oxyl-2,2,5,5,-tetramethyl-3-pyrroline-3-methyl)methane sulfonate
MW	molecular weight
MWCO	molecular weight cut-off
NMR	Nuclear magnetic resonance
NOE	Nuclear Overhauser effect
NOESY	Nuclear Overhauser effect spectroscopy
N-terminal	Amino-terminal
OD_{600}	Optical density at 600 nanometers
PAGE	Polyacrylamide gel electrophoresis
PDB	Protein Data Bank
PEG	Polyethylene glycol
PMSF	phenylmethylsulphonyl fluoride
ppm	parts per million
PRE	paramagnetic relaxation enhancement
Rad23	Radiation sensitive mutant complementation gene 23
RDC	Residual dipolar coupling
rmsd	Root mean square deviation
RP	Regulator particle
Rpm	Revolutions per minute
S5a	proteasome subunit 5a
SAXS	small angle X-ray scattering
S. cerevisiae	*Saccharomyces cerevisiae*

SDS	Sodium dodecyl sulfate
SL	Spin label
SPR	Surface plasmon resonance
SUMO	Similar to ubiquitin modifier
TLCK	Na-Tosyl-Lysine-chloromethylketone
TOCSY	Total correlation spectroscopy
Tris	2-amino-2-(hydroxymethyl)-1,3-propanediol
Ub	Ubiquitin
UBA	Ubiquitin-associated domain
UBD	Ubiquitin-binding domain
UBL	Ubiquitin-like domain
Ub_n	(n)-polyubiquitin chain
UIM	Ubiquitin-interacting motif
UPP	Ubiquitin-proteasome pathway
UV	Ultraviolet
VWA	von Willebrand factor A
WT	wildtype

Chapter 1: Introduction to Ubiquitin and the Ubiquitination cycle

1.1 Overview

Proteins undergo a variety of post-translational modifications (acetylation, biotinylation, methylation, phosphorylation, glycosylation, sulfation, prenylation, etc.) as signals that regulate cellular pathways. In the late 1970's, Hershko, Ciechanover, and Rose found that a heat-stable protein, ubiquitin, covalently attaches to proteins in rabbit reticulocyte lysates and signals for proteolysis. Biochemical studies thereafter have determined that the covalent linkage of substrate proteins to ubiquitin, termed ubiquitination, signals for a multitude of cellular outcomes (reviewed in [1]).

Ubiquitin is a 76-residue globular protein that is highly conserved in all eukaryotes. Attachment to substrates takes place via its flexible C-terminal segment that forms isopeptide bonds with the ε-amine of a lysine on a target protein, including another ubiquitin. Ubiquitination is catalyzed by a series of Ub activating (E1), conjugating (E2), and ligase (E3) enzymes. The isopeptide bond can be reversed by unique proteases called de-ubiquitinating enzymes (DUBs) (Fig. 1.1). Since there are seven lysines on the surface of Ub, polyUb chains of varying lengths can be formed with different lysine linkages. The remarkable versatility and complexity of ubiquitin signaling is acquired from these variations. Thus, the outcome of ubiquitination depends on whether a protein is attached to a single Ub or a polyUb chain and the specific lysine involved in forming the chains [2].

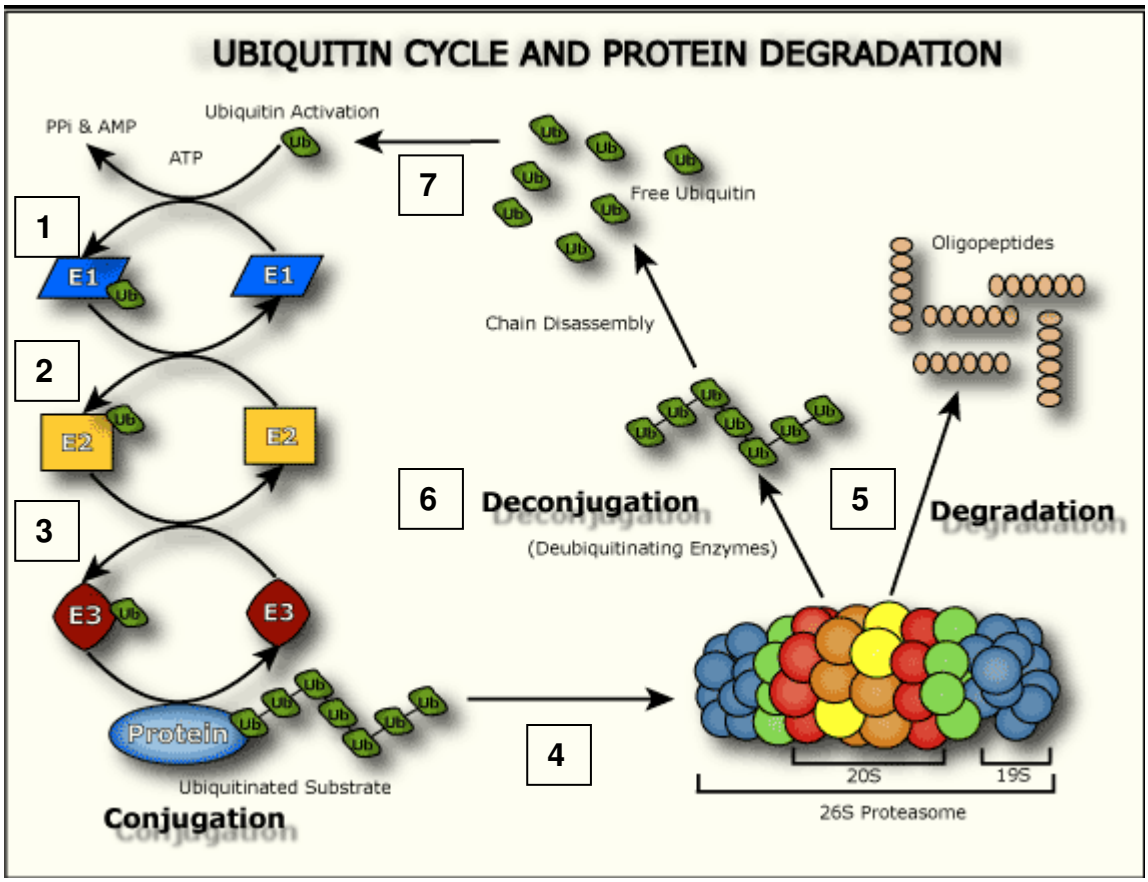

Figure 1.1: Overview of the Ubiquitin Proteasome Pathway
1) ATP-dependent activation by E1 (Ub-activating enzyme). 2) Transfer to E2 (Ub-conjugating enzyme). 3) Interaction of E2 and E3 (Ub-ligase) and covalent attachment of Ub to substrate protein. 4) Recognition of polyUb by proteasome. 5) Degradation of the substrate protein by proteasome. 6) De-conjugation of polyUb from substrate by De-ubiquitinating enzyme (DUB). 7) Hydrolysis and recycling of ubiquitins.
The diagram was reproduced from the website of Boston Biochem, Inc. (www.bostonbiochem.com/incl/images/content/UPP_diagram.gif)

1.2 Enzymatic Conjugation

In an ATP-dependent process, a thioester bond is formed between the carboxy-terminal Gly76 of Ub and the active site cysteine of an activating enzyme, E1. In this reaction, E1 binds to Ub, ATP is hydrolyzed to AMP and the Ub carboxy terminus is adenylated releasing inorganic diphosphate. Nucleophilic attack by the active site cysteine forms a thioester bond with the C-terminal glycine of Ub. The highly conserved diglycine C-terminal sequence in Ub has been shown to be critical for this reaction,

whereas mutation of the C-terminal glycine to any other amino acid or its extension by even one residue inhibits the reaction [3]. The next step for Ub conjugation involves transfer of the activated Ub from E1 to the active site cysteine of an E2 enzyme. Dozens of E2s have been identified in different eukaryotes and several of their structures have been determined [4-8]. The human E2s E2-25K [9] and Mms2/Ubc13 [10] have been shown to catalyze the synthesis of Lys48- and Lys63-linked polyUb chains, respectively. All E2s have a conserved catalytic domain and an active site cysteine which forms a thioester bond with Gly76 of the activated Ub through a trans-thioesterification from E1. The final step of ubiquitination is transfer of Ub to the substrate protein is catalyzed by an E3 enzyme [11]. Ubiquitination occurs at lysine residues on a substrate protein via a single Ub or a polyUb chain at a single or multiple sites [12]. E3s have been classified in two groups based on the mechanism by which Ub is transferred to the substrate protein. In HECT (Homologous to E6AP C-terminus)-domain E3s, Ub is transferred from the active site of E2 to an active site cysteine on the E3 in a transthioesterification reaction. The Ub is finally transferred to a substrate protein bound on a different site on the E3. A smaller group of E3s, the RING (Really Interesting New Gene)-domain E3s, bind E2 and the protein substrate and directly transfer Ub to the substrate without first forming a thioester intermediate [3]. Notably, there are hundreds of E3 ligases with different substrates and E2 specificities, dozens of E2s, but only one E1 gene has been identified per organism [13]. The superfamily of E3s share little sequence homology and this diversity is necessary in order to bind to numerous ubiquitination targets.

1.3 Functional roles of Ubiquitination

Modification with monoUb or polyUb signals for various cellular outcomes depending on the nature of the modification. The diversity in signaling has been attributed to the different conformations adopted by polyUb chains as a result of various lysine linkages and chain lengths. The known functions of polyUb chains linked through different lysines has been reviewed in [2] and are illustrated in Figure 1.2. Although the role of Ub in proteasomal degradation was first detected in the 1970's and has been studied extensively, recently it has become apparent that Ub is also involved in a variety of other cellular pathways.

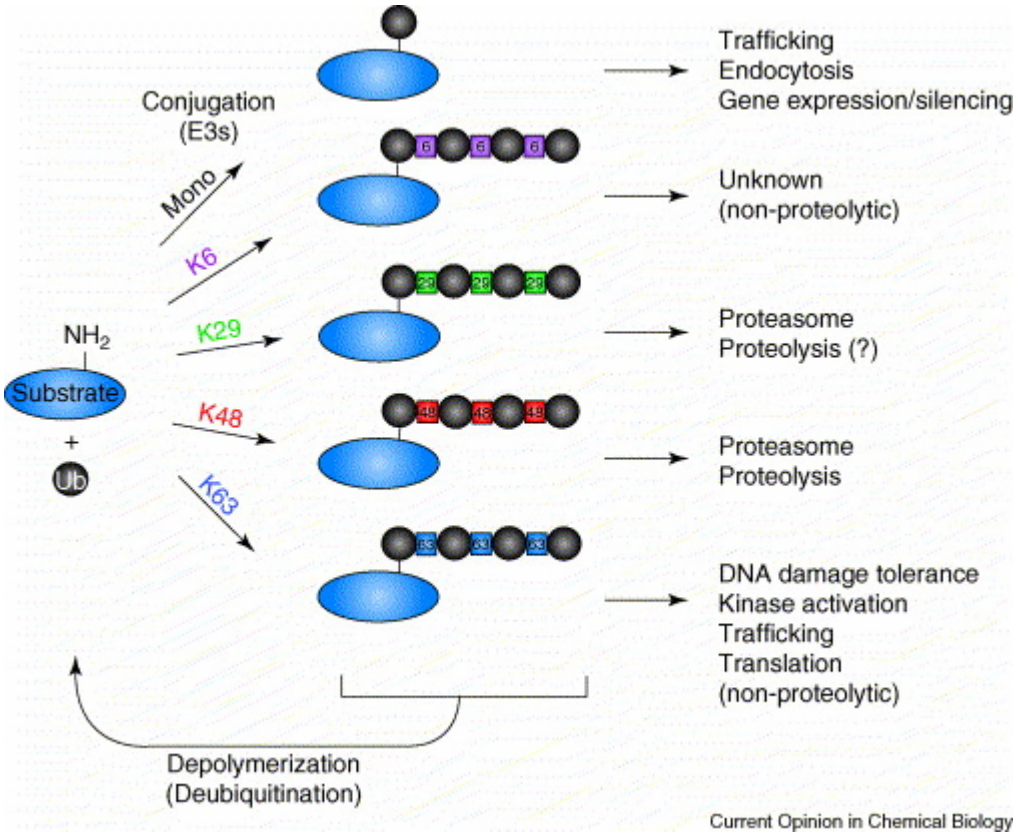

Figure 1.2: Cellular Outcomes of Ubiquitination based on Lysine linkage. The various linkages of polyUb chains are represented by the colored squares. Figure reproduced from [2].

1.3.1 Ubiquitin-Proteasome Pathway (UPP)

The selective degradation of cellular proteins is a precisely regulated process required for various cellular functions (reviewed in [3]) including apoptosis, biogenesis of organelles, cell cycle and division, DNA transcription, modulation of cell surface receptors, ion channels and the secretory pathway, stress response to extracellular modulators and viral infection, and likely many other still undiscovered pathways. Responsibility for the breakdown of many short-lived regulatory proteins, enzymes, and structural proteins falls upon the ubiquitin/proteasome system. PolyUb chains of 4 or more Ub moieties linked via Lys48 act as a universal recognition signal that targets proteins for proteasomal degradation [14]. Regulation of the levels of cellular proteins is critical for maintaining cellular homeostasis. For example, most neurodegenerative diseases are characterized by abnormal protein folding, processing, and/or aggregation [15, 16]. Specifically, impaired degradation leads to Alzheimer's and Parkinson's diseases [17], while overactive protein degradation has been linked to Cystic Fibrosis [18]. Also, the development of several types of cancer has been attributed to defects in the ubiquitin-proteasome pathway, which is integral to the destruction of cyclins that mediate cell cycle progression; such defects can lead to uncontrolled cell division and tumorogenesis [19].

The proteasome is a large, multisubunit ATP-dependent protease found in the cytosol and nucleus of most eukaryotic cells, as well as at the surface of the endoplasmic reticulum [20-22]. The 2.5 MDa eukaryotic 26S proteasome complex is composed of a 20S (700 kDa) proteolytic subunit, and two 19S subunits that serve as a gate that regulates access to the 20S subunit [3, 23-26] (Fig. 1.3). The 20S subunit of the

proteasome is a hollow, cylindrical stack of four 7-membered rings that provides an enclosed active site for degradation, and allows targeted proteins to enter at openings at both ends. However, unassociated 20S subunits are unable to unfold and hydrolyse tagged proteins [27]. The targeted protein undergoes ATP-dependent unfolding at the 19S subunits and passes through the 13Å entrance of the 20S catalytic channel, while the ubiquitin tag is recycled. The 19S subunit is a 900 kDa complex comprised of at least 17 subunits containing ATPases, deubiquitinating enzymes, Ub binding sites, Ub ligases and many other regulatory domains. The 19S is referred to as the Regulatory Particle (RP) since it recognizes Ub chains, binds to the substrate and unfolds it, and disassembles the polyUb tag. The narrow entrance ensures that only appropriately targeted proteins enter the proteasome. Once inside the 20S compartment, interaction with nucleophilic threonine residues leads to degradation of the unfolded protein to short peptides ranging from 3 to 25 amino acids. The sites have broad proteolytic activities such that peptides of different sequences can be cleaved [28]. Deubiquitinating enzymes on the 19S remove the polyUb tag from the substrate and can disassemble the chain into free Ubs. The Rpn10/S5a subunits (Regulatory Particle non-ATPase 10 in yeast/ Subunit 5a in mammals) of the 19S particles have been identified to have 1 and 2 Ub binding regions dubbed UIMs (Ubiquitin Interacting Motifs), respectively.

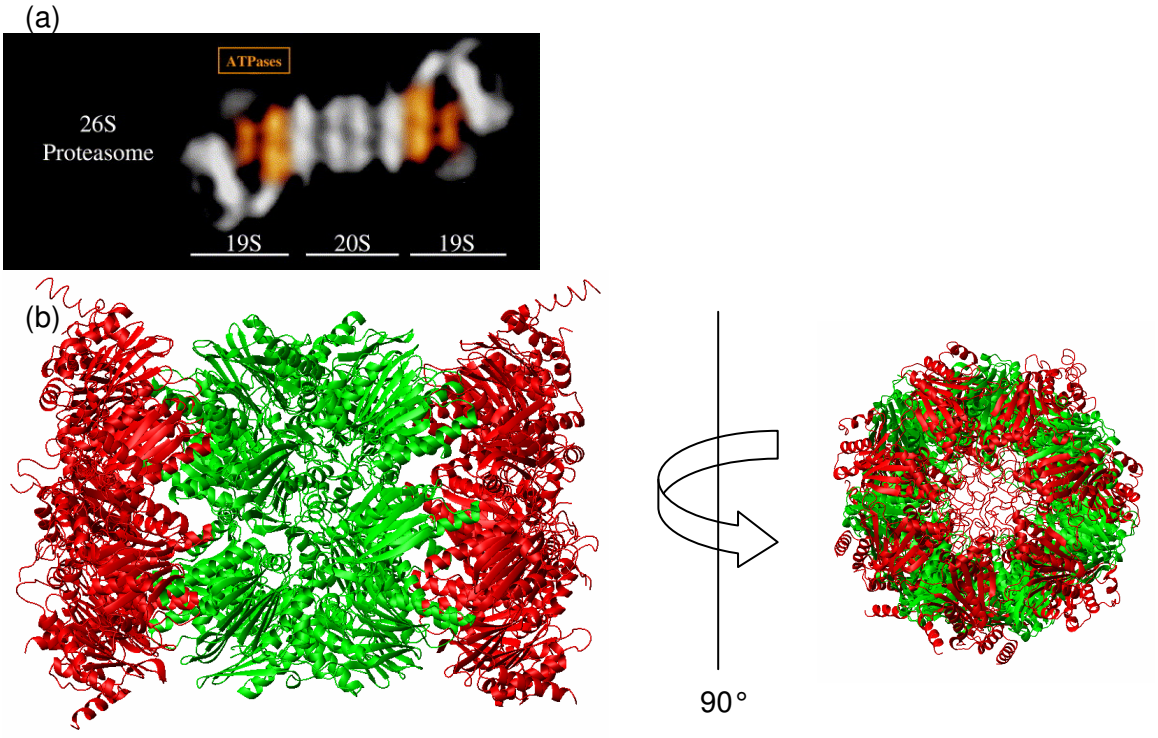

Figure 1.3: Structures of the proteasome obtained by electron microscopy and crystallography a) EM image of 26S proteasome from *Xenopus laevis* oocytes ATPase subunits are colored orange (image from [26]). b) bovine 20S proteasome (PDB ID: 1IRU) ref.[25], the α-subunits are colored red and the β-subunits are colored green. Figures throughout this dissertation were prepared in Molmol [29] and Pymol [30].

A complex network of Ub-associated (UBA) and Ub-like (UBL) domains have been implicated in the Ubiquitin Proteasome Pathway (UPP), however the functional roles of these proteins require further characterization. Intriguingly, such proteins, including Rad23 and Dsk2, have been observed to bind to both Rpn10/S5a and polyUb suggesting that they may act as shuttles to deliver polyubiquitinated conjugates to the proteasome [31-34]. The presence of UBL and UBA domains within the same peptide suggests an elegant regulatory mechanism. Unlike Rpn10, Rad23 is not an integral subunit of the proteasome. Rad23 associates with the proteasome by binding to the

proteasomal subunit Rpn1 [35, 36] . Both receptors can bind Lys48-linked polyUb [37], although neither is essential for yeast cell viability.

Cell cycle progression is driven by oscillations in the activities of cyclin-dependent kinases (Cdks). Cdk activity is controlled by periodic synthesis and degradation of cyclins, fluctuations in the level of Cdk inhibitors (Ckis), and reversible phosphorylation. There are specific cyclins for different phases of the cell cycle that activate Cdks at the appropriate times and are then degraded to inactivate kinase activity. The level of some Ckis also fluctuates at specific times to regulate Cdk/cyclin activity. The ubiquitin-mediated degradation of cyclins, Ckis, and other cell-cycle regulators plays a critical role in cell-cycle control (reviewed in [19]).

1.3.2 Endoplasmic Reticulum Associated Degradation (ERAD)

Compartmentalized, membrane-anchored, and secretory proteins fold and are modified in the endoplasmic reticulum (ER), and subsequently assembled into multisubunit complexes. Proteins that fail to fold or oligomerize properly are degraded via association with chaperones in the "ER quality control" machinery. The unwanted proteins are tagged with Lys48-linked chains within the ER, and are then retro-translocated into the cytosol with the aid of ATPases located on the 19S subunit of proteasomes lining the cytosolic ER membrane. The proteins then undergo proteasomal degradation in the cytosol. Although the underlying mechanism that distinguishes between normal proteins in the process of folding and misfolded proteins is unknown, it has been suggested that chaperones play an important role in translocation of proteins destined for degradation [19].

1.3.3 Protein trafficking

Eukaryotic organisms maintain cellular homeostasis through the internalization process referred to as endocytosis. Ub is involved in targeting proteins from plasma membranes and the trans-Golgi network to endosome, lysosome, and vacuole compartments [38]. There are a growing number of membrane proteins that have been shown to be ubiquitinated and internalized including G-protein coupled receptors [39], epidermal growth factors [40], and ABC transporter proteins [41]. Although monoUb is the best characterized tag for endocytosis, evidence suggests that Lys63-linked chains are more competent endocytic signals [42]. While the role of ubiquitination in endocytosis is not fully understood, it has been suggested that endocytic proteins with ubiquitin binding domains (UBDs) may act as adaptors by associating with ubiquitinated proteins and plasma membranes to promote internalization.

While the previous paragraph describes Ub's role in associating with plasma membranes to facilitate protein internalization, monoubiquitination also signals for transport in the opposite direction. Ub is required for budding of enveloped viruses from plasma membranes of infected cells [43, 44], as well as budding of protein cargo in vesicles from multivesicular bodies (MVBs) [45]. Enveloped proteins from MVBs are targeted for degradation in the lysosome/vesicle pathway. Retroviruses including HIV exploit this system to facilitate the virus budding away from the cytosol [46]. Studies of p53 have shown how tagging with monoUb can signal for a completely different cellular pathway than proteasomal degradation for polyUb-tagged p53. In normal cells, p53 has a short half-life and is polyubiquitinated for proteasomal degradation. However, stressed cells contain monoubiquitinated p53 that is exported to the cytoplasm [47]. While the

actual reason for nuclear export is unknown, it is evident that monoubiquitinated p53 escapes proteasomal degradation, and it has been suggested that the entry of p53 to the cytosol makes it available to promote apoptosis [48]. In summary, it appears that monoubiquitination is a trafficking signal that is recognized by cellular machinery involved in the transport of proteins across plasma membranes.

1.3.4 Transcription regulation through histone modification

Meiosis in yeast has been shown to depend on histone ubiquitination, whereby mutation of the ubiquitination site of H2B decreases cell division by inhibiting sporulation (reviewed in [49]). H2B is a "linker" histone and is the only histone in yeast that is ubiquitinated. Its ubiquitination is required for methylation of H3 which regulates transcriptional activity [50]. Intriguingly, a protein in *Drosophila*, TAF250, has been identified as a requirement for transcription and possesses both E1 and E2 domains [51]. Thus, it has been suggested that TAF250 uniquely targets histones for monoubiquitination.

1.3.5 DNA repair

If DNA lesions are not repaired prior to S phase, replication forks accumulate and post-replicative DNA damage repair is initiated. An E3 enzyme, RAD6, mediates Ub targeting the DNA polymerase processivity factor PCNA (proliferating cell nuclear antigen) to initiate this type of DNA repair [52]. Remarkably, two pathways involving Ub are involved based on the length of the Ub tag; the first pathway occurs when PCNA is monoubiquitinated and entails recruitment of specialized DNA polymerases to the DNA lesion [53]. This pathway leads to error-prone lesion bypass at the replication fork.

The other pathway takes place when PCNA is polyubiquitinated with Lys63-linked chains and results in error-free repair via template switching of the DNA strand [54, 55].

1.3.6 Inflammatory response

Activation of IκBα kinase (IKK) via Lys63-linked chains leads to the degradation of IκBα, which in turn activates the transcription factor NF-κB for innate immune response [56]. In unstimulated cells, NF-κB is associated with IκBα in the cytoplasm, however, upon contact with proinflammatory stimuli such as the tumour-necrosis factor TNFα, viruses, and components of bacterial cell walls, NF-κB is free to translocate to the nucleus to induce inflammatory response [57] [58]. It is important to note that proteasomal degradation is not required for IKK activation. Thus, it has been suggested that Lys63-linked chains likely function as a tag to recruit other proteins in the IKK pathway [59].

1.3.7 Protein stabilization

Several studies have provided evidence that Lys6-linked polyUb chains protect substrates from proteasomal degradation [60-63]. A breast and ovarian cancer-specific tumor suppressor complex, (BRCA1/BARD1), functions as an E3 to construct Lys6-linked polyUb chains. While these chains successfully form conjugates and are recognized by the 26S proteasome, the substrates are not degraded *in vitro* [61, 62]. Thus, in stark contrast to ubiquitination with Lys48-linked chains which leads to proteasomal degradation, it appears that tagging with Lys6-linked chains leads to stabilization.

1.4 Functions of Ubiquitin-Like proteins (UBLs)

While Ub's role as a post-translation modifier has been studied extensively, there is a growing family of UBLs that modify targets in pathways that are related to the UPP but distinct from that of ubiquitin. These alternative modifiers show various degrees of sequence conservation compared to Ub, however they maintain very similar folds and surface topologies and are processed, activated, conjugated and released from conjugates by enzymatic steps that are similar to the corresponding mechanisms for Ub. Some examples of UBLs include SUMO, NEDD8, ISG15 (UCRP), APG8, APG12, FAT10, URM1, and Hub1. These molecules have distinct functions from Ub and do not induce degradation of tagged substrates. However, they do work in parallel with the UPP to influence a diverse set of biological processes. These molecules may be evolutionary offshoots of the UPP which have contributed additional layers of regulation to various pathways. Along the same lines, UBLs have their own specific E1, E2, and E3s and isopeptidases. Thus, it is not surprising that some of these modifiers are unique to higher organisms. For example, ISG15, a signal for interferon signal transduction and the immune response, is found exclusively in vertebrates [64].

Proteins can become modified by one or more UBLs suggesting that multiple regulatory pathways may concurrently affect the same protein. SUMO modification often acts antagonistically to that of ubiquitination and serves to stabilize protein substrates. Proteins conjugated to UBLs are typically not targeted for degradation by the proteasome, but rather function in diverse regulatory activities. NEDD8 activates cullin-RING Ub ligases involved in the cell cycle, signaling, and embryogenesis [65], while

proteins in the SUMO family have been implicated in regulating transcription, DNA repair, nuclear transport, chromosomal function, and signal transduction (reviewed in [66]). The roles of other UBLs remain largely uncharacterized, however it is likely that the attachment of UBLs may alter substrate conformation, affect the affinity for ligands or other interacting molecules, alter substrate localization, and influence protein stability (reviewed in [67]).

1.5 Structural review of Ub and polyUb chains

Ubiquitin is a heat stable [68] and highly rigid [69] protein found in relatively high concentrations in eukaryotic cells ([Ub]> 10 μM) [70]. In addition, Ub is one of the most conserved proteins in eukaryotes, with only three amino acid substitutions between vertebrates and yeast, suggesting strong selective pressure. The differences between yeast and human ubiquitin are as follows: Ser19 to Pro19, Asp24 to Glu24, and Ser28 to Ala28. It is also important to note that Ub does not contain any cysteines, thus disulfide bond formation between individual Ubs or with substrates can be excluded. The crystal structure of human Ub revealed a globular fold comprised of a long α-helix, two single turn 3_{10} helices, as well as five β-strands forming a β-sheet that packs against the helix [71]. The structure of yeast ubiquitin is quite similar to that of human ubiquitin on the basis of difference Fourier electron density maps from X-ray analyses [72]. Additionally, excluding mutated residues and their immediate neighbors (residues i, i+1), the chemical shift positions of amide resonances of yeast ubiquitin are essentially identical to those reported for human ubiquitin [73]. At the center of the β-sheet is a hydrophobic surface comprised of residues Leu8, Ile44, and Val 70 whose sidechains are exposed to solvent. The hydrophobic surface is the main interaction site with many UBDs [74-77] (Fig. 1.4).

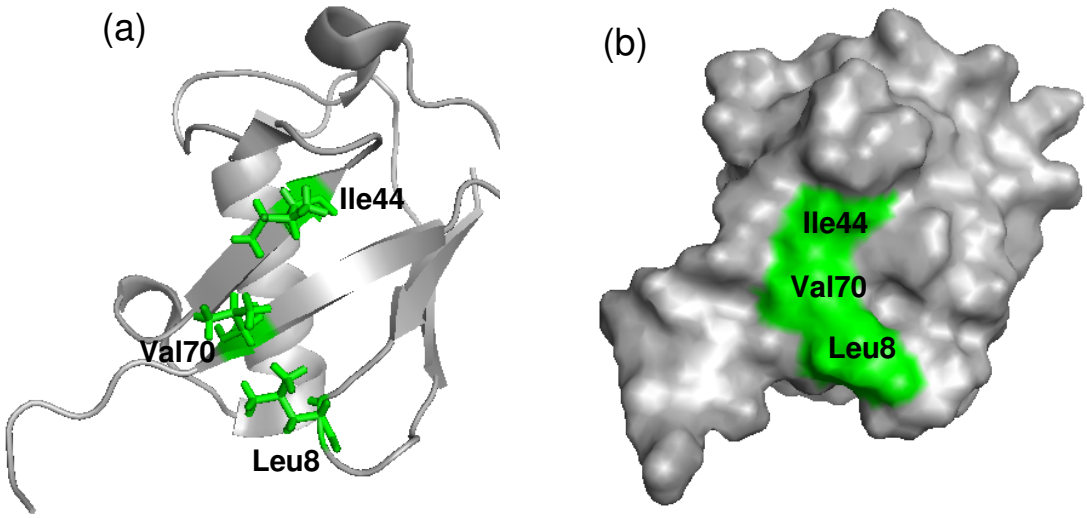

Figure 1.4: Structure of monoubiquitin a) Ribbon representation of Ub showing hydrophobic patch residues in green. b) Surface representation of the same. (coordinates from 1D3Z.pdb [78]).

The stability and rigidity of Ub are in large part due to efficient packing of side chains in the hydrophobic core. The 4 C-terminal residues are flexible and solvent-exposed allowing Gly76 to be available for conjugation to lysine residues of substrates. In addition to the hydrophobic patch and C-terminal residues, several basic residues flanking the hydrophobic patch (Arg42, Lys48, and Arg72) are required to support yeast viability as determined from alanine mutation experiments (Fig. 1.5) [79].

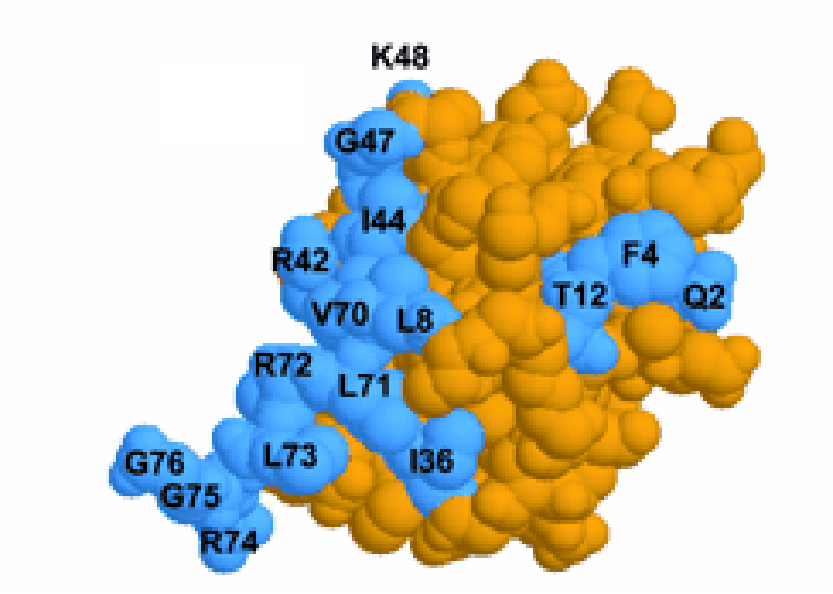

Figure 1.5: Ubiquitin surface residues essential for yeast viability. Surface amino acids are represented as spheres; blue spheres represent essential amino acids. Figure reproduced from [79] .

1.5.1 Ub_2 chain structures

There are seven lysine residues (Lys6, Lys11, Lys27, Lys29, Lys33, Lys48, and Lys63) on Ub that can participate in polyUb chain formation (Fig. 1.6). Mass spectrometric analysis of Ub conjugates in *S. cerevisiae* has determined that polyUb chains are found in relative abundance Lys48 > Lys63 and Lys11 >> Lys33, Lys29, Lys27, and Lys6 [80]. Substrates conjugated with Ub on multiple sites, as well as polyUb chains linked via different lysines, were also detected. The diversity in Ub-mediated signaling is believed to be a result of substrates conjugated to Ub chains of different lengths and linkages.

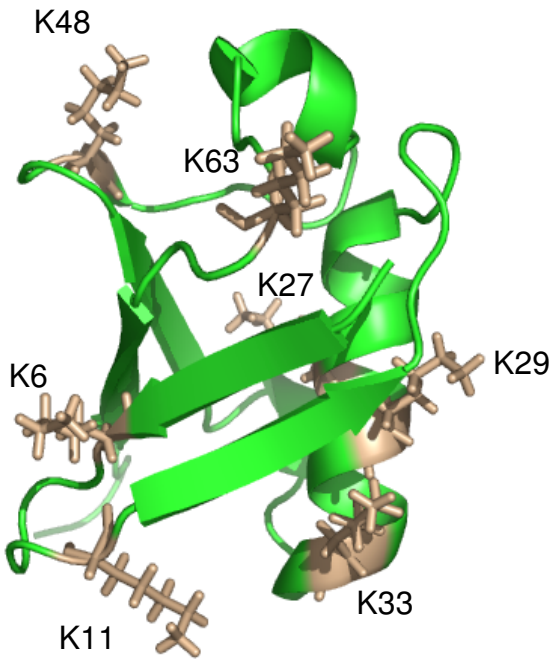

Figure 1.6: Lysines of ubiquitin Cartoon representation of Ub showing each lysine sidechain colored tan (coordinates from 1D3Z.pdb).

PolyUb chains linked via different lysines adopt different conformations. The conformation of Lys48-linked polyUb chains have been studied by crystallography and NMR. The first polyUb structure, determined in 1992, was Lys48-linked Ub_2 crystallized at pH 4.5. The Ub moieties adopted a closed conformation involving direct contacts between the hydrophobic patches (Leu8, Ile44, Val70) of the Ubs (Fig. 1.7a) [4]. NMR studies have shown that the closed conformation is the predominant conformation (85% populated) in solution at pH 6.8, however lowering pH disrupts the interface between the hydrophobic patches leading to a more open conformation (Fig. 1.7b,c) [81, 82]. The shift in conformation, from closed to open with decreasing pH, likely depends on the protonation states of the histidine sidechains (pKa = 5.5) [83] which protrude into the center of the interface between the Ubs in the closed conformation (Fig. 1.7a). The interaction between the two Ubs is weak and there is rapid

exchange between the open and closed conformations (~10ns timescale) [82]. Thus, although the functionally important hydrophobic patch residues are sequestered at the interface in the closed conformation, the interface is dynamic and can be readily disrupted to allow interactions with UBDs. A chain locked in the closed conformation would greatly reduce ligand's access to the ligand-binding sites on ubiquitins, and could render polyUb binding incompetent. For example, cyclization of Lys48-linked Ub_2 by a cross-linker that restricted interface opening strongly impeded the ability of this chain to bind UBA domain in a high-affinity sandwich-like mode [84].

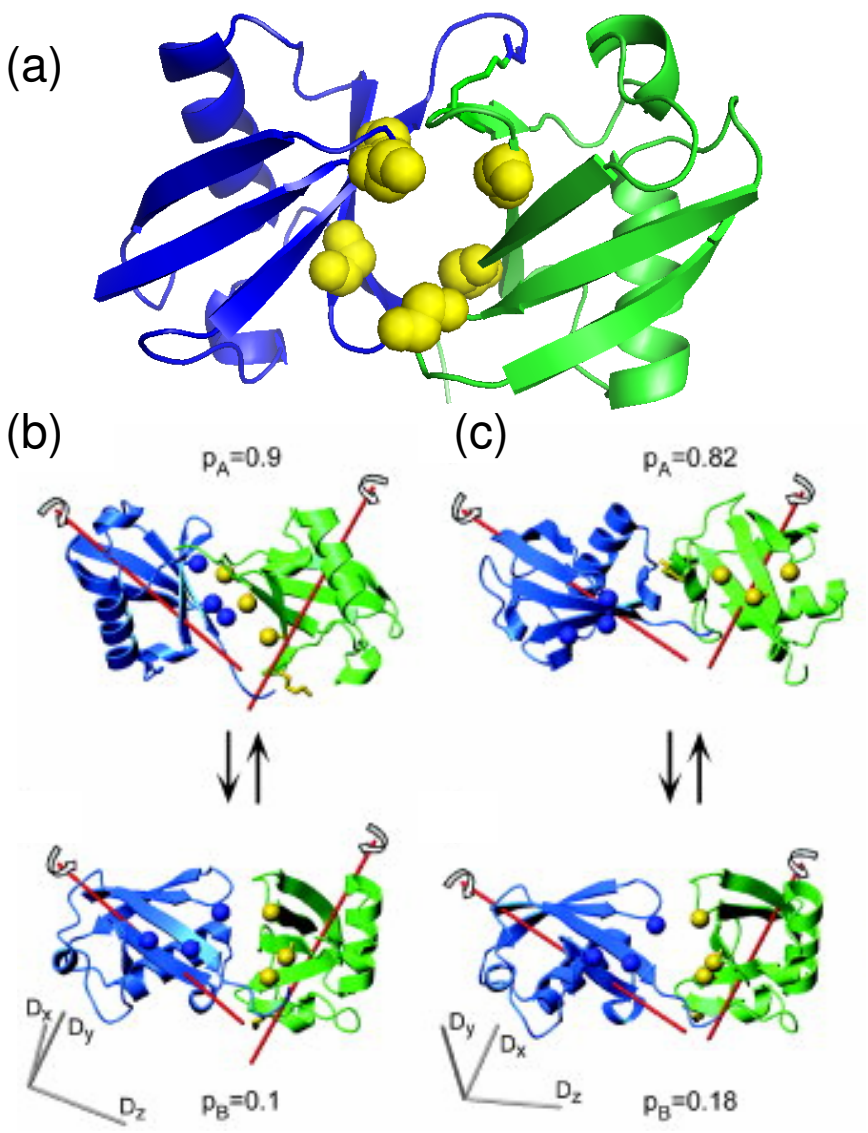

Figure 1.7: Conformations of Lys48-linked di-ubiquitin a) Crystal structure of Lys48-linked Ub_2 (PDB ID: 1AAR) [85]. The distal Ub is colored blue, proximal is green. Residues Leu8, Ile44, Val70 represented by yellow spheres. b) Conformations of the Lys48-linked Ub_2 at pH 6.8 and c) pH 4.5. Relative populated states at each pH are represented by p_A and p_B. Figures b and c adapted from [82].

The diversity of polyUb signaling has been ascribed to the ability of differentially linked chains to bind to various effector proteins [86]. Therefore, polyUb chains linked via different lysines would presumably adopt different conformations in accordance with this theory. This presumption was supported by characterization of the conformation

adopted by Ub_2 linked via Lys63 by NMR [87]. The sidechain of Lys63 is located at the opposite extremity of Ub from the C-terminus (Fig. 1.8a), imparting linear geometry to chains extended via this linkage. The solution structure at pH 6.8 reveals an extended conformation where the hydrophobic patches on each Ub do not interact and are solvent-exposed (Fig. 1.8c) [87]. Although there are no structures for longer polyUb chains linked via Lys63, studies using small angle X-ray scattering (SAXS) have shown that Ub_4 linked via Lys63 adopts a more extended conformation than Ub_4 linked via Lys48 [88]. In stark contrast, residues that comprise the hydrophobic patch (Leu8, Ile44 and Val70) in Lys48-linked chains show significant chemical shift perturbations when compared with the same residues in monoUb, indicating a defined interface between the Ubs in the chains linked via Lys48 [81, 88].

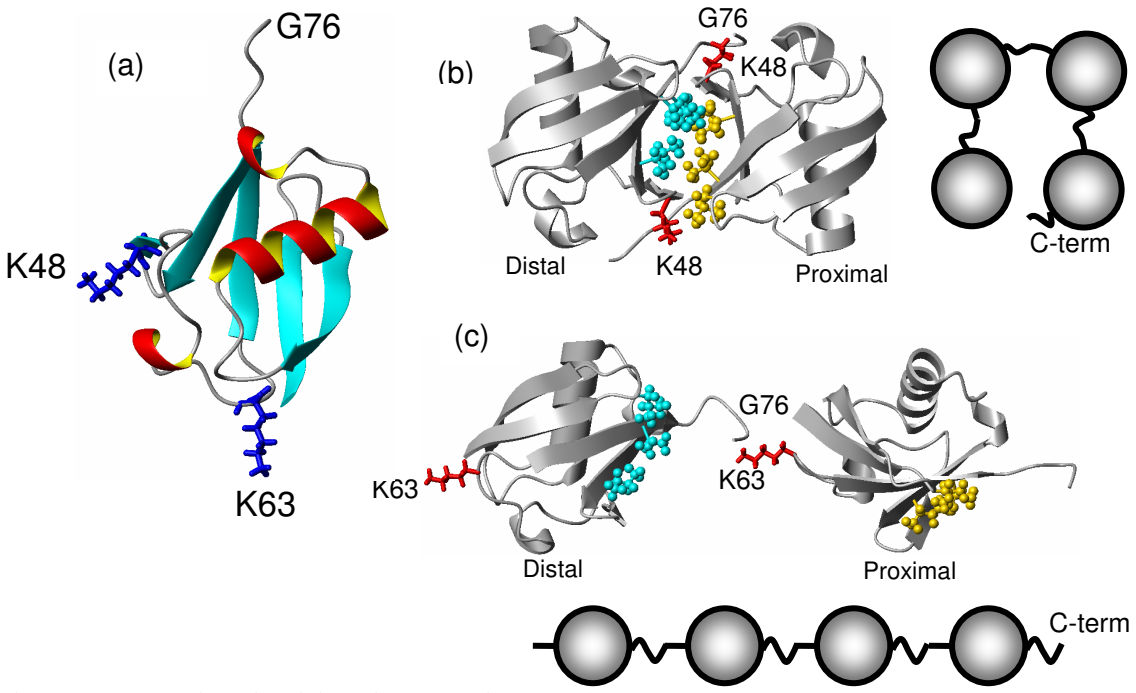

Figure 1.8: Di-ubiquitin linked via Lys48 versus Lys63 a) Ubiquitin structure, sidechains of Lys48 and Lys63 shown as blue sticks. b) crystal structure of Lys48-linked Ub_2 [85] with sidechains of Leu8, Ile44, Val70 shown as cyan ball and stick model on distal Ub and yellow on the proximal Ub. Red sticks designate position of sidechains of Gly76 and Lys48. c) solution structure of Lys63-linked Ub_2 [87] with sidechains of Leu8, Ile44, Val70 shown as cyan ball and stick model on distal Ub and yellow on the proximal Ub. Red sticks designate position of sidechains of Gly76 and Lys63. Courtesy Dr. David Fushman.

1.5.2 Ub_4 chain structures

Three crystal structures have been reported for Lys48-linked Ub_4, each showing a different conformation adopted by the Ub moieties [89-91]. The first structure, solved in 1994, showed translational and rotational 2-fold symmetry exposing the hydrophobic β-sheet surfaces to the solvent [89] (Fig. 1.9b). Another crystal structure of Lys48 linked Ub_4, published in 2000, has two possible chain conformations both of which differ from the previously solved structure [90]. One conformation is referred to as extended, and does not include any contacts between the hydrophobic patch residues. The second conformation is a closed circular conformation, in which the hydrophobic surfaces are

buried but not directly interacting with each other (Fig. 1.9c). Interestingly, both crystal structures described above were from crystals grown in acidic conditions (pH < 5). Recently, a crystal structure of Lys48-linked Ub_4 was solved at near neutral pH (6.7) (Fig. 1.9a) [91]. The overall conformation is a dimer of di-ubiquitins, and is consistent with NMR studies in solution using data derived from site-directed spin labeling and CSP mapping. The structure shows that ubiquitins 1 and 3 form closed interfaces with ubiquitins 2 and 4, respectively. Ubiquitin 1 refers to the first Ub in the polyUb chain that can be conjugated to a substrate lysine residue (has the free C-terminus) and the subsequent Ubs are numbered 2, 3 and 4. Importantly, both sets of dimers adopt a conformation very similar to the "closed" conformations observed by NMR [81] and crystallography [71]. The variety of Ub_4 conformations observed in crystals, as well as in NMR studies, demonstrates the inherent flexibility in Lys48-linked polyUb chains and reveals that these conformations appear to behave in a pH-dependent manner.

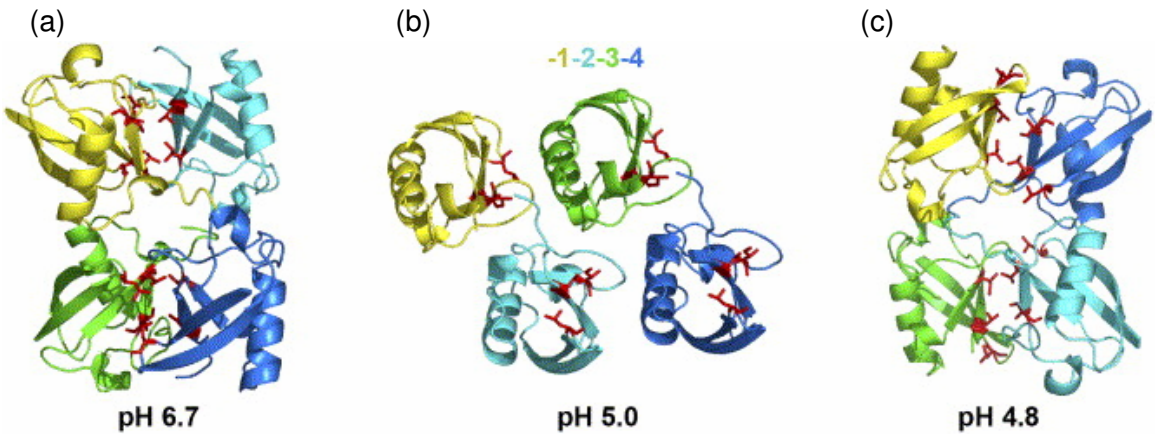

Figure 1.9: Comparison of the three tetraubiquitin crystal structures The tetraubiquitin coloring from proximal ubiquitin to distal ubiquitin is: yellow–cyan–green–blue (1–2–3–4). Hydrophobic patch residues, Leu8, Ile44, and Val70 are shown as red sticks. a) pH 6.7 Ub4 structure (2O6V.pdb) [91], b) pH 5.0 structure (1TBE.pdb) [92], c) pH 4.8 structure [93]. (Figure reproduced from [91]).

Chapter 2: Introduction to Ubiquitin Binding Domains and specific aims

2.1 Ubiquitin Binding Domains

Many of the proteins involved in the various cellular processes described above contain Ub Binding Domains (UBDs) including E2s, E3s, DUBs, substrate adaptors, etc. The largest class of UBDs are α-helical and include UBAs (Ub Associated), UIMs (Ub Interacting Motif), MIUs (Motif Interacting with Ub), and CUEs (Coupling of Ub conjugation to Endoplasmic reticulum degradation) (reviewed in [94]).

2.1.1 Ubiquitin Interacting Motifs (UIMs)

The UIM is a single helix with the consensus sequence e-e-e-x-φ-x-x-A-x-x-x-S-x-x-e, (e- acidic residue, x- helix favoring residue, φ- large hydrophobic residue, A- alanine, S- serine) [95]. Within this consensus sequence, UIMs usually contain a sequence of alternating long and short hydrophobic residues. In the complex, UIMs typically lie along β5 of Ub and form hydrophobic contacts with Leu8, Ile44, Val70, as well as electrostatic contacts with Arg42 and Arg72 on Ub [74, 96]. The solution structure of the UIM-1 and UIM-2 domains of S5a, each bound to monoUb are shown in Fig. 2.1 [74]. The UIM is found in many trafficking proteins that recognize Ub-conjugated cargo, the Rpn10/S5a subunit of the proteasome, and other proteins [74, 96, 97]. The human proteasome subunit S5a contains 2 UIMs, while the yeast orthologue, Rpn10, contains a single UIM [31, 98]. Rpn10/S5a is known to bind to Rad23 and Dsk2 proteins which contain UBL and UBA domains. Consequently, since Rpn10/S5a is

found on the 19S subunit of the proteasome [97], as well as free in the cytosol [99], it was suggested that a complex network of UBDs appears to be involved in shuttling ubiquitinated cargo to the proteasome.

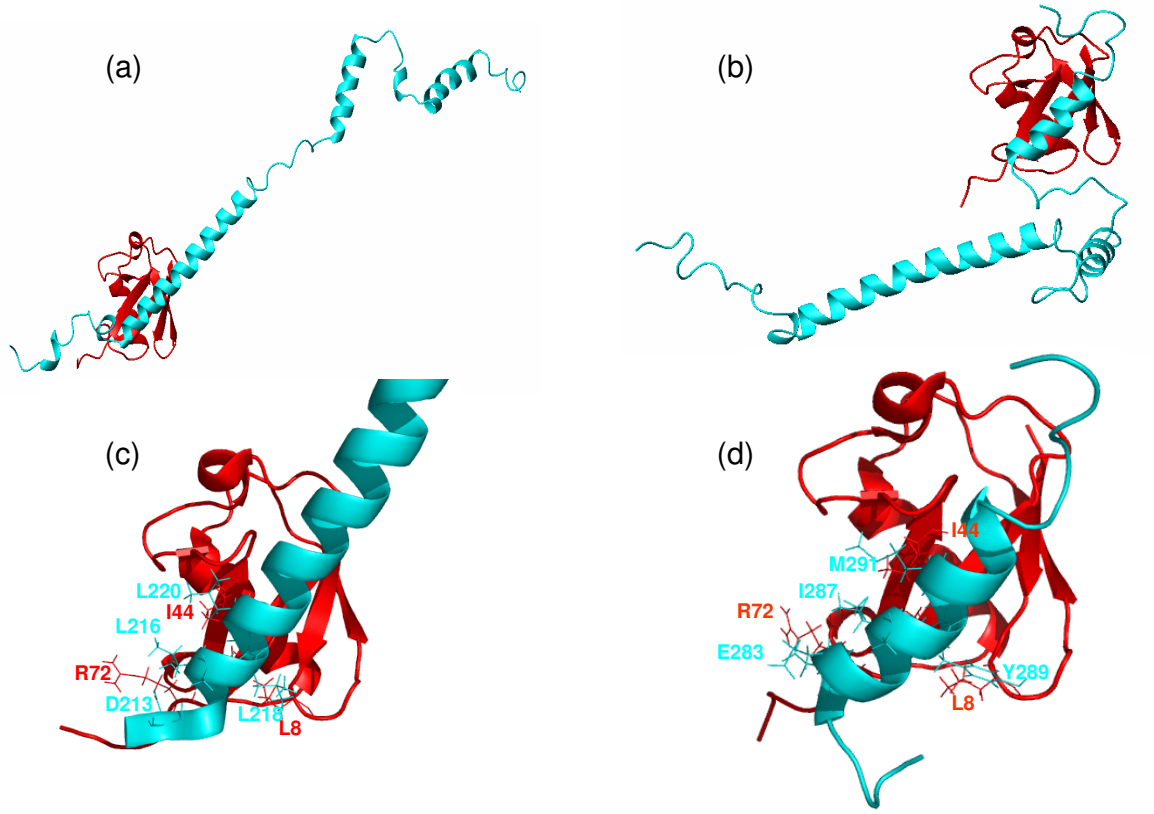

Figure 2.1: Structure of monoUb in complex with UIM-1 and UIM-2 of S5a$_{196\text{-}306}$ a) Ribbon representation of UIM-1 of S5a (cyan) in complex with Ub (red) (PDB ID: 1YX5) b) UIM-2 of S5a (cyan) in complex with Ub (red) (PDB ID: 1YX6). Close-up views of the interacting residues are also shown (c) and (d) below the corresponding structures. [74]

Several groups have reported binding of UIM-containing peptides to monoUb with relatively low affinity ($K_d \sim 300$ µM) [74, 83, 98, 100, 101], although stronger (~70 µM) binding was observed for UIM-2 of S5a [74, 75]. The UIM-2 domains of S5a and Vps27 bind Ub with higher affinity than UIM-1 (5- and 2-fold stronger binding, respectively, in the case of S5a [74] and Vps27 [102]). A similar difference between the

UIMs of S5a was observed in polyUb binding, wherein isolated UIM-2 showed a 10-fold greater affinity[98]. Interestingly, the finding that the UBL domain of hHR23A (human homologue of Rad23A) binds with high affinity to UIM-2 of S5a (K_d ~ 12 μM) [103] provides further credence to the role of Rad23 in the UPP.

S5a has been shown to have a strong preference for longer Lys48-linked polyUb chains (> 3 Ubs) [98], in agreement with the observation that Lys48-linked Ub_4 is the minimum signal for efficient targeting to proteasomes [98]. Recently, several studies using SPR and pulldown assays have provided evidence that S5a binds with relatively similar strength to Lys48- and Lys63-linked polyUb chains [74, 98].

In addition to two UIM domains connected by a long, (~40 residue) flexible linker, S5a contains a domain that is homologous to the A-domain of the von Willebrand factor, referred to as VWA. The von Willebrand factor is a large multimeric protein shown to mediate cell adhesion [104]. Although Rpn10 is not essential for yeast viability, it has been shown to promote proteasomal degradation [31]. Interestingly, while Rpn10 and Rad23 are important for degradation of cell cycle substrates such as Sic1, Rad23 requires the VWA domain of Rpn10 in order to rescue proteasomal degradation when Rpn10 is deleted [105]. This is somewhat surprising since polyUb binding to the proteasome does not require the presence of the VWA domain. Since deletion of the VWA domain results in dissociation of lid subunits Rpn3 and Rpn12 [97], the VWA domain has been suggested to have the important structural role of binding with other subunits on the lid of the proteasome to maintain functionality of the 19S regulatory machinery.

The human endocytic proteins, Epsin 1 and Eps15, contain 3 and 2 UIMs, respectively. Epsin and Eps15 appear to be central components of the vertebrate poly/multiubiquitin-sorting endocytic clathrin machinery. The UIM region of Epsin 1 associates directly with polyUb chains, but has poor affinity for monoUb. Epsin 1 interacts with Eps15 as well as several core components of the endocytic clathrin coat and polyUb chains to promote rapid internalization [106]. Interestingly, the yeast homologue of Eps15, Ede1, contains a single UBA domain, rather than UIMs.

The structural and mechanistic details of polyUb recognition by the proteasome are not yet clear. Since S5a acts as a proteasomal polyUb-tag receptor, characterization of the interaction of the S5a UIMs with polyUb chains is required for understanding this mechanism.

2.1.2 Ubiquitin Associated Domains (UBAs)

UBAs are compact 3-helix bundles connected by two short loops and are identified as a region of homology in many proteins either involved in ubiquitination cascades or containing UBL domains, or both [107]. Although UBAs have low sequence homology (15-35%), structural homology is maintained within the family [108-112]. The common characteristic of UBA domains is the conserved M/L-G-F/Y motif which is essential for Ub binding [75, 109, 110, 113, 114]. Additionally, several conserved acidic residues at the N-terminus of helix 3 also contribute to the interaction. A wide range of binding affinities have been observed for UBA/monoUb interactions, between ~15 μM for Dsk2 UBA [109] to > 500 μM for hHR23A UBA domains [76]. Several structures of Ub/UBA complexes have been solved and show that hydrophobic residues on the

surface formed by helices 1 and 3 of UBA mediate the interaction with the hydrophobic patch of Ub and UBL [109, 110, 114-116].

The Ede1 UBA domain contacts the Ub hydrophobic patch via helix 1 and helix 3 and residues in the loop (referred to as MGF-loop) connecting helices 1 and 2 [110] (Fig. 2.2). Interestingly, Ede1 UBA has relatively higher affinity for monoUb (K_d ~75-90 μM) [116] than many other UBA domains, including hHR23A UBA-2 (K_d ~500 μM) [76, 115, 117], CUE2-CUE (K_d ~155 μM) [118], and E2-25K (K_d ~400 μM) [115]. Although the hHR23A UBA domains engage the hydrophobic patch surface of Ub through an analogous surface found in the Ede1 UBA, the relative orientations of the hHR23A UBA domains differ by at least 45° and as much as 90° [76, 110]. While the various UBAs have specific and distinct roles in the cell and bind Ub in fundamentally distinct modes, there are also similarities in recognition, namely by the hydrophobic patch of Ub and the conserved hydrophobic and acidic residues on the UBAs.

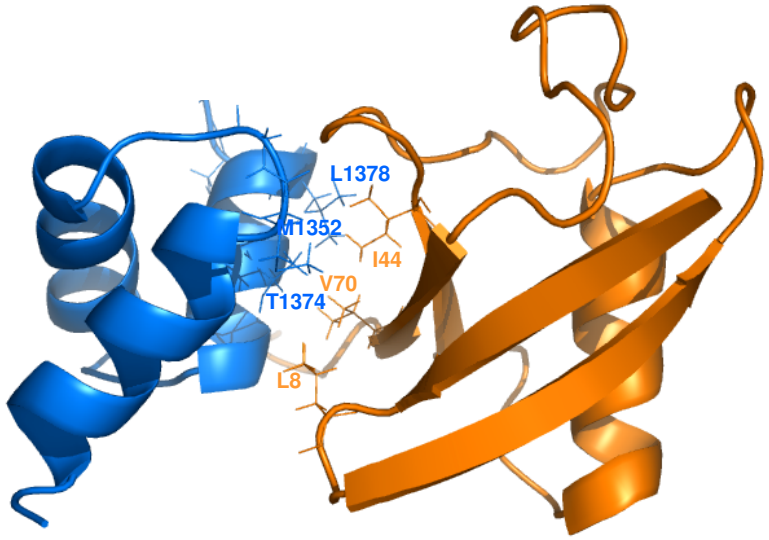

Figure 2.2: Structure of monoUb in complex with the UBA of Ede1. Cartoon representation of UBA (blue) in complex with Ub (orange) (PDB ID: 2G3Q) [110]

Whereas the majority of binding studies have focused on monoUb/UBA binding, a recent study of the interaction of 30 different UBA domains with polyUb chains formed through different types of linkage identified four major specificity classes [115]. Class 1, which contains Rad23/hHR23A UBA-2 and Mud1 UBA, selectively binds to Lys48-linked polyUb; class 2, which contains Rad23/hHR23A UBA-1 and Ede1 UBA, binds preferentially to Lys63-linked polyUb; class 3 UBA domains were not observed to bind to monoUb or polyUb; and class 4 UBA domains bind to polyUb chains without any linkage specificity. While UBAs in classes 1, 2, and 4 also bind monoUb, it is typically with lower affinity, although there are exceptions.

The mechanism of linkage-specific recognition is largely uncharacterized and remains a mystery. Binding of hHR23A UBA-2 [117] and Mud1 UBA [119] to Lys48-linked Ub_2 has been studied structurally by NMR. The structures reveal that these UBA

domains bind in the center of the two Ub moieties in a 'sandwich' to interact with the hydrophobic patch of both Ubs. The closed conformation of Lys48-linked chains creates a hydrophobic binding pocket for hHR23A UBA-2, where helices 1 and 3 contact the distal Ub while the proximal Ub interacts with helices 2 and 3, as well as additional contacts with the Lys48-Gly76 linker region (Fig. 2.3). The binding affinity was enhanced >100 fold and >25 fold for Mud1 UBA [119] and hHR23A UBA-2 [120] binding to Lys48-linked Ub_2, respectively, when compared with binding to monoUb. These studies have provided very useful insights into polyUb binding of Class 1 UBAs, however the basis for the binding specificity for longer and alternatively linked chains remains unsolved.

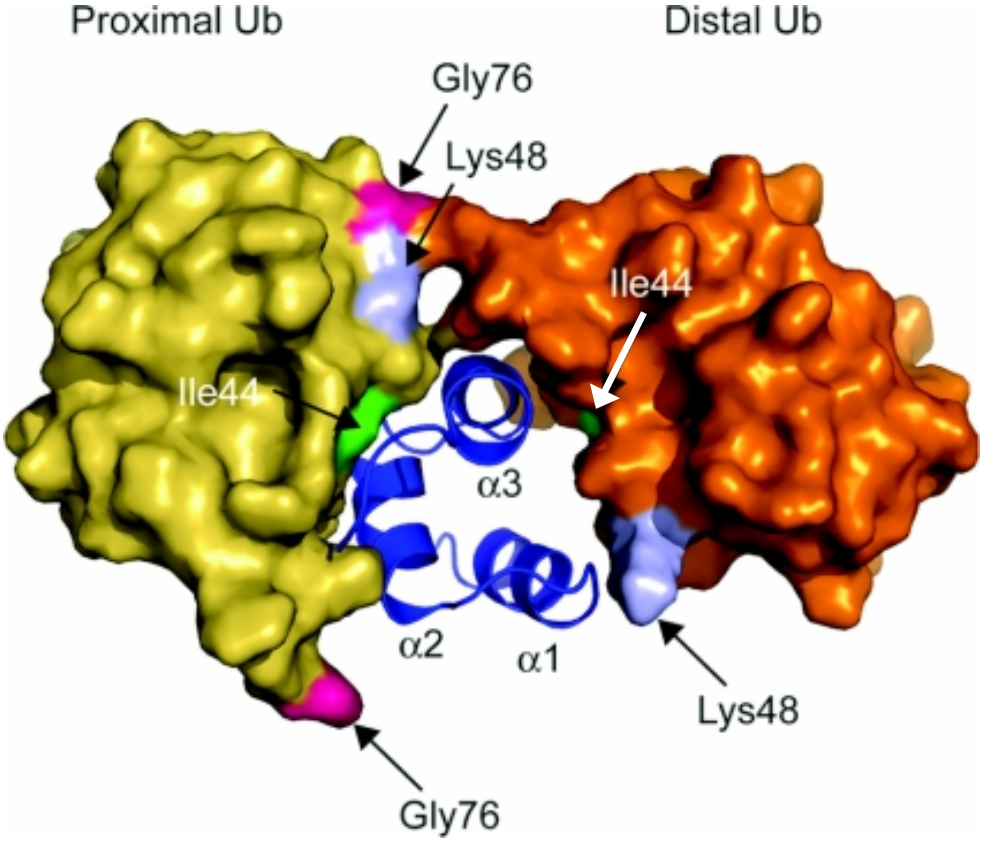

Figure 2.3: The UBA-2 domain of hHR23A in complex with Lys48-linked di-Ubiquitin. UBA-2 is shown as a ribbon (blue) and helices are denoted. Gly76 (pink) and Lys48 (light blue) are shown on both the distal Ub (orange) and the proximal Ub (yellow) to show the sites of covalent linkage and possible chain extension in longer chains. (PDB ID: 1ZO6) [117]. This figure is adapted from [94].

2.1.3 Coupling of Ub conjugation to ER degradation Domains (CUEs)

CUE domains have sequence and structural similarity to UBAs although they are classified as a different domain. Similar to UBA domains, CUEs are also compact 3-helix bundles and bind Ub via conserved hydrophobic residues on helices 1 and 3, however they are found in Ub binding proteins at the plasma membrane [121]. The Cue2-1 domain is a close structural homologue of hHR23A UBA-2, however it binds monoUb with relatively stronger affinity (~155 μM vs. ~500 μM) [76, 118].

The CUE domain from the yeast vacuolar sorting protein, Vps9p, was found to exist as a domain swapped dimer in solution. It binds to the Ub hydrophobic patch, but

contacts extend well beyond to a region around Leu8 and Ile36 (Fig. 1.13). These interactions bury almost 900 $Å^2$ of solvent accessible surface area, more than most other ubiquitin-binding domains (e.g. ~410-440 $Å^2$ for UBA-1 and UBA-2 of hHR23A [109], and ~370 $Å^2$ for UBA of Ede1 [110] bound to Ub). The affinity for this interaction is stronger than other CUE family members identified to date (K_d ~1- 20 μM, depending on the technique used) [121, 122]. It has been suggested that the Vps9 CUE domain binds Ub with high affinity because it can form domain-swapped dimers, and thus interact with a secondary site on Ub. The principle of oligomerization and domain swapping in these Ub-binding domains is an intriguing concept in the context of polyUb chain binding.

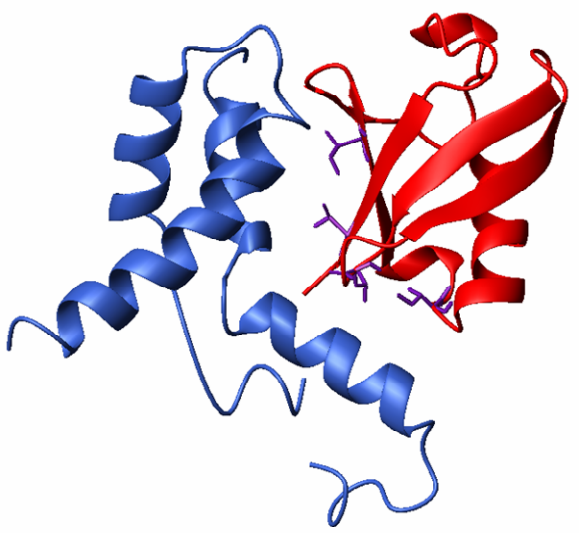

Figure 2.4: Structure of monoUb in complex with the Vps9 CUE.
Ribbon representation of UBA showing domain swapping (blue) in complex with Ub (red) (PDB ID: 1P3Q) [121].

2.2 Specific Aims

The functional diversity of Ub and polyUb chains of various linkages is complex and not well-understood. Elucidating the molecular details of the interaction of Ub with its receptors is vital to understanding of various Ub signaling pathways. This work is

aimed at exploring the structural basis for binding of UIMs and UBAs to monoUb, Lys48- and Lys63-linked polyUb chains.

Despite significant progress in characterization of various cellular pathways involving Ub, understanding of the structural details of polyUb chain recognition by downstream cellular effectors is missing. Since Lys48-linked chains are the principal signal for proteasomal degradation, while Lys63-linked chains act as nonproteolytic signals, the interaction of S5a UIMs with Lys48- and Lys63- linked di-ubiquitin (the simplest model for polyUb chain) can provide insights into the mechanism of polyUb recognition by the proteasome. To this effect, the specific questions answered in Chapter 4 are: What is the mode of interaction of S5a UIMs with Lys48- and Lys63-linked Ub_2? How are the interactions affected by the different conformations adopted by the differently linked chains?

Studies in the past have focused on the identification of functionally important surface residues in Ub [123], however little is known about the biological role of Ub's stability and dynamics. In order to address this question, Chapter 5 focuses on the effect of mutating leucine residues that are part of the hydrophobic core to a polar residue (serine). The structural, biochemical, and functional properties of Ub hydrophobic core mutants L67S and L69S are described.

Although monoUb is the most well-studied tag for endocytosis, evidence suggests that Lys63-linked chains are more competent endocytic signals [42]. However, the role of polyUb chains in endocytosis is not well-understood, and the Ede1 UBA/polyUb interaction has not been characterized. Given the strong structural similarity (rmsd ~0.8Å) between the Ede1 and hHR23A UBA domains and the conservation of residues

comprising the α1-α3 hydrophobic patch, it is not clear why these domains would interact differently with polyUb chains. Chapter 6 aims to elucidate the molecular basis for the preferential binding of the Ede1 UBA to Lys63-linked chains.

Mutation of Lys6 of Ub has been shown to inhibit proteasomal degradation [62, 79, 124] and endocytosis [79]. To gain insights into the structural basis for this inhibition, structural studies of the interactions of K6W Ub with UBAs of a proteasomal receptor protein, hHR23A, and an endocytic receptor protein, Ede1, are detailed in Chapter 7.

Chapter 3: Methods

3.1 Protein expression and purification

3.1.1 Growth media and conditions

To insert plasmid DNA constructs into E. coli BL21(DE3) pLysS cells, 1-2 µl of plasmid DNA was incubated with 50 µl of BL21(DE3) pLysS competent cells (Invitrogen) for 30 minutes on ice. The cells were then heated in a 42°C water bath for exactly 30 seconds and added to 250 µl of S.O.C. growth medium (2% tryptone, 0.5% yeast extract, 10 mM sodium chloride, 2.5 mM potassium chloride, 10 mM magnesium chloride, 10 mM magnesium sulfate, 20 mM glucose) and incubated for 30 minutes at 37°C. The cells were grown on LB-agar plates (1.0% Tryptone, 0.5% yeast extract, 1.0% NaCl, 1.5% agar) for 14-16 hours.

Starter cultures were grown in Lauria-Bertani (LB) medium (1.0% Tryptone, 0.5% yeast extract, 1.0% NaCl) for 6-8 hours at 37°C to an OD_{600} ~0.6 using isolated colonies from a fresh plate. For most protein expression cultures, the autoinducing ZYP-5052 medium [125] (1.0% Tryptone, 0.5% yeast extract, 50mM Na_2HPO_4, 50 mM KH_2PO_4, 25 mM $(NH_4)_2SO_4$, 0.5% glycerol, 0.05% glucose, 0.2% α-lactose monohydrate) supplemented with ampicillin and chloramphenicol (100 mg and 50 mg per liter, respectively, as needed) was incubated at 37°C in a shaker incubator with continuous agitation at 220 rpm for 14-16 hours. For S5a UIMs expression, starter cultures were grown in LB medium as described above, diluted 10 fold and grown to OD_{600} ~0.6, then diluted 10 fold again. Once OD_{600} was between 0.3 and 0.5, IPTG was added to a final concentration of 300 µM and the incubator temperature was reduced to

30°C. Antibiotic supplementation was chloramphenicol and kanamycin (50 mg per liter of each).

For uniform ^{15}N isotope incorporation in proteins other than S5a UIMs, cell cultures were grown in minimal autoinducing ZYP-5052 medium [125] replacing $(NH_4)_2SO_4$ with $^{15}NH_4Cl$ (1g per liter of culture) and Na_2SO_4, such that $^{15}NH_4Cl$ provided the sole source of nitrogen in the medium. The medium was supplemented with 1mM $MgSO_4$, 0.4mM $CaCl_2$, and 0.08% ferric citrate.

For growth of ^{15}N labeled S5a UIMs, LB medium was replaced with M9 minimal medium (6 g Na_2HPO_4, 3 g KH_2PO_4, 0.5 g NaCl per liter of medium), supplemented with 1mM $MgSO_4$, 0.4mM $CaCl_2$, 0.08% ferric citrate and expressed using IPTG as described above.

3.1.2 Protein Purification

All cell pellets were frozen at -80°C for at least 30 minutes prior to lysis. Cells used for expression of Ub and Ub mutants were lysed in PBS buffer, 0.02% Triton X-100, 0.4 mg/ml lysozyme, DNase1 (to 20 µg/ml), 10 mM magnesium chloride and protease inhibitors: 1mM PMSF, 50 µM TLCK, 5 µg/ml soybean trypsin inhibitor, and 2.5 µg/ml leupeptin. Cells were centrifuged at 25000 rpm for 25 minutes in a preparative ultracentrifuge 45Ti rotor. The soluble extract was stirred and kept on ice, and ~300 µl 70% perchloric acid was added drop-wise. Most proteins except ubiquitin and lysozyme precipitated at this step. The extract was ultracentrifuged again at 25000 rpm for 25 minutes in a 45Ti rotor. The supernatant was dialyzed for 14-16 hours at 4°C in a 3.5 kDa MWCO dialysis tube against 2 liters of 50 mM ammonium acetate buffer at pH 4.5.

The dialyzed sample was purified by cation exchange chromatography on a 5 ml SP Sepharose Fast Flow column (GE Healthcare). The column was equilibrated with 50mM ammonium acetate pH 4.5 and Ub was purified using a salt gradient. Ub eluted at approximately 0.29 M NaCl. The purified protein was checked on a 15% SDS gel, concentrated using Amicon Ultra centrifugal filter device with a 5 kDa MWCO and exchanged into the desired buffer (20 mM sodium phosphate buffer pH 6.8 for most NMR experiments or 50 mM Tris pH 8 for polyUb synthesis). Protein concentrations were determined using UV absorbance at 280 nm. The extinction coefficient for WT Ub and D77, Lys48R, Lys48C, Lys63C, Lys63R, L69S, L67S Ub mutants and are 1490 M^{-1} cm^{-1} at 280 nm measured in water. The extinction coefficient for K6W Ub mutant is 6990 M^{-1} cm^{-1} at 280 nm measured in water.

Two S5a constructs were used in this study; one containing residue numbers 263-307 and the other containing residues 196-306. Both constructs had an additional N-terminal histidine tag $MG(H)_{12}$SSGHIEGRH. Plasmid DNA constructs were a generous gift from Dr. Patrick Young (Stockholm University). Cells used for expression of S5a UIMs were suspended in 25mM MOPS, 100mM NaCl, 50mM sodium acetate, NP-40 0.025% pH 7.5, as well as DNase1 and magnesium chloride and the protease inhibitors described above and Lysed via sonication. Cells were centrifuged at 25000 rpm for 25 minutes in a preparative ultracentrifuge 45Ti rotor. The supernatant was loaded on 1 ml HiTrap Chelating HP (GE Healthcare). The column was equilibrated with 0.1M $NiSO_4$ and washed with dH_2O to remove unbound nickel. The lysate was loaded onto the column and the column was washed with 20 ml column wash buffer (50mM sodium phosphate, 300 mM NaCl, 30 mM imidazole pH 8.0) to elute unbound proteins. The His-

tagged protein was eluted with 500 mM imidazole pH 7.0. The purified protein was checked on a 15% SDS gel, concentrated using Amicon Ultra centrifugal filter device with a 5 kDa MWCO and exchanged into 20 mM sodium phosphate, 150 mM NaCl buffer pH 6.8. The extinction coefficient for either length of S5a is 1490 M^{-1} cm^{-1} at 280 nm measured in water.

Two constructs encoding the UBA domain of Ede1 (residues 1337-1381) were purified. The cells containing the GST-tagged construct were suspended in PBS buffer (pH 7.4) containing magnesium chloride, DNase1, the protease inhibitors mentioned above and 0.1% (v/v) Triton X-100. The cells were lysed using 0.4 mg/mL lysozyme, centrifuged at 25000 rpm for 25 minutes in a preparative ultracentrifuge 45Ti rotor and the supernatant was loaded onto glutathione agarose linked through sulfur resin (Molecular Probes, 10 mls per bead suspension per liter culture) equilibrated with PBS buffer, pH 7.4 and incubated for 2 hours. The resin was washed with 10 column volumes PBS buffer (pH 7.4) to remove loosely bound proteins. Bound proteins were cleaved using 20 units of thrombin per liter of cells and eluted with 50mM Tris pH 8. UBA was further purified using a HiTrap benzamidine FF column (Molecular Probes). The column was equilibrated with PBS and the protein was eluted with 0.5M NaCl.

The His_{10}-tagged construct of Ede1 UBA was cloned in a pET16b (Novagen) expression vector. The cells were grown in BL21(DE3) pLysS cells as previously mentioned. Frozen cells were suspended in 20mM sodium phosphate buffer pH 8 containing magnesium chloride, DNase1, protease inhibitors, and 0.1% Triton X-100 as above. The cells were lysed via sonication and centrifuged at 25000 rpm for 25 minutes in a preparative ultracentrifuge 45Ti rotor. The supernatant was loaded on a 1 ml HiTrap

Chelating HP (GE Healthcare) equilibrated with 0.1M $NiSO_4$ and washed as above. The protein was eluted with 250 mM imidazole, 300mM NaCl pH 8.0. The purified protein was checked on a 15% SDS gel, concentrated using Amicon Ultra centrifugal filter device with a 5 kDa MWCO and exchanged into 20 mM sodium phosphate pH 6.8, 2mM DTT. The extinction coefficient of the UBA domain of Ede1 is 5500 M^{-1} cm^{-1} at 280 nm measured in water. ^{15}N labeled His-tagged Ede1 UBA was generously provided by Joshua Sims (Johns Hopkins).

The UBA-1 (residues 156-204) and UBA-2 (residues 319-346) domains of hHR23a were expressed as GST-fused proteins in the ZYP-5052 medium described above. Cells were lysed in PBS buffer, pH 7.4, DNase1, protease inhibitors and lysozyme as described. The protein was purified and checked on SDS-PAGE using the same protocol for the GST-fused Ede1 UBA described in the previous paragraph. Protein concentrations were determined by UV-Vis absorbance. The extinction coefficients are 5120 and 1490 M^{-1} cm^{-1} at 280 nm measured in water for the UBA-1 and UBA-2 domains of hHR23a, respectively.

3.2 PolyUb Chain Synthesis

3.2.1 Background

PolyUb chains were comprised of Ub monomers linked via an isopeptide bond between a C-terminal glycine and the ε-amine of either Lys48 or Lys63. This isopeptide bond can be formed using E1 and E2 enzymes [126] as described in the next paragraph. In experiments requiring spectroscopic examination of Ub moieties in polyUb chains, segmental isotope labeling was employed [81]. For this process one Ub unit was

expressed in ^{15}N medium prior to chain synthesis, and then linked to a Ub moiety expressed in ^{14}N medium to overcome the spectroscopic equivalence of the Ub monomers comprising the chains. The notation used in this text to describe the isotope labeling of chains are 'Ub_2-P' and 'Ub_2-D', referring to the ^{15}N labeling of the Ub at the proximal or distal position with respect to a possible substrate.

3.2.2 Ub_2 chain synthesis

Ub_2-P chains were synthesized using ^{15}N labeled D77 Ub and unlabeled K48C, K48R, or K63R Ub, while Ub_2-D chains were synthesized using unlabeled D77 and ^{15}N labeled K48C, K48R, or K63R Ub. All chemicals were from Sigma and E1 was obtained from Boston Biochemicals. Additional E1 was generously provided by Dr. Robert Cohen (Johns Hopkins). The chain reactions took place in 50mM Tris pH 8, 5mM $MgCl_2$, 10mM creatine phosphate, 0.6U/ml inorganic phosphatase and creatine phosphokinase, 2mM ATP, 0.5mM DTT, 7.5 mg/ml each of Ub (D77 and K48C or K48R for synthesis of Lys48-linked chains and D77 and K63R for synthesis of Lys63-linked chains), 30µM E2 (GST-E2-25k for Lys48-linked chains or an equimolar mixture of Ubc13 and Mms2 for Lys63-linked chains), and 0.1 µM E1. K48R and K63R mutants were used to block the formation of longer chains at the lysines targeted by the respective E2s, while the C-terminal extension with Asp, namely D77, was used to block extension via the C-terminus as described in [126]. The ingredients were mixed up to a final volume of 2 mls (for a total of 30 mg of Ub) and incubated for 14-16 hours at 37°C. Next, the reaction was quenched by addition of 4mM DTT and 20 µl of undiluted acetic acid. The formation of Ub_2 was confirmed by SDS-PAGE. In order to separate Ub_2 from unreacted monomers, the reaction mixture was applied to a HiLoad Sephadex 16/60 column in 50

mM sodium acetate buffer pH 5.5, 2 mM DTT, and 4mM EDTA. Typically, approximately 8-10 mg of Ub_2 was obtained after purification from a 30 mg initial reaction. The purified protein was checked on a 15% SDS gel, concentrated using Amicon Ultra centrifugal filter device with a 5 kDa MWCO and exchanged into 20 mM sodium phosphate pH 6.8, 0.02% sodium azide, 7% D_2O. The extinction coefficient of the Ub_2 is 2980 M^{-1} cm^{-1} at 280 nm measured in water. Some Lys63-linked Ub_2 was generously provided by Joshua Sims (Johns Hopkins).

3.3 NMR binding experiments

3.3.1 Chemical shift perturbation mapping

All NMR measurements were performed on a Bruker Avance-600 spectrometer at 14.1 T, 23-24 °C, and all titration samples contained 0.02% sodium azide and 7% D_2O**.** Backbone amide resonances for each residue were observed using ^{1}H-^{15}N HSQC and ^{1}H-^{15}N SOFAST-HMQC experiments [127]. The combined amide chemical shift perturbation was calculated as

$$\Delta\delta = [(\Delta\delta_H)^2 + (\Delta\delta_N/5)^2]^{1/2} \quad \text{(Eq. 1)}$$

where $\Delta\delta_H$ and $\Delta\delta_N$ are the chemical shift changes for ^{1}H and ^{15}N, respectively. Differences in the resonance frequencies of signals detected in the absence and presence of ligand, under identical experimental conditions, indicate a change in the microenvironment of the observed nuclei as a result of interaction with the ligand.

3.3.2 Binding models and equations

Binding of Ub or polyUb to UBDs was monitored in NMR titration experiments performed as a series of ^{1}H-^{15}N HSQC or ^{1}H-^{15}N SOFAST-HMQC experiments. The sample, referred to as the protein, was ^{15}N labeled, and the titrant, referred to as the ligand, was typically unlabeled. Increasing amounts of ligand were added and binding was monitored through changes in peak positions and intensities. Titrations were continued until no or very little chemical shift changes were observed. Combined amide chemical shift differences were calculated as described in the previous paragraph and changes in NMR signal intensities due to line broadening and slower chemical exchange regimes were measured by scaling the spectra to compensate for the increasing molecular weight of the complexes. The signal attenuation for each residue was calculated as the ratio of peak intensities of the free and bound protein.

The affinities of protein-ligand complexes in the fast-exchange regime on the NMR timescale were estimated from titration curves assuming that the observed chemical shift $\Delta\delta$, at each step in the titration was an average weighted by the population of free (p_F) and bound states of the protein (p_B) such that $p_F + p_B = 1$ and $\Delta\delta = \delta_F.p_F + \delta_B.p_B$ whereas δ_F and δ_B are the chemical shifts corresponding to free and bound states of the protein, respectively.

Three equations were used for analysis of binding affinity depending on the protein complexes being studied and their mode of binding. To describe simple 1:1 (Ub:UBD or UBD:Ub_x) binding with a single binding site:

$$p_B = ([P_t] + [L_t] + K_d - \sqrt{([P_t] + [L_t] + K_d)^2 - 4[P_t][L_t]})/(2[P_t]) \quad \text{(Eq. 2)}$$

1:1 (UBD:Ub_2) binding when there are 2 equivalent binding sites available, but only one site can be occupied by a ligand at a time:

$$p_B = ([P_t] + [L_t] + \frac{1}{2}K_d - \sqrt{([P_t] + [L_t] + \frac{1}{2}K_d)^2 - 4[P_t][L_t]})/(4[P_t]) \quad \text{(Eq. 3)}$$

and 2:1 (UBD:Ub_2) binding when there are 2 equivalent and independent binding sites available:

$$p_B = (2[P_t] + [L_t] + K_d - \sqrt{(2[P_l] + [L_t] + K_d)^2 - 8[P_t][L_t]})/(4[P_t]) \quad \text{(Eq. 4)}$$

where P_t and L_t are the total molar concentrations of protein and ligand and K_d is the dissociation constant. Titration curves for each residue were fit to the appropriate model using the least squares method in MATLAB.

3.3.3 Determination of stoichiometry using ^{15}N relaxation rates

The molecular weights of proteins and protein complexes were estimated using ^{15}N longitudinal relaxation time (T_1). T_1 is sensitive to the overall tumbling rate, which is proportional to the molecular weight of the molecule under observation. A calibration curve plotting T_1 versus MW has been previously developed in the lab [81, 128]. The theoretical dependence of T_1 on MW predicted by the calibration curve is in good agreement with the measured T_1s of the proteins GB3, Ub_1, Ub_2 and Ub_4:

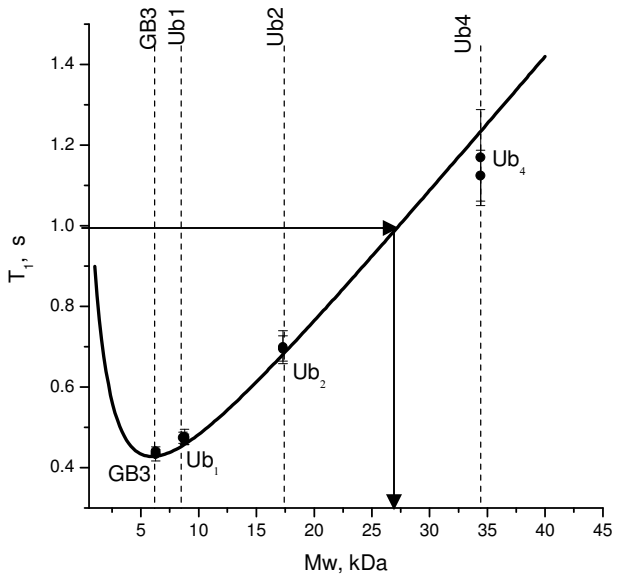

Figure 3.1 Estimation of molecular weight from ^{15}N relaxation times. The solid curve represents the theoretical dependence of ^{15}N T_1 on the molecular weight, calculated as described below. The arrows show how molecular weight is estimated based on measured ^{15}N T_1. The measured ^{15}N T_1 relaxation times for the proteins GB3, Ub_1, Ub_2 and Ub_4 are shown as data points with error bars. The molecular weight of each protein is marked by dashed vertical lines. The figure is adapted from [117].

The theoretical dependence of T_1 on the molecular weight was calculated from:

$$T_1 = [(d^2/10)[J(\omega_H - \omega_N) + 3J(\omega_N) + 6J(\omega_H+\omega_N)] + (3c^2/10)J(\omega_N)]^{-1} \quad \text{(Eq. 5)}$$

where the spectral density function is given by:

$$J(\omega) = (1 - S^2)(\tau_{eff} / 1+ \omega^2 \tau^2_{eff}) + S^2(\tau_c / 1+ \omega^2 \tau_c^2) \quad \text{(Eq. 6)}$$

where $\tau_{eff} = \tau_{loc}\ \tau_c / (\tau_{loc} + \tau_c)$, τ_c is the overall correlation time, τ_{eff} and τ_{loc} are the effective and local correlation times (the latter was taken as 10ps for the simulation of the theoretical dependence), respectively. S^2 is the Lipari-Szabo order parameter (taken as 0.83 for the simulation of the theoretical dependence), c^2 and d^2 are factors that represent the chemical shift anisotropy and dipolar contributions to T_1. τ_c is the overall tumbling time of the molecule given by the Stokes-Einstein-Debye relationship:

$$\tau_c = \eta V MW/kT \quad \text{(Eq. 7)}$$

where η is the viscosity of the medium, MW is the molecular weight, and *V* is the specific volume of the molecule (taken as 0.76 cm^3/g). The overall tumbling was assumed isotropic. The values of τ_c obtained from the Stokes-Einstein-Debye equation are scaled by a factor of 1.5 to account for the effect of a hydration shell. The molecular weights of proteins and protein complexes can be estimated from their measured T_1 using this calibration curve.

3.4 Site-directed spin labeling

The spin label (1-oxyl-2,2,5,5,-tetramethyl-3-pyrroline-3-methyl)methane sulfonate (MTSL, Toronto Research Chemicals) was covalently linked to the sidechain of a cysteine residue of K48C Ub, Ub_2-D or Ede1 UBA (Cys1366). The spin labeling reactions were performed in 50mM Tris pH 8 with 2 molar excess of MTSL. MTSL was dissolved in acetonitrile to a final concentration of 40mM. The reaction tube was incubated in the dark for 14 hours. Unreacted MTSL was removed from the protein solution using an Amicon Ultra centrifugal filter device with a 5 kDa MWCO and exchanged into 20 mM sodium phosphate buffer pH 6.8. MTSL enhances paramagnetic relaxation depending on the electron-nucleus distance. The increase in the ^1H transverse relaxation rate 'R_2' due to the presence of a paramagnetic spin 'S' at a distance 'r' from the nucleus under observation is given by

$$\Delta R_{2para} = K[4\tau_c + 3\tau_c / (1 + \omega_H^2 \tau_c^2)]/r^6 \qquad \text{(Eq. 8)}$$

where $K = (1/15)S(S+1)\gamma_H^2\beta_e^2 g_e^2$, g_e is the electronic g-factor, γ_H is the gyromagnetic ratio of hydrogen, where S is the quantum number for a paramagnetic spin (taken as 1/2), and β_e is the Bohr magneton.

The ^{1}H paramagnetic relaxation rate enhancement (PRE) ΔR_{2para} for the NH groups were calculated from the ratio of the signal intensities in ^{1}H-^{15}N HSQC or ^{1}H-^{15}N SOFAST-HMQC spectra acquired with the spin-label in oxidized (paramagnetic) and reduced states, I_{ox} and I_{red} respectively using

$$\Delta R_{2para} = \Delta R_{2ox} - \Delta R_{2red} = \ln(I_{red}/I_{ox})/t \quad \text{(Eq. 9)}$$

where t is the experimental time during which the ^{1}H magnetization undergoes paramagnetic relaxation in the transverse plane. PREs were reported as %PRE and were calculated by:

$$PRE\ \% = (1-I_{ox}/I_{red})*100\% \quad \text{(Eq. 10)}$$

where z is a scaling factor to normalize the observed signal intensities. The PREs were used to determine the position of the unpaired electron with respect to the protein using an in-house MATLAB program called SL_FIT.

3.5 L69S Ubiquitin Structure Calculation

The ^{1}H- ^{15}N HSQC spectrum of L69S Ub was assigned using 2D TOCSY, 2D NOESY, and 3D ^{15}N-edited TOCSY spectra. $^{1}J_{HnH\alpha}$ couplings obtained from HMQC-J spectra[129] were used to confirm secondary structure assignment. The J-coupling between the H_N and H_α proton provides information about the peptide backbone conformation as it relates to the φ angle by the Karplus relationship[130]:

$$J_{HnH\alpha} = 6.51\cos^2\theta - 1.76\cos\theta + 1.60 \quad \text{(Eq. 11)}$$

where $\theta = \varphi - 60°$. Peaks with J-coupling constants smaller than 5 Hz were confirmed to comprise helices and peaks with J-coupling constants larger than 5 Hz correspond to β-strands.

The solution structure was solved using a combination of NOE-derived distance restraints, dihedral angle constraints predicted using TALOS[131], hydrogen-bonding constraints derived from backbone H_N to H_N NOEs, and experimentally derived orientational restraints from RDCs.

NOESY spectra provide a powerful means for detecting two protons that are separated by less than ~5Å. NOESY peaks were assigned and used to put a loose restraint on the distance between the two protons. Furthermore, since the size of NOE peaks depends inversely on the distance ($1/r^6$), distance constraints between protons were estimated using the NOESY peak volumes using DYANA [132].

The dipolar interaction between two nuclei in the magnetic field samples all conformations in isotropic solutions and is averaged to zero. However, when the medium is not isotropic, some orientations are more likely than others and the dipolar coupling can be observed. A dilute liquid crystalline medium composed of n-alkyl-poly(ethylene glycol) (C12E5) (5% by weight) with n-hexanol (molar ratio of 0.85) was used as described [133]. Steric and electrostatic interactions between the protein and the medium resulted in partial alignment of the proteins. The ^{1}H- ^{15}N couplings were measured using IPAP ^{1}H- ^{15}N HSQC experiments [134] with 512 t1 increments. The RDCs were calculated from the difference in the ^{1}H- ^{15}N couplings observed in the aligned phase (24°C) and isotropic phase (35°C). Simulated annealing was performed using CNS [135] with ARIA [136] extensions.

3.6 Hydrogen-Deuterium Exchange

Backbone amide hydrogen exchange rates were measured in a series of ^{1}H- ^{15}N SOFAST-HMQC experiments with 64 t1 increments. ^{15}N labeled samples of 16 mg/ml

Yeast WT Ub and L69S Ub in 20mM sodium phosphate pH 5.8 buffer were frozen, lyophilized for 8 hours, and resuspended in 99.99% D_2O. The samples were immediately transferred to a NMR tube and data collection was initiated such that the first spectrum was obtained only 90 seconds after dissolution. Spectra were recorded at regular intervals for 15.8 hours in the L69S Ub sample and 20.0 hours for WT Ub. The decays in signal intensity were fit to monoexponentials to derive H/D exchange rates.

3.7 Protein Relaxation and Dynamics

The overall tumbling of the protein as a whole and the internal dynamics of heteronuclear bonds are two motions that are assumed to contribute to relaxation of isotropically tumbling proteins. These motions modulate dipolar interactions between the spins and the interaction of each spin with the magnetic field. Therefore, the relaxation rates of proteins are affected primarily by dipolar interactions and chemical shift anisotropy (CSA). After excitation with a radio-frequency pulse, a magnetic moment relaxes back to equilibrium with time t. Two components comprise the magnetization vector used to describe this relaxation for isotropic systems in the absence of chemical exchange: longitudinal (T_1) and transverse (T_2).

Longitudinal relaxation (T_1) is the component of the magnetization vector parallel to the magnetic field B_0, referred to as M_z. After excitation, the return to equilibrium magnetization, M_0, with respect to time is described by the equation:

$$dM_z / dt = -(M_z - M_0) / T_1 \qquad \text{(Eq. 12)}$$

Transverse relaxation (T_2) is the component of the magnetization vector perpendicular to the magnetic field B_0, referred to as M_{xy}. The return to equilibrium with respect to time in the xy plane is described by the equation:

$$dM_{xy} / dt = - M_{xy} / T_2 \quad \text{(Eq. 13)}$$

The equation for ^{15}N T_1 is shown above (Eq. 6), and for ^{15}N T_2 [137]:

$$1/T_2 = (d^2+c^2/20)[4J(0)+ 3J(\omega_N)] +$$

$$(d^2/20)[J(\omega_H - \omega_N) +6J(\omega_H)+6J(\omega_H+\omega_N)]+R_{ex} \quad \text{(Eq. 14)}$$

where c^2 is the contribution from CSA, d^2 is the dipolar contribution and R_{ex} is the contribution from chemical exchange.

The ^1H (T_2) and ^{15}N relaxation measurements (T_1, T_2, and hetero-NOE) were performed using standard methods [128]. ^{15}N T_1 and T_2 were derived from least square fitting of monoexponential signal decay measured in a series of ^1H- ^{15}N HSQC spectra using the equation:

$$I(\tau) = I(0)e^{-R\tau} \quad \text{(Eq. 15)}$$

where I is peak intensity as a function of relaxation time, τ. R is the relaxation rate (R_1 or R_2), and I(0) is the intensity at $\tau = 0$.

The Nuclear Overhauser Effect (NOE) measures how perturbation of the ground and excited state populations of one spin affects the populations of another coupled spin. If the two coupled spins are unlike, such as the ^{15}N-^1H group, it is referred to as the heteronuclear NOE. Hetero-NOE is used to characterize the motional properties of ^{15}N-H bond vectors and reports on fast (ps-ns) local backbone dynamics. The hetero-NOE is calculated from the ratio of peak intensities of signals in an experiment with proton presaturation to the intensities obtained without presaturation. The equation for the hetero-NOE is [137]:

$$NOE= 1+ (\gamma_H / 10\gamma_N)d^2[6J(\omega_H + \omega_N) - J(\omega_H - \omega_N)]T_1 \quad \text{(Eq. 16)}$$

The experimental data were analyzed using a suite of in-house Matlab programs. The overall rotational diffusion of the protein was analyzed using the program ROTDIF[138], the backbone dynamics parameters were obtained using the program DYNAMICS [128].

Chapter 4: Interaction of S5a UIMs with Lys48- and Lys63-linked Ub_2

4.1 Background and Objectives

S5a has two ubiquitin-interacting motifs (UIM), which adopt α-helical structures [74] and contain a short stretch of residues of alternating long and short hydrophobic side-chains (LALAL motif in UIM-1 and IAYAM in UIM-2) serving as the primary interacting surface with the hydrophobic patch on Ub [74, 100, 139]. This pattern is critical for binding to polyUb, as determined by mutational studies showing that either scrambling the order of the LALAL motif in UIM-1 or replacing with all leucines or all alanines reduced Ub-binding by ≥ 99.4% [98]. When compared with UIM-1, UIM-2 has been shown to bind mono-Ub [74] and Lys48-linked polyUb [98] with 5 and 10 fold stronger affinity, respectively. The solution structure of a S5a fragment, $S5a_{196–306}$, encompassing both UIMs, in complex with monoUb, shows that each UIM interacts independently with the corresponding Ub molecule [74]. It has been suggested that the hydrophobic contacts between the so-called N-terminal turn in UIM-2 (residues 276–282) and L8, V70, and L71 of Ub confer stronger binding affinity compared to UIM-1. The fact that in the $S5a_{196–306}$:monoUb complex UIM-1 and UIM-2 are each bound to a separate Ub molecule suggests that the full-length S5a would optimally bind multiple (at least two) Ub monomers in polyUb. In fact, S5a shows strong binding preference toward longer (n ≥ 4) polyUb chains [139-141]. Intriguingly, however, the individual UIMs of S5a also exhibit much higher binding affinity for Lys48-linked polyUb than for monoUb [140]. This suggests that the S5a's binding preference toward polyUb cannot be

attributed solely to the presence of two UIMs (note in this regard that Rpn10, the yeast homologue of S5a, contains a single UIM, homologous to UIM-1). This also raises the possibility that polyUb chains might bind UIMs in a different mode compared to monoUb.

While it is known that Lys48-linked chains are the principal signal for proteasomal degradation, and Lys63-linked chains act as nonproteolytic signals, understanding of the structural details of polyUb chain recognition by downstream cellular effectors is missing. The objective of this chapter is to structurally study the interaction of the proteasomal receptor, S5a, with polyUb chains of different linkages. This study uses NMR to probe the interaction of UIMs of the proteasomal subunit S5a with di-ubiquitin, the simplest model for polyubiquitin chain, to gain insights into the mechanism of polyubiquitin recognition by the proteasome.

4.2 Interaction of UIM-2 with monoUb and Ub_2

4.2.1 Interaction of $S5a_{263-307}$ and monoUb

Binding of the isolated UIM-2 containing peptide ($S5a_{263-307}$) to monoUb was investigated using the chemical shift perturbation (CSP) mapping approach (e.g. [142]). The CSPs observed in ^{15}N-labeled monoUb upon addition of $S5a_{263-307}$ (Fig. 4.1a,e) cluster around residues Leu8, Ile44, and Val70, consistent with $S5a_{263-307}$ binding to the hydrophobic patch on the surface of Ub.

In $S5a_{263-307}$, the addition of monoUb caused a considerable change in chemical shifts of more than 10 residues, most of them located in the helical region and the

remaining few in the region flanking the α-helix (Fig. 4.2a, also 4.3). The magnitude of the perturbations increased with ubiquitin concentration and saturated at [Ub] / [$S5a_{263-307}$] > 1. The largest CSPs were observed in residues Met291, Met293, Leu295, as well as Ile287 and Gln296, indicating that monoUb binding involves the hydrophobic IAYAM motif (287-291) and the C-terminus of the UIM-2's helix. Significant chemical shift changes were also observed in Ser279-Thr282 located in the N-terminal turn which has been implicated in the helix stabilization and binding interactions with both monoUb [141] and the UBL domain of hHR23A [83, 103]. Interestingly, chemical shifts in the bound state were nearly identical to those observed in UIM-2 complexed with UBL of hHR23A [103], indicating that UIM-2's interactions with UBL and monoUb are, indeed, similar.

The stoichiometry of the $S5a_{263-307}$:monoUb complex was determined by ^1H transverse relaxation measurements. Relaxation time T_2 is inversely proportional to the overall tumbling time of a protein, which, in turn, is proportional to protein's molecular weight. Using the ^1H T_2 values for monoUb (50 ms, molecular weight 8.8 kDa) and Ub_2 (26 ms, 17.4 kDa) [87] as "molecular weight markers", the T_2 of 28 ms measured for the $S5a_{263-307}$:monoUb complex corresponds to ~16.1 kDa, which indicates a 1:1 stoichiometry (16.5 kDa expected). The CSP mapping and relaxation data both indicate that monoUb binds a single $S5a_{263-307}$ molecule and the interaction involves Ub's hydrophobic patch (Fig. 4.1). The surface mapped from this data agrees well with the solution structure of monoUb:UIM-2 complex [141] (Fig. 4.1i). Note that the signal of Lys48 was only slightly shifted ($\Delta\delta$ = 0.06 ppm) upon binding, consistent with the

observation [141] that this residue is not directly involved in Ub's interaction with the UIMs of S5a.

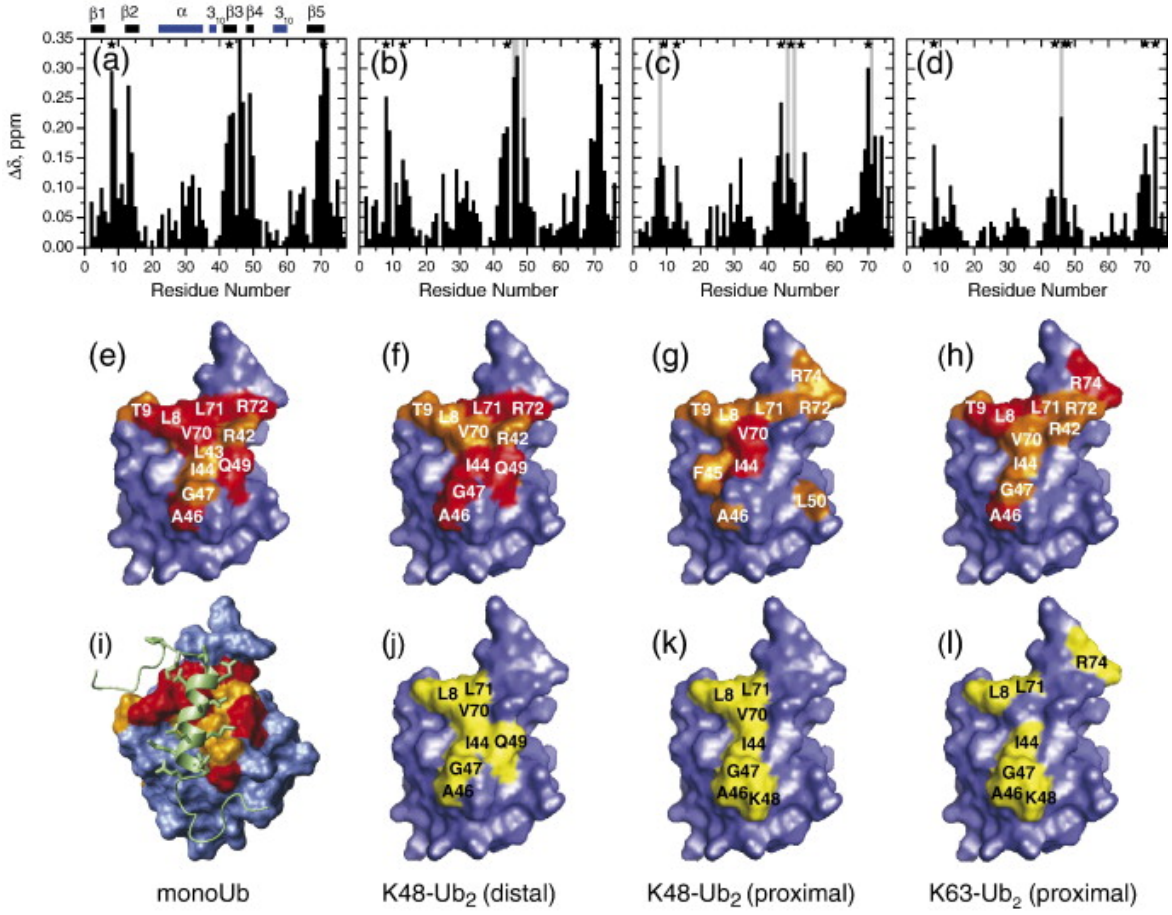

Figure 4.1 NMR mapping of the S5a$_{263–307}$-binding surface on monoUb and Ub units in the Ub$_2$ constructs studied. The top row shows CSPs at saturation as a function of the residue number for the (a) monoUb, (b) distal, and (c) proximal Ubs in K48-linked Ub$_2$ and (d) for the proximal Ub in K63-linked Ub$_2$. (e–h) Sites mapped with significant CSPs on the surface of ubiquitin. The coloring of the CSPs is as follows: (e) $\Delta\delta \geq 0.25$ ppm (red), $0.25 > \Delta\delta \geq 0.15$ (orange) (f) $\Delta\delta > 0.2$ ppm (red), 0.2 ppm $> \Delta\delta > 0.15$ ppm (orange), (g) $\Delta\delta > 0.2$ ppm (red), 0.2 ppm $> \Delta\delta > 0.125$ ppm (orange), (h) $\Delta\delta > 0.15$ ppm (red), 0.15 ppm $> \Delta\delta > 0.075$ ppm (orange). (j–l) Residues that show signal attenuation > 60% (colored yellow) in the ubiquitin units of the corresponding Ub$_2$ constructs. The structure of the monoUb:UIM-2 complex is shown in (i) (Protein Data Bank code 1YX6 [74]). Asterisks in (a–d) mark sites showing intermediate exchange (attenuation > 60%) and the vertical gray bars mark sites exhibiting slow exchange. Horizontal bars at the top of (a) indicate the elements of secondary structure in ubiquitin; the β-strands are colored black and helices are blue.

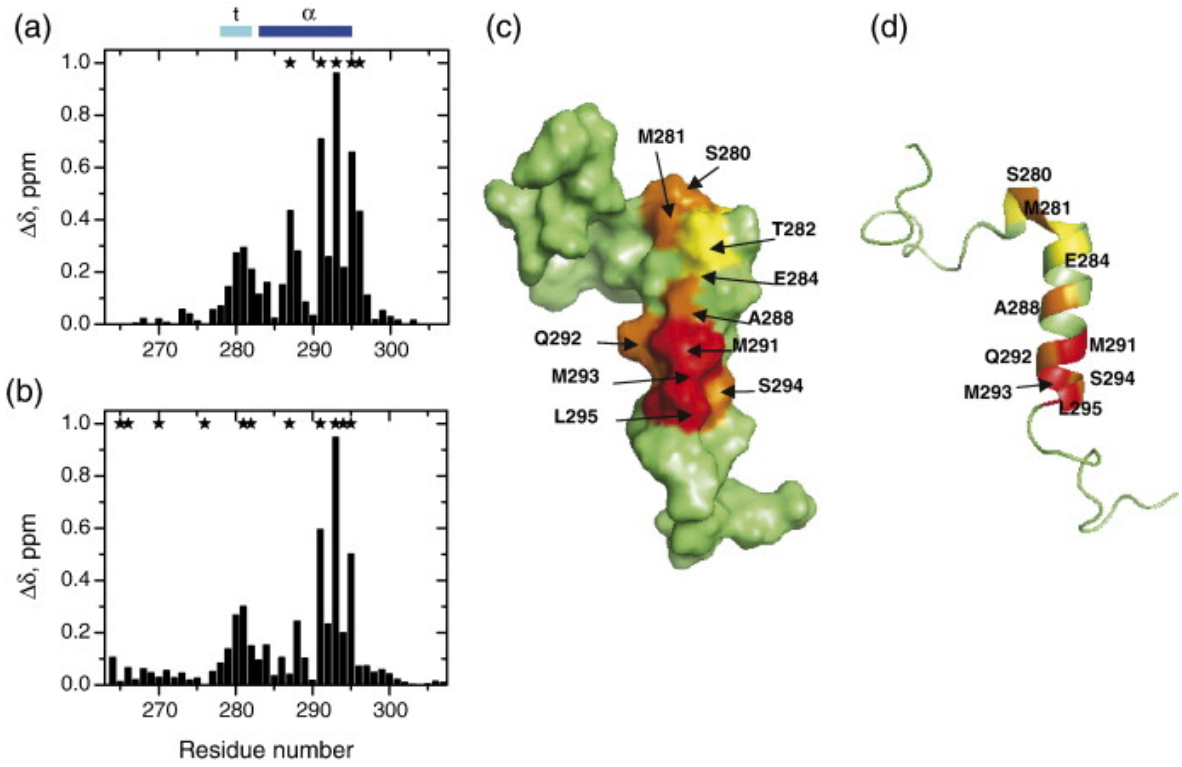

Figure 4.2 NMR mapping of S5a$_{263–307}$ residues affected by binding to monomeric Ub and K48-linked Ub$_2$. (a) and (b) depict the CSPs in S5a$_{263–307}$ at saturation with monoUb and Ub$_2$, respectively, as a function of the residue number. Sites showing significant signal attenuation (>60%) due to intermediate or slow exchange are marked by asterisks. (c) and (d) map these CSPs on the surface (c) and the cartoon representation (d) of UIM-2; the coloring is as follows: $\Delta\delta > 0.4$ ppm (red), 0.4 ppm $> \Delta\delta >$ 0.2 ppm (orange), 0.2 ppm $> \Delta\delta >$ 0.125 ppm (yellow). Horizontal bars at the top of (a) indicate the elements of secondary structure in S5a$_{263–307}$; the helix is blue and the N-terminal turn in S5a$_{263–307}$ (labeled t) is cyan.

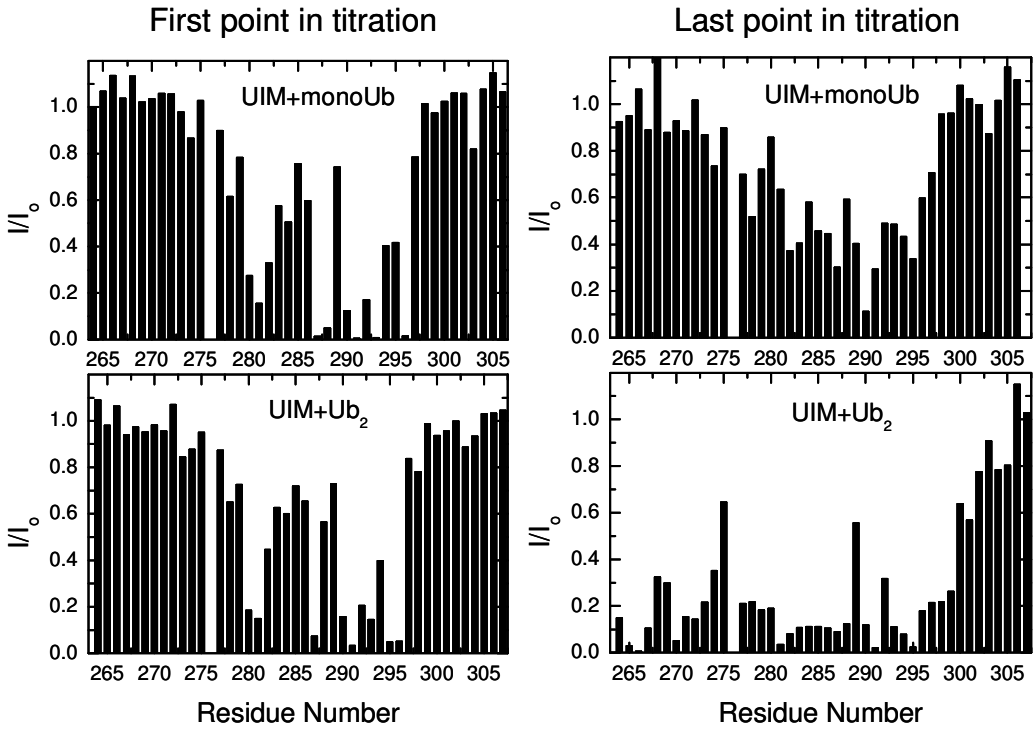

Figure 4.3 Ratio of signal intensities in S5a$_{263-307}$ at the first (left column) or last (right column) point in titration (I) and prior to titration (Io), as a function of residue number. Upper and lower rows correspond to titration with monoUb and Lys48-linked Ub_2, respectively. To compensate for the higher molecular weight of the complex and for the differences in experimental settings, the ratio of intensities was scaled such that it approximately equals 1 for C-terminal residues. A decrease in signal intensity at the first point in titration (when the amount of bound S5a$_{263-307}$ is small) primarily reflects true signal attenuation due to slow or intermediate exchange, whereas the attenuations at the last point (at saturation, when most of S5a$_{263-307}$ molecules are in the bound state) also reflects slow molecular tumbling due to higher molecular weight of the complex. Note that for signals in slow exchange, the latter plot represents (increasing) signal intensities of the bound peaks.

4.2.2 Interaction of S5a$_{263-307}$ and Lys48-linked Ub_2

Using segmentally ^{15}N-labeled Lys48-linked Ub_2 chains synthesized as described in Section 3.2.2, perturbations in the distal and proximal units of Ub_2 induced by S5a$_{263-307}$ binding were monitored separately. As evident from Fig. 4.1, the perturbations (CSPs and signal attenuations) observed in both Ubs are clustered around the hydrophobic patch

residues Leu8, Ile44, and Val70, and the perturbed sites are generally consistent with those in monoUb. Moreover, the magnitudes and the directions of the shifts in the signals are different from those associated with the opening of the hydrophobic interface in Ub_2 (Fig. 4.4). These are important observations, because they indicate, for the first time, that UIM-2 enters the Ub/Ub interface and binds directly to the hydrophobic patch on either Ub domain in Lys48-linked Ub_2.

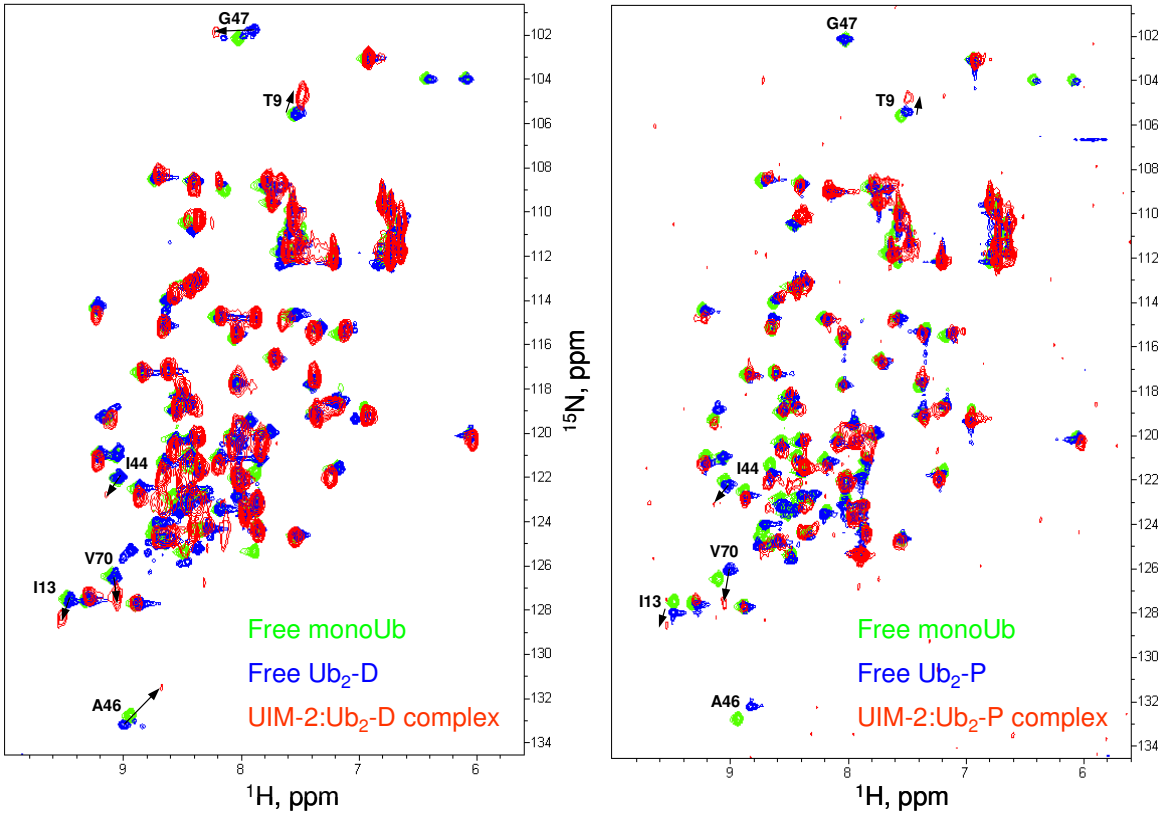

Figure 4.4 Overlay of ^{1}H-^{15}N HSQC spectra of monoUb (green), free Lys48-linked Ub_2 (blue), and $S5a_{263-307}$:Ub_2 complex (red). The left and right panels correspond to the distal and proximal Ubs, respectively.

The binding surface on $S5a_{263-307}$ was also studied. The CSPs in most residues in $S5a_{263-307}$ in the presence of Lys48-linked Ub_2 were almost identical to those observed in the titration with monoUb (Fig. 4.2), both in the magnitude and the direction of the shifts

(Fig. 4.5). The magnitude of the perturbations increased with Ub_2 concentration and saturated at $[Ub_2] / [S5a_{263-307}] > 1$. Noticeably weaker CSPs (accompanied by significant signal attenuation, 75% and 50%, respectively) were observed in Ile287 and Gln296 located at the binding interface between UIM-2 and monoUb, while residues C-terminal to Gln296 as well as at the N-terminus of the $S5a_{263-307}$ construct (Thr264, Ser266, Gln268) show small but significant resonance shifts in the presence of Ub_2, indicative of their possible involvement in the binding. Interestingly, most amides at the N-terminus of $S5a_{263-307}$ (residues 264-274) show signal attenuation comparable to that in the α-helix and other Ub-binding sites in this construct, whereas the C-terminal residues (300-307) show a relative increase in intensity. The latter is consistent with the high flexibility of the C-terminus, which makes these residues practically insensitive to the slower tumbling of the Ub_2-bound part of the construct. This is in contrast with monoUb binding where the N- and C-termini both behave as flexible in the UIM-2:monoUb complex, and only the middle part of $S5a_{263-307}$ (278-295) shows a relative overall decrease in signal intensity reflecting the increased overall tumbling time of the complex (Fig. 4.3). All these observations suggest a possible involvement of the N-terminal residues of $S5a_{263-307}$ in binding to Ub_2.

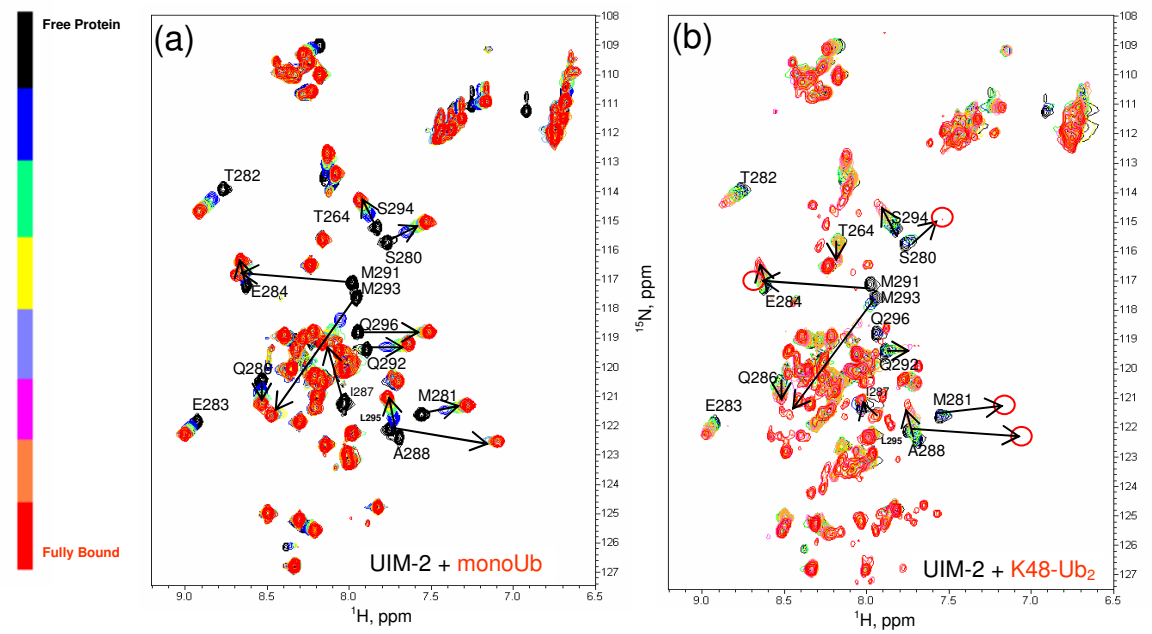

Figure 4.5 Overlay of ^{1}H-^{15}N HSQC spectra of S5a$_{263-307}$ in the course of its titration with (a) monoUb and (b) Lys48-linked Ub$_2$. The coloring scale for the contours is shown on the left, while there are less titration steps in the (a). Arrows indicate the direction and the magnitude of the shift. Circles indicate the position of the signals that are present in the spectra but not seen here because they are below the selected lowest threshold for drawing the contour level. While the magnitude of the shift depends on the binding equilibrium and on the strength of ligand-induced perturbations in a protein, the direction of the shift reflects differences and similarities in the relative perturbations in the electronic environment of ^{15}N and ^{1}H nuclei in the amide group. Thus it is natural to expect that similarity in the direction of the shifts for the signals corresponding to a given residue in two Ub domains probably reflects similar mechanism of interaction with the ligand, while a difference in these directions might indicate subtle differences in the local interactions with the ligand.

The stoichiometry of the S5a$_{263-307}$:Ub$_2$ complex was determined using ^{1}H transverse (T_2) and ^{15}N longitudinal (T_1) relaxation time measurements. A comparison of the measured ^{1}H T_2s with those for Ub$_2$ (26 ms, 17.4 kDa) and Ub$_4$ (13 ms, 34.4 kDa) [87] was used to estimate the molecular weight of the S5a$_{263-307}$:Ub$_2$ complex. The ^{1}H T_2 of 13.6 ms observed independently for two Lys48-linked Ub$_2$ samples (Ub$_2$-D and Ub$_2$-P), as well as for Lys63-linked Ub$_2$ (Ub$_2$-P), in the presence of saturating amounts of

$S5a_{263-307}$, corresponds to 32.9 kDa, in good agreement with 32.8 kDa expected for a 2:1 $S5a_{263-307}$:Ub_2 complex. In order to further characterize the binding event, a series of ^{15}N T_1 relaxation measurements were performed with increasing $S5a_{263-307}$:Ub_2 molar ratio for Lys48-linked Ub_2 (Table 4.1). At [$S5a_{263-307}$]:[Ub_2] = 0.5, the ^{15}N T_1 averaged over residues belonging to Ub core was 796 ± 25 ms (mean ± std), corresponding to a molecular weight of ~22 kDa, smaller than 25.1 kDa expected for a 1:1 $S5a_{263-307}$:Ub_2 complex (Fig. 4.6). At a 1:1 molar ratio, the average ^{15}N T_1 was 909 ± 73 ms, which corresponds to a molecular weight range of 22-27 kDa, consistent with the expected molecular weight for a 1:1 complex. At [$S5a_{263-307}$]:[Ub_2] =2, the ^{15}N T_1 was 1022 ± 130 ms, corresponding to a molecular weight range of 24-32 kDa, comparable with 32.8 kDa expected for a 2:1 complex. The results of all these independent measurements thus indicate that a single Lys48-linked Ub_2 chain can bind up to two UIMs.

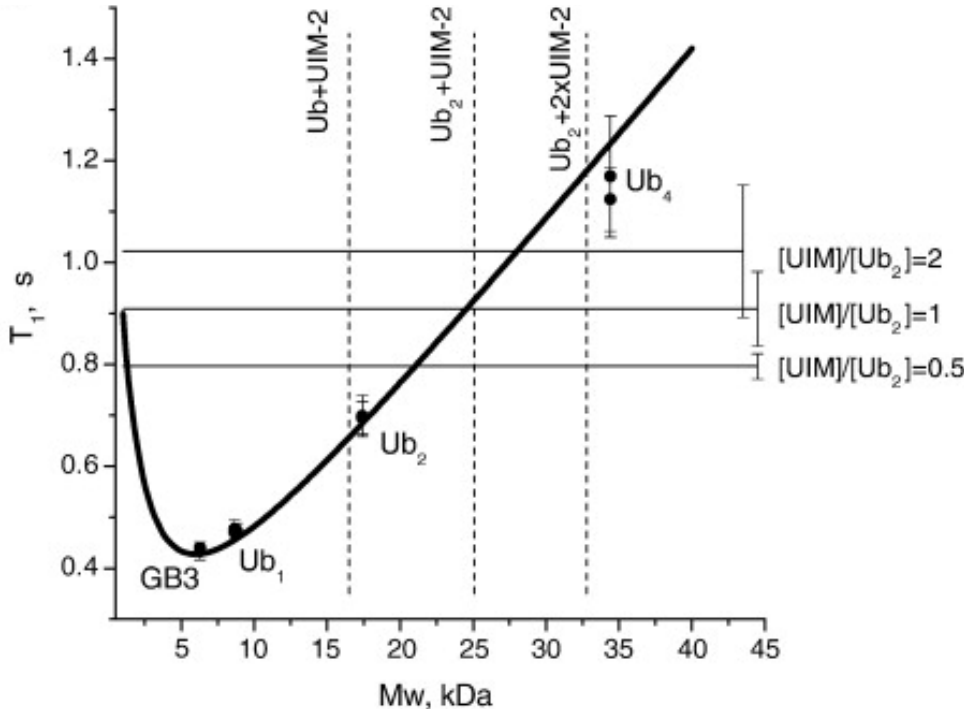

Figure 4.6 NMR characterization of the stoichiometry of Ub_2:S5a$_{263–307}$ binding using ^{15}N longitudinal relaxation rate measurements. The "molecular weight calibration" curve representing the molecular mass dependence of ^{15}N T_1 in proteins was calibrated as described [117]. The horizontal lines correspond to ^{15}N T_1 values measured in Ub_2-P at various titration steps, as indicated (see also Table 4.1); the error bars represent standard deviations in T_1 over core residues in Ub. The dashed vertical lines are molecular weight markers indicating the expected mass of the corresponding constructs.

Table 4.1 Using ^{15}N relaxation time T_1 to verify the stoichiometry of the S5a$_{263-307}$:Ub_2 complex at various titration points.

[S5a]/[Ub_2]	^{15}N T_1 (ms)[a]	Molecular weight range (kDa) corresponding to the ^{15}N T_1 value[b]	Molecular weight (kDa) expected for this stoichiometry
0.5	796 ± 25	20-22	< 25.1
1	909 ± 73	22-27	25.1
2	1022 ± 130	24-32	32.8

[a] ^{15}N longitudinal relaxation time (mean ± standard deviation over the core residues) in Lys48-linked Ub_2 (Ub_2-P) in the presence of the specified molar amounts of S5a$_{263-307}$.
[b]The molecular weight was estimated based on the measured ^{15}N T_1 value using the calibration curve in Fig.4.6.

The fact that the CSPs are seen on the same "face" of UIM as in the titration with monoUb, indicates that there is no secondary binding site on S5a$_{263-307}$ for the other

ubiquitin moiety in Ub_2. These mapping data then indicate that UIM-2 binds Lys48-linked Ub_2 in a mode which is different from that observed for hHR23A UBA-2, where both Ub domains wrap around a single UBA molecule in a sandwich-like manner [117]. Moreover, combined with the mapping data for Ub domains (Fig. 4.1), these results suggest that two UIM-2 molecules are bound to Ub_2.

In addition to the strong similarity in the magnitude of the CSPs in UIM-2 bound to monoUb and Ub_2, slow exchange phenomenon was observed in $S5a_{263-307}$ both in the presence of monoUb and Ub_2. Thus, residues Met291, Met293, Leu295, and Gln296 located at the C-terminus of the helix, as well as Ile287 (of the IAYAM motif) clearly showed a slow-exchange behavior when titrated with monoUb. A similar picture was observed upon addition of Lys48-linked Ub_2, where signals from the same residues, Met291, Met293, Leu295, Ile287, as well as Met281 (N-terminal turn) showed strong signal attenuation from the beginning of titration and attenuated significantly (>80%) already in the presence of 0.2 molar equivalent of Ub_2; these signals reappeared at a different position in the spectrum at the end of the titration (Fig. 4.5).

There are, however, differences in the behavior of $S5a_{263-307}$ signals upon binding to monoUb and Ub_2. Thus, Ser280, Met281, Gln292, and Ser294 exhibit a typical fast exchange behavior upon addition of monoUb, but are in slow (Ser280, Met281) or intermediate (Gln292, Ser294) exchange in the presence of Ub_2. Intriguingly, significant signal attenuation (>90%) was detected in the N-terminal residues Thr265, Ile266, and Glu270 in $S5a_{263-307}$ upon binding to Ub_2, while no such attenuation was observed in its complex with monoUb. Together with the abovementioned CSPs in this part of the construct, these data indicate that the N-terminus of $S5a_{263-307}$ might be involved in

interaction with Ub_2. The greater number of sites showing slow or intermediate exchange (reflecting slower off-rates, hence higher binding affinity) suggests stronger $S5a_{263-307}$ binding to Ub_2 than to monoUb. In the UIM-2:monoUb complex, the C-terminus of the UIM helix containing Met291 and Met293 contacts Ile44, Gly47, and Val70 of Ub while Leu295 is in contact with Ala46 and Gly47 [141]. Residues Ser280 and Met281 are located in the N-terminal turn that caps the hydrophobic Ub surface formed by Leu8, Val70, and Leu71. Interestingly, all these Ub sites in both domains in Ub_2 also show slow or intermediate exchange behavior (Fig. 4.7).

Figure 4.7 Site-specific shifts in the NMR spectra over the course of titration. Shown are overlays of the ^{1}H-^{15}N HSQC spectra corresponding to various titration points for selected Ub residues, as indicated on the right. The coloring scale for the contours is shown on the left. Arrows indicate the direction and the magnitude of the shift. Dashed arrows are used to connect peaks in slow exchange.

A gel mobility assay of $S5a_{263-307}$ binding to monoUb and Lys48-linked Ub_2 provides a qualitative glimpse into preferential binding of $S5a_{263-307}$ to Ub_2. As shown in Figure 4.8a, in a mixture of Ub_2 and $S5a_{263-307}$ (the rightmost lane on the gel), a significant portion of $S5a_{263-307}$ migrates with Ub_2 as evident from the decrease in intensity of the $S5a_{263-307}$ band in the presence of Ub_2.

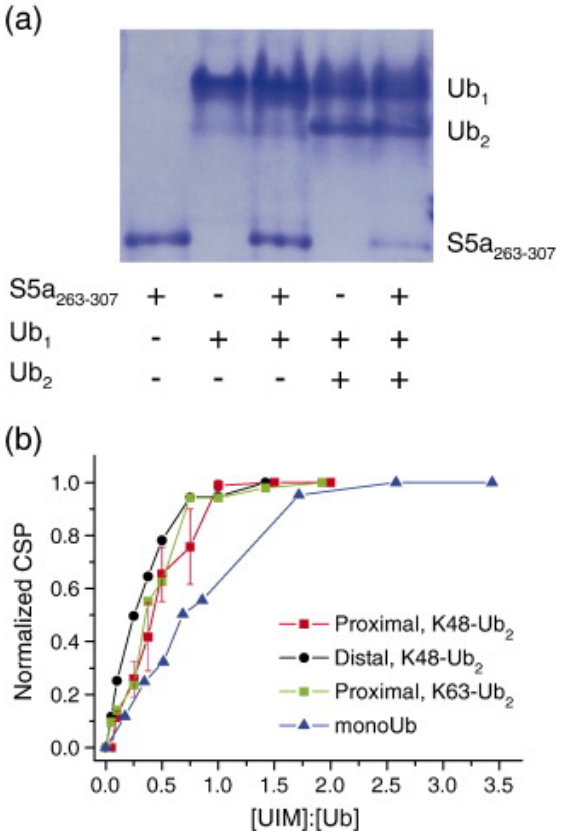

Figure 4.8 Comparison of $S5a_{263–307}$ binding to monoUb and Ub_2. (a) Gel mobility assay comparing binding of $S5a_{263–307}$ to monoUb (lane 3) and Ub_2 (lane 5). A nonreducing, nondenaturing polyacrylamide gel was loaded with equimolar amount of the proteins (2 nmol each). (b) NMR titration curves presenting normalized chemical shift perturbations (averaged over Ub residues His68, Leu69, Val70) for monoUb, Lys48-, and Lys63-linked Ub_2 (as indicated) plotted as a function of the $S5a_{263–307}$:Ub molar ratio, i.e., the number of $S5a_{263–307}$ molecules per Ub unit. The normalization was achieved by dividing all CSPs for a given residue by its CSP at the endpoint of the titration. The error bars in (b) represent the standard deviation (among selected residues) for each averaged CSP value in the proximal Ub. The molar ratios shown on the abscissa axis in (b) were normalized according to the number of available binding sites.

In the UIM-2:monoUb structure, the UIM helix is positioned parallel to and in direct contact with the β5 strand of Ub. Therefore, titration data for residues His68, Leu69, Val70 in this strand were used to monitor and compare UIM binding to Ub units in all the constructs considered here. Figure 4.8b illustrates an increase and subsequent saturation of the CSPs in all Ub units upon addition of $S5a_{263-307}$, which clearly indicates the complex formation. When plotted against the number of $S5a_{263-307}$ molecules per Ub unit, [$S5a_{263-307}$]/[Ub], the CSPs in all Ub_2 constructs studied here saturate at [$S5a_{263-307}$]/[Ub] ~1 (Fig. 4.8b). This is consistent with the binding stoichiometry of one $S5a_{263-307}$ per Ub unit. The fact that the CSPs in monoUb saturate at a higher [$S5a_{263-307}$]/[Ub] ratio (Fig. 4.8b) suggests a higher apparent affinity of $S5a_{263-307}$ for individual Ub units in Ub_2 compared to monoUb. This is likely due to the effect of local Ub concentration: one could anticipate that, when $S5a_{263-307}$ dissociates from a Ub unit, it has a higher probability to bind to another Ub in the same molecule rather than to a Ub in a different chain. Even stronger binding could then be expected in the case of tetraUb and longer chains. This is in agreement with the well known binding preference of S5a for longer chains [141, 143], where the literature data suggest possible binding cooperativity in addition to the increase in the number of Ubs due to chain elongation.

Despite the overall similarity between the two Ub units in terms of the binding surface, the CSPs observed in the distal domain are overall larger than in the proximal (Fig. 4.1). Larger CSPs at saturation could indicate stronger binding, although the precise relationship between the side-chain conformations and the backbone NH chemical shifts in proteins is not fully understood. On the other hand, as evident from Fig. 4.8b, the averaged normalized titration curves for the two domains are not very different from each

other. Although the CSPs in the proximal Ub show a shallow increase (compared to the distal Ub) upon addition of $S5a_{263-307}$ (Fig. 4.1, 4.8b), which could indicate a somewhat weaker UIM-2 binding, accurate quantification of this observation in terms of the difference in the K_d values turned out problematic due to the site-so-site variations in the titration curves likely reflecting the complexity of the binding (Fig. 4.9) and the conformational changes in Ub_2 occurring upon addition of the ligand. Accurate fitting of these titration curves to simple models (e.g., two independent binding sites model) was not possible, likely due to the complex nature of $S5a_{263–307}$ binding to Ub_2. However, from the fact that the Ub_2 CSPs are close to saturation (>90%) at [$S5a_{263–307}$]/ [Ub] = 1, when the molar concentrations of Ub_2 and $S5a_{263–307}$, respectively, are 0.45 and 0.9 mM (proximal Ub titration), 0.44 and 0.88 mM (distal Ub), and 0.37 and 0.74 mM (proximal Ub in Lys63-linked Ub_2), the microscopic K_d is estimated to be on the order of 10 μM, assuming that Ub_2 contains two independent and equivalent binding sites for $S5a_{263–307}$. For comparison, the level of saturation (~60%) observed in monoUb at a similar point in the titration ([$S5a_{263–307}$]/ [Ub] = 0.86, the molar concentrations 0.395 and 0.339 mM) corresponds to Kd ~70 μM, consistent with the literature data [74].

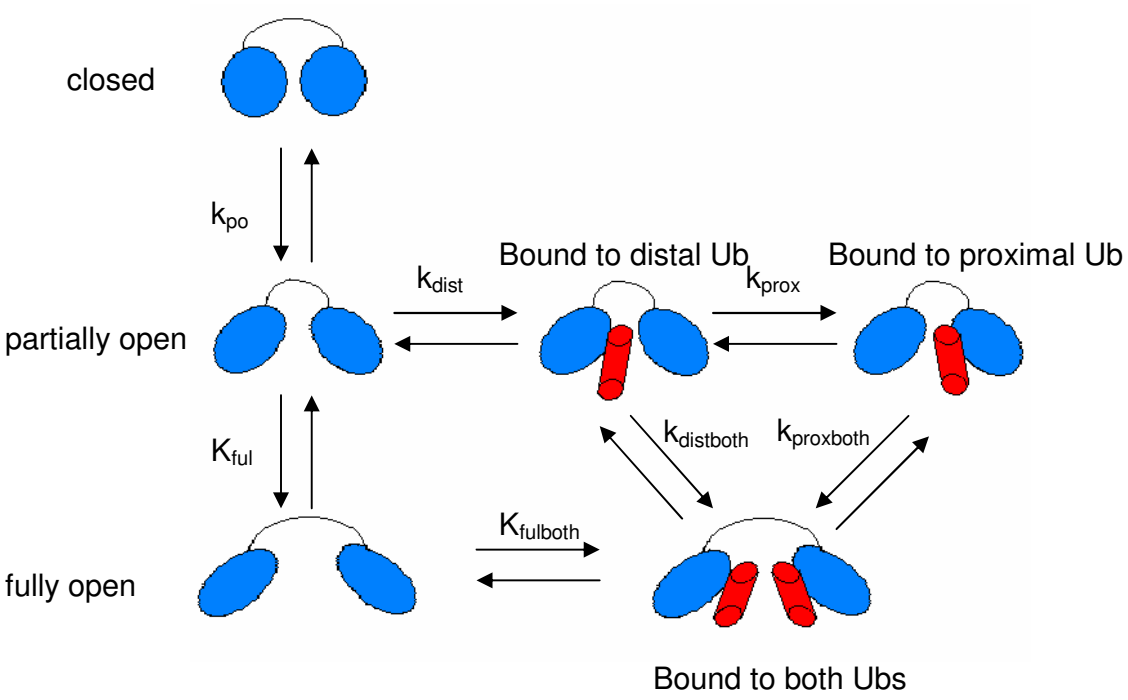

Figure 4.9 UIM:Lys48-linked Ub_2 binding possibilities. The equilibrium between the "closed" and "open" states of Lys48-linked Ub_2 is shown on the left. A combination of the various processes, each with individual equilibria contributes to the binding curves observed.

A detailed analysis revealed further differences between UIM-2 binding to the proximal and distal Ubs in Lys48-linked Ub_2. Thus, the CSP pattern in the distal Ub is very similar to that in monoUb. This is not surprising, given that the only differences between the distal Ub and the D77 Ub mutant used in the monoUb binding studies include a K48C mutation in the former and modifications of the C-terminus (not involved in UIM-2 binding): the Gly76-Lys48(proximal) isopeptide bond in the former and the D77 extension in the latter. The CSP pattern in the proximal Ub is somewhat different. Here the largest CSPs were observed in Ile44, Leu69, Val70, located in the hydrophobic patch, as well as in Arg72, Arg74 at the flexible C-terminus. The differences between the distal and the proximal Ub in the β3-β4 region (residues 45-51), evident from Fig. 4.1,

suggest that the involvement of Lys48 of the proximal Ub in the isopeptide linkage is the likely reason for the observed differences in the $S5a_{263-307}$-induced perturbations in these domains. Although Lys48 in monoUb does not directly interact with UIM-2 (see above), this modification could sterically affect UIM's access to and local interaction with neighboring surface residues in the proximal Ub. Note in this regard that in the proximal Ub, the Lys48 signal itself shows a stronger CSP ($\Delta\delta$ = 0.11 ppm) than in the distal Ub and a slow-exchange behavior.

It should be mentioned, however, that not all sites in the proximal Ub show a somewhat weaker $S5a_{263-307}$ binding compared to their counterparts in the distal Ub. Thus, Leu8 and Leu71, located at the opening of the Ub/Ub interface, show slow exchange in the proximal but not in the distal Ub, indicative of stronger UIM binding to these particular sites. In addition, Val70 in the proximal Ub has a stronger CSP than in both monoUb and the distal Ub (Fig. 4.1, 4.7). These observations emphasize the complexity of the UIM interaction with Ub_2, as well as the ability of NMR titration experiments to provide a detailed site-specific picture of a binding event.

4.2.3 Interaction of $S5a_{263-307}$ and Lys63-linked Ub_2

Binding interactions of UIM-2 with Lys63-linked Ub_2 were aimed at understanding the molecular basis for chain linkage specificity in proteasomal degradation. One of the goals was to test whether the sequestration of the hydrophobic patches in the closed conformation of Lys48-linked Ub_2 has any hindering effect on UIM's binding to Ub_2. Because the closed Ub/Ub interface is not formed in Lys63-linked Ub_2 (hence no hindering expected), this chain serves as a control for such study. Another

goal was to examine if the involvement of Lys48 in the isopeptide linker has any effect on the UIM binding properties of the proximal Ub in Lys48-linked Ub_2. In the Lys63-linked Ub_2, Lys48 is not modified, and Lys63 is located far away from the UIM-binding sites, hence one could expect that the proximal domain binds UIM similarly to the distal Ub in Lys63- or Lys48-linked chain. Another important question is whether the extended hydrophobic binding pocket in Ub_2 [117], which is formed due to the Gly76-Lys48 linkage and allows Ub_2 to bind UBA domains in a sandwich-like fashion [117, 119], plays any role in the $S5a_{263-307}$ binding. If this was true, one could expect that the absence of such a pocket in Lys63-linked Ub_2 would result in weaker $S5a_{263-307}$ binding to this chain.

The CSPs in the proximal Ub in Lys63-linked Ub_2 clearly demonstrate that $S5a_{263-307}$ binding occurs at the same hydrophobic Ub surface as in monoUb and Lys48-linked Ub_2. The NMR titration curve is also similar to that for the Lys48-linked Ub_2 (Fig. 4.8b); the magnitude of the perturbations increases with $S5a_{263-307}$ concentration and saturates at $[S5a_{263-307}]/[Ub_2] \sim 2$ (or $[S5a_{263-307}]/[Ub] \sim 1$). The CSP pattern (Fig. 4.1d) and the directions of the signal shifts (Fig. 4.7) here are similar to those in monoUb and in the distal Ub of Lys48-linked Ub_2, suggesting a similar mode of the UIM:Ub interaction. Similar sites in Lys63-linked Ub_2 show signal attenuations upon addition of $S5a_{263-307}$; the gradual shifts of the corresponding signals accompanied by their broadening (Fig. 4.7) indicate intermediate exchange, also observed in the Lys48-linked Ub_2. Also the averaged normalized titration curve for the β5 strand (Fig. 4.8b) is strikingly similar to that for the proximal as well as for the distal Ub in Lys48-linked Ub_2. All these data point to the conclusion that, despite the differences in local perturbations,

the involvement of Lys48 in the isopeptide linkage does not significantly affect the affinity of UIM-2 binding to the proximal Ub. On the other hand, however, the overall magnitude of the CSPs is markedly smaller even compared to the proximal Ub of Lys48-linked Ub_2. The reasons for this are not yet clear and could be related to the linkage-dependence of Ub_2's conformation.

4.2.4 Discussion

Ligand binding to polyUb could be complicated by the presence of the intramolecular interaction between Ub monomers in the chain [81]. Thus the predominant (85% populated) conformation of Lys48-linked Ub_2 in solution at neutral pH is characterized by a close contact between the two ubiquitins[81, 82], which bind to each other via their hydrophobic patches, effectively burying the functionally important residues Leu8-Ile44-Val70 at the Ub/Ub interface. The same contacts are present in Lys48-linked Ub_4 [81, 88, 91, 117]. The opening of the Ub/Ub interface is essential for polyUb's binding to UIM or any other ligand targeting the hydrophobic patch on Ub. One could then expect that the predominantly closed conformation of Lys48-linked Ub_2 and the necessity for a ligand (here UIM-2) to compete with the Ub/Ub interaction might control its binding to the chain. Thus, ligand binding to polyUb would depend on several factors, including (i) the strength of the ligand:Ub versus Ub/Ub interaction, (ii) the entropic contributions including the hydrophobic effect and the cost of ligand's immobilization (see e.g. [87]), and (iii) the rate of interface opening, which depends on the height of the corresponding activation barrier between the closed and open states of Lys48-linked Ub_2.

The total buried surface area between UIM-2 and monoUb is 1,197 $Å^2$, compared to ~1,500-1,750 A^2 between Ub units in Ub_2. This suggests that the formation of a 1:1 $S5a_{263-307}$:Ub_2 complex using the same $S5a_{263-307}$:Ub contacts as in the case of monoUb and thus exposing the hydrophobic surface of one of the two Ub units, is not entropically favorable. In the case of two $S5a_{263-307}$ molecules bound per Ub_2, the total buried area is expected to be about 2,240 A^2, which would make the formation of such a complex more favorable with regard to the hydrophobic effect. This gain, however, could be offset by the entropy loss due to the immobilization of an additional UIM moiety. The NMR titration data indicates that, in fact, $S5a_{263-307}$ binding to either Ub unit in Ub_2 is tighter than to monoUb. This is in agreement with the published pull-down data indicating that S5a, as well as the individual UIMs, bind polyUb more efficiently than monoUb [140, 141].

Because two UIM molecules ultimately bind to Ub_2, the complex must remain open or continue opening after binding of the first UIM, rather than wrapping around it to form a Ub-UIM-Ub sandwich. This conclusion is supported by the NMR mapping data presented above. Indeed, the Ub_2-binding surface on $S5a_{263-307}$ involves the same "face" of the UIM helix as in binding to monoUb, and no additional perturbations were observed on the opposite "face" of UIM-2 (Fig. 4.2) thus excluding the sandwich model. In addition, the $S5a_{263-307}$-binding surfaces on both Lys48- and Lys63-linked Ub_2 constructs (Fig. 4.1) agree well with that on monoUb (Fig. 4.1a,e) and with the published structure of the UIM-2:monoUb complex [141]. Moreover, there is no indication of any interaction between the two $S5a_{263-307}$ molecules in the fully loaded, 2:1 $S5a_{263-307}$:Ub_2 complex, thus rendering unlikely a more complex model where the two UIMs, bound to the individual

Ub domains, interact with each other (e.g. sandwiched within the Ub_2's hydrophobic pocket). Note that sedimentation velocity measurements, as well as NMR studies showed that S5a UIMs do not interact with each other [102, 141]. It seems then reasonable to model the formation of the UIM:Ub_2 complex as a two-step process in which the binding of one UIM shifts the equilibrium towards an open conformation of Ub_2, thus causing a conformational change in the chain which, in turn, exposes the hydrophobic patch on the other domain and makes it available for binding to a second UIM.

4.2.5 Structural models of UIM-2 binding to Lys48- and Lys63-linked Ub_2

Model structures of the complexes of UIM-2 with Lys48-and Lys63-linked Ub_2 were created based on the data and are shown in Fig.4.10 and 4.11. The Ub_2 structure in the complex with the hHR23A UBA-2 domain (PDB code 1ZO6, [117]) was used as a structural model for the open conformation of Lys48-linked Ub_2, while the (extended) conformation of free Lys63-linked Ub_2 in solution was used in Fig. 4.11. The UIM-2:monoUb structure [141] was used to model the UIM-2/Ub contact for both Ub units in each chain. It should be mentioned that, based on the NMR analysis of the equilibrium dynamics in Lys48-linked Ub_2, the relative orientation of the two Ub domains in the open state of free Ub_2 at pH6.8 is similar to that in the Ub_2:UBA-2 complex [82, 87], therefore we used this structure as a model for the open state of Ub_2. The structure model shown in Fig. 4.10 illustrates how two UIMs can be accommodated in the hydrophobic pocket of Lys48-linked Ub_2. The steric clashes involving flexible regions flanking the UIMs may be relieved by further opening of the two Ub domains (which seems plausible due to the flexibility of the Ub-Ub linker) as well as by structural rearrangement of the clashing

flexible fragments. No steric clashes are seen in the Lys63-linked Ub_2:UIM complex, in which the Ub units are expected to bind two UIM-2 molecules independently, in analogy to that observed in the chain's binding to hHR23A UBA-2 domains [87].

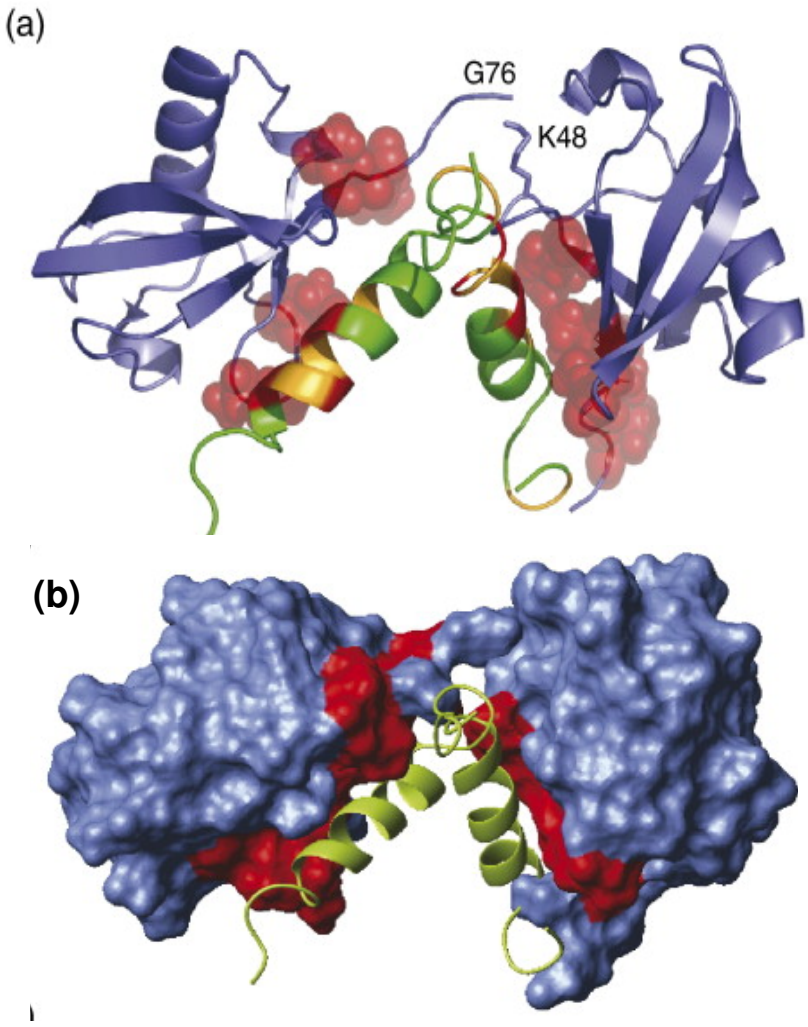

Figure 4.10 Models of two UIM-2 helices bound to Lys48-linked Ub_2. Side-chains of Ub_2 residues with $\Delta\delta > 0.2$ ppm are represented by red spheres, while CSPs on UIM-2 (in (a)) are colored as follows: $\Delta\delta \geq 0.4$ ppm (red), $0.4 \text{ ppm} > \Delta\delta > 0.125$ ppm (orange). These structures were obtained assuming that each UIM-2 binds to the corresponding Ub unit in the chain in the same way/orientation as to monoUb (Protein Data Bank code 1YX6) and using the structure of Lys48-linked Ub_2 in its complex with UBA-2 (Protein Data Bank code 1ZO6) as a structural model of the open conformation. The resulting structures were obtained by direct superimposition of ubiquitin atoms in the UIM:Ub complex with those for each Ub unit in Ub_2. (b) The same complex as in (a), with Ub_2 shown in surface representation, painted red for those sites on both Ub units that show significant CSPs and/or signal attenuations.

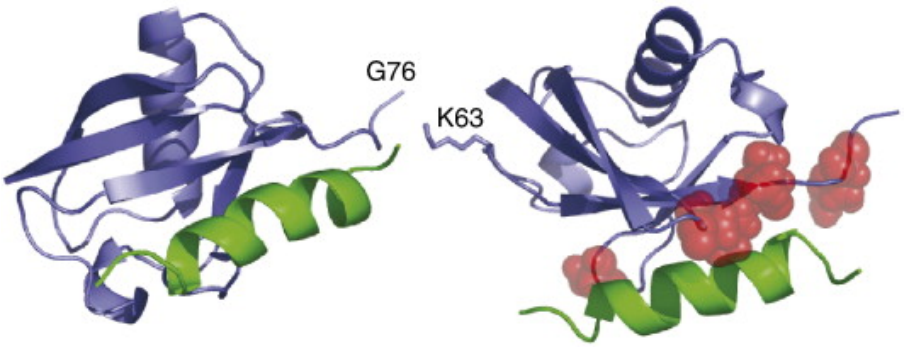

Figure 4.11 Models of two UIM-2 helices bound to Lys63-linked Ub_2. Side-chains of Ub_2 residues with $\Delta\delta > 0.2$ ppm are represented by red spheres. The structure was obtained assuming that each UIM-2 binds to the corresponding Ub unit in the chain in the same way/orientation as to monoUb (Protein Data Bank code 1YX6) and using the structures of free Lys63-linked Ub_2 [87] as a structural model.

The similarity in UIM-2 binding between Lys48- and Lys63-linked Ub_2s is in contrast to their interaction with hHR23A UBA-2. This is in agreement with the SPR data [115] indicating that, unlike the UBA-2 domain, S5a does not discriminate between Lys48- and Lys63-linked Ub_4. It is important to emphasize here that the binding preference toward a particular chain linkage depends on a combination of (1) the Ub-binding properties of a ligand and (2) the ability (dictated by the linkage) of a given polyUb chain to adopt a specific conformation necessary to bind this ligand in the energetically most favorable way. For example, the three-helix bundle structure of UBA-2 allows it to interact simultaneously with both Ubs in the Lys48- but not in the Lys63-linked Ub_2, where the conformational properties of the chain do not allow a similar, high-affinity binding mode. This, however, cannot be generalized for all UBAs, which exhibit diverse chain-linkage preferences [115]. The nondiscriminatory binding of polyUb chains by UIM-2 of S5a could be a result of UIM-2 being a single, one-sided Ub-binding helix.

It is possible that the tandem UIM S5a and other UIMs are linkage selective, for example, those from Eps15 and Hrs, predicted to exhibit double-sided binding [144].

The binding data show that a single UIM-2 binds per Ub unit in Ub_2. Moreover, as mentioned above, the footprints of UIM-2 on both Ub units in Ub_2 are very similar to those on monoUb (Fig. 4.1); and likewise similar are the perturbations in UIM-2 caused by Ub_2 and monoUb (Fig. 4.2). This suggests that the mode of UIM-2 binding to each Ub unit in Ub_2 is similar to that in the UIM-2:monoUb complex. Detailed structural characterization of these complexes is required in order to fully address this issue.

4.3 Interaction of tandem UIM-1/UIM-2 S5a construct with Lys48- and Lys63-linked Ub_2

The work described in this section is part of a collaborative project with the Walters Lab at the University of Minnesota. Since this project is ongoing, the data and interpretations are preliminary and require further analysis.

The tandem UIM-1/UIM-2 construct (referred to as $S5a_{196-306}$ in this text) contains three structured regions spanning residues Pro214-Glu245, Asp257-Glu269, and Leu278-Gln296 (Fig. 4.12a) [74]. Flexible, randomly coiled linker regions connect the structured elements and prevent them from being defined relative to each other. NMR and gel-filtration studies have shown that the UIM-1 and UIM-2 domains do not interact with each other, and sedimentation velocity experiments up to 2mg/ml of $S5a_{196-306}$ indicate a monomeric state for the tandem construct. [74].

The first helix is comprised of nine helical turns and includes the well-known UIM-1 hydrophobic patch LALAL (216-220) within the first two turns. In addition to

hydrophobic residues, the presence of charged residues C-terminal to UIM-1 (Glu215) is important for interactions with Lys6 and His68 of monoUb [74, 100]. The middle helix in S5a has not been implicated in binding to Ub, and the region linking UIM-1 and UIM-2 is flexible and allows the S5a UIMs to span long distances which may be integral in binding to polyUb chains of different lengths and linkages [74]. It was suggested that this feature of S5a may explain the dramatically higher binding affinity for longer polyUb chains (estimated K_d ~23 μM for Lys48-linked Ub_2 and K_d < 18nM for polyUb chains more than 7 Ubs in length [145]), since longer polyUb chains provide a greater number of available binding sites to the two UIMs. The third helix of $S5a_{196-306}$, UIM-2, is comprised of four helical turns including the hydrophobic patch $I^{287}AYAM^{291}$ and an N-terminal hairpin loop (Leu287, Ser279, Ser280). Charged residues N-terminal to UIM-2 (Glu283, Glu284, Glu285) make contacts with monoUb [74]. A conserved serine residue at the C-terminus of both UIMs also contributes to Ub binding [74]. An important difference between UIM-1 and UIM-2 is the positioning of the hydrophobic LALAL/IAYAM sequence. In UIM-1 this sequence is positioned at the N-terminal end of the α-helix, whereas in UIM-2 it resides in the second and third helical turn (Fig. 4.12a). The positioning of the hydrophobic patch has been suggested to play a major role in stronger UIM-2/Ub binding compared to UIM-1 [74].

While Lys48-linked chains bind $S5a_{196-306}$ and are the most well-known signals for proteasomal degradation, Lys6- and Lys11-linked chains [145], as well as Lys63-linked chains, also bind to $S5a_{196-306}$ [74]. Importantly, Lys63-linked chains have also been observed to signal for proteasome-mediated degradation *in vitro* [10] and bind to hHR23A, although with lower affinity than Lys48-linked polyUb [146]. Accordingly,

Lys48-linked polyUb may be the most competent proteolytic tag consistent with a proposed scenario in which S5a and hHR23A collaborate to shuttle polyubiquitinated substrates to the proteasome [74]. This model is based on an NMR study [147] that observed a ternary complex involving $S5a_{196-306}$, Lys48-linked Ub_4, and hHR23a in solution. The proposed mechanism asserts that UBA-2 of hHR23A binds polyUb, while UBL of hHR23A binds to UIM-2 of $S5a_{196-306}$ and shuttles polyUb to UIM-1 [147]. However, studies have shown that the UIMs of S5a are not essential for proteasomal degradation [31], therefore, this may be one of several possible pathways for recognition of ubiquitinated substrates by the proteasome. While this NMR analysis provides very useful insights into how ubiquitinated substrates may be shuttled to the proteasome, a detailed study of S5a binding to Lys48- and Lys63-linked polyUb is needed in order to understand chain linkage specificity and evaluate the prevailing belief in the Ub field that Lys48-linked chains are the principal signal for polyUb-mediated proteasomal degradation.

The finding that each Ub moiety in Lys48-linked Ub_2 binds to a single UIM, combined with the fact that each UIM in S5a binds a monoUb [74], suggests a 1:1 stoichiometry model for Ub_2's complex with $S5a_{196-306}$. In order to test this hypothesis, and gain insights into the polyUb chain-linkage effect on the tandem UIM S5a, the interaction of $S5a_{196-306}$ with Lys48- and Lys63-linked Ub_2 was studied.

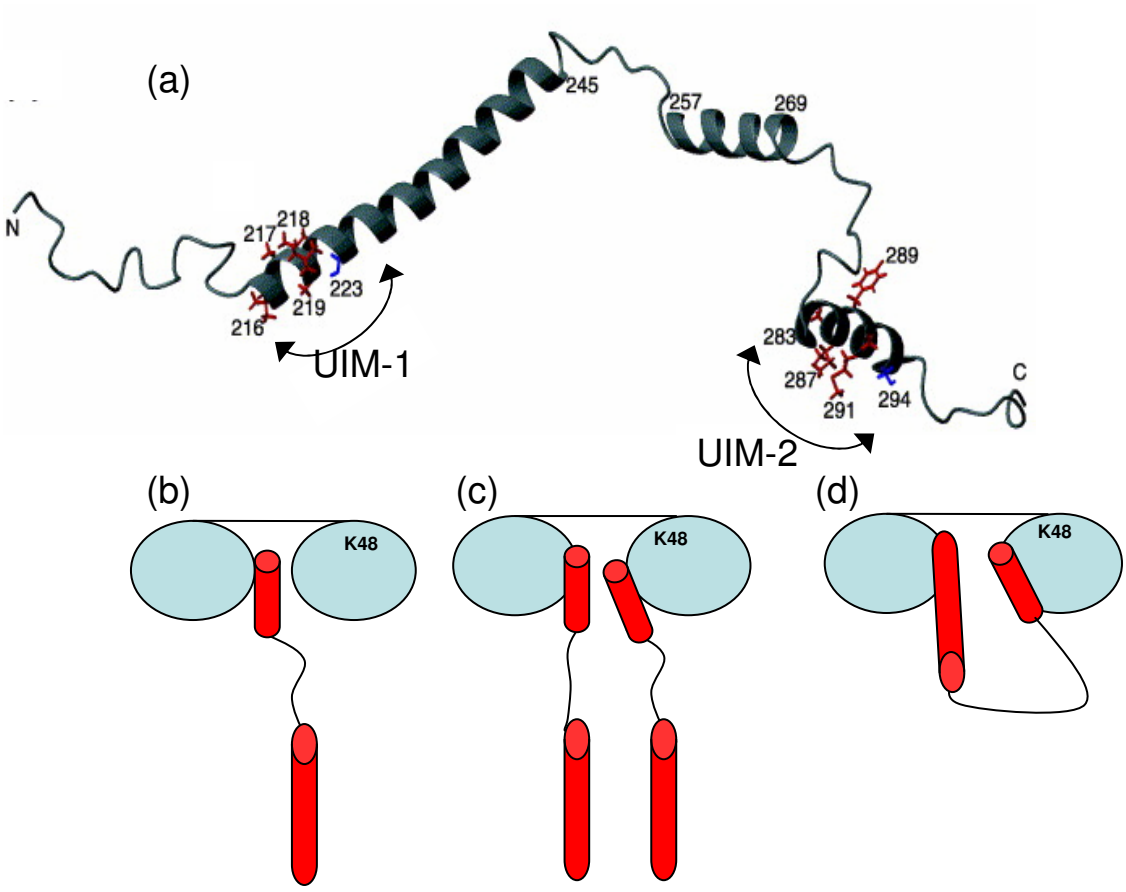

Figure 4.12: Structure of S5a and possible modes of binding to Ub_2. a) Ribbon representation of $S5a_{196-306}$ showing 3 alpha helix regions (coordinates from 1YX4.pdb). The hydrophobic LALAL/IAYAM residues within each UIM are highlighted in red, and the conserved serine residue is colored blue. Figure adapted from [74]. Schematic representations of b) S5a binding to Lys48-linked Ub_2 via one UIM, c) 2 S5a molecules binding to Lys48-linked Ub_2, d) S5a binding to Lys48-linked Ub_2 via both UIMs.

4.3.1 Interaction of $S5a_{196-306}$ and Lys48-linked Ub_2

While the data above show that Lys48-linked Ub_2 binds to two free UIM-2s, its mode of binding with the tandem UIM-1/UIM-2 $S5a_{196-306}$ was unclear. At least three possible modes could be imagined (Fig. 4.12b,c,d). One possibility would involve a single UIM of $S5a_{196-306}$ binding to either domain in Lys48-linked Ub_2 (Fig. 4.12b). The second possibility would involve two $S5a_{196-306}$s binding to Ub_2 via a single UIM on each $S5a_{196-306}$ (Fig. 4.12c). A third possibility is binding of a single $S5a_{196-306}$ to Ub_2, via both

UIMs, each UIM binding to one of the Ub moieties (Fig. 4.12d). NMR relaxation measurements were used to determine the stoichiometry. Here, ^{1}H T_2 was 14.3 ms (at the 1:1 molar ratio), and ^{15}N T_1 was 1103 ±112 ms and 1077 ± 156 ms at [S5a]/[Ub_2] = 0.8 and 1.5, respectively, which corresponds to the molecular weight range of 26-33 kDa, in agreement with 30 kDa expected for a 1:1 complex. Thus, the model describing Lys48-linked Ub_2 bound to two $S5a_{196-306}$ constructs (Fig. 4.12c) (42.4 kDa expected) can be excluded.

In order to differentiate between the remaining two possible modes of binding, the chemical shift perturbation mapping approach was used to determine the binding surfaces. Strong CSPs and signal attenuations were observed in both UIM-1 and UIM-2 of $S5a_{196-306}$ in a titration with Lys48-linked Ub_2 (Fig. 4.13c) (unpublished data and plots courtesy Drs. Qinghua Wang and Kylie Walters, Univ. of Minnesota). The data show that both UIMs of S5a are involved in binding to Lys48-linked Ub_2, thus it appears that the model with only one UIM of $S5a_{196-306}$ involved in binding (Fig. 4.12b) can also be discarded, leaving only the model shown in Fig. 4.12d. Since UIM-1 binds 5-10 times weaker than UIM-2 to Ub [74, 98] and the pattern of signal attenuations in both UIMs are strong throughout the titration, it is unlikely that there is alternating binding by UIMs (i.e. only UIM-1 binding to Ub_2, then only UIM-2 binding and vice versa).

The pattern of CSPs observed in the UIM-2 region of $S5a_{196-306}$ bound to Lys48-linked Ub_2 (Fig. 4.13c) was mostly similar to the pattern observed when $S5a_{196-306}$ was bound to monoUb (Fig. 4.13a), while the CSP in signals belonging to most UIM-1 residues could not be reliably quantified due to the significant decrease in signal intensities in this region as a result of slow exchange regimes. Furthermore, a third

region, N-terminal to UIM-2 (residues 262-268), was also perturbed as a result of the binding interaction with Lys48-linked Ub_2. Notably, perturbations in this region were also observed in the isolated UIM-2 upon binding to Lys48-linked Ub_2 (Fig. 4.2b), but not detected in complex with monoUb (Fig. 4.2a).

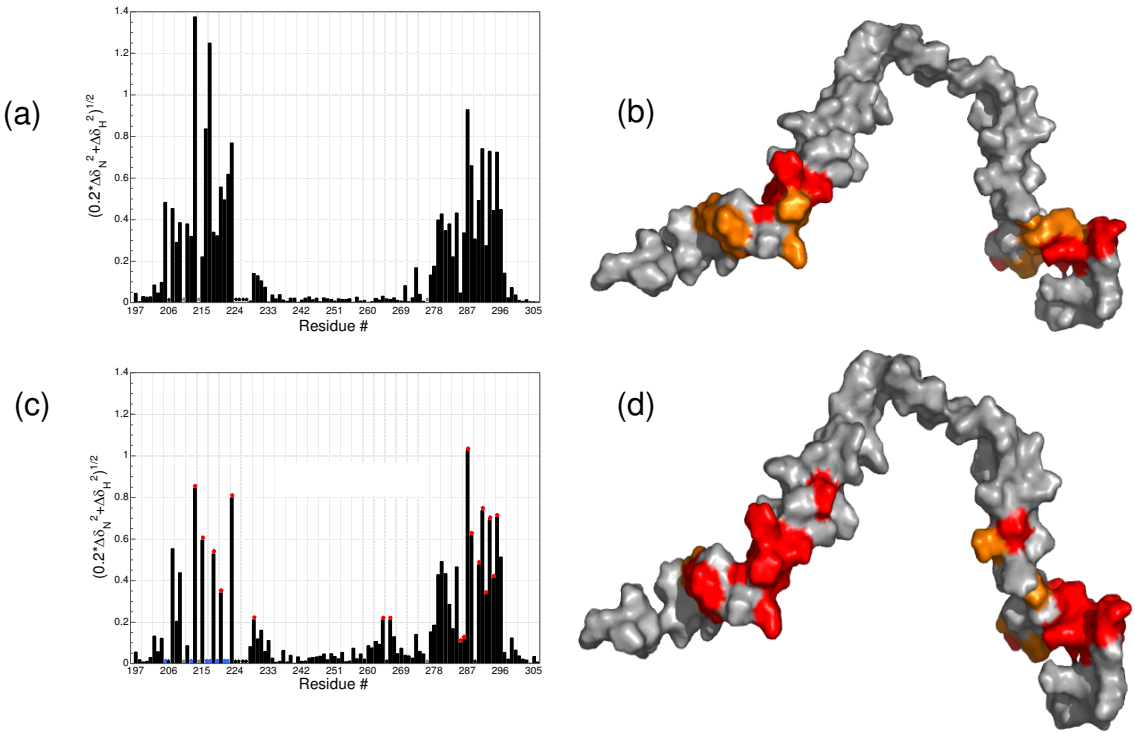

Figure 4.13 NMR mapping of $S5a_{196–306}$ residues affected by binding to monoUb and Lys48-linked Ub_2. (a) CSPs in $S5a_{196-306}$ at saturation (1:4 [S5a]:[Ub]) with monoUb and (c) Lys48-linked Ub_2 (1:3 [S5a]:[Ub_2]) as a function of the residue number. (b,d) Surface representation of the perturbations mapped on the surface of S5a using the coloring scheme: $\Delta\delta \geq 0.4$ ppm and slow exchange regimes (red), $0.4 > \Delta\delta \geq 0.15$ (orange). Red and blue Stars in (c) mark sites showing slow exchange regimes. Gray stars denote prolines and unfilled stars denote unassigned residues. Panels (a,c) contain unpublished data from experiments done in the Walters Lab at Univ. of Minnesota.

Based on our chemical shift perturbation mapping, the binding surface on the distal Ub of Lys48-linked Ub_2 (Fig. 4.14a,c,e) was mostly similar to the binding surface

with the isolated UIM-2 (see Fig. 4.1b,f,j), although strong CSPs and signal attenuations were also observed in the linker region between the Ub moieties (residues 72-76). This is important since it suggests an additional surface involved in the interaction. Also, strong signal attenuation, an indication of slow exchange, was observed in many Ub residues, as well as both UIM regions of $S5a_{196-306}$, indicating that the binding interaction with $S5a_{196-306}$ is relatively stronger than with the isolated UIM-2 ($S5a_{263-307}$).

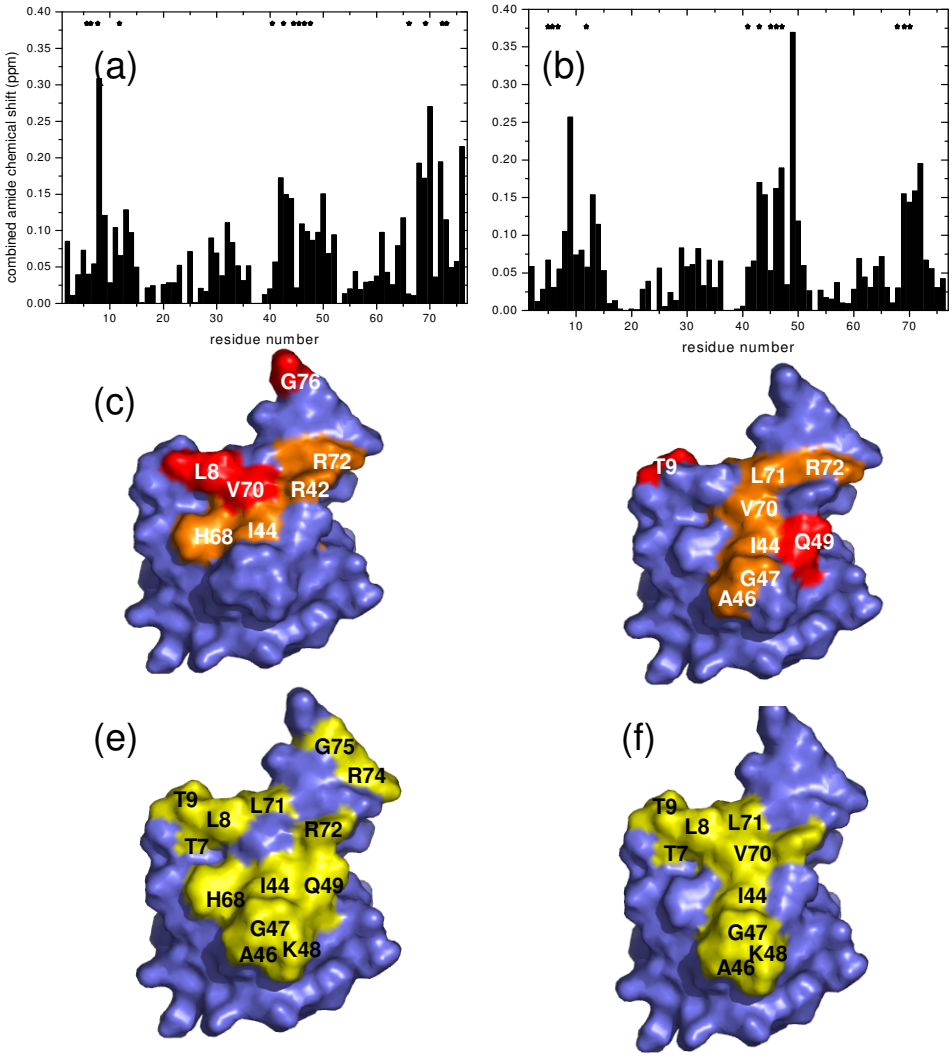

Figure 4.14 NMR mapping of the S5a$_{196–306}$-binding surface on distal Ub units in the Ub$_2$ constructs studied. The top row shows CSPs at saturation as a function of the residue number for the distal Ubs in (a) Lys48- and (b) Lys63-linked Ub$_2$ (c,d) Sites mapped with significant CSPs on the surface of ubiquitin. The coloring of the CSPs is as follows: $\Delta\delta \geq 0.20$ ppm (red), $0.20 > \Delta\delta \geq 0.15$ (orange) (e,f) Residues that show signal attenuation > 60% (colored yellow) in the corresponding Ub$_2$ constructs.

The titration curves for residues not in slow or intermediate exchange on the distal Ub of Lys48-linked Ub$_2$ were fit to a simple binding model (Eq. 2, section 3.3.2) to determine K_d = 59 ±23 μM (Fig. 4.15a). Binding curves for residues in S5a$_{196-306}$ titrated with unlabeled Lys48-linked Ub$_2$ could not be reliably fit due to significant intermediate and slow exchange behavior observed in these spectra.

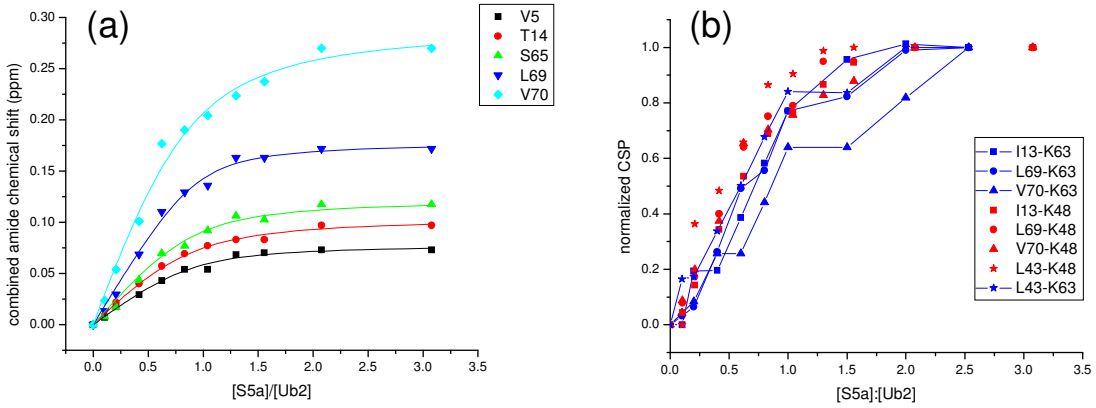

Figure 4.15 Comparison of S5a$_{196–306}$ binding to Lys48- and Lys63-linked Ub$_2$. (a) NMR titration curves presenting chemical shift perturbations in residues Val5, Thr14, Ser65, Leu69, Val70 of the distal Ub in Lys48-linked Ub$_2$ plotted as a function of the S5a$_{196–306}$:Ub$_2$ molar ratio. (b) NMR titration curves plotting the normalized CSPs in residues Ile13, Leu43, Leu69, Val70 (squares,stars,circles,triangles) of the distal Ub of (red) Lys48-linked Ub$_2$ and (blue) Lys63-linked Ub$_2$ plotted as a function of the S5a$_{196–306}$:Ub$_2$ molar ratio.

Since both UIMs of S5a$_{196-306}$ appear to be involved in binding to Lys48-linked Ub$_2$, a putative model of the complex of S5a$_{196-306}$ and Lys48-linked Ub$_2$ was proposed (schematically shown in Fig. 4.16a,b). In this model, both UIMs of S5a$_{196-306}$ are bound, each to a separate Ub unit in the chain. This model is based on superimpositions of the intermolecular UIM:Ub contacts in the S5a$_{196-306}$/monoUb solution structure [74] with the structure of Lys48-linked Ub$_2$ in a partially open, UBA-bound state [117]. Because UIM-2 binds mono/polyUb stronger than UIM-1 does [140, 141], it is natural to assume that its binding preferences could dictate the structure of the S5a$_{196-306}$:Ub$_2$ complex. However, an isolated UIM-2 does not show strong preference for a particular Ub unit in Ub$_2$, so both possible scenarios are considered here, i.e. with UIM-2 bound to the distal (Fig. 4.16a,c) or to the proximal Ub (Fig. 4.16b,d), and UIM-1 bound to the other Ub unit in Ub$_2$. Structural superimposition models of such a complex, based on the complexes of

these UIMs with monoUb can be found in Fig. 4.16c,d. The positioning of the LALAL motif in UIM-1 at the N-terminus of a very long α-helix (9 turns compared to 4 turns in UIM-2) could potentially cause steric clashes between the helices as well as with the Ub-Ub linker (Fig. 4.16a,c). On the other hand, this orientation may allow additional interactions with the Ub/Ub linker. Interestingly, in this model, the N-terminal UIM-2 region is positioned close to the Ub/Ub linker and, in fact, significant CSPs are observed in these residues as described above. Moreover, in the scenario shown in Fig. 4.16b,d in which UIM-2 is bound to the proximal Ub, possible steric clashes between UIM-1 and UIM-2 near the Ub-Ub linker are avoided and, in addition, the flexible part of $S5a_{196-306}$ (between the UIMs) would extend away from this region. A spin-labeling experiment was used to test the predicted models.

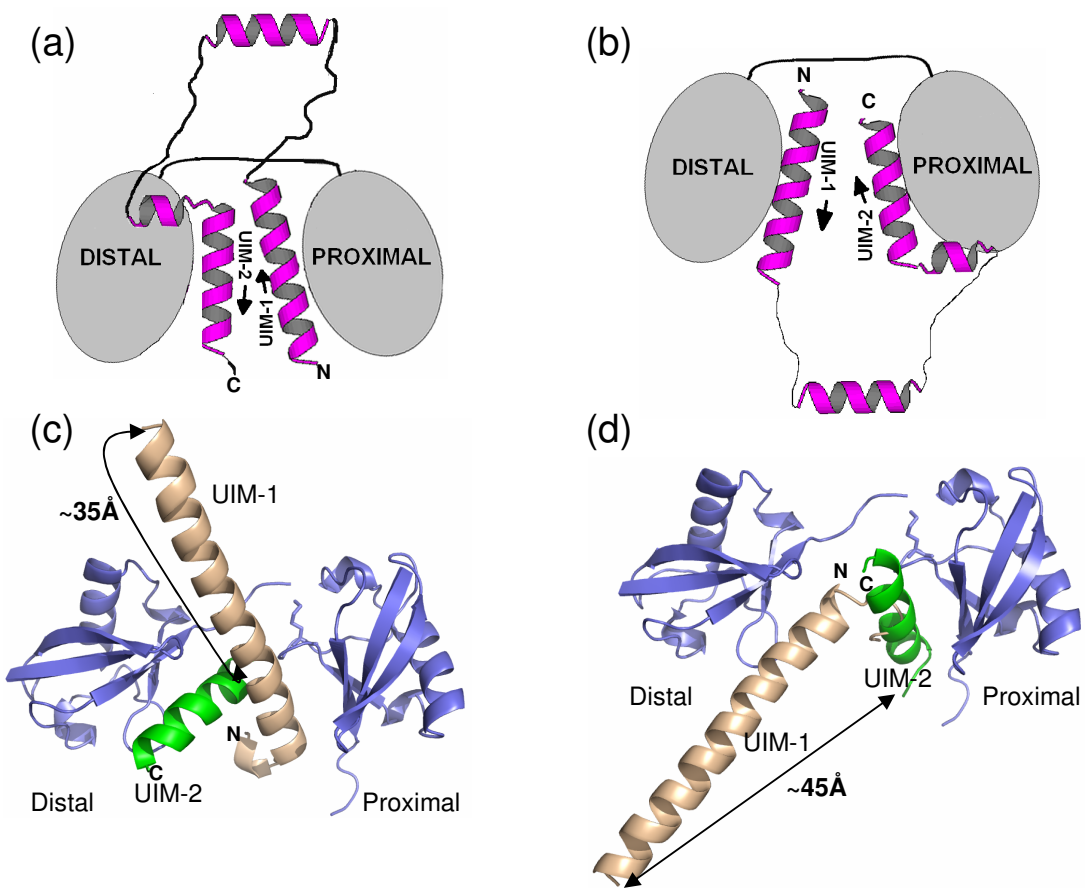

Figure 4.16 Putative models for the complex of Lys48-linked Ub_2 and the tandem-UIM fragment of $S5a_{196-306}$. (a) and (b) show two possible ways in which the $S5a_{196-306}$ UIMs can contact individual Ub units in Ub_2. The linker connecting UIMs in S5a is flexible in solution [74]. (c) and (d) Preliminary structural models of the complex obtained by superimposition of the structures of the corresponding UIM/monoUb complexes [PDB codes 1YX5 for UIM-1 and 1YX6 for UIM-2].

Site-specific attachment of a spin-label (MTSL) can provide distance constraints since it causes paramagnetic relaxation enhancement (PRE) in atoms close to it in space. Signal attenuation caused by MTSL decreases with distance ($1/r^6$). In this experiment, MTSL was attached to a single mutated cysteine (K48C) on the distal Ub in Lys48-linked Ub_2 and PRE effects in $S5a_{196-306}$ residues were recorded (Fig. 4.17). The hypothesis was that the strongest PRE effects would be observed in the UIM bound to the distal ubiquitin since it would be closest to MTSL. In both models, the S5a linker region is predicted to

extend away from MTSL, and as expected, PREs were not observed in this region. Indeed, PREs were observed in most UIM-2 residues and some UIM-1 residues. While the effect appears to be stronger in UIM-2 (Fig. 4.17a), supporting the model shown in Fig. 4.16c, the results are not conclusive since it was not possible to assign many UIM-1 residues due to strong signal attenuation upon binding to Ub and/or peak overlap. Thus, without a complete data set, it was not possible to rule out either model. Atomic-resolution structural studies are required to determine the mode of binding between $S5a_{196-306}$ and Lys48-linked Ub_2 and longer chains, and to verify if specific UIMs bind to each particular Ub domain in the chain.

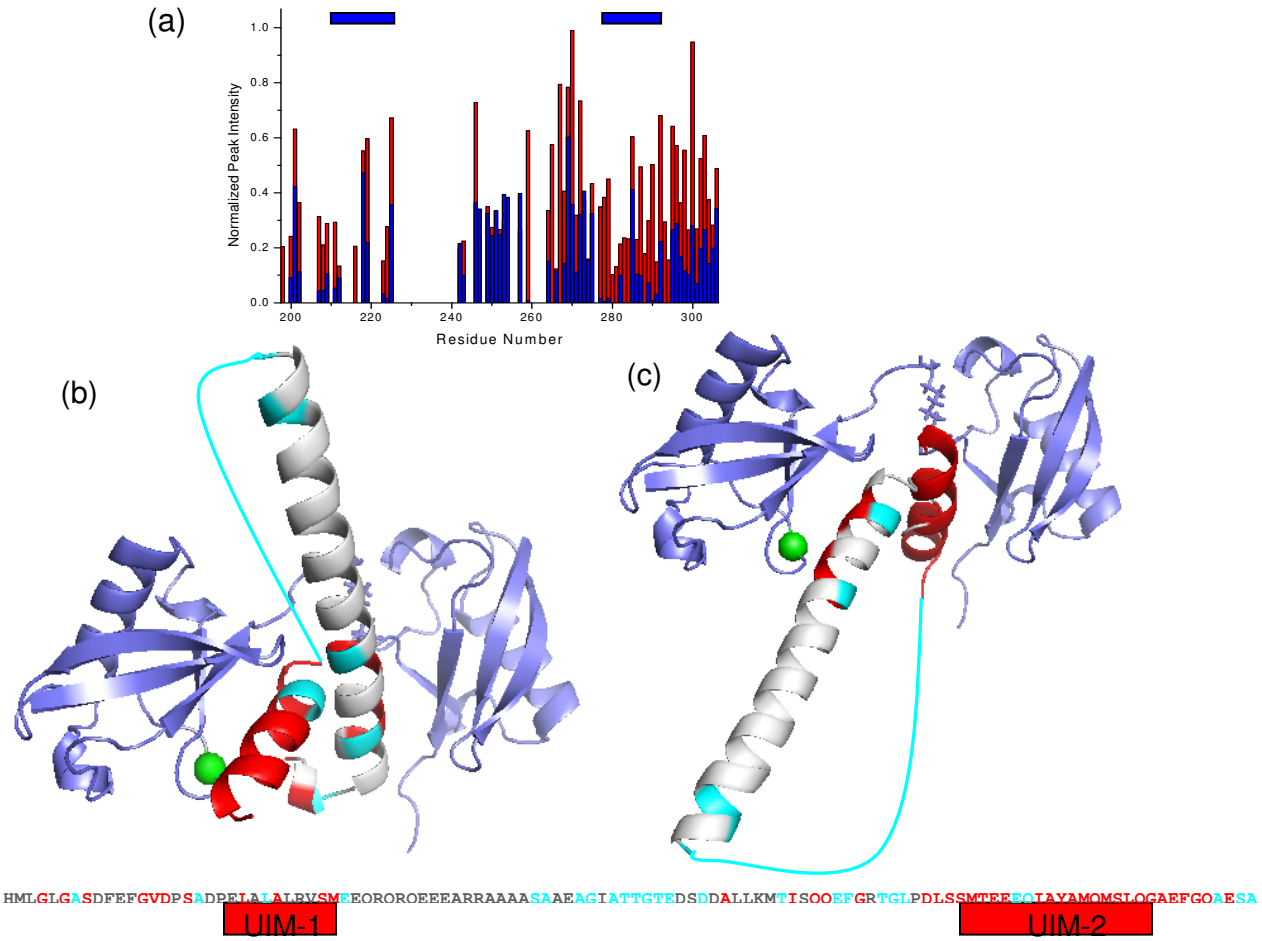

Figure 4.17 Spin labeling experiments to test models of S5a/Lys48-linked Ub_2 interaction. a) Overlay of peak intensities of ^{15}N $S5a_{196-306}$ in complex with Lys48-linked Ub_2 (1:1.5 molar ratio $S5a_{196-306}$:Ub_2) in the presence (blue) and absence (red) of MTSL. Unassigned residues are left blank. Peak intensities in the spectrum with MTSL present were scaled by 55x to normalize the intensities between the two experiments. Horizontal blue bars at the top indicate position of UIMs. Two models of S5a bound to Lys48-linked are shown in b) and c). Ubiquitin is colored blue and the site of attachment of MTSL is shown as a green sphere. PREs >50% are colored red, while PREs <50% are colored cyan. Unassigned residues are gray. The flexible linker between the UIMs is represented by a cyan line since its structure is not known and all assigned residues in this region show PREs < 50%. The sequence of $S5a_{196-306}$ is colored as described.

4.3.2 Interaction of $S5a_{196-306}$ and Lys63-linked Ub_2

To compare the binding interaction of S5a with alternatively linked polyUb chains, binding of $S5a_{196-306}$ to Lys63-linked Ub_2 was examined. The hypothesis being

tested is that since Lys48-linked polyUb is believed to be the preferred polyUb tag for proteasomal degradation and S5a is its receptor, then S5a should bind more strongly to chains linked via Lys48 rather than chains linked via Lys63. The Ub binding surfaces in Lys63-linked Ub_2 do not contact each other and are extended farther apart than in Lys48-linked Ub_2 which forms a closed Ub/Ub interface, thus, one of the goals of this study was to determine if the different conformation adopted by Lys63-linked chains affected binding to $S5a_{196-306}$. It is possible that the closed conformations of Lys48-linked Ub_2 may provide additional binding interactions via the Ub/Ub linker region which comprises a hydrophobic binding pocket in Lys48-linked Ub_2 as observed in the Ub_2/UBA-2 complex [117]. On the other hand, because the hydrophobic surfaces on Lys63-linked Ub_2 are solvent exposed, the gain from burying these surfaces may be greater. In order to test the validity of these speculations, NMR studies were used to examine the interaction of S5a with Lys63-linked Ub_2.

Chemical shift mapping of S5a in complex with Lys63-linked Ub_2 is shown in Figure 4.18a,c. While large CSPs were observed in both UIM-1 and UIM-2, significant CSPs were not detected in the region N-terminal to UIM-2 (residues 262-268), as were observed in complex with Lys48-linked Ub_2. Based on the above data, it appears that S5a binds to Lys63-linked Ub_2 in a different mode compared to Lys48-linked Ub_2. While residues in UIM-1 were in slow exchange and attenuated completely upon binding, residues in the flexible linker showed insignificant CSPs (>0.05 ppm), and most residues in UIM-2 reached the fully bound state upon addition of a small amount of Ub_2 (~0.2 molar equivalents-plots not shown). To measure binding affinity, titration curves were fit to a simple 1:1 binding model (Eq. 2, section 3.3.2). While many residues were in the

slow and intermediate exchange regimes and could not be monitored using this type of analysis, the fitted curves for residues Leu278, located in the N-terminal hairpin loop of UIM-2, and Glu283 and Glu284 located at the N-terminus of the UIM-2 helix, are shown in Figure 4.18b. Based on these fits, K_ds of 108, 2, and 3 μM, respectively, were determined. Since NMR titrations require protein concentrations above ~200 μM for adequate signal intensity, binding affinities in the low μM range cannot be accurately measured by this method. The different types of chemical exchange and CSPs observed suggest that the different regions of $S5a_{196-306}$ bind differently to Ub_2. Binding to UIM-1 was impossible to quantify due to signal attenuations, binding to the UIM-2 was too strong to be precisely measured at these concentrations (apparent K_d ~2-3 μM), and the N-terminal hairpin loop of UIM-2 appeared to bind with much lower affinity (~108 μM). The lack of CSPs in the flexible linker region indicates that there were no contacts made between this region and Lys63-linked Ub_2.

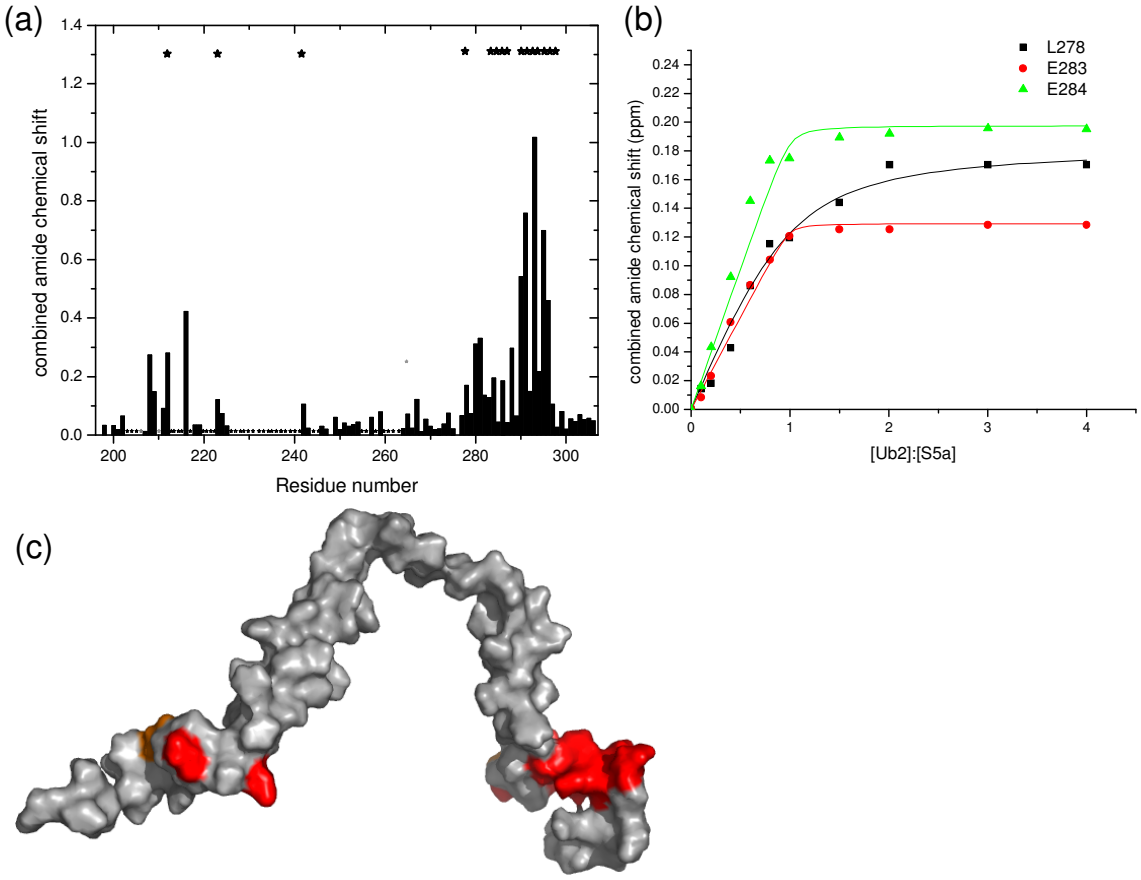

Figure 4.18 NMR mapping and titration curves of $S5a_{196–306}$ residues affected by binding Lys63-linked Ub_2. (a) CSPs in $S5a_{196-306}$ in complex with Lys63-linked Ub_2 (1:4 [S5a]:[Ub_2]) as a function of the residue number. Gray stars denote prolines and unfilled stars denote unassigned residues. Black asterisk at the top denote residues in slow and intermediate exchange. (b) NMR titration curves presenting chemical shift perturbations in residues Leu278, Glu283, Glu284 of $S5a_{196-306}$ plotted as a function of the Ub_2:S5a molar ratio. (c) Surface representation of the perturbations mapped on the surface of S5a (PDB:1YX4) using the coloring scheme: $\Delta\delta \geq 0.4$ ppm and slow exchange regimes (red), $0.4 > \Delta\delta \geq 0.15$ (orange).

To investigate the binding surface on Ub, the reverse titration was performed with Lys63-linked Ub_2, ^{15}N labeled on the distal Ub. The perturbed surface involves the canonical hydrophobic Ub binding surface (Fig. 4.14b,d,f), however, the pattern of perturbations differs from that observed in the distal domain of Lys48-linked Ub_2 (Fig. 4.14a,c,e). The magnitude of CSPs in the distal Ub of Lys63-linked Ub_2 is larger in the

β3 and β4 and smaller in β5 compared to the distal domain of Lys48-linked Ub_2. Additionally, while significant CSPs and signal attenuations are observed in the C-terminal residues of the distal Ub in Lys48-linked Ub_2 which comprise the linking region between the Ubs, no significant perturbation is observed in this region of Lys63-linked Ub_2 in complex with $S5a_{196-306}$. Thus, comparison of the data for the distal Ubs in Lys48- and Lys63-linked Ub_2, which are chemically identical (save for K48R and K63R mutations, respectively), indicated a smaller $S5a_{196-306}$ binding surface on the distal Ub of Lys63-linked Ub_2.

Titration curves for residues Ile13, Leu43, Leu69, and Val70 of the distal Ubs of Lys48- and Lys63-linked Ub_2 were overlaid to qualitatively compare the binding interaction. Since the concentration ranges are different in the two experiments, the data were normalized to account for the difference in final CSP (Fig. 4.15b). The magnitude of CSPs in Lys63-linked Ub_2 increased less steeply than those in Lys48-linked Ub_2 indicating somewhat weaker binding. Importantly, the shape of the titration curves for Lys63-linked Ub_2 was complex, including a shallow increase in CSPs observed in many residues at the beginning of the titration (1:0.2) and a plateau between 1:1 and 1:1.5 [Ub_2]:[S5a], thus excluding the application of simple binding models for K_d determination.

The relative orientation of the UIM binding sites of Lys63-linked Ub_2, suggests that there is one preferred arrangement of S5a on Lys63-linked Ub_2. The models shown in Figure 4.21 orient each UIM on each Ub based on the solution structure of Lys63-linked Ub_2 [87] superimposed with the UIM-1/monoUb and UIM-2/monoUb solution structures [74]. This model is based on the similarity of the CSPs and attenuations in

each UIM when bound to Lys63-linked Ub_2 (Fig. 4.18a) and monoUb (Fig. 4.13a). If UIM-1 is bound to the distal Ub, the C-terminus extends in the opposite direction from the proximal Ub (Fig. 4.19b). In this orientation, for UIM-2 to be able to bind to the proximal Ub, a sharp U-shaped turn and extension of at least 88Å of the linker is required. Based on the number of residues in the linker, in order to span a length of 88Å helix 2 of $S5a_{196-306}$ would have to unfold and a nearly completely extended peptide chain would be required. This mode of interaction seems highly unlikely, hence it is postulated that the model shown in Fig. 4.19a, where UIM-2 is bound to the distal Ub and UIM-1 is bound to the proximal Ub, appears to be more likely. Both models exclude interaction of $S5a_{196-306}$ with the Ub/Ub linker, in good agreement with the data. While, these models assume a rigid conformation of Lys63-linked Ub_2, the dimer is actually dynamic and flexible [87] and may adopt other conformations. Atomic-level resolution structural studies are required to better understand the interaction.

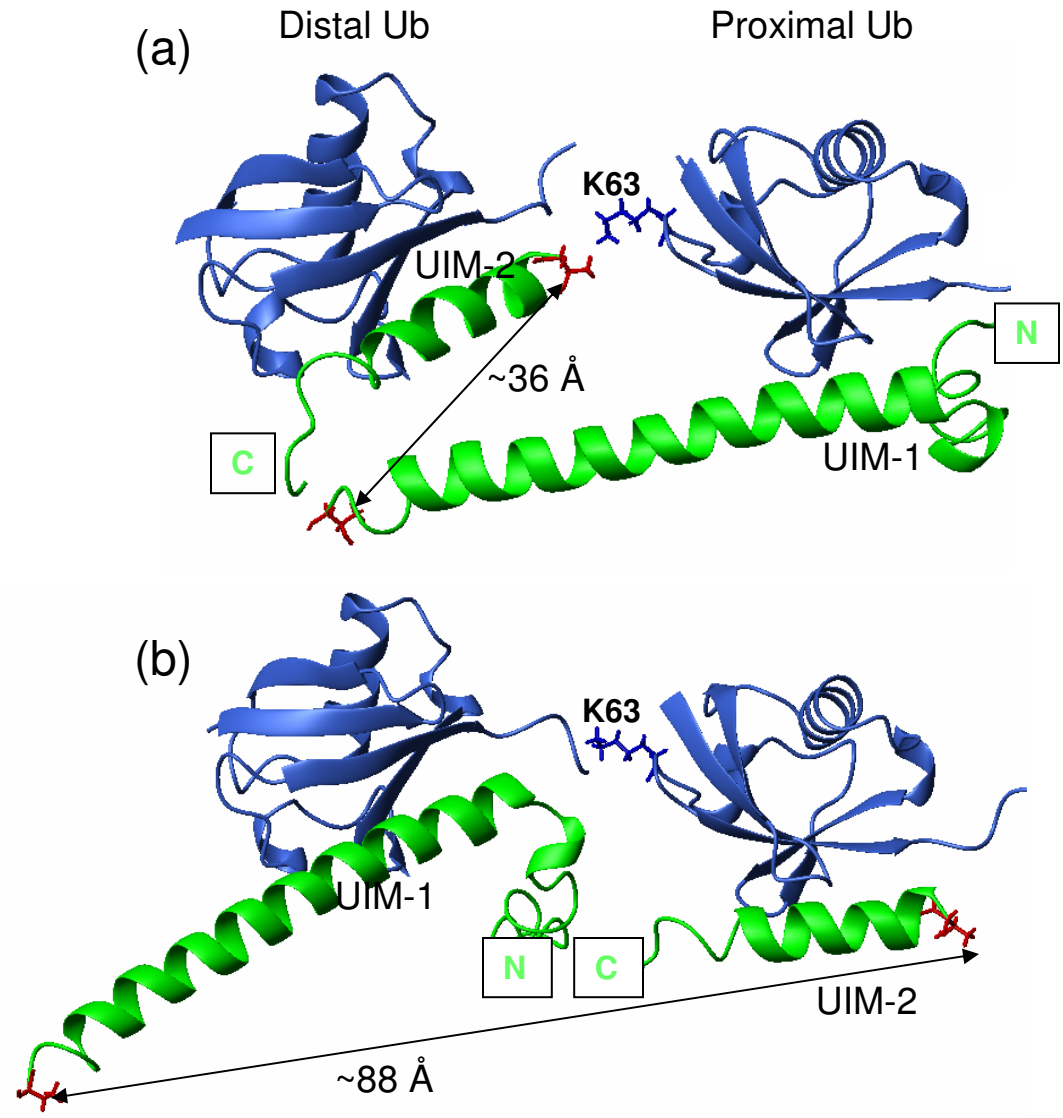

Figure 4.19 Structural models for the complex of Lys63-linked Ub_2 and the tandem-UIM fragment of S5a. (a) and (b) show two possible structural models of the S5a UIMs (green) bound to individual Ub units in Ub_2 (blue) obtained by superimposition of the structures of the corresponding UIM/monoUb complexes [PDB codes 1YX5 for UIM-1 and 1YX6 for UIM-2]. Amino- and carboxy-termini are marked by N and C, respectively.

4.3.3 Discussion

Here we mapped the interacting surfaces involved in binding of monoUb, Lys48- and Lys63-linked Ub_2 to $S5a_{196-306}$. The data also suggest that S5a binds Lys48-linked

Ub_2 via both UIMs concurrently. Based on the data, putative structural models of the interaction with Lys48- and Lys63-linked Ub_2 are proposed.

The difference in binding affinities determined from CSP titration curves observed in the distal domain of Ub_2s with those observed in $S5a_{196-306}$ requires further analysis. The observation of slowly exchanging peaks in UIM-1, Lys48- and Lys63-linked Ub_2, as well as the relatively small apparent K_d measured in UIM-2 of $S5a_{196-306}$ in complex with Lys63-linked Ub_2 (2-3 μM) indicate that the binding affinity determined from the analyses of distal Ub of Lys48-linked Ub_2 does not fully account for the strength of the interaction. Also noteworthy is the plateau, and subsequent resumption of CSP increase observed between the addition of 1:1 and 1:2 molar equivalents of $S5a_{196-306}$ to distal ^{15}N-labeled Lys63-linked Ub_2 (see Fig. 4.15b). This behavior may be indicative of a change in the mode of binding and it is not yet clear how to quantify the interaction.

The evidence above shows that $S5a_{196-306}$ interactions with Lys48-linked Ub_2 involve additional binding surfaces when compared with the $S5a_{196-306}$/Lys63-linked Ub_2 complex. The additional interactions may occur via the Ub/Ub linker region, as well as the N-terminal UIM-2 region, suggesting that $S5a_{196-306}$ may preferentially bind to Lys48-linked Ub_2. The additional contacts may be due to the relative orientation of the Ub moieties and the linker between them. Since there is not yet enough evidence to show that $S5a_{196-306}$ binds more strongly to Lys48-linked Ub_2 compared with Lys63-linked Ub_2, it is put forth only as a hypothesis in this dissertation as a basis for future studies. Lys48-linked Ub_4 has been estimated to bind to S5a with strong affinity (K_d range 10^{-6}-10^{-7} M) [145] and SPR studies have shown that S5a binds to Lys48- and Lys63-linked Ub_4 with similar strength[115]. Thus, it would be somewhat surprising if preference for

Lys48-linked chains existed in Ub_2 but not in Ub_4. A possible explanation for the difference in linkage-specificity in Ub_2 and Ub_4 is that the conformational dynamics of polyUb chains, especially as the number of available binding sites increase in longer chains, allows additional possible binding modes. Models of $S5a_{196-306}$ binding in various conformations to Lys48-linked Ub_4 were presented in [74]. S5a may sample many different UIM/Ub combinations to find the most favorable conformation with chains of either linkage resulting in similar binding affinity with Lys48- and Lys63-linked Ub_4. Assuming S5a does bind to Lys48- and Lys63-linked Ub_4 with similar affinity, the "extrinsic" proteasomal receptor, hHR23A, preferentially binds Lys48-linked polyUb [146]. Thus, the polyUb linkage specificity of degradation is likely not due to S5a's preference, but rather may depend on extrinsic factors such as binding to hHR23A, cellular levels and localization of polyUb chains, or how the chains are processed after recognition by proteasomal machinery (i.e. de-ubiquitinating enzymes). It is however intriguing that an additional binding surface was observed with Lys48-linked Ub_2. Further structural and biochemical studies are required to elucidate the interaction of S5a with Ub chains linked via Lys48 and Lys63 for better understanding of the S5a/polyUb system.

Chapter 5: Mutations in the hydrophobic core of Ub differentially affect its recognition of UBAs and UIMs

5.1 Background and Objectives

Ubiquitin is one of the most highly conserved signaling proteins in eukaryotes. In carrying out its myriad functions, Ub conjugated to substrate proteins interacts with dozens of different receptor proteins that link the Ub signal to various biological outcomes. The ability of Ub to interact with such a variety of receptor molecules is remarkable. A detailed understanding of the structural determinants of the binding properties of Ub is therefore required, in order to be able to predict its interaction with various downstream receptors, as well as the ability of polyUb chains to act as diverse signals. Of interest in this study are proteins that act as the proteasomal receptors for polyUb chains: Rpn10 in yeast (S5a in mammals), a subunit of the 19S regulatory complex [98, 143], and Rad23 [31, 105].

Ub is extremely stable to heat denaturation; temperatures close to 100 °C are required to unfold it [68]. This melting temperature is unusually high for a protein from organisms that live at moderate temperature [148]. In addition to its extreme thermal stability, Ub is highly rigid, based on amide proton exchange measurements [69]. These unusual physical properties may be important for Ub's function, or they may be a random byproduct of evolution. To address the question as to how the high stability and rigidity displayed by Ub impact its interactions with binding partners, the point mutants (L67S and L69S) were used in order to disrupt packing in the hydrophobic core of Ub.

5.2 Stability and Structure

5.2.1 Core mutations altered the stability of Ub

The L67S and L69S mutants and wild type Ub had similar CD spectra at 25 °C indicating that at this temperature all three proteins were folded and had similar secondary structure content (Fig. 5.1a). Also, both mutants and wild type Ub cooperatively unfolded when exposed to increasing concentrations of the denaturant guanidinium chloride (Fig. 5.1b) confirming that all three proteins were folded in the absence of denaturant. Thermodynamic fits of the data showed that compared to wild-type Ub (ΔG_{unfold} = 23.6 kJ/mol), the stability of L67S (10.1 kJ/mol) and L69S (11.6 kJ/mol) were both reduced by more than 50%. The thermodynamic destabilization of L67S and L69S is likely due to loss of favorable leucine interactions in the folded state (hydrophobic and van der Waals) and the unfavorable burial of a polar hydroxyl group from the introduced serine (see also below). Despite this large thermodynamic destabilization, both L67S and L69S remained well folded at temperatures up to 55 ºC as judged by circular dichroism (Fig. 5.1c). For comparison, wild-type Ub remained well folded at temperatures approaching 100 °C at neutral pH [68]. While the stability of L67S and L69S were greatly reduced relative to wild type, these mutants were well folded at physiologically relevant temperatures.

The work presented in this subsection was performed by Michael Twarog and Dr. Dan Bolon in the Bolon Lab (Univ. of Massachusetts Medical School, Worcester, MA).

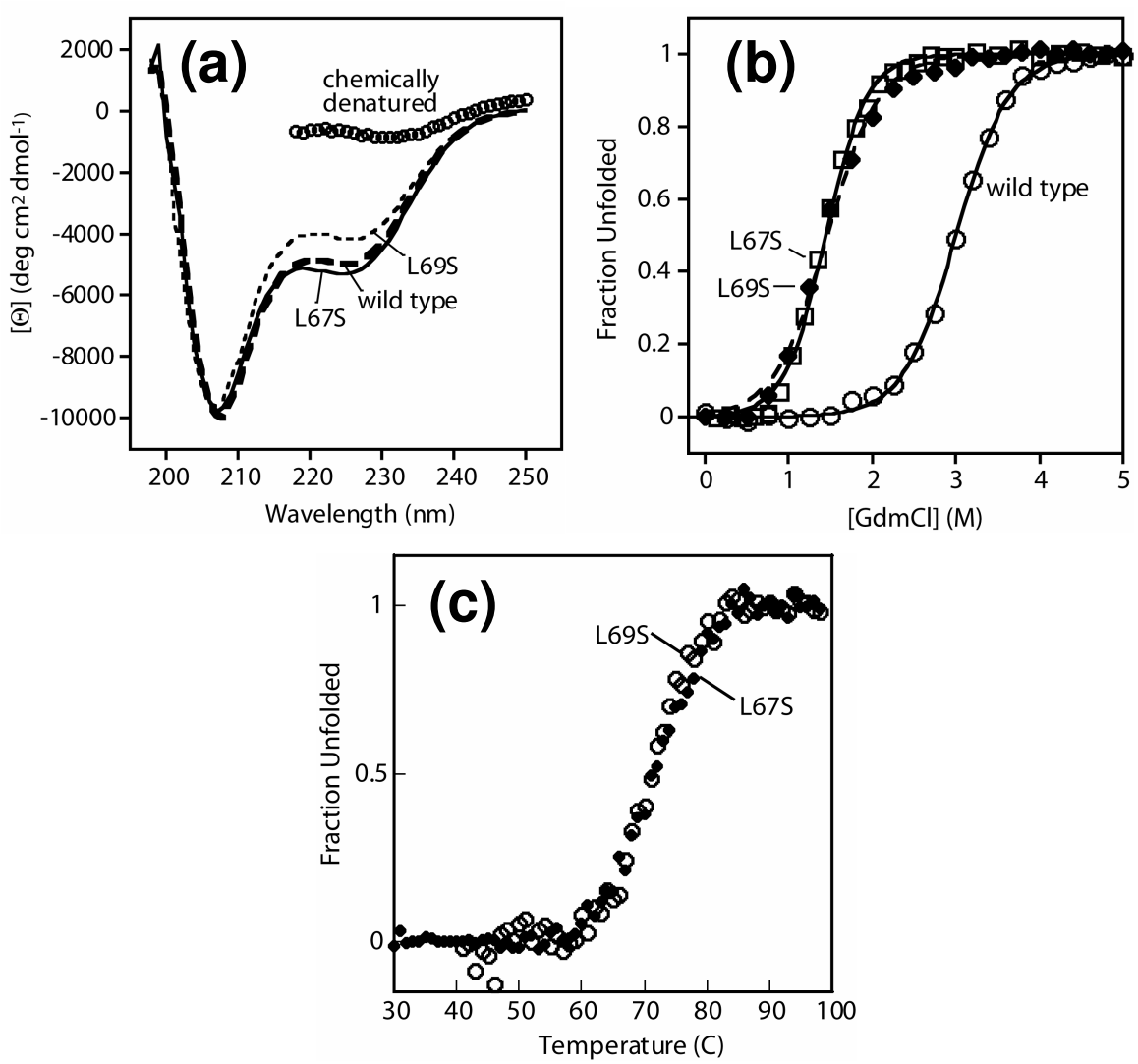

Figure 5.1 Comparison of the thermodynamic stability of purified wild type, L67S, and L69S ubiquitins. (a) Circular dichroism (CD) spectra at 25 ºC indicate that all three proteins have similar secondary structure content. (b) Stability to guanidinium chloride denaturation monitored at 25 ºC by loss of CD signal at 222 nm. Both L67S and L69S are greatly reduced in stability compared to wild type ubiquitin. (c) Temperature denaturation curves for L67S and L69S monitored by CD signal at 222 nm. Both mutants have $T_m \approx 72^oC$, and are well folded at temperatures below 55^oC.

5.2.2 Three-dimensional structure of L69S

To directly compare the overall structural similarity between the wild type and mutant Ubs, the three-dimensional structure of L69S was solved in solution by NMR. The resonance assignments were made using a combination of ^1H-^{15}N HSQC, 2D

TOCSY, 3D ^{15}N TOCSY, and 2D NOESY spectra. The assignment of residues located in helices and β-sheets was confirmed using $^{1}J_{HNH\alpha}$ couplings obtained from HMQC-J spectra [129].

The structure calculation was performed using the simulated annealing program CNS [135] with ARIA [136] extensions as described in section 3.5. Figure 5.2a shows the superposition of the 10 lowest energy structures from a total of 75 in the final round of calculation. The ensemble is well defined with an rmsd from the mean structure of 0.2 Å for backbone atoms of secondary structure elements. For all atoms over the ordered region (residues 2-71), the rmsds from the mean structure are 0.35 Å for backbone atoms and 0.79 Å for heavy atoms. The number of restraints (1224 NOE, 173 long-range NOE, 38 hydrogen-bond, 137 dihedral angle, and 70 dipolar coupling restraints) and statistics reflect the high quality of the structures (Table 5.1). The five C-terminal residues are disordered and no inter-residue NOE restraints were detected. Flexibility in this region is confirmed by order parameters (see Section 5.6.3). The resulting ensemble of NMR structures was indeed similar to that for the wild type Ub (Fig.5.2a,b). Because the mutations involve only buried side chains, the exterior surface should be the same as for wild-type Ub. According to the current understanding of the structure-function relationship in Ub the surface of Ub mediates its binding to UBDs. Therefore, based on the structural and surface similarity, one would expect the mutants to be functional.

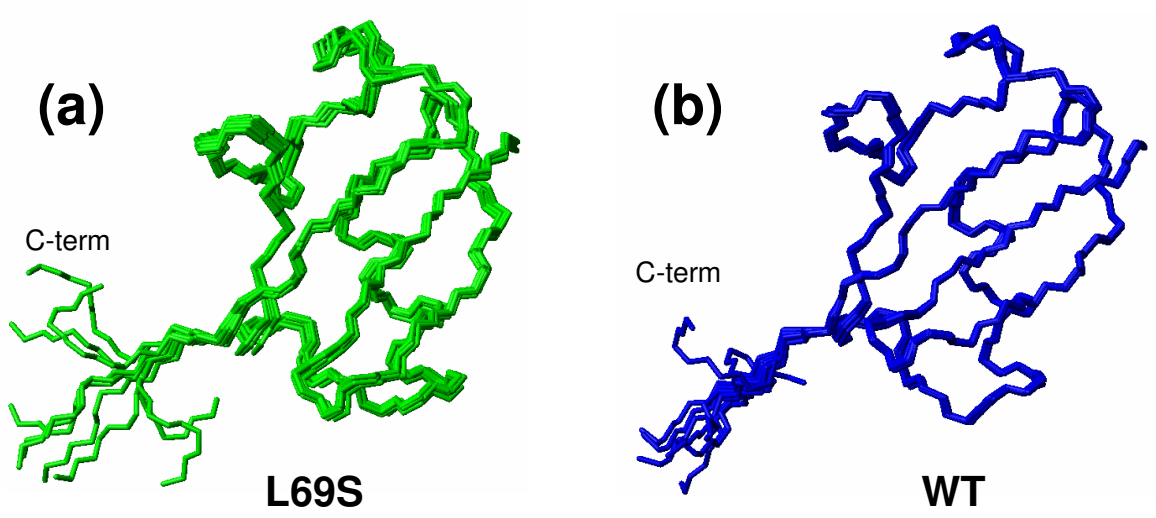

Figure 5.2 Comparison of the structure of L69S and wild type ubiquitins. (a) The ensemble of 10 lowest-energy solution NMR structures of L69S determined here has strong similarity to that of wild type ubiquitin (PDB code 1D3Z [78], shown in panel b). The NMR data (NOEs, backbone dihedral angles) as well as the calculated structures show that the same secondary structure elements are present in both L69S and wild type Ub structures.

Table 5.1 Statistics of the experimental restraints and calculated ensemble of 10 NMR structures of L69S Ub.

NOE distance restraints	
Ambiguous	1224
Unambiguous	1216
Intraresidue	815
Sequential	251
Medium range ($2 \leq \|i-j\| \leq 4$)	58
Long range ($\|i-j\| > 4$)	173
Hydrogen bond restraints	38 (19 H bonds)
Dihedral angle restraints from TALOS	137
Orientational restraints from RDCs	70
RMS deviations from the experimental data	
Average distance restraint (Å)	0.134 ± 0.006
Average dihedral angle restraint (°)	4.78 ± 0.19
Energy (kcal/mol)	
NOE	1.015 ± 0.093
Dihedral	0.501 ± 0.005
Bonds	0.427 ± 0.010

Angles	0.541 ± 0.014
Impropers	0.147 ± 0.016
Van der Waals	-0.614 ± 0.008
Ramachandran statistics	
Residues in most favored regions (%)	87.9
Residues in additionally allowed regions (%)	8.7
Residues in generously allowed regions (%)	1.8
Residues in disallowed regions (%)	1.7
Average atomic RMSDs from average structure (Å)	
Heavy atoms	
All residues	1.37
Residues 2-71 (i.e. without the C terminus)	0.79
Secondary structure residues	0.74
Backbone atoms (N,C^{α},C')	
All residues	1.15
Residues 2-71	0.35
Secondary structure residues	0.20

5.3 Mutant Ubs are lethal for budding yeast when provided as the sole source of Ub

The effect of expressing L67S or L69S Ub was tested in yeast. In the SUB328 strain wild-type Ub expression is controlled from a galactose-induced promoter and can be shut off by dextrose. Mutant Ub expressed from a strong constitutive GPD promoter on a high-copy plasmid was introduced. When grown on medium containing galactose, the mutants did not prevent or slow yeast growth (Fig. 5.3). This result indicates that neither L67S nor L69S Ub is toxic to cells containing wild-type Ub. However, when wild-type Ub expression was shut off, neither L67S nor L69S Ub rescued growth. This result is surprising and indicates that L67S and L69S are defective for some essential process in yeast.

To gain molecular insight into the growth arrest phenotype upon shutoff of wild-type Ub Western Blot analysis was used to monitor the level of free Ub as well as high-

MW ubiquitinated species (Fig. 5.3c). Expression of wild-type Ub from this plasmid system is similar to that of ubiquitin from its endogenous promoters (Fig. 5.4). When wild-type Ub was present, neither L67S nor L69S perturbed the steady state level of high-MW ubiquitinated species, suggesting that either the mutants were not incorporated into these high-MW species or they were incorporated along with wild-type Ub into chimeric chains that can be processed inside cells. After sufficient time in dextrose media to stall growth (25 hours – Fig. 5.3a,b), cells lacking any Ub rescue plasmid were depleted of free Ub and had low levels of high-MW ubiquitinated species (Fig. 5.3c,d). In contrast, cells expressing L67S or L69S had a large store of free mutant Ub that was greater than the level of free Ub in cells expressing wild-type Ub (Fig. 5.4). This result indicates that yeast growth is not impeded by low expression levels of the mutants and instead is hindered by subsequent interactions of the mutant Ubs with other cellular components. Cells containing L67S or L69S as the sole source of Ub had increased levels of high-MW ubiquitinated species, suggesting that the mutant Ubs were activated by E1 and assembled into chains by E2 and E3 enzymes, but that polyUb chains composed of mutant Ub subunits were not properly metabolized.

p

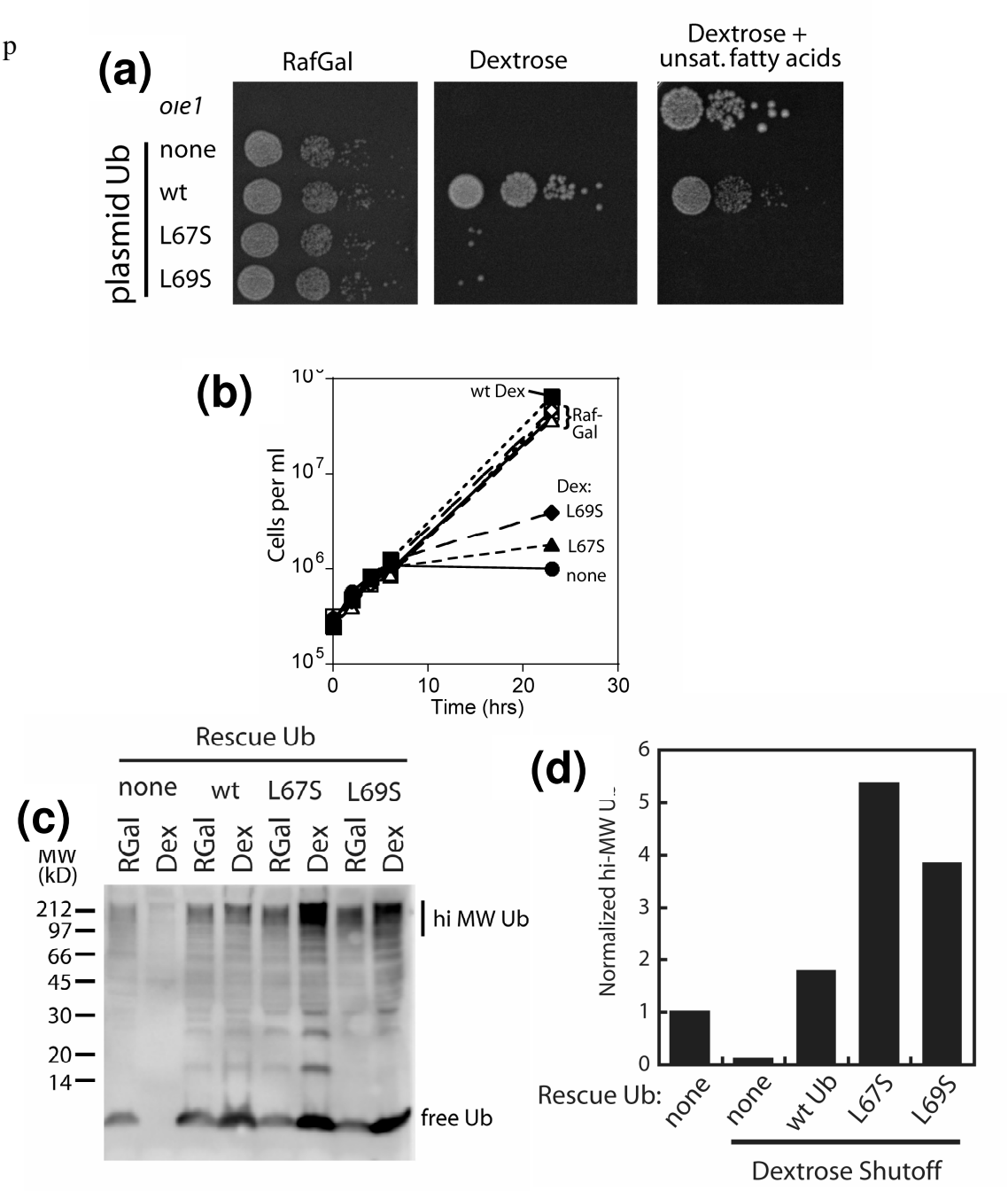

Figure 5.3 L67S and L69S Ub mutants are incapable of sustaining yeast cell growth. (a) Comparison of SUB328 cell growth in RafGal media and under Ub expression shutoff in glucose media (Dextrose, Dextrose+unsaturated fatty acids). The type of Ub introduced on a plasmid is indicated ("none" corresponds to control plasmid lacking Ub). Also shown is growth of the *ole1* strain that is incapable of synthesizing unsaturated fatty acids. (b) Cell density as a function of time grown on dextrose. (c) Comparison of the accumulation of high-MW ubiquitinated species in SUB328 cells after 25 hours in RafGal and under cell growth arrest in dextrose media. (d) Quantitative comparison of the amounts of accumulated high-MW species for the various rescue plasmids used in this study.

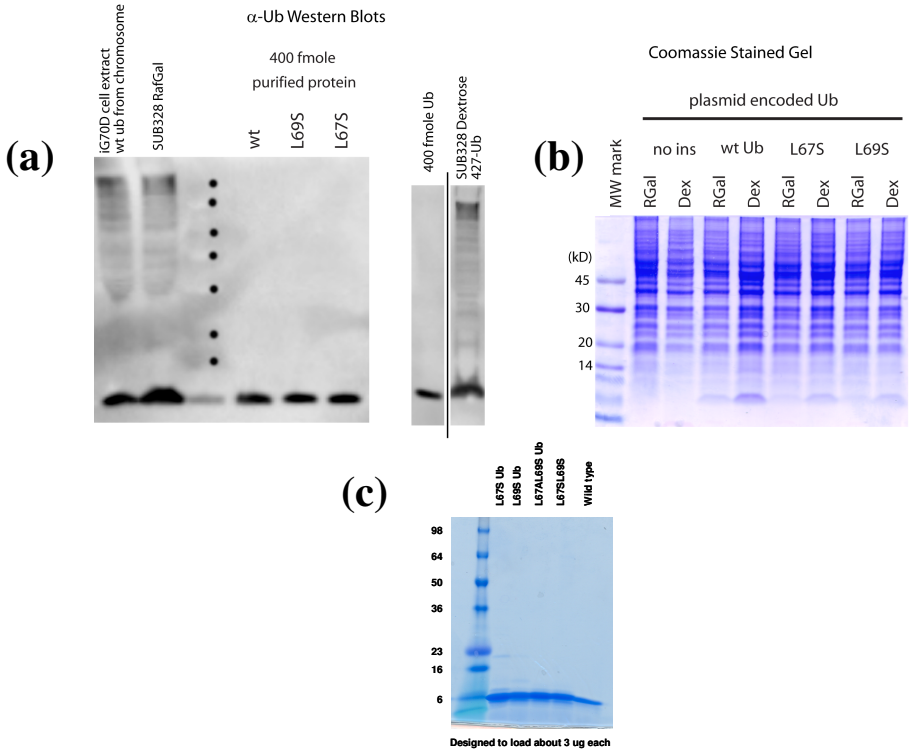

Figure 5.4 Controls showing expression of WT and mutant Ubs in our in vivo and in vitro assays. (a) Western blot and (b) PAGE show that (1) expression of WT Ub from our plasmid system is similar to that of Ub from its endogenous promoters and (2) that cells expressing L67S or L69S had a large store of free mutant Ub that was greater than the level of free Ub in cells expressing wild-type Ub. (c) Mutants containing single, and double mutations in the core of Ub can be expressed, and purified from *E.coli***.**

The work presented in this section was performed by Michael Twarog and Dr. Dan Bolon in the Bolon Lab (Univ. of Massachusetts Medical School, Worcester, MA).

5.4 Recognition by UBAs and UIMs

5.4.1 Chains assembled from mutant Ub can be recognized by UBA-containing Rad23, but not by UIM-containing Rpn10

To determine the molecular basis of the observed *in vivo* lethality of the Ub mutants, functional *in vitro* assays were performed using Sic1 as a substrate. Sic1 restrains chromosome duplication by binding to and inhibiting the S phase-promoting

cyclin-dependent kinase. At the end of G1 phase, which precedes S phase, SCFCdc4 binds Sic1 and attaches ubiquitin to it. Ubiquitin-modified Sic1 is then degraded by the 26S proteasome [149]. The results (Fig. 5.5a) confirm the *in vivo* results by showing that single Ub mutants could be charged by E1/E2 (Cdc34) and conjugated onto a substrate (MbpSic1) by SCF to generate high molecular weight conjugates that were indistinguishable from those formed with wild-type Ub. However, these high-MW conjugates were not degraded by purified 26S proteasomes (Fig. 5.5b). To determine whether this was due to a failure of the proteasome to recognize polyubiquitinated MbpSic1, binding of these chains to the proteasome substrate receptors, Rpn10 and Rad23 was assayed. The results (Fig. 5.5c) show that mutant-ubiquitinated MbpSic1 did not bind to the UIM-containing receptor protein Rpn10, but was still capable of binding to Rad23. This result by itself can explain the stability of Sic1 conjugates formed with mutant ubiquitin, because proteasomes lacking Rpn10 are unable to degrade Sic1 *in* v*itro* [105].

In contrast to Rpn10, Rad23 is an "extrinsic" receptor, and assays with 26S proteasome purified from *rpn10*Δ cells showed that their inability to degrade UbSic1 can be rescued by Rad23, provided the VWA domain of Rpn10 is provided *in trans* [105]. However, Sic1 conjugated with mutant Ub was not degraded by *rpn10*Δ 26S proteasomes supplemented with Rad23 and the VWA domain (data not shown). Speculatively, despite the ability of Rad23 to bind the mutant chains, the inability of purified proteasomes to degrade Sic1 conjugated with mutant chains suggests that other events downstream from the polyUb chain recognition step are affected by the mutations. Since degradation of Ub-

conjugated substrates is essential, this defect could suffice to explain the inability of the mutant Ubs to sustain life.

To explore in more depth whether the mutant Ubs might have other defects, their ability to be conjugated by Ubc4–Rsp5 was tested. Whereas SCF is representative of the largest class of ligases that is based on a RING domain, Rsp5 is representative of the second, mechanistically distinct branch of ubiquitin ligases whose activity is dependent upon a HECT domain [150]. As shown in Fig. 5.5d, the Ub mutants could not be conjugated to the PYP-reporter substrate using Rsp5 and Ubc4. This is in contrast to the results for the Cdc34-SCF combination and indicates that the Ub mutations have differential effects on different Ub conjugation pathways. The inability of Ubc4-Rsp5 to conjugate mutant Ub is unlikely to account for the lethality of the L67S and L69S mutations, because the addition of unsaturated fatty acids to growth medium, which suppresses the essential requirement for Rsp5 [151], did not allow for growth of cells in which L67S and L69S were the only source of Ub (Fig. 5.3a). Given the central role of Ub in many different essential biological processes, the L67S and L69S mutants could be defective in multiple pathways.

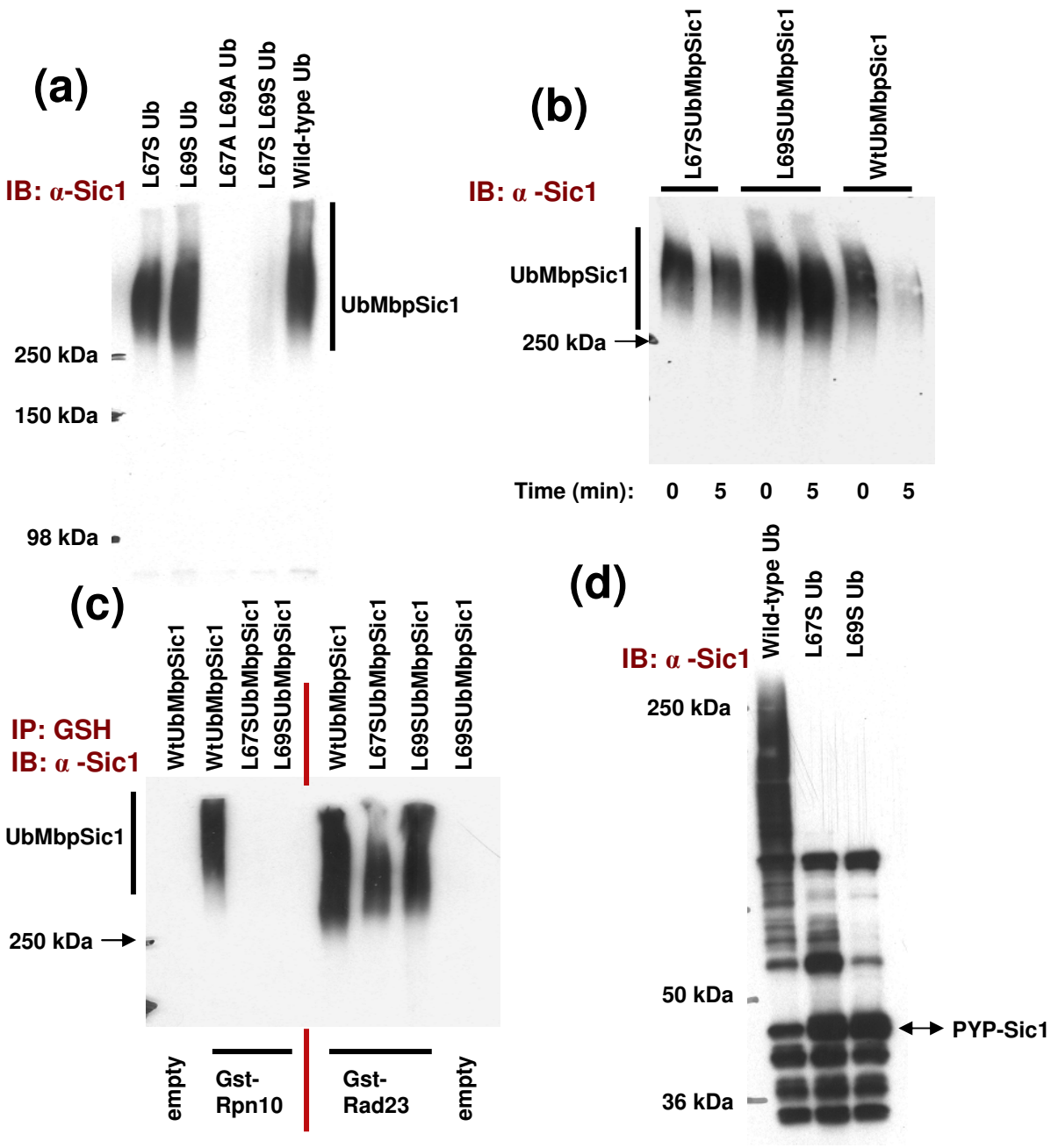

Figure 5.5 Functional in vitro assays. (a) Single Ub mutants (L67S or L69S) could be charged by E1/E2 (Cdc34) and conjugated onto a substrate (MbpSic1) by SCF^{Cdc4} to generate high molecular weight conjugates that were indistinguishable from wild-type Ub conjugates. (b) The high-MW conjugates generated from Ub mutants are not degraded by the 26S proteasome. (c) The mutant high-MW conjugates bind to Rad23 but not to Rpn10. (d) Mutant Ub could not be conjugated to the PYP-reporter substrate using Rsp5 and Ubc4.

*The work presented in this subsection was performed by Rati Verma and Dr. Ray Deshaies in the Deshaies Lab (*California Institute of Technology, *Pasadena, CA).*

5.4.2 NMR studies of ligand binding to L69S Ub

The observed ability of mutant polyUb chains to discriminate between Rpn10 and Rad23 is surprising. To verify that this specificity happens at the level of the individual Ub units (as opposed to polyUb chains), binding of the monomeric Ub mutants to UIMs of S5a and to the UBA-1 domain of hHR23A, a human homologue of Rad23 was studied.

Consistent with the binding assays presented above (Fig. 5.5a), no measurable perturbations were observed in L69S spectra upon titration with increasing amounts of the UIM-2 motif from S5a (residues 263-307), thus indicating a lack of binding (Fig. 5.6a). Also no binding was observed between L67S and an S5a construct containing both UIM-1 and UIM-2 motifs (Fig. 5.6b). While UIM-1 of S5a is highly homologous to the single UIM of Rpn10, the UIM-2 has a lesser sequence homology to Rpn10 and binds wild type Ub and chains stronger than UIM-1 does [74, 98].

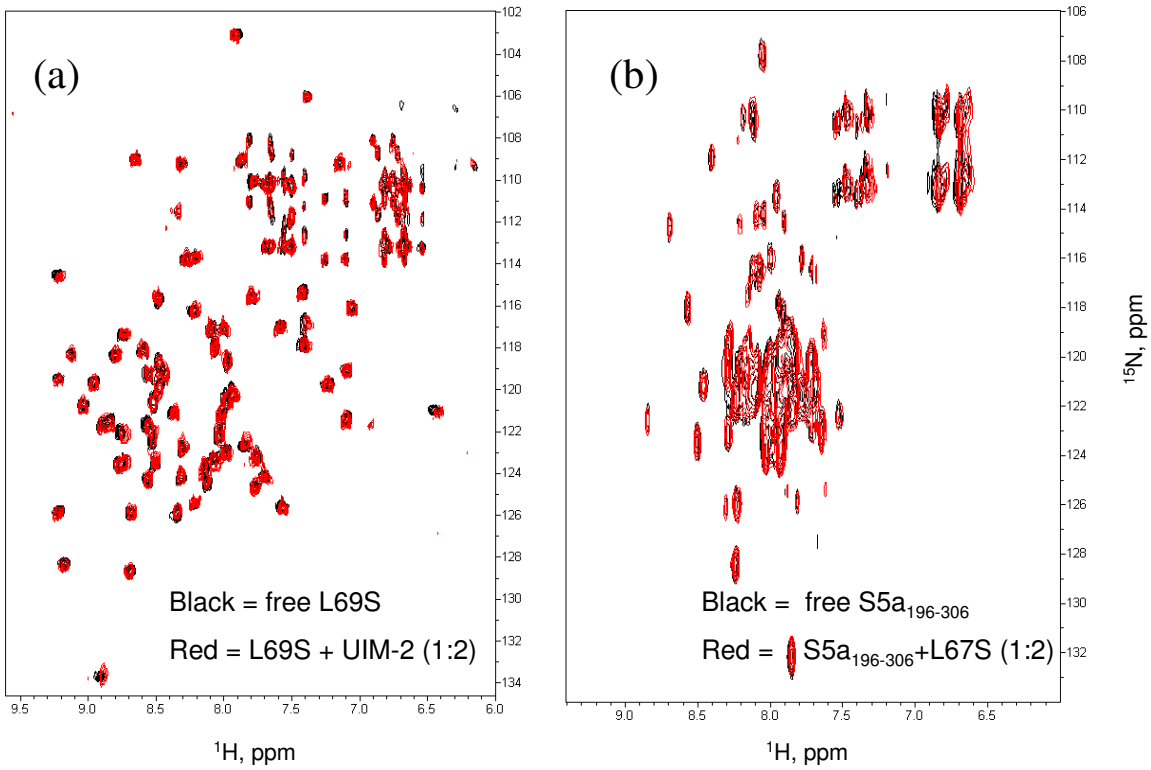

Figure 5.6 NMR binding assays: no measurable binding is observed between L69S and UIMs of S5a. (a) Overlay of the ^{1}H-^{15}N HSQC spectra of L69S free (black) and in the presence of a 2:1 molar excess of UIM-2 of S5a (red): no measurable binding is observed. (b) Overlay of the ^{1}H-^{15}N HSQC spectra of S5a$_{196-306}$ containing both UIM-1 and UIM-2: free (black) and in the presence of a 2:1 molar excess of L67S (red).

In contrast with UIM-2, titration with the UBA-1 domain of hHR23A resulted in strong perturbations in the ^{1}H-^{15}N HSQC spectra of L69S (Fig. 5.7a,c). The largest chemical shift perturbations (CSPs) were observed in residues Thr7, Leu8, Ile13, Arg42, Leu43, Ile44, Lys48, Gln49, and Val70. In addition, several amides (most notably, Thr7, Leu8, Thr9, Lys11, and Leu71) showed strong signal attenuations indicative of an intermediate or slow exchange (on the NMR time scale) between the free and bound states of L69S. The perturbed surface is located on one side of Ub structure (Fig. 5.7d,e) and includes the same hydrophobic patch (Leu8-Ile44-Val70) involved in UBA-1 binding to WT Ub (Fig. 5.7e) [152, 153]. The same surface of WT Ub is also involved in its

interactions with many other Ub-binding proteins (e.g. [2]) including UIM-2 of S5a [74, 77, 152]. Titration curves were fit to a single-site 1:1 binding model yielding an average dissociation constant of 161 ± 29 μM (Fig. 5.7b, Table 5.2). This K_d value is 2-3 fold smaller than reported for UBA-1 binding to WT yeast Ub (~500 μM [153]) or to WT human Ub (310 ± 20 μM [152]), which could be due to additional interaction between UBA-1 and L69S involving β5 strand residues Val70 and His68 of Ub (see below).

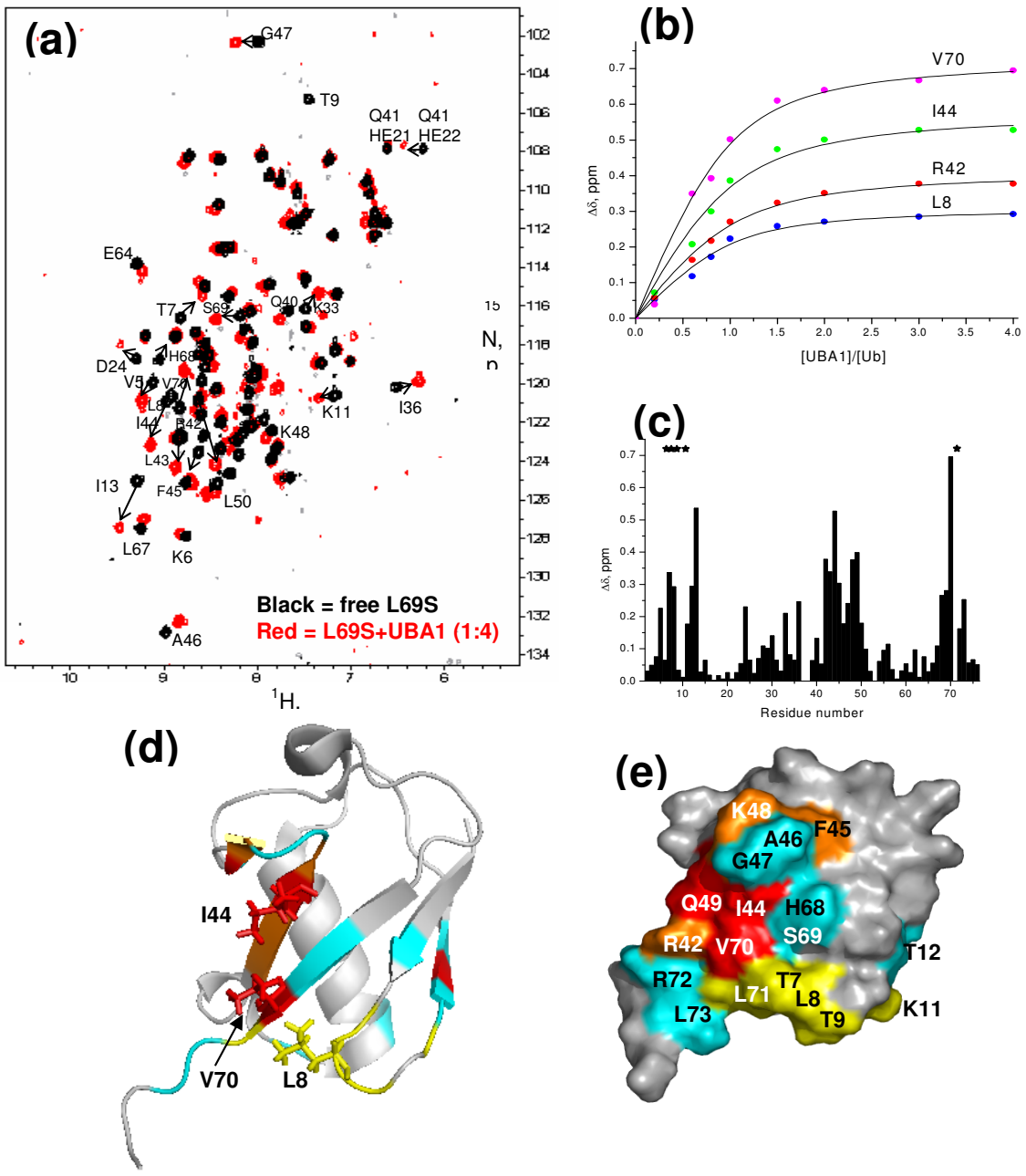

Figure 5.7 NMR titration studies of UBA-1 binding to L69S Ub. (a) Overlay of the ^{1}H-^{15}N HSQC spectra of the free (black) and UBA-1-bound (red) L69S at saturation (UBA-1:Ub molar ratio is 4:1). (b) Representative titration curves for several amides (as indicated). (c) CSPs in L69S at the last titration point ([UBA-1]/[Ub]=4:1) as a function of residue number. Asterisks in (c) indicate residues that show >70% signal attenuation in the presence of UBA-1. (d) Ribbon representation of Ub structure color-coded by the CSP values and with the side chains of Leu8, Ile44, and Val70 indicated. (e) Surface representation of Ub with the perturbed sites colored by CSPs as follows: $\Delta\delta > 0.4$ ppm (red), $0.4 > \Delta\delta > 0.3$ ppm (orange), and $0.3 > \Delta\delta > 0.16$ ppm (cyan), while residues showing significant signal attenuation (>70%) in the bound state are painted yellow.

Table 5.2 The dissociation constants for UBA-1/Ub(L69S) binding, derived from NMR titration experiments.

Residues	K_d (μM)
Val5	157
Thr7	191
Leu8	128
Ile13	143
Arg42	175
Leu43	174
Ile44	171
Phe45	165
Ala46	174
Leu67	206
His68	197
Ser69	106
Val70	130
Arg72	140
Mean	161 ± 29

Interestingly, a comparison of the chemical shifts in WT vs. L69S after titration with UBA-1 reveals that the difference between these proteins in the final position of peaks is significantly less than in the unbound state. In fact, the chemical shift of most residues differs by less than 0.2 ppm (Fig. 5.8a), with a few exceptions such as Leu/Ser69, Val70, Arg42, Thr12, Thr14, Ile36, Asp32, Leu56 and Thr7. Ignoring residues at position 69 and Val70 which are perturbed due to the mutation, there are only 7 amides (residues 7, 12, 14, 32, 36, 42, and 56) that have a chemical shift position difference larger than 0.2 ppm in the fully bound states of L69S and WT, compared to 16 amides that differ by more than 0.2 ppm in the unbound state (Fig. 5.10b). This analysis suggests that upon binding to UBA-1, L69S may be stabilized relative to the unbound state, and perhaps behave more like WT Ub, thus, chemical shift positions appear similar to WT Ub in the bound state. A comparison of order parameters of L69S in the bound and unbound state (Fig. 5.8b) shows increased S^2 in β3, β4, and C-terminal residues

Leu71, Arg72, Leu73, and Arg74 in L69S bound to UBA-1, an indication of greater structural rigidity upon ligand binding.

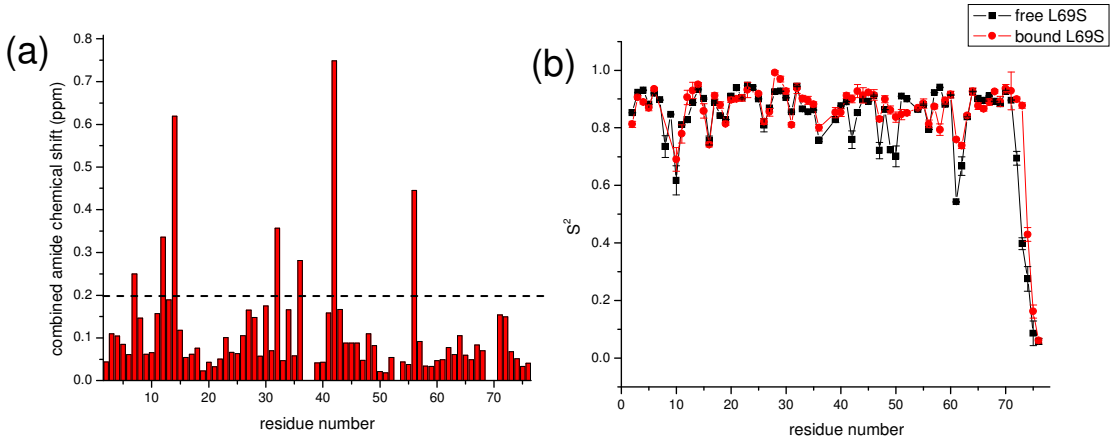

Figure 5.8 Comparison of chemical shift positions in bound state and backbone dynamics of L69S bound to UBA-1. (a) the difference between the final chemical shift positions of L69S bound to UBA-1 and WT Ub bound to UBA-1 are shown. Residues 69 and V70 are not shown since large CSP in these residues is a direct result of mutation. (b) Comparison of order parameters in unbound L69S (black) and L69S bound to UBA-1 (red).

5.5 Structural Comparisons

5.5.1 Structural differences between wild type and L69S Ubs

The observed striking effect of L69S and L67S point mutations on the ligand specificity of Ub is unprecedented. Given the overall structural similarity of the proteins and identical composition of the surface residues, this effect is likely caused by subtle changes in Ub structure and/or differences in protein dynamics introduced by these core mutations.

In order to understand the structural basis of the observed effect, structural differences between L69S and wild type Ub were analyzed in detail. The backbone atoms

of the lowest-energy structure of L69S Ub superimpose with those of WT solution structure (PDB code 1D3Z [78]) with the rmsd of 1.14 Å (residues 2-71) or 0.93 Å for the secondary structure elements. Atom coordinates of yeast WT Ub are not available in the Protein Data Bank, therefore the structure of the human variant was used for the comparison here, This is justified by (1) the comparison of the electron density maps indicating similar structures of yeast and human ubiquitin [72] and (2) by the fact the only difference in the amino acid sequence between the two WT variants is in three surface residues (19, 24, and 28) that are located away from structural changes introduced by the L69S mutation and (3) by the HSQC spectra of yeast and human WT Ub are very similar, with only local perturbations in the signals corresponding to mutated residues and those adjacent to them (Fig. 5.11). The structural differences between L69S and WT Ub are significantly greater than the rmsds within each ensemble of structures (Table 5.1). Figure 5.9 shows a direct comparison of the L69S and WT Ub structures, superimposed by the α-helix and the strands β1 and β2 (backbone rmsd = 0.76 Å for the superimposed residues). These elements were chosen because the distance between them remains almost unchanged upon the mutation (Table 5.3); in contrast, there is a significant increase in the distance between the α-helix and strands β3 and β5. This superimposition emphasizes an important structural difference between the two proteins, in that the strand β5 in L69S is tilted and displaced away from the core of the protein. Distance analysis indicates that the C-terminal part of this strand (residues 68-71) is on average approximately 2 Å farther away from the α-helix (Cα of Leu30) than in WT Ub (Table 5.3). This displacement of β5 away from the core is not unexpected, given the hydrophobic side-chain of Leu69 that "anchors" this strand to the core in WT Ub (Fig.

5.9) is replaced by a shorter, polar Ser side-chain in the mutant. Several independent lines of evidence presented below indicate that, although subtle, these differences between the wild type and L69S Ubs are real.

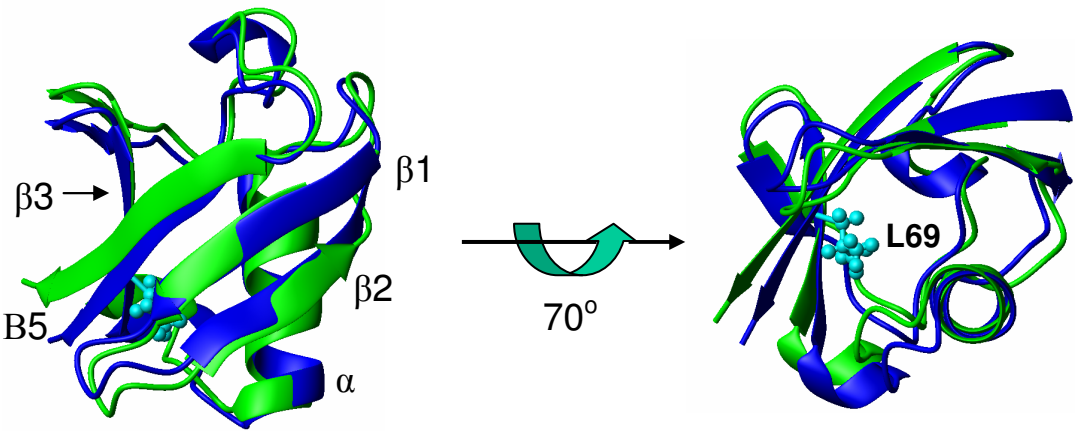

Figure 5.9 Structural differences between L69S and WT Ub. A cartoon representation of the backbone superimposition of the structures of yeast L69S (green) and human WT Ub (blue). Residues 2-7 (β1), 12-17 (β2), and 23-34 (α) were used for the superimposition. Shown in ball-and-stick (cyan) is the side chain of Leu69 in WT Ub. The unstructured flexible C terminus (residues 73-76) is not shown.

Table 5.3 Distances between the Cα atoms of Leu30 and the residues in the strands β1, β2, β3, and β5.

Residue	Strand	L69S [Å] (*)	WT [Å] (*)	□(L69S-WT) [Å]
4	β1	10.71 (0.17)	10.99 (0.06)	-0.28
5	β1	9.55 (0.29)	9.02 (0.06)	0.53
6	β1	11.56 (0.25)	11.28 (0.08)	0.28
7	β1	10.90 (0.25)	11.13 (0.08)	-0.23
				Mean = 0.08
12	β2	10.77 (0.08)	11.55 (0.05)	-0.78
13	β2	8.24 (0.07)	8.58 (0.06)	-0.34
14	β2	9.31 (0.15)	9.68 (0.06)	-0.37
15	β2	7.53 (0.24)	8.22 (0.06)	-0.69
16	β2	9.86 (0.33)	10.84 (0.08)	-0.98
17	β2	10.85 (0.21)	11.49 (0.08)	-0.64
				Mean =-0.63
41	β3	10.52 (0.18)	9.20 (0.12)	1.32
42	β3	12.49 (0.19)	11.33 (0.12)	1.16
43	β3	12.01 (0.22)	10.79 (0.10)	1.22
44	β3	15.53 (0.24)	14.04 (0.09)	1.49
45	β3	17.79 (0.28)	15.73 (0.07)	2.06

				Mean = 1.45
66	β5	14.63 (0.21)	14.02 (0.05)	0.61
67	β5	13.29 (0.27)	11.89 (0.10)	1.40
68	β5	13.71 (0.27)	12.04 (0.10)	1.67
69	β5	11.32 (0.27)	9.77 (0.12)	1.55
70	β5	13.96 (0.29)	12.15 (0.11)	1.81
71	β5	14.76 (0.37)	12.24 (0.19)	2.52
72		17.35 (0.39)	14.83 (0.13)	2.52
				Mean = 1.73

*Numbers in the parentheses represent standard deviations within the corresponding ensemble of 10 NMR structures.

5.5.2 Spectral differences between the mutants and WT Ub

Chemical shifts reflect local electronic environment of a nucleus under observation, and amides are particularly sensitive to changes in both secondary and tertiary structure of a protein. The ^{1}H-^{15}N HSQC spectra of both WT Ub and L69S Ub (Fig. 5.10a) show well-dispersed signals indicative of a well-defined tertiary fold with a significant β-sheet content, characteristic of Ub. Surprisingly, however, a large number of amides, not only those adjacent to the site of mutation, show significant perturbations in L69S (Fig. 5.10b), well above the experimental uncertainty in signal positions. This dissimilarity between the two spectra exceeds the level typically observed for a point mutation of surface residues (see e.g. Fig. 5.11), where most perturbations are typically local, and suggests a possibility of a rearrangement in the core of the protein and/or in its tertiary structure.

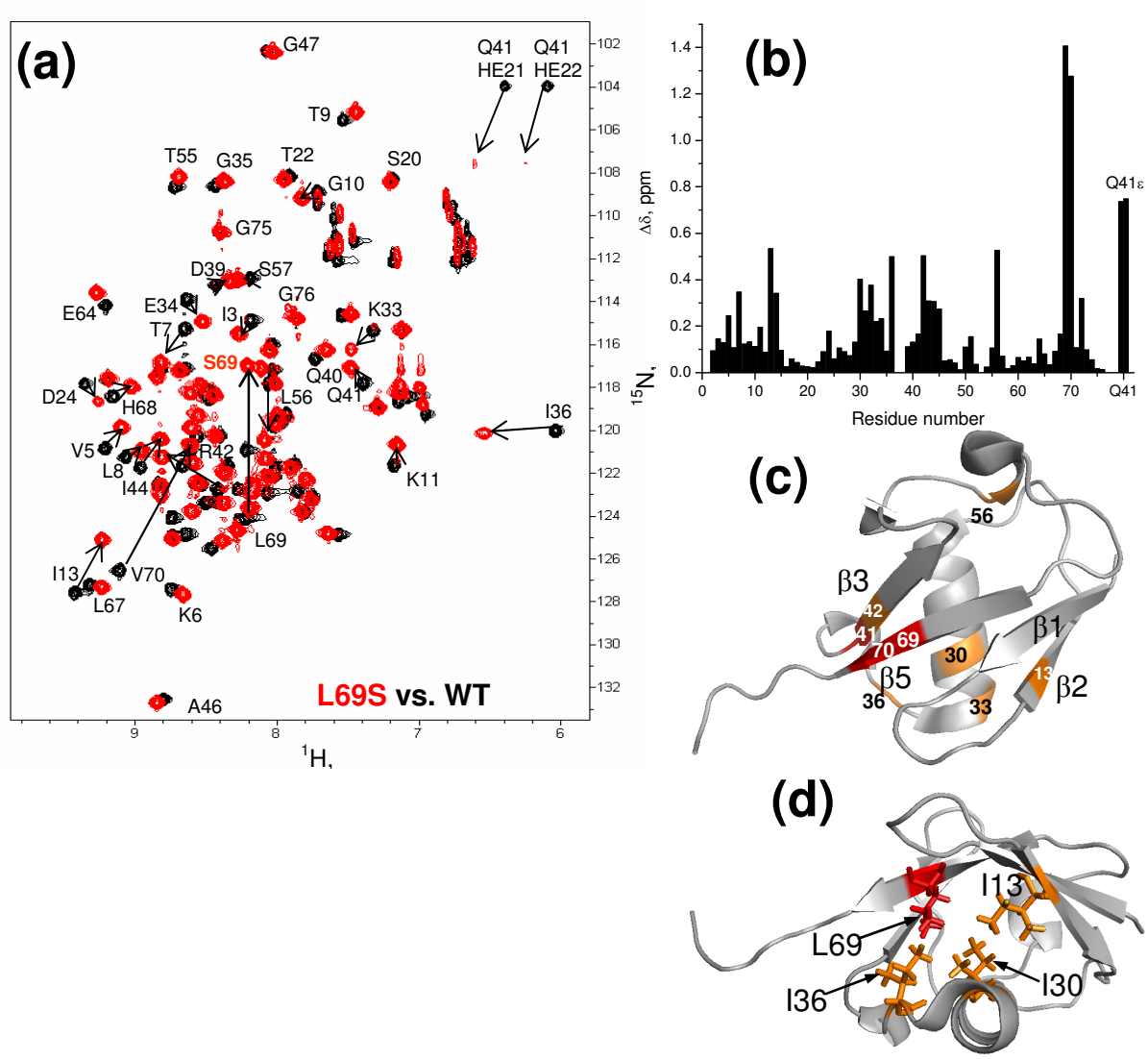

Figure 5.10 Structural differences between L69S and WT Ub. (a) Superposition of the ^{1}H-^{15}N HSQC spectra of L69S (red contours) and WT Ub (black contours). Shifted resonances are indicated. (b) Combined amide chemical shift differences between the two proteins as a function of residue number. The experimental uncertainty in $\Delta\delta$ is ≤ 0.02 ppm. The site of mutation is indicated by the arrow. (c) Cartoon representation of the 3D structure of WT Ub with the residues showing the biggest CSPs colored (from yellow to red, in increasing $\Delta\delta$). (d) Cartoon representation of the WT Ub structure, with the side chains of the perturbed residues forming or adjacent to the protein's core shown in stick representation.

Particularly large resonance shifts are observed in Ser69 and Val70 (located in the strand β5) as expected due to the mutation. Less expected are strong CSPs in Arg42 and

Thr7, located in the strands β3 and β1 flanking β5 on both sides and in a close proximity to the site of mutation (Fig. 5.10c). These CSPs likely indicate disruption in the hydrogen bond contacts (supported by the H-D exchange data, see below) between the strands, specifically, between Val70 and Arg42 (both NH and CO groups of these two residues are involved) and between NH of Leu69 and CO of Lys6 (the peptide plane that includes NH of Thr7). The strong CSP in Thr7 could also reflect the fact that in the WT Ub this residue makes side chain van der Waals contacts with Leu69. Intriguingly, significant changes in amide resonances are also observed in Ile30 in the α-helix, Ile13 in strand β2, and Ile36 in the α/β3 loop. In WT Ub, the side chains of Ile30 and Ile13 extend into the protein core forming hydrophobic contacts with the side chains of Leu69 and Ile36 (Fig. 5.10d). Since the side chain of Ile36 contacts side chains of Gln41 and Leu69 in WT Ub, the large shift in the resonance of Ile36 in L69S can be attributed to the mutation as well as changes in the relative positions of β3 and β5. This is further corroborated by a strong CSP of the side chain amino group (NH_2) of Gln41 (Fig. 5.10a,b), suggesting a substantial change in the local environment of this side chain. Indeed, Gln41 side chain is oriented differently in L69S and WT Ub, although in both cases it points toward the protein core. Another strongly perturbed residue is Leu56, located proximal to the N-terminus of the α-helix, and also involved in the formation/stabilization of the core of Ub. All these spectral perturbations agree with the rearrangements in the core of Ub which involve change in the relative positions of the β-strands and the α-helix.

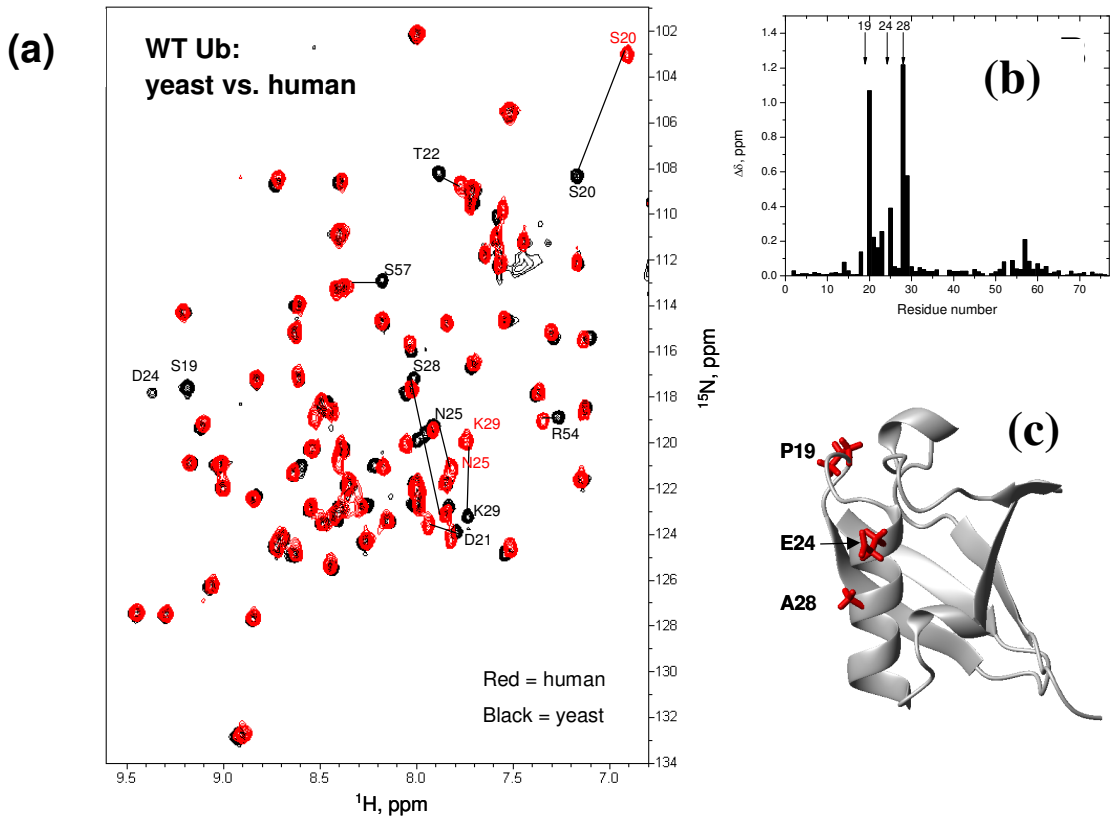

Figure 5.11 Comparison of the ^{1}H-^{15}N HSQC spectra of Yeast versus Human WT Ub. (a) Overlay of the ^{1}H-^{15}N HSQC spectra of yeast (black) and human (red) Ub. (b) Amide chemical shift perturbations as a function of residue number show that the observed perturbations are very local, practically only in the mutated residues and their immediate neighbors (residues i+1). The arrows indicate the location of the three amino acids that are different between yeast and human. Of these 3 mutated residues, only resonance shift in residue 28 can be quantified. The signals of residues 19 and 24 are present in yeast but not in human Ub spectra, because Pro19 (human Ub) has no ^{1}H-^{15}N HSQC signal, and the signal of Glu24 (human Ub) could not be reliably observed (likely exchange-broadened beyond detection). Signal of Ser20 is shifted due to mutation of residue 19, Asn25 is shifted due to mutation of residue 24, and Lys29 is shifted due to mutation of residue 28. (c) Cartoon representation of human Ub structure with the three residues mutated in yeast Ub indicated.

The ^{1}H-^{15}N HSQC spectrum of L67S also shows significant differences from that of WT Ub (Fig. 5.12a,b). The CSP pattern in L67S is distinct from that of L69S, with generally fewer perturbed residues, but with a greater number of strong perturbations ($\Delta\delta$ >1 ppm). Strong signal shifts were observed in L67S in most of the residues in strand β5,

as well as in Phe4 and Gln2, both located in the β1 strand and (in WT Ub) hydrogen-bonded to Leu67/Ser65 and Glu64, respectively. These CSPs likely reflect a perturbation in the hydrogen bonding between β5 and flanking it strands β1 and β3 (Fig. 5.12c). Smaller perturbations are observed in the α-helix, consistent with the CD spectra indicating a closer correlation in the secondary structure between WT Ub and L67S, compared to L69S.

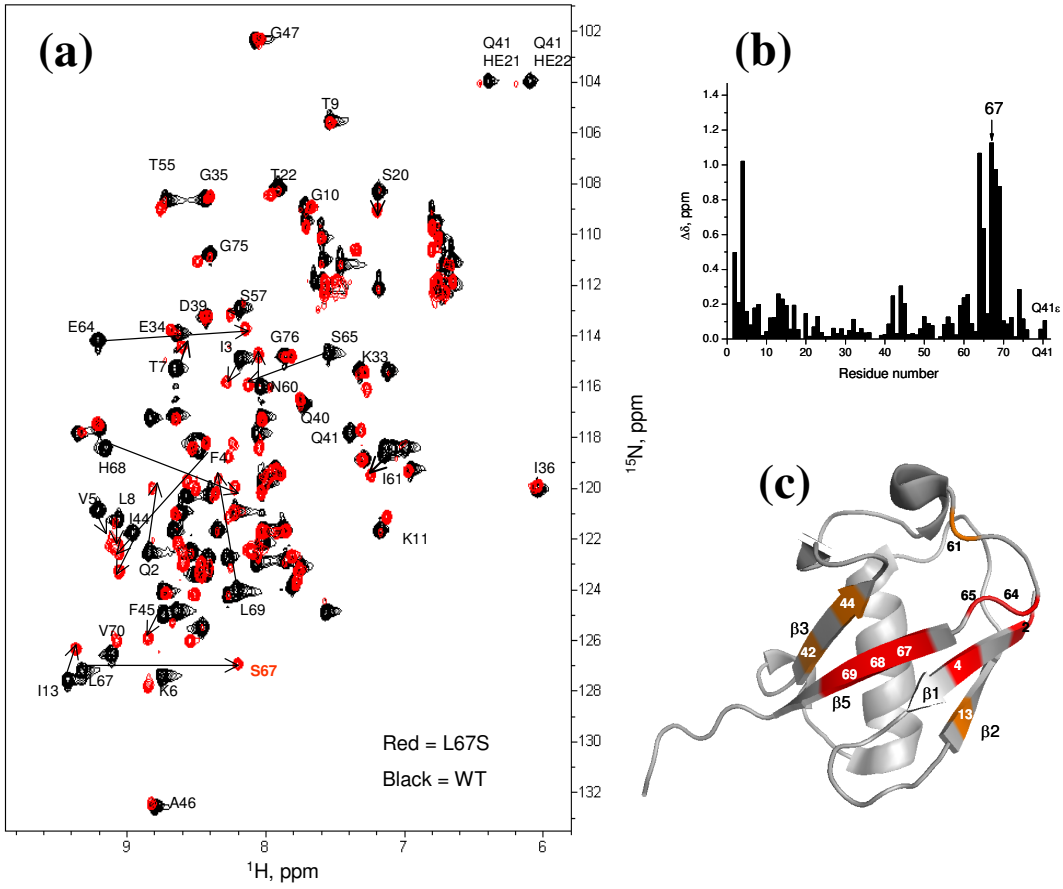

Figure 5.12 Spectral differences between L67S and WT Ub. (a) Overlay of the ^{1}H-^{15}N HSQC spectra of wild type ubiquitin (black) with L67S (red). (b) Amide chemical shift differences between the two proteins as a function of residue number. The site of mutation is indicated by the arrow. (c) Cartoon representation of the 3D structure of WT Ub with the residues showing the biggest CSPs colored (from orange to red, in increasing Δδ).

5.5.3 Residual dipolar couplings

The ^{1}H-^{15}N residual dipolar couplings (RDCs) report directly on the orientation of the NH bonds in a protein and therefore are highly sensitive to structural changes. While the structure of L69S is in excellent agreement with the RDCs measured for this protein (and included in its refinement), it agrees less well with the experimental RDCs for WT Ub, and *vice versa* (Fig. 5.13). Thus, the correlation coefficient between the experimental RDCs for L69S and those calculated for WT Ub is 0.97, while it is 0.99 for L69S structure; the quality factors [154] are 0.19 and 0.09, respectively. Overall, the RDC differences for the WT structure are approximately a factor of 2 bigger than for L69S. In a reverse comparison, using the published experimental data for WT human Ub (from [78]), the corresponding correlation coefficients are 0.998 and 0.95, for WT Ub and L69S, respectively, and the quality factors are 0.042 and 0.193. All these discrepancies between the experimental RDCs for one protein and predicted for the other indicate subtle although measurable structural differences between the two proteins, resulting in a different orientation of NH bonds in some of the structural elements.

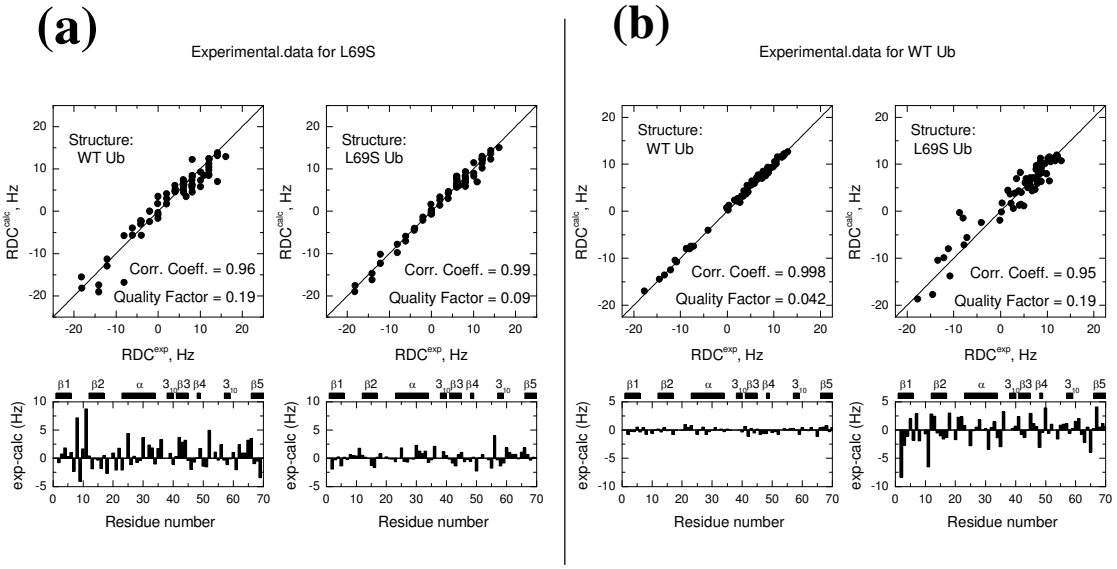

Figure 5.13 Residual dipolar couplings indicate structural differences between L67S and WT Ub. (a) Comparison of the experimental RDCs measured in L69S with their predicted values based on the structures of WT Ub and L69S. (b) Comparison of the experimental RDCs reported for WT Ub with their predicted values based on the structures of WT Ub and L69S. The bottom plots show the difference between experimental and calculated RDCs for each residue.

The rearrangement in the local position/orientation of the β5 strand with respect to strands β1, β2, and β3 and the α-helix would change the topography/landscape of the part of Ub's surface that includes the hydrophobic patch, and therefore could have a profound effect on its binding properties, as discussed below. The displacement of β5 away from the protein core is also expected to weaken its hydrogen-bond contacts with the neighboring strands β1 and β3, which would further enhance the destabilizing effect of the mutation.

5.6 Rigidity and Dynamics

5.6.1 H-D exchange indicates a reduced rigidity of the mutant

To verify the weakening in the inter-strand hydrogen bonding in L69S, hydrogen protection factors were assayed by monitoring H-D exchange in L69S Ub as well as in WT Ub, as a control. A relatively slow H-D exchange was observed in the β1 and β2 strands, consistent with the presence of hydrogen bonds between these strands. However, all β5 residues as well as residues 40-43 in β3 showed fast H-D exchange in L69S Ub, thus indicating that the N-terminal part of β3 is not protected by hydrogen bonding with β5. The fast exchange in these parts of the L69S mutant is in stark contrast with that in WT yeast (Fig. 5.14) and human Ub (data not shown, see also [69]). The observed 7-646 fold increase in the H-D exchange rate in L69S (Fig. 5.14b) clearly indicates a reduction in the hydrogen protection as a result of the structural changes introduced by the mutation. The location of the affected residues agrees with the displacement of β5 in the L69S structure. Intriguingly, there is also an increase in the H-D exchange in amides of the α-helix residues 29-31, which also show chemical shift perturbations as a result of the mutation.

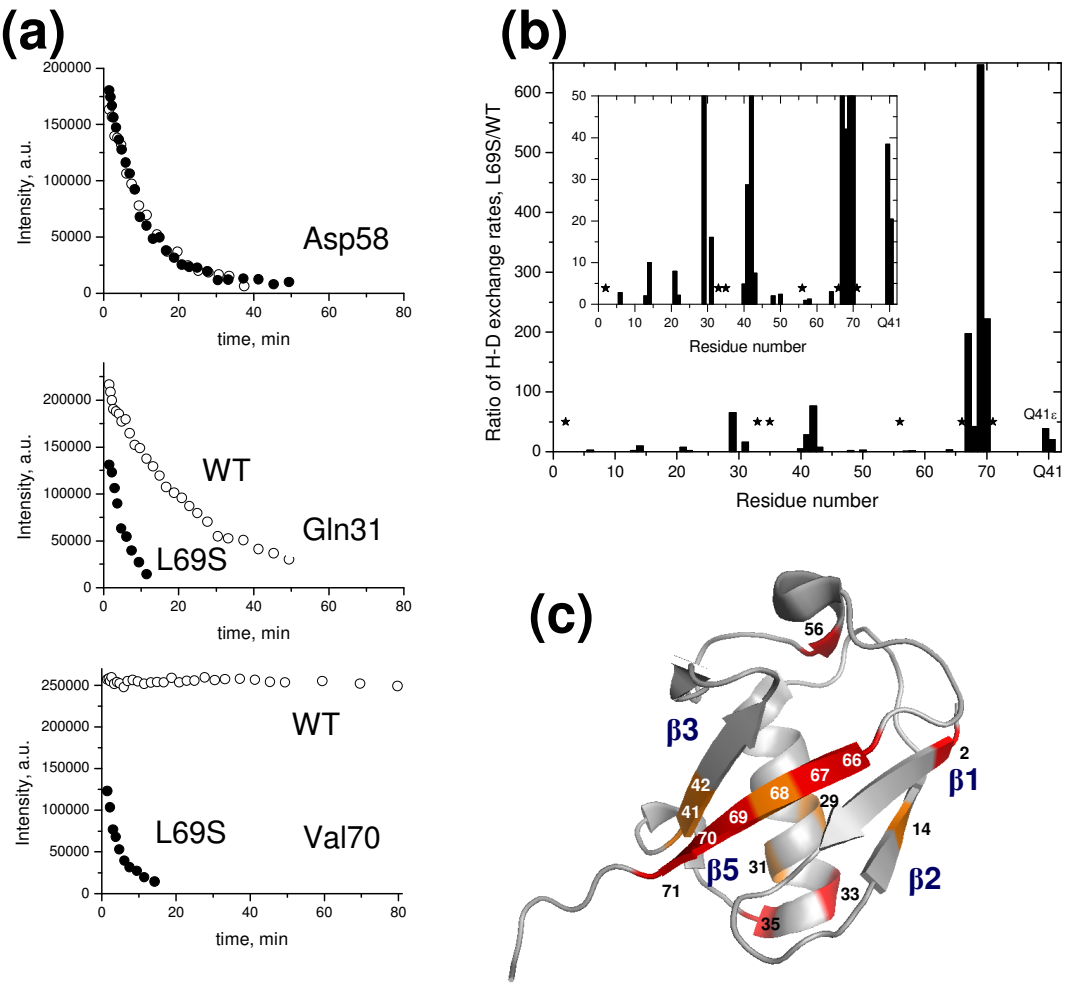

Figure 5.14 The results of H-D exchange assays. (a) Representative exchange kinetics for selected amides in WT (open symbols) and L69S (closed symbols). (b) The ratio of H-D exchange rates in L69S and WT ubiquitins. The inset zooms in on a smaller range of ratios. Not shown are data for several residues (marked with asterisks) where the ratio was > 1, but accurate quantification of the effect was not possible. These include Thr66 (β5) which exchanges essentially immediately in L69S (hence no reportable ratio) and Ile44 (β3); the latter amide did not exchange in WT Ub over the time course of the experiments (up to 20 h), but it did exchange although slowly in L69S. (c) A cartoon representation of the structure of Ub, with the residues showing significant increase in the exchange rate colored red (ratio > 100) and orange (ratio between 10 and 100). Overall, faster H-D exchange in L69S is localized to areas which show spectral perturbations as a result of the mutation, while the uninvolved sites retain their rigidity.

Based on the H-D exchange data, of the possible hydrogen bonds between β5 and the neighboring strands present in WT Ub, only Glu64-Gln2, Ile44-His68, and Phe4-

Ser65 (donor-acceptor) pairs were included in the structure calculation of L69S. For these pairs interstrand NOEs were also observed consistent with hydrogen bonding. It is worth mentioning here that these hydrogen bond constraints had little effect on the relative positioning of strands β1, β3 and β5, which is well defined by the network of NOE constraints. Thus, calculations with no β5-β3 or even β1-β5-β3 hydrogen bonds yielded L69S structures very similar to the one presented here, they superimpose with the backbone rmsd of 0.5Å or 0.4Å, respectively (residues 2-71). Interstrand NOEs consistent with possible other hydrogen bond pairs (Leu69-Lys6, Arg42-Val70, His68-Ile44, Lys6-Leu67) were observed; however, given the fast H-D exchange in the amides these likely represent transient NOEs and were not included in the calculation.

5.6.2 L69S has a well-folded structure

As shown above, the mutations reduced the thermodynamic stability and structural rigidity of ubiquitin. To independently verify that the L69S mutant is a well-folded protein under the conditions of these studies, ^{15}N R_1 and R_2 relaxation rates and heteronuclear ^{15}N-^{1}H NOEs in L69S and in WT Ub, as a control, were measured. These parameters report on the overall rotational diffusion of a protein (reflecting its size and shape) as well as the backbone dynamics on a ps-ms time scale. The overall similarity between the mutant and WT Ub in their ^{15}N relaxation data (Fig. 5.15) clearly indicates that L69S Ub behaves as a well-folded protein. This conclusion is further supported by a detailed analysis of the relaxation data (Fig. 5.15). The overall rotational correlation time of L69S and WT are very similar (~5 ns), suggesting a similar size of both proteins.

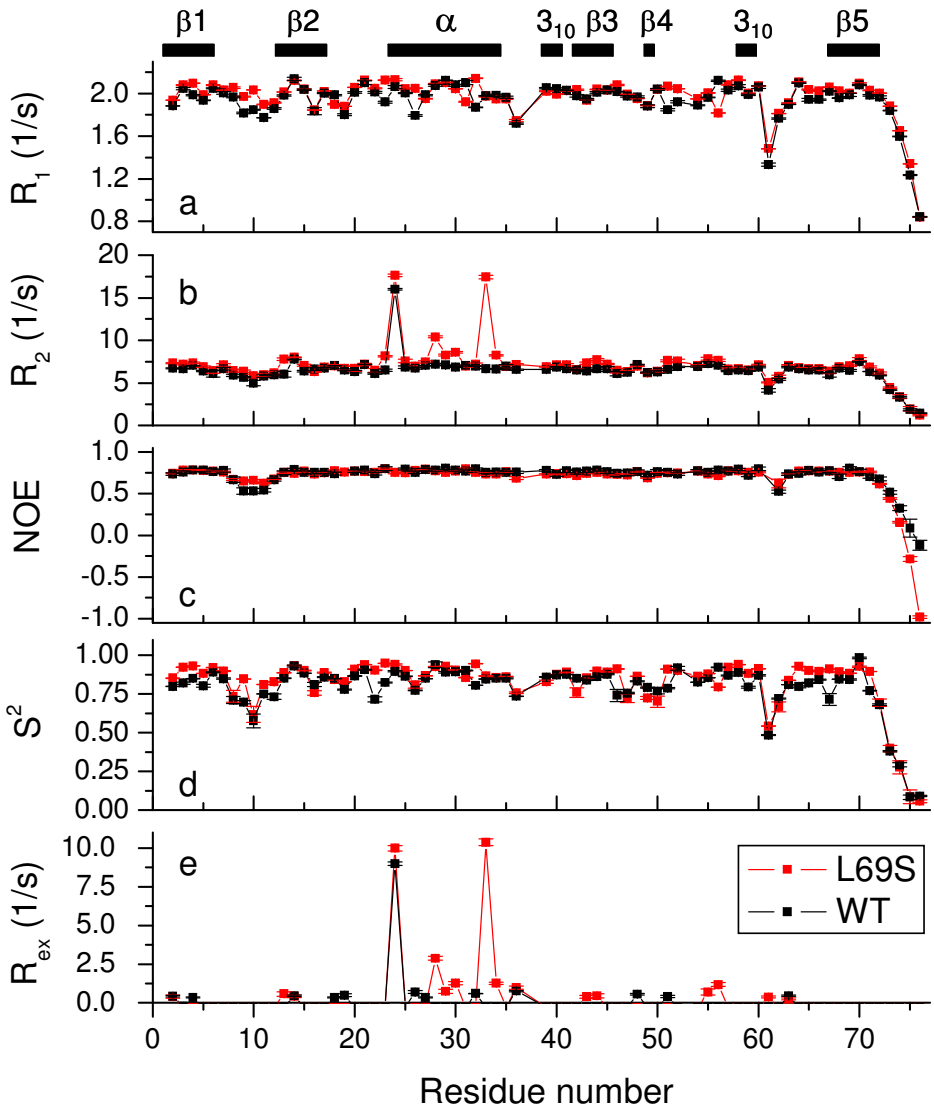

Figure 5.15 Comparison of the ^{15}N relaxation data. (a-c) and parameters of the backbone dynamics (d-e) in L69S (red) and yeast WT Ub (black). The overall rotational correlation time estimated from the ^{15}N relaxation data for L69S and WT Ub was 5.04 ± 0.4 and 4.95 ± 0.6 ns, respectively.

5.6.3 Comparison of the backbone dynamics in L69S and WT Ub

The values of the backbone order parameter (S^2, Fig. 5.15d) in L69S are very similar to those in WT Ub and typical for a well-folded protein, thus indicating retention of structural rigidity on a ps-μs time scale despite the lesser temperature and chemical

denaturation stability of the mutant. Interestingly however, several amides in L69S show significantly elevated R_2 values (Fig. 5.15b) indicative of conformational exchange motions on a μs-ms time scale. Indeed, the analysis of ^{15}N relaxation data (Fig. 5.15e) indicates the presence of conformational exchange (on a μs-ms time scale) in Ser28, Lys29, Ile30, Lys33, Glu34, Thr55, and Thr56 in L69S but not in WT Ub. The location of these sites, in the middle and the C-terminus of the α-helix as well as in the $\beta 4/3_{10}$ loop flanking the N-terminal end of the α-helix, combined with the fact that the side chains of most of these residues face the hydrophobic core of Ub, suggest that the observed conformational exchange could reflect some μs-ms -time scale rearrangements/motions in the hydrophobic core of the mutant. Note that many of these residues (30, 33, 34, and 56) show strong CSPs in L69S and some of them (Lys29, Gln31) have elevated H-D exchange rates (Fig. 5.14b). The presence of R_{ex} terms in most of these residues was independently confirmed by the comparison of ^{15}N R_2s with the ^{15}N CSA/dipolar cross-correlation rates (not shown). It should be pointed out that the conformational exchange motions are not unique to the L69S mutant, as some of the residues (especially Asp24 and Ile36) show strong R_{ex} contributions both in L69S and WT Ub (Fig. 5.15e).

The findings that the L69S mutation has practically no effect on the fast (ps-ns) local backbone dynamics, some effect on slow (μs-ms) motions, and a dramatic effect on much slower motions (seconds and longer) suggest that while the secondary structure elements remain essentially intact, their contacts and packing which form the tertiary structure of Ub are affected.

5.7 Discussion

Biochemical, biophysical, and *in vivo* assays demonstrated that the Ser mutations of Leu67 and Leu69 have a dramatic effect on Ub's function, stability, and the slow time scale dynamics. Although the effect of these mutations on the three-dimensional structure of the protein is modest, the displacement/rearrangement of the β strands that form the hydrophobic patch–containing face of Ub is the likely structural basis for its altered binding properties. In fact, this surface comprising the Leu8-Ile4-Val70 hydrophobic patch is targeted by most currently known UBDs (e.g. [94, 155]), and the structural features of this surface should be critical for Ub's ability to recognize a vast variety of structurally different ligands. Mutations in these hydrophobic patch residues have been shown to have a strong effect on Ub function [156] and cell growth [79]. The results indicate that even more subtle modifications that preserve the amino acid composition of the surface but alter the dynamics of the protein and the structure/topography of its surface could have a profound effect on the binding specificity. Sequence alignment (Table 5.4) shows that Leu is conserved in Ub at positions 67 and 69 in all eukaryotes, and there is also high sequence homology in both positions amongst the UBL domains. This implies that hydrophobic residues in strand β5 at positions analogous to 67 and 69 play a significant role in stabilizing the β sheet not only in ubiquitin but possibly in the UBLs.

Table 5.4 Structure-based sequence alignment of ubiquitin and related proteins (UBL, NEDD and SUMO) indicate high conservation of the hydrophobic side chains in positions corresponding to L67 and L69 in Ub.

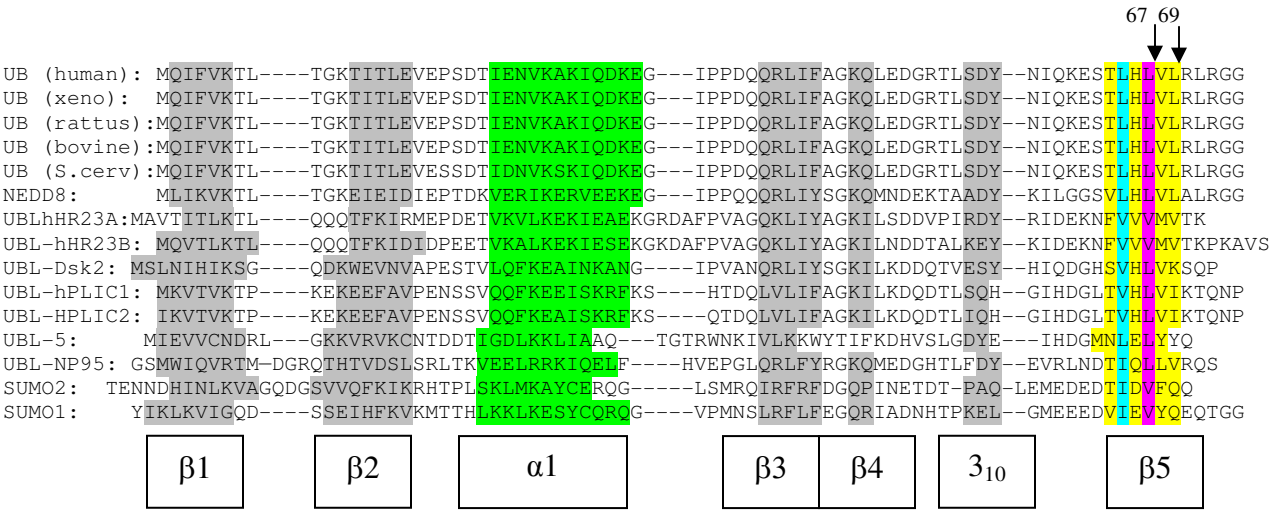

The L69S mutation, while preserving the overall three-dimensional structure of Ub, caused perturbations in the structural arrangement and hydrogen bond contacts between β5 and the adjacent strands β1 and β3. This weakened the stability of the protein and dramatically increased its flexibility on the slow time scale, while the size of the protein and the subnanosecond backbone dynamics remain unaffected.

5.7.1 Why does L69S lack binding affinity for UIM?

To understand possible reasons for the lack of Rpn10 and S5a UIM binding to the mutants, the L69S Ub structure was superimposed onto the solution structure of the WT Ub/UIM-2 complex (1YX6.pdb) [74]. When bound to WT Ub, UIM-2 lies along the β5 strand, forming hydrophobic contacts with Val70 and His68 via its IAYAM motif, as well as electrostatic contacts with Arg72 via Glu283. The complex is further stabilized by favorable interactions of UIM-2 with several residues in the adjacent β1 and β3 strands of ubiquitin, in particular, with Leu8 via Tyr289, Arg42 via Glu283, Ala46 via Leu295, and

Ile44 via Ala290, Met291, and Met292. The superimposed model (Fig. 5.16a) suggests that the steric clashes caused by the displacement/elevation of β5 could weaken or disrupt these interactions, e.g. by moving the UIM farther away from the rest of the hydrophobic patch. The ~2 Å elevation of the C-terminal part of β5 above the β-sheet of Ub is expected to affect UIM's electrostatic interactions with Arg42, as well as the van der Waals contacts with Leu8 and possibly Ala46, thus effectively sterically hindering UIM's binding to Ub. A superimposition with the Ub/UIM-1 complex (1YX6.pdb) [74] (Fig. 5.16c) suggests that a similar conclusion holds for L69S binding to UIM-1 of S5a. Due to the sequence similarity between the UIM of Rpn10 and UIM-1 of S5a, it is natural to expect that this could also explain the lack of L69S binding to Rpn10. Moreover, the analysis of all currently available structures of Ub:UIM complexes (Fig. 5.17) shows that other UIMs also bind to and are positioned along the β5 strand; thus their binding could be affected by this mutation.

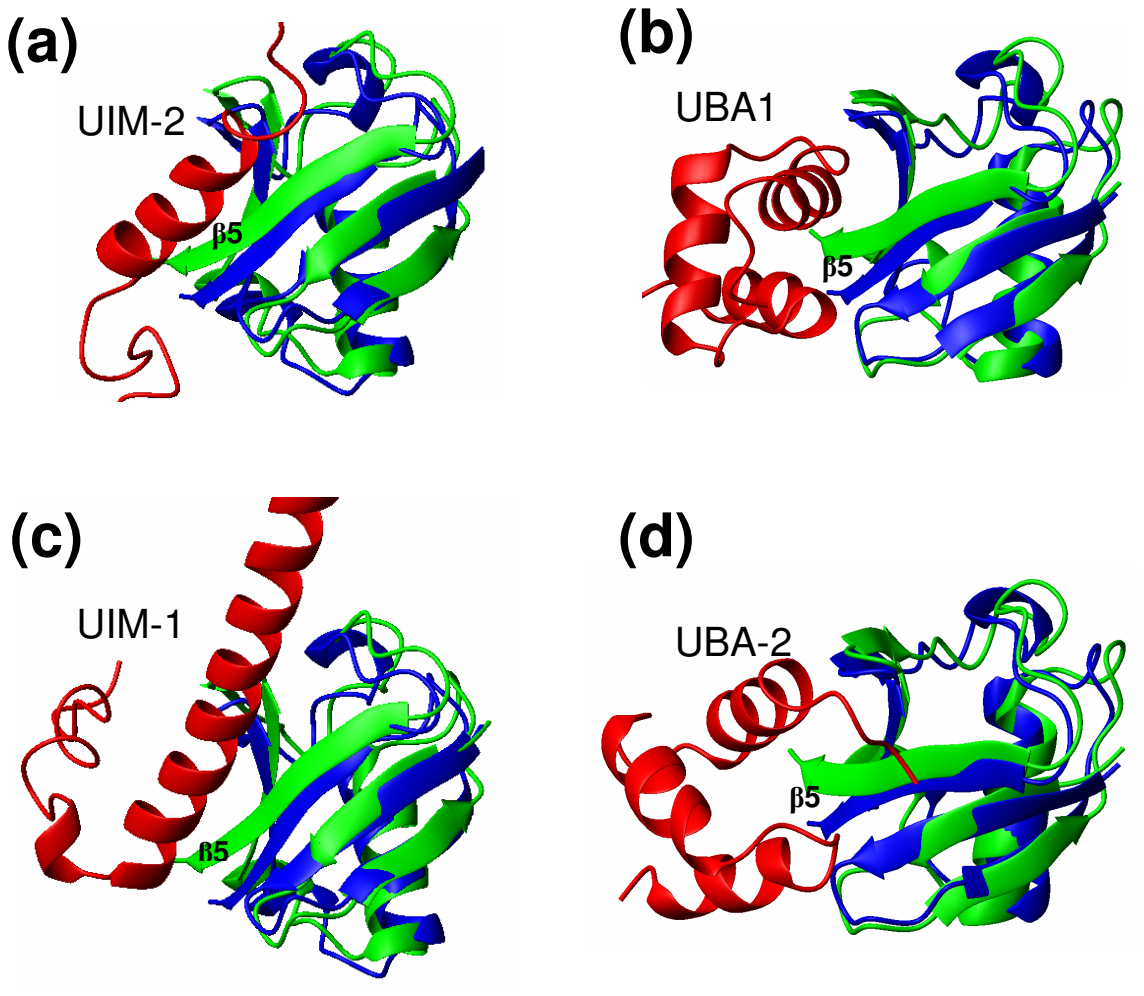

Figure 5.16 Structural superposition models show how the displacement of β5 in L69S could affect its binding to UIMs of S5a but not to UBAs of hHR23A. Shown is a superimposition of L69S Ub structure on the known structures of WT Ub complexes: (a) Ub:UIM-2 (PDB: 1YX6) (b) Ub:UBA-1 (c) Ub:UIM-1 (PDB: 1YX6) and (d) Ub:UBA-2. WT Ub is colored blue, L69S Ub is green, the UIM or UBA domains are red. The Ub:UIM structures are from[74], the Ub:UBA docked models are from [153].

5.7.2 Why does L69S retain binding affinity for UBA domain?

According to the NMR-based model of the WT Ub:UBA-1 complex [153], UBA-1 contacts Lys6, Leu8, and Gly10 of the Ub's β1/β2 loop via His192, while the side chains of Met173 and Tyr175 contact Ile44 and Arg42 in β3, respectively. Chemical

shift perturbation in Val70 of WT Ub when bound to UBA-1 (compared with free Ub) is below the level of significance [153]. Moreover, no direct sidechain-to-sidechain contacts with β5-strand residues are present in the WT Ub:UBA-1 complex [153]. In contrast, when UBA-1 is added to L69S, the largest CSP is observed in Val70 (Fig. 5.7c). In addition, strong signal attenuations (>70%) are present in Thr7, Leu8, Thr9, Lys11, and Leu71, indicating strong interaction of UBA-1 with residues in the β1/β2 loop, as well as with the C-terminus of β5. This is consistent with the structure of L69S. Indeed, superimposition of the L69S structure on the WT Ub:UBA-1 complex (Fig.5.16b) reveals that the elevation of β5 in L69S positions Val70 properly to form a hydrophobic interaction with Met173. Also, His68 of L69S Ub is positioned properly for a hydrogen bonding interaction with Glu168. These additional interactions may be responsible for the observed increase in the binding affinity of L69S for UBA-1 (see above) compared with the reported data for WT binding to UBA-1 [152, 153]. A similar superimposition with the UBA-2/Ub structure (Fig. 5.16d) suggests that L69S is expected to bind UBA-2 of hHR23a as well. This is in striking contrast with the UIM:Ub complex discussed above (Fig. 5.16a,c), where the displacement of β5 is expected to cause steric clashes with the UIM.

It should be pointed out here that the structural factors discussed above presumably affect the enthalpy of binding. A complete picture should account for the effect of the mutation on the entropic cost of binding. The increased structural flexibility on a slow time scale (obvious from the increased H-D exchange) suggests lower activation barriers separating various conformational states, and possibly a greater conformational ensemble available to the mutant in the native state. This would then

imply a greater entropic cost associated with the rigidification of the protein upon ligand binding. Further studies are necessary to fully unveil the nature of the observed binding selectivity of the two Ub mutants studied here.

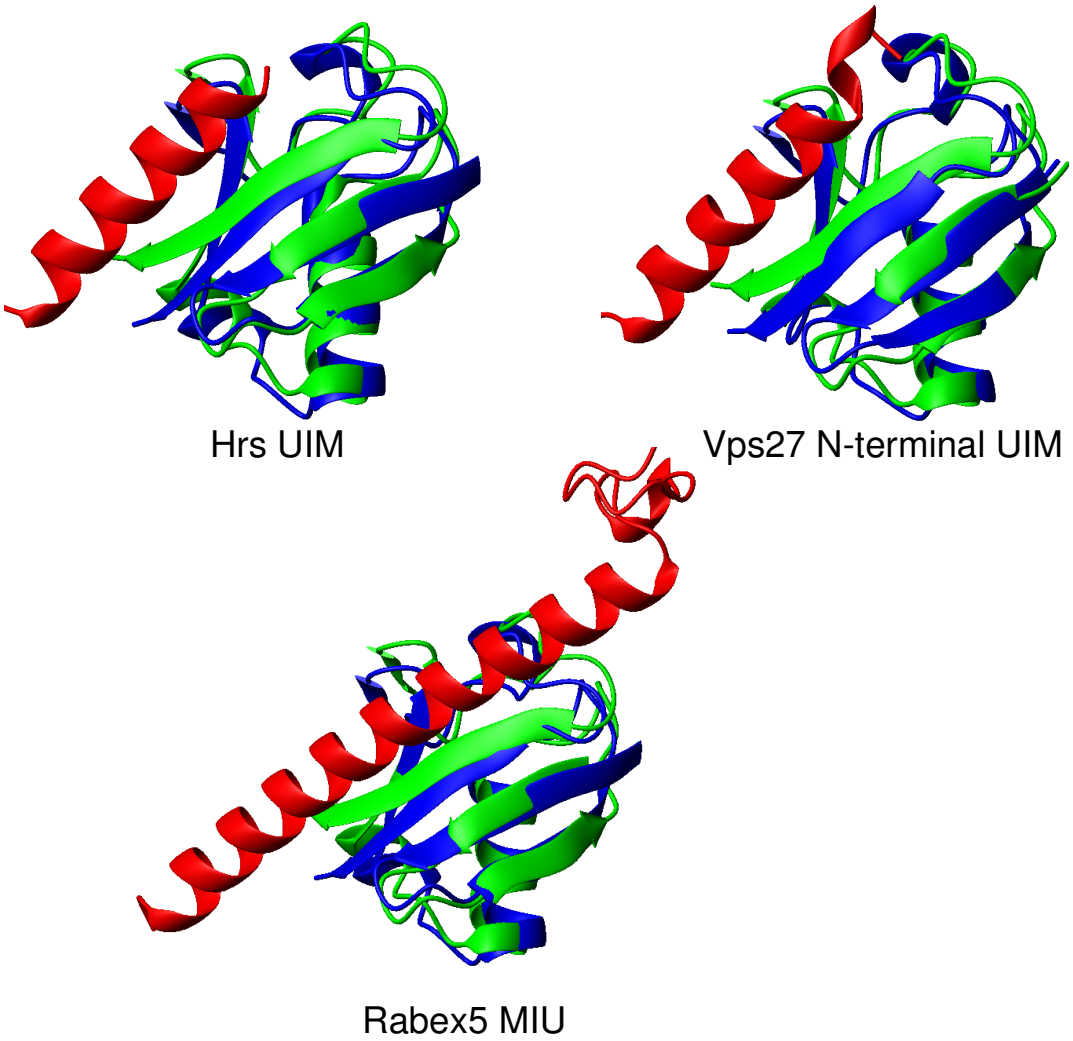

Figure 5.17 Structural comparison with other known UIM/Ub complexes. Superimposition of L69S (green) onto the known structures of UIM:Ub complexes (red=UIM, blue=WT Ub) suggests that the displacement of β5 could affect UIM binding to L69S. The flexible C-terminal residues (73-76) in Ubs are not shown.

5.7.3 A clue to the sequence conservation of Ub

The inability of L67S and L69S to support yeast growth is surprising, given the modest changes in the structure and dynamics of these mutants relative to wild-type Ub.

These results demonstrate that Ub's function is exquisitely sensitive to small perturbations in its structure and dynamics. Ub is one of the most highly conserved proteins in the eukaryotic kingdom, with yeast and human Ub differing in only 3 out of 76 residues. The results provide a rationalization for this unusually high degree of sequence conservation. Ub must interact with a wide array of different proteins to perform its biological functions. Given Ub's small size and its large number of binding partners, it appears that there is extraordinary pressure on Ub to retain its sequence, because even relatively modest structural perturbations caused by mutations in residues that are not surface-exposed can compromise the binding of some partners (Rpn10) but not others (Rad23). Ub is a central component in many different biological pathways. Theoretical studies predict that protein hubs which intersect multiple pathways will be more sensitive to mutations than proteins that operate more independently [157]. Perhaps this is the reason that even small perturbations to the structure and dynamics of Ub are not tolerated in the cell.

With respect to the ability of Ub to bind Rad23 but not Rpn10, the L67S and L69S mutants represent separation-of-function alleles that may be useful as tools to distinguish biological functions of Ub that depend on these two receptor proteins. If this discrimination extends to other UBA and UIM domain proteins, the L67S and L69S mutants may prove to be valuable reagents to identify effector functions of Ub that are read out by UIM domains. Indeed, analysis of all currently known complexes between Ub and UIM, UBA, and CUE domains (Figs. 5.17,5.18), suggests that the ability of L69S to discriminate between UIM and UBA could be a general feature of this mutant. Since a number of proteins involved in trafficking of cargo between different membrane

compartments contain either a UBA or UIM domain (reviewed in [158]), the mutants could effectively be used to sort out steps in the endosomal pathway.

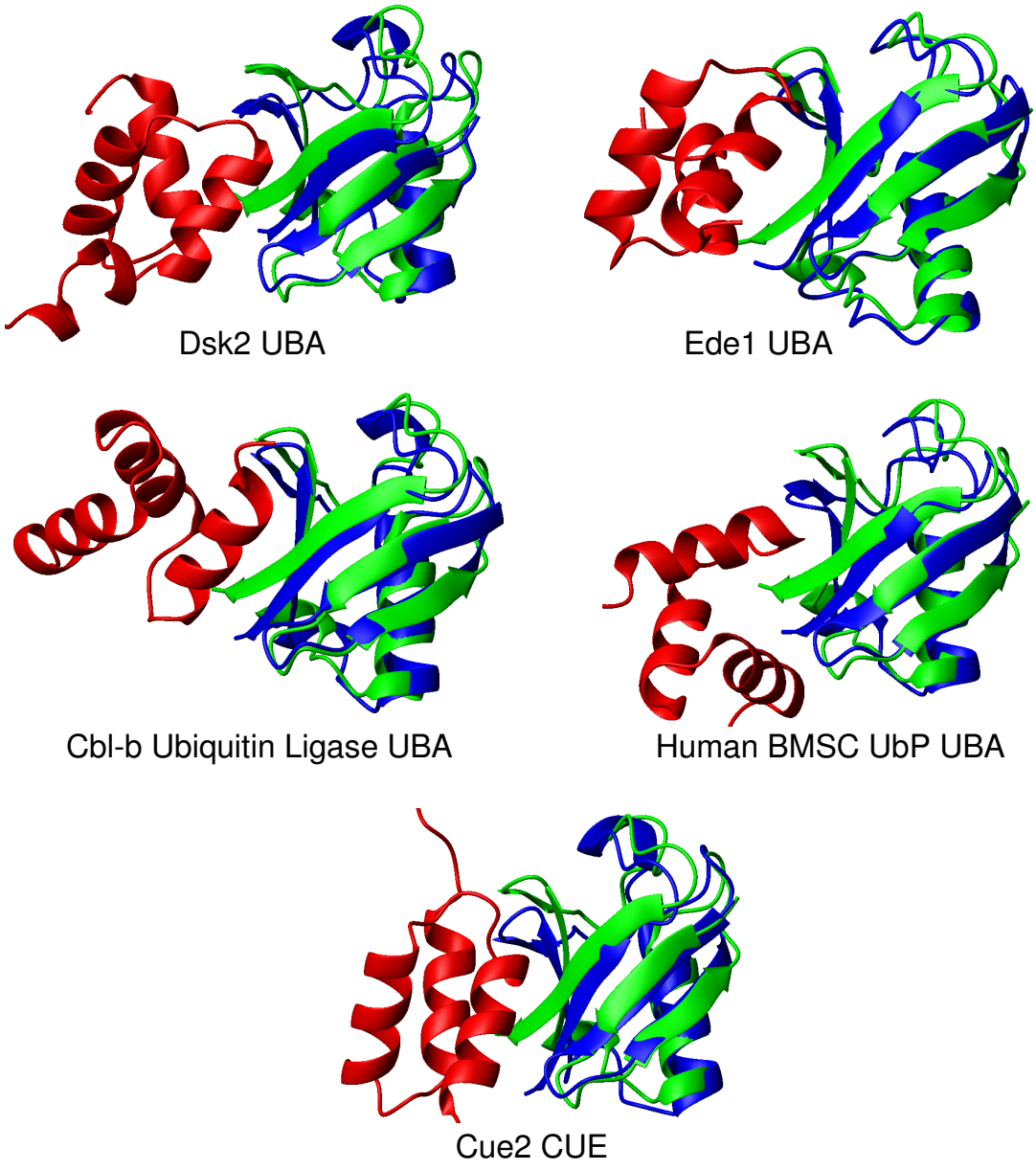

Figure 5.18 Structural comparisons with other known Ub complexes with UBA or CUE domains. Superimposition of L69S (green) onto the known structures of Ub's complexes with UBA and Cue domains (red=UBA or Cue, blue=WT Ub) suggests that, contrary to UIM:Ub binding, the displacement of β5 could have little effect on UBA binding to L69S. The flexible C-terminal residues (73-76) in Ubs are not shown.

5.8 Summary

Ub is highly promiscuous with regard to its binding partners, ranging from small organic molecules like ubistatins [159] to protein domains [94]. The knowledge of what elements and features of Ub's surface contribute to this property of Ub is important for the understanding of what recognition signals various polyUb chains present. All binding data published to date have demonstrated that UIM and UBA domains can function interchangeably in binding polyUb, and both do not discriminate between Lys48- and Lys63-linked chains [74, 115]. Biochemical studies presented here show that, for the first time, point mutations in its core bestow upon Ub the ability to discriminate between the two proteasomal Ub-receptor proteins, Rad23 and Rpn10.

Chapter 6: Structural insights into polyubiquitin chain linkage specificity of the UBA domain of Ede1

6.1 Background and Objectives

Eukaryotic organisms maintain cellular homeostasis through endocytosis. In yeast, a non-essential endocytic protein, Ede1, is required for efficient internalization of ubiquitinated proteins [160]. Ede1 binds Ub via its Ub-associated (UBA) domain, comprised of a 40-residue three-helix bundle, whereas its human homologue, Eps15, contains a pair of single-helix UIM domains. The Ede1 UBA domain has been reported to bind to Ub with moderate affinity (K_d = 83 ± 9 μM) [116]. The solution structure of the Ede1 UBA/monoUb complex reveals that UBA contacts the hydrophobic patch of Ub via residues in its helices α1 and α3 and the α1/α2 loop [110]. In addition to hydrophobic interactions with Leu8, Ile44, and Val70 (Fig. 1.11), Ede1 UBA also makes contacts with Ala46, Gly47 in the β3-β4 loop region, and Lys48, Gln49 in β4, as well as electrostatic interactions via Glu1348 with Lys6 and His68 located in β1 and β5, respectively.

Although monoUb is the best studied tag for endocytosis, evidence suggests that Lys63-linked chains are more competent endocytic signals [42]. Accordingly, preferential binding of Lys63-linked polyUb by Ede1 UBA is presumably a critical factor. However, the role of polyUb chains in endocytosis is not well understood and the Ede1/polyUb interaction has not yet been characterized. It is also interesting to explore the structural basis for linkage-specificity in polyUb/UBA interactions (described in Section 2.1.2). NMR was used to gain insight into the interaction of the UBA domain of

Ede1 with Ub chains linked via either Lys48 or Lys63, in order to elucidate the structural basis for its purported preferential binding to Lys63-linked polyUb.

6.2 Mapping the interactions sites between Ede1 UBA and monoUb

As control experiments, increasing amounts of unlabeled Ede1 UBA were titrated into a 0.8 mM ^{15}N-labeled monoUb sample up to a Ede1 UBA:Ub_2 molar ratio of 3, and unlabeled monoUb was titrated into a 0.45 mM ^{15}N labeled Ede1 UBA sample up to a Ub:UBA molar ratio of 2.8.

The CSPs observed in ^{15}N-labeled monoUb upon addition of Ede1 UBA (Fig. 6.1a) cluster around residues Leu8, Ile44, and Val70, consistent with binding to the hydrophobic patch on Ub's surface. The largest CSPs were observed in residues Ala46, Gln49, and His68, while significant signal attenuation was detected in Lys48 and Leu71. The magnitude of the perturbations increased with Ede1 UBA concentration and saturated at [UBA] /[Ub] > 1.

The observed CSPs in ^{15}N-labeled Ede1 UBA titrated with unlabeled monoUb (Fig. 6.1b) agree well with the published data[110] and reveal a nearly identical ^{1}H-^{15}N chemical shift map for the Ub-bound state. Interestingly, Ala1372 and Ala1381 located in α3 showed slow exchange indicative of tighter binding to this part of UBA.

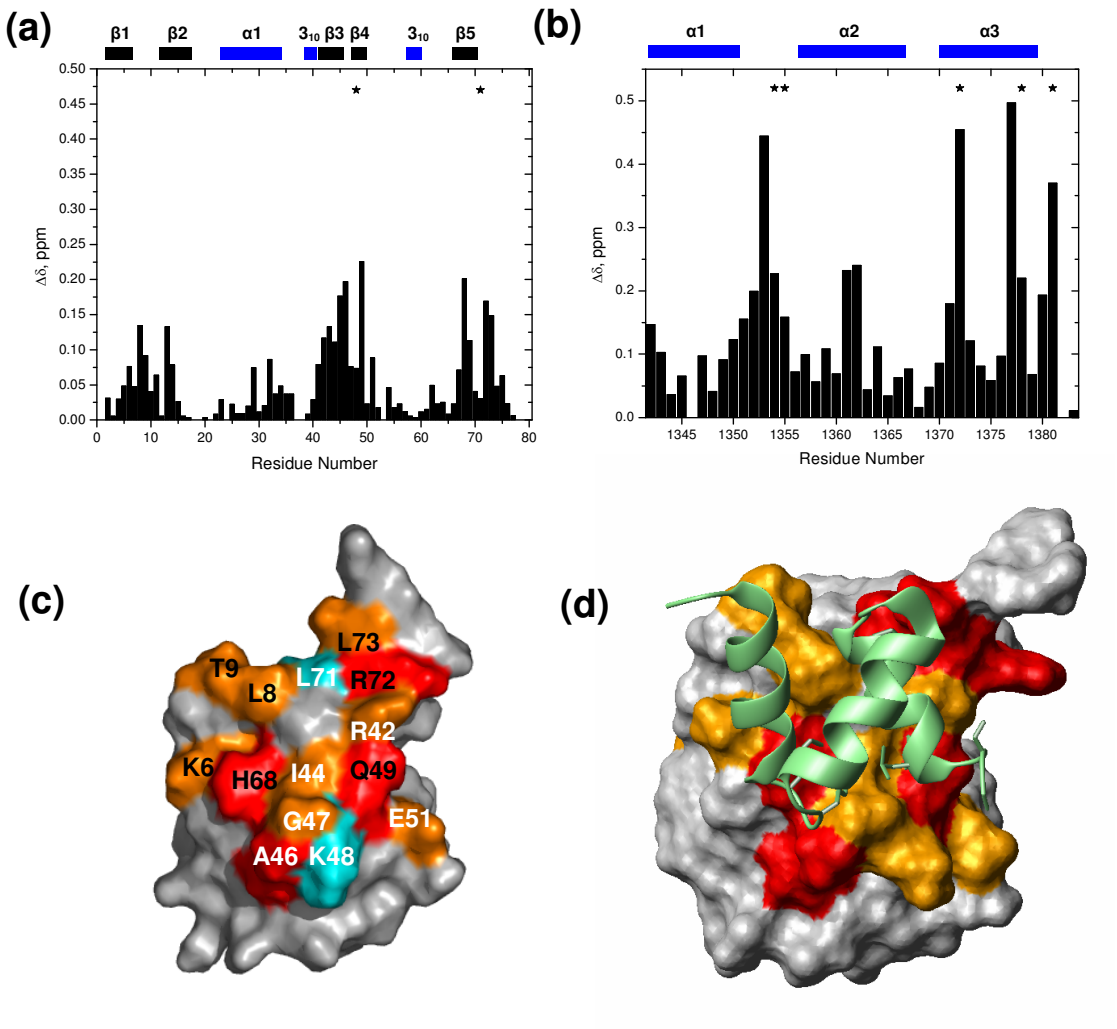

Figure 6.1 NMR mapping of ubiquitin and UBA residues affected by binding. (a) The CSPs in ubiquitin at saturation with UBA, as a function of the residue number. (b) The CSPs in UBA at saturation with monoUb, as a function of the residue number. The CSP shown at position 1383 is for the indole amine of W1368. Sites showing significant signal attenuation (>60%) due to intermediate or slow exchange are marked by asterisks. (c) Surface representation of Ub with the sites colored by the observed CSPs as follows: $\Delta\delta > 0.15$ ppm (red), $0.15 \text{ ppm} > \Delta\delta > 0.075$ ppm (orange). Residues with signal attenuation > 60% are colored cyan. (d) The structure of the monoUb:Ede1 UBA complex (PDB code 2G3Q)[110]. Horizontal bars at the top of (a) and (b) indicate elements of secondary structure; β-strands are colored black and helices are blue.

6.3 Interaction of Ede1 UBA with Lys48- and Lys63-linked Ub_2

6.3.1 Experimental background

To determine the UBA-binding surface on the distal or proximal Ub in Ub_2, 0.35 and 0.6 mM ^{15}N-labeled Lys48-linked Ub_2 samples (Ub_2-D or Ub_2-P, respectively) were titrated with increasing amounts of unlabeled Ede1 UBA (from a stock solution). Titration for the proximal and distal Ub continued up to Ede1 UBA:Ub_2 molar ratio of 4. Similar studies were performed on 0.5 and 0.75 mM ^{15}N-labeled Lys63-linked Ub_2-D and Ub_2-P samples up to a Ede1 UBA:Ub_2 molar ratio of 2.9 and 4, respectively. Two sets of the reverse titration experiments were performed. The first set was at lower concentrations, with 0.2 mM and 0.4 mM ^{15}N-labeled Ede1 UBA samples titrated with increasing amounts of unlabeled Lys63- and Lys48-linked Ub_2 to [Ub_2]/[Ede1 UBA] = 2.9 and 5.5, respectively. The second set was at higher concentrations, with 0.6 and 0.61 mM ^{15}N-labeled UBA titrated with Lys63- and Lys48-linked Ub_2s, respectively, up to [Ub_2]/[Ede1 UBA] = 3.5.

6.3.2 Di-ubiquitin chains bind up to two UBAs

The stoichiometry of the UBA:Ub_2 complexes was determined using ^{15}N longitudinal (T_1) relaxation time measurements performed under fully saturating conditions. In the titrations with low starting Ub_2 concentrations (0.33 and 0.5 mM, respectively, for Lys48-Ub_2-P and Lys63-Ub_2-D), the ^{15}N T_1 averaged over residues belonging to Ub core was 894 ± 97 ms for Lys48-linked Ub_2, corresponding to a molecular weight range of 21-27 kDa, compared with 24.7 kDa expected for a 1:1 UBA:Ub_2 complex (Table 6.1). For Lys63-linked Ub_2 the ^{15}N T_1 was 898 ± 56 ms,

corresponding to a molecular weight of 22-26 kDa, compared with 22.3[a] kDa expected for a 1:1 UBA:Ub_2 complex, but also close to 27.2[a] kDa expected for a 1:2 UBA:Ub_2complex, suggesting that there may be a mixture of singly and doubly UBA-bound Lys63-linked Ub_2s. In the titrations starting with higher Ub_2 concentrations (0.61 and 0.75 mM, for Lys48-Ub_2-D and Lys63-Ub_2-P, respectively) the average ^{15}N T_1 for Lys48-linked Ub_2 fully saturated with UBA was 1299 ± 167 ms, corresponding to a molecular weight range from 31 to >40 kDa, while the average ^{15}N T_1 for Lys63-linked Ub_2 was 1249 ± 64 ms, corresponding to a molecular weight range of 33-37 kDa, compared with 32.4 kDa expected for a 2:1 UBA:Ub_2 complex. The results of these independent measurements thus indicate that Ub_2 linked via Lys48 and Lys63 can bind up to two Ede1 UBA domains. The discrepancy between the T_1 values (hence the apparent molecular weights) measured at lower and higher concentrations could indicate a true change in the binding stoichiometry with the concentration or could merely reflect the fact that a greater fraction of the protein is in the bound state at higher concentrations.

Similar conclusions were obtained from ^{15}N T_1 measurements in Ede1 UBA in the presence of Ub_2 where the average ^{15}N T_1 for UBA fully saturated with Lys48-linked Ub_2 was 1007 ± 51 ms, corresponding to a molecular weight range from 26 to 29 kDa, while the average ^{15}N T_1 for UBA saturated with Lys63-linked Ub_2 was 1132 ± 52 ms, corresponding to a molecular weight range of 30-33 kDa.

Table 6.1: ^{15}N T1 values and the estimated stoichiometries of Ub_2:UBA complexes at various experimental conditions.

Sample [Ratio of final concentrations (mM)]	^{15}N T_1 (ms)	Apparent molecular mass range (kDa) corresponding to the ^{15}N T_1 value	Expected molecular mass (kDa) for this stoichiometry	# of UBAs bound
Lys48-linked Ub_2:UBA [0.29:0.88]	921 ± 59	23-27	22.3[a] -27.2[b]	1-2
Lys48-linked Ub_2:UBA [0.40:1.19]	852 ± 88	19-26	22.3[a] -27.2[b]	1-2
Lys63-linked Ub_2:UBA [0.40:1.61]	834 ± 145	18-27	22.3[a] -27.2[b]	1-2
Lys63-linked Ub_2:UBA [0.25:0.71]	898 ± 56	22-26	22.3[a] -27.2[b]	1-2
Lys48-linked Ub_2:UBA [0.20:0.86]	894 ± 97	21-27	24.7	1
Lys48-linked Ub_2:UBA [0.46:1.39]	1278 ± 233	29-40	32.4	2
Lys63-linked Ub_2:UBA [0.40:1.61]	1252 ± 112	32-38	32.4	2
UBA: Lys48-linked Ub_2 [0.27:0.94]	1007 ± 51	26-29	32.3	2
UBA: Lys63-linked Ub_2 [0.34:0.69]	1132 ± 52	30-33	32.3	2

[a] UBA samples used for these measurements were GST-cleaved constructs.
[b]The expected molecular weight if a second UBA bound to these complexes is 27.2 kDa.

6.3.3 UBA-binding surfaces on Lys48-linked Ub_2

Using segmentally ^{15}N-labeled Lys48-linked Ub_2 chains, we monitored separately perturbations induced by UBA binding in the proximal and distal Ub units of Ub_2 (Fig. 6.2a,b). Significant CSPs observed in and around the hydrophobic residues in strands β3-β5, and the β1/β2 loop are similar to those in monoUb (Fig. 6.1a,c) and suggest that the interaction is primarily hydrophobic, similar to previously described UBA:Ub complexes [117]. Additionally, significant signal attenuations were observed in the β3/β4 turn and

strand β4. Overall, the magnitude of the CSPs in the distal Ub is about twice as large as the perturbations in the proximal Ub. The differences in the overall CSP profiles between the two domains indicate that the mode of interaction may differ between the two Ubs in Lys48-linked Ub_2. While the largest CSPs in the distal Ub were in β3, the largest CSPs in the proximal Ub were observed in Thr7 and Leu8 in the β1/β2 loop and Val70 (β5), as well as in Arg72 and Leu73 located at the free C-terminus. Significant signal attenuations were also detected in strands β3 and β4 of the proximal Ub indicative of slower exchange regimes hence possibly stronger binding to these sites. Upon addition of UBA, Leu71 is completely attenuated, and significant perturbations are observed in Arg72 and Leu73 in both domains, implicating the C-terminal portion of β5 as an important interaction site. Notably, Val70 is not significantly perturbed or attenuated in the distal Ub (as in the case of monoUb), however it is strongly perturbed in the proximal domain ($\Delta\delta$~0.16ppm).

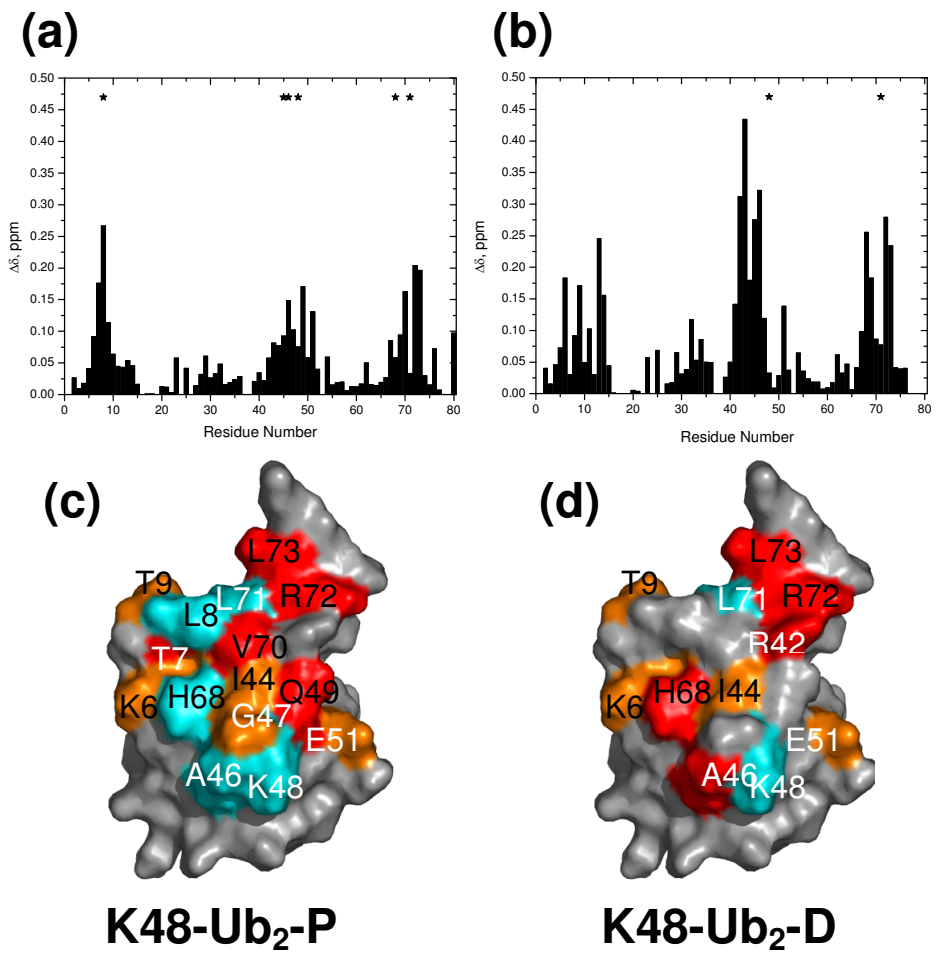

Figure 6.2 NMR mapping of the Ede1 UBA-binding surface on the Ub units in Lys48-linked Ub_2. The top row shows CSPs at saturation as a function of the residue number for the (a) proximal and (b) distal Ubs in Lys48-linked Ub_2. Asterisks mark residues with significant signal attenuation (>60%). (c,d) Surface representations of Ub with the sites showing significant CSPs colored as follows: (c) $\Delta\delta \geq 0.15$ ppm (red), $0.15 > \Delta\delta \geq 0.075$ (orange) (d) $\Delta\delta > 0.2$ ppm (red), 0.2 ppm $> \Delta\delta >$ 0.125 ppm (orange). Residues with signal attenuation > 60% are colored cyan. Also shown in (a) (at position 80) is the CSP of the ε-amine of Lys48-linked Ub_2-P.

Fitting the titration curves for the distal Ub to a 2:1 (UBA:Ub_2) stoichiometry model (Eq. 4, Section 3.3.2) resulted in the microscopic dissociation constant of 64 ± 22 μM (Fig. 6.3a, red curves). The CSPs observed in the proximal Ub did not fit well to this model; instead, they fit better to Eq. 3 (Section 3.3.2) (1 UBA per Ub_2), yielding a K_d of 88 ± 58 μM (Fig. 6.3b, red curves). The latter likely reflects the complexity of ligand

binding to Lys48-linked Ub_2, which requires a conformational transition (interface opening) to provide access to the hydrophobic patches on the two Ub units. Thus a simplified, noncooperative model of independent UBA-binding sites on Ub_2 might not be adequate in this case. Note also that the T_1 measured at saturation conditions at the end of this titration does correspond to a single UBA bound to Ub_2.

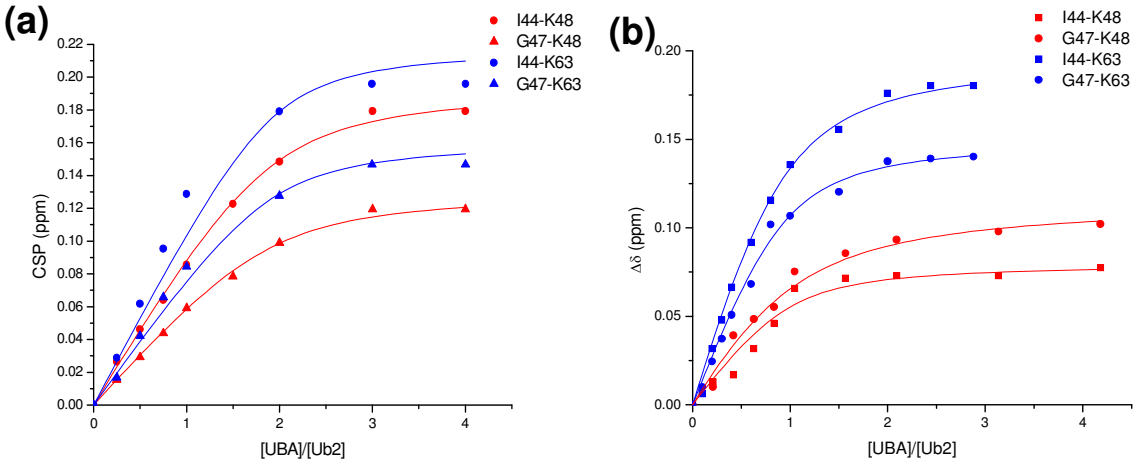

Figure 6.3 Comparison of Ede1 UBA binding to Lys48- and Lys63-linked Ub_2. Shown are NMR titration curves presenting CSPs as a function of the UBA:Ub_2 molar ratio for Ub residues Ile44 and Gly47 in Lys48- (red), and Lys63-linked Ub_2 (blue). Panels (a) and (b) correspond to titrations performed with different starting Ub_2 concentrations: $[Ub_2] \geq 0.6$mM (a) and $[Ub_2] \leq 0.5$ mM (b).

6.3.4 UBA's surface involved in binding to Lys48-linked Ub_2

In a reverse titration assay, unlabeled Lys48-linked Ub_2 was titrated into a solution containing ^{15}N-labeled UBA. The magnitude of the perturbations increased with Ub_2 concentration and saturated at $[Ub_2]/[UBA] > 2$ (Fig. 6.4a), however the increase in CSP magnitudes at low $[Ub_2]/[UBA]$ was atypically shallow. A comparison of the CSP map with that in monoUb/Ede1 UBA interaction reveals a very similar CSP pattern, with the largest perturbations in the α1/α2 loop and the C terminus of α3 (Fig. 6.5a,c). Intriguingly, significant signal attenuations were observed in Lys1342 and His1362

located on the "back" side of UBA's surface that is not involved in binding to monoUb (Fig. 6.5b,d). Strong signal attenuations (>50%) and slow exchange behavior were observed in residues Phe1354 (α1/α2 loop), Ala1372, Leu1377, and Ala1381 (α3) indicative of slow off-rates on the NMR timescale. Since the titration curves were not hyperbolic-like (Fig. 6.4b) – likely reflecting the complex nature of ligand binding to Lys48-linked chains, they could not be fit to standard binding models. Due to this complication, in order to obtain a direct comparison of UBA binding to chains of both types of linkages, ^{15}N UBA from the same stock was titrated with Lys63-linked Ub_2 at nearly identical conditions (temperature, pH, buffer, protein/ligand concentrations). From comparison of the resulting binding curves (Fig. 6.4c) it is obvious that Ede1 UBA binds Lys63-linked Ub_2 tighter than Lys48-linked Ub_2 (see below).

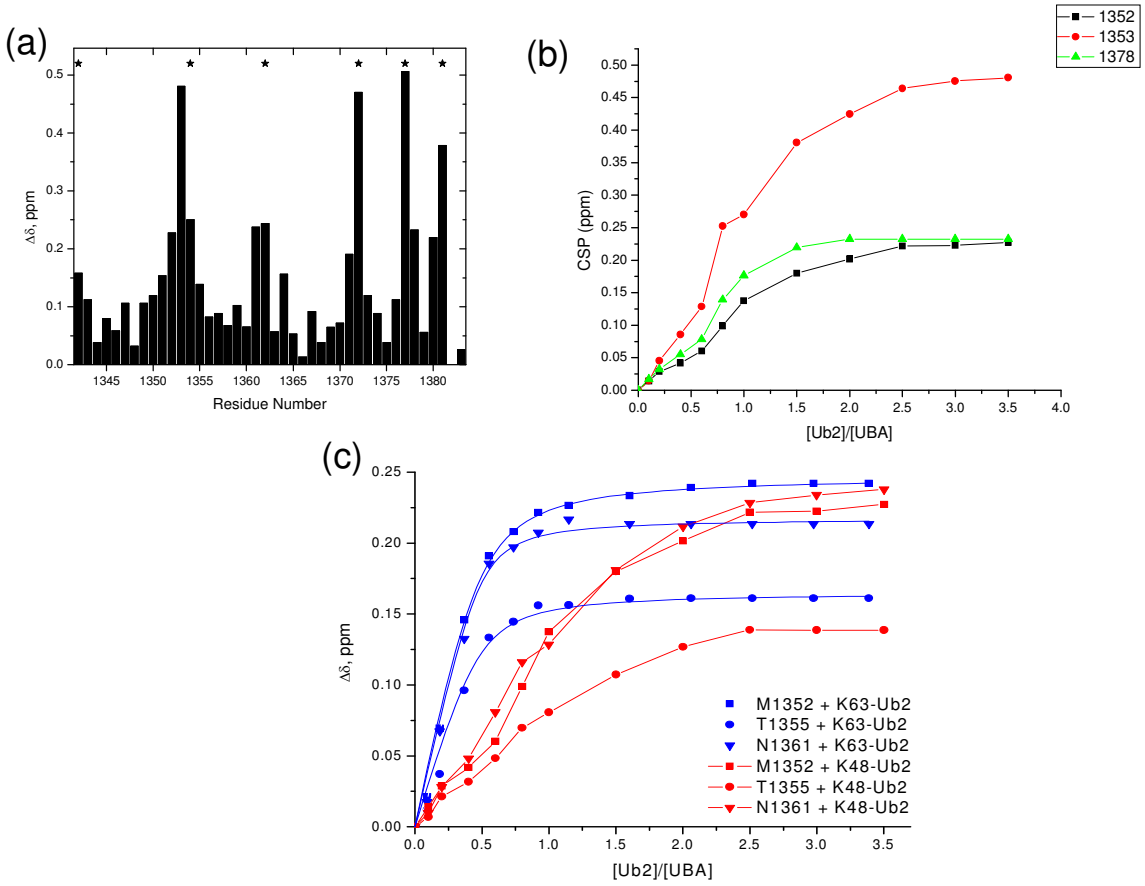

Figure 6.4 NMR characterization of Ede1 UBA residues affected by binding to Lys48- and Lys63-linked Ub_2s. (a) CSPs and attenuations as a function of residue number for UBA bound to Lys48-linked Ub_2. Sites showing significant signal attenuation (>60%) due to intermediate or slow exchange are marked by asterisks. The CSP shown at #1383 is for the indole NH of Trp1368. (b) titration data for CSPs of UBA residues Met1352, Gly1353 and Leu1378 upon addition of Lys48-linked Ub_2 (c) comparison of NMR titration curves presenting chemical shift perturbations (for UBA residues Met1352, Thr1355, and Asn1361) titrated with Lys48- (red), and Lys63-linked Ub_2 (blue) plotted as a function of the Ub_2:UBA molar ratio.

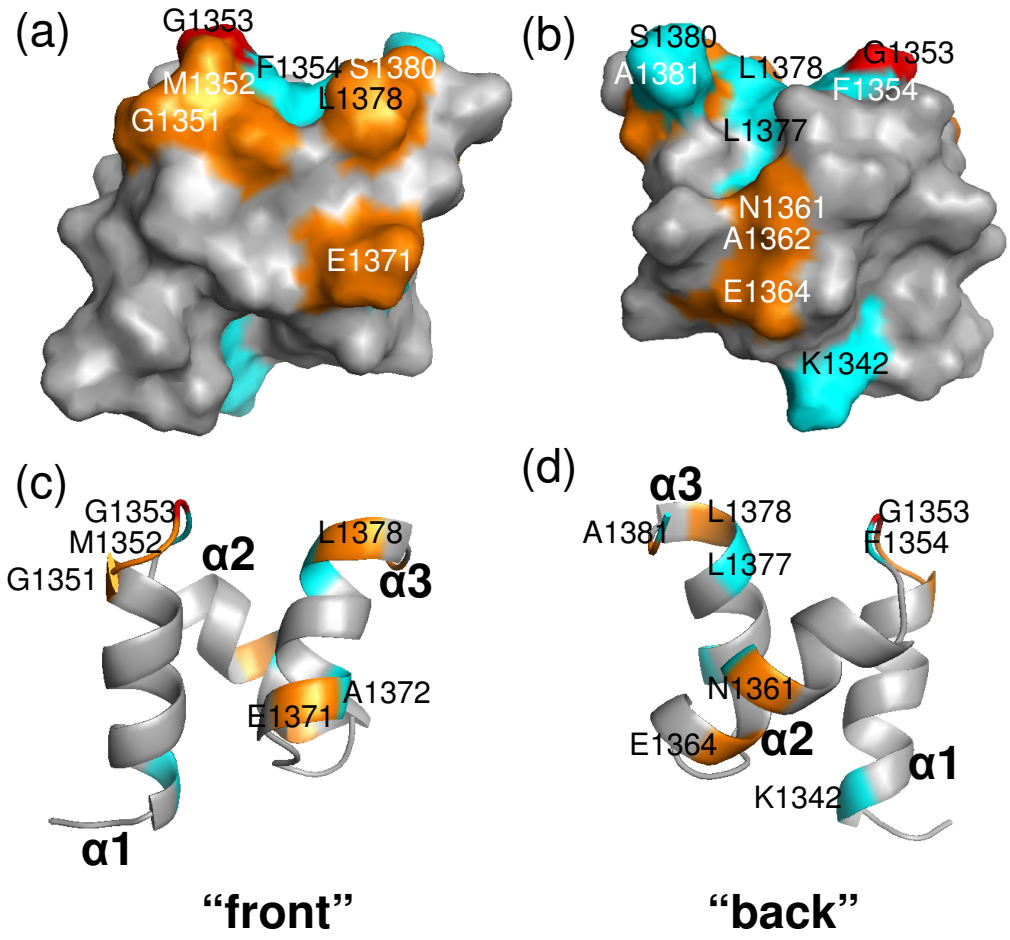

Figure 6.5 Surface mapping of the Lys48-linked Ub_2 binding surface on Ede1 UBA. From the CSPs and attenuations shown in Figure 6.4, the binding surface of UBA was mapped. The coloring is as follows: $\Delta\delta > 0.3$ ppm (red), 0.3 ppm $> \Delta\delta > 0.15$ ppm (orange). Signals attenuated >60% are colored cyan. Cyan coloring is selected over red in residues showing both large CSPs and significant attenuations. The denotations “front” and “back” signify the surface of UBA which faces towards (front) or away (back) from Ub in the monoUb/UBA complex (Protein Data Bank code 2G3Q) [110].

6.3.5 UBA-binding surfaces on Lys63-linked Ub_2

Similar experiments were performed to determine the binding surfaces on Lys63-linked Ub_2. The pattern and magnitude of CSPs, as well as the signal attenuations, were very similar between the distal and proximal domains of Ub_2 (Fig. 6.6a,b). In addition, the CSP profile is also very similar to UBA-bound states of both monoUb and the distal

Ub of Lys48-linked Ub_2, but distinct from the CSP pattern observed for the proximal Ub of Lys48-linked Ub_2.

It is noteworthy that immediately upon addition of UBA, the signal of Lys48 attenuates almost completely, and there is a large CSP in Gln49 of the distal Ub. These observations, as well as large CSPs and attenuations detected in Phe45 and Ala46, implicate the β3/β4 loop and β4 as important UBA-interacting sites in Lys63-linked Ub_2. Interestingly, significant CSPs were observed in Arg72 and Leu73 in both domains, indicating that these residues interact with Ede1 UBA not only in the context of the Ub-Ub linker, but also as part of the free C-terminus of Lys63-Ub_2. The observed pattern of perturbations very closely mimics that for monoUb, suggesting that Ede1 UBA binds each Ub in Lys63-linked Ub_2 in a mode similar to the monoUb:UBA interaction. Fitting the titration data for the proximal Ub to Eq. 4 (Section 3.3.2) yielded a microscopic dissociation constant of 55 ± 19 μM (Fig. 6.3a, blue curves), in agreement with the corresponding K_d values for UBA binding to monoUb as well as to the distal Ub in Lys48-linked Ub_2 (Table 6.2). This is not unexpected, given the similarity of the perturbation patterns which suggest that these Ub domains bind Ede1 UBA in a similar mode. Surprisingly, the same model does not fit well the binding curves for the distal Ub in Lys63-linked Ub_2; instead, model 1 was a better fit, although with very similar microscopic K_d values (48 ± 13 μM) (Fig. 6.3b, blue curves). Note in this regards that, as in the abovementioned case of the proximal domain in Lys48-Ub_2, the T_1 values measured at the endpoint of the titration correspond to one UBA bound per chain.

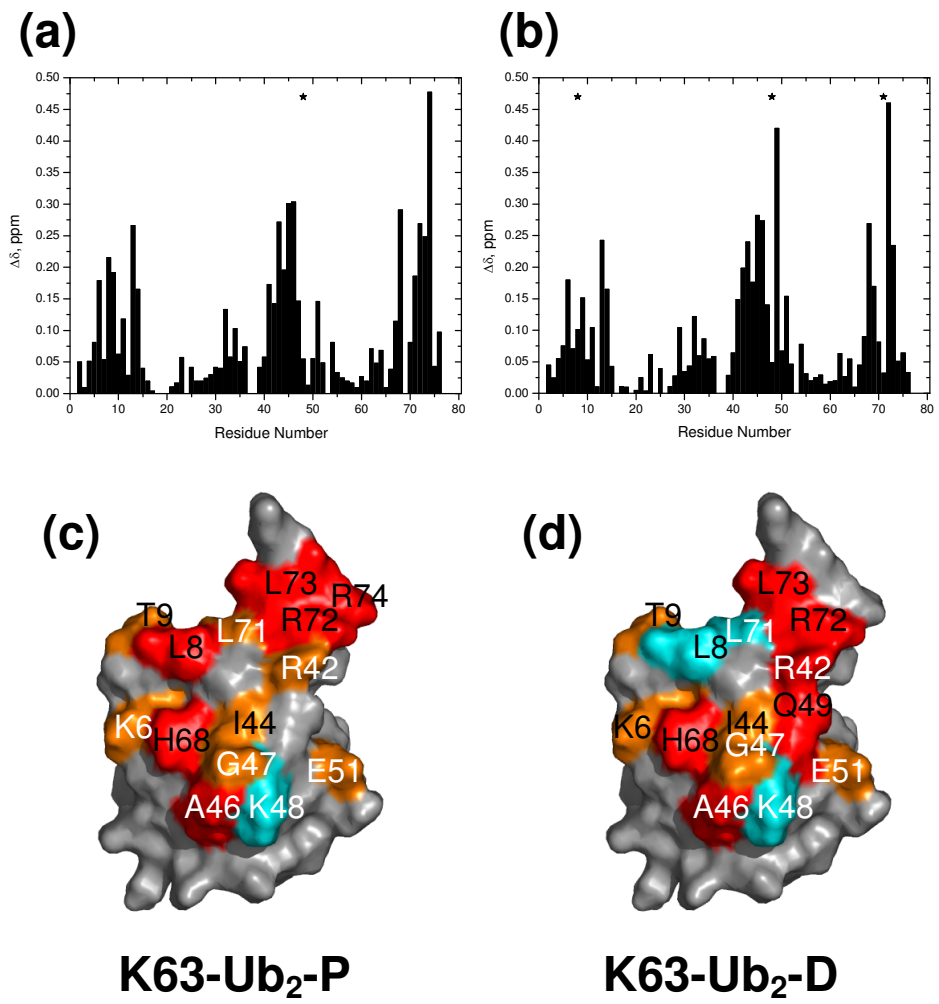

Figure 6.6 NMR mapping of the Ede1 UBA-binding surface on the Ub units in Lys63-linked Ub_2. The top row shows CSPs at saturation as a function of the residue number for the (a) proximal and (b) distal Ubs in Lys63-linked Ub_2. Asterisks mark residues with significant signal attenuation (>60%). (c,d) Surface representations of Ub with the sites showing significant CSPs colored as follows: $\Delta\delta > 0.2$ ppm (red), 0.2 ppm > $\Delta\delta$ > 0.125 ppm (orange). Residues with signal attenuation > 60% are colored cyan.

6.3.6 Binding surface on UBA in complex with Lys63-linked Ub_2

To identify the binding surface on UBA, unlabeled Lys63-linked Ub_2 was titrated into a solution containing ^{15}N labeled UBA. The magnitude of the perturbations increased with Ub_2 concentration and saturated at [Ub_2]:[UBA] ~1 (Fig. 6.7a). Importantly, the

increase in CSP magnitudes was steeper in this titration compared with the Lys48-Ub_2 titration. The strongest CSPs were in the α1/α2 loop and in α3, while significant CSPs and signal attenuations were also detected in α2 (Fig. 6.7d,e). A comparison of the CSPs with those from UBA titration with monoUb (Fig. 6.1b) and Lys48-linked Ub_2 (Fig. 6.4a) reveals a generally similar perturbation map in all three cases. The only exception is helix α2 (the "back-side" of Ede1 UBA), where binding to Lys63-Ub_2 caused stronger perturbations, particularly pronounced in Glu1364 and Lys1365 (Fig. 6.7c,e). The apparent K_d value for UBA:Lys63-Ub_2 binding determined by fitting the titration curves in Fig. 6.4c assuming a single Ub_2-binding site on the UBA was 48 ± 12 μM, in agreement with the K_ds determined from reverse NMR titrations (Table 6.2).

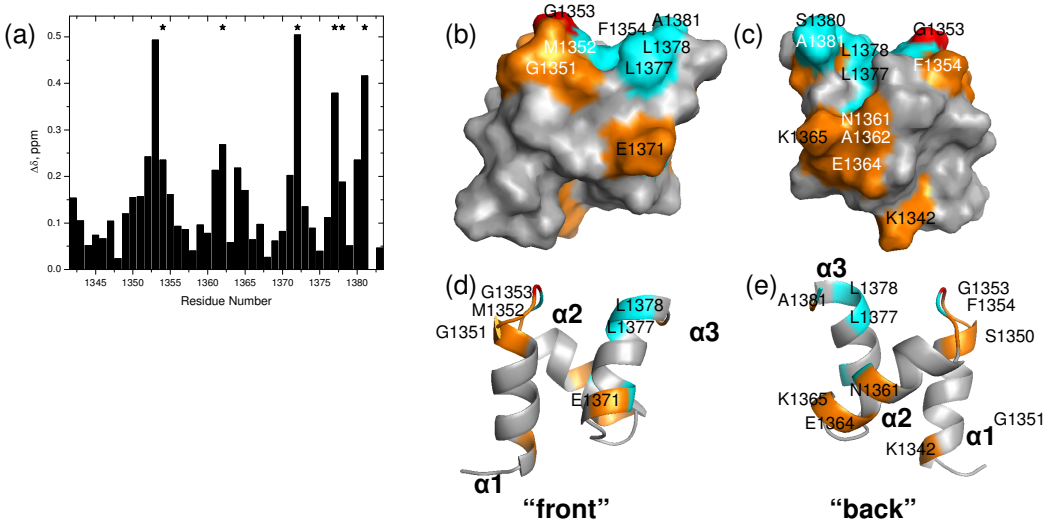

Figure 6.7 Surface mapping of the Lys48-linked Ub_2 binding surface on Ede1 UBA. (a) CSPs and attenuations as a function of residue number for UBA bound to Lys63-linked Ub_2. Sites showing significant signal attenuation (>60%) due to intermediate or slow exchange are marked by asterisks. The CSP shown at #1383 is for the indole NH of Trp1368. The surface of UBA is colored based on CSPs and signal attenuations in (b-e). The coloring is as follows: $\Delta\delta > 0.3$ ppm (red), 0.3 ppm $> \Delta\delta > 0.15$ ppm (orange). Cyan coloring is selected over red in residues showing both large CSPs and significant attenuations. The denotations "front" and "back" signify the surface of UBA which faces towards (front) or away (back) from Ub in the monoUb/UBA complex (Protein Data Bank code 2G3Q).

A direct comparison of the binding curves for residues Met1352, Thr1355, and Asn1361 of UBA upon titration with Lys48- and Lys63-linked Ub_2 (Fig. 6.4c) illustrates the difference in Ede1 UBA binding to these chains. These assays were performed at almost identical concentrations and the same buffer/temperature conditions. Because the CSPs are directly proportional to the fraction of UBA in the bound state, the fact that reaching the saturation requires less Lys63-linked Ub_2 compared to Lys48-linked Ub_2 clearly indicates the UBA's binding preference for the Lys63-linked chain. This finding is in agreement with the previously reported linkage selectivity of Ede1 UBA [115].

Table 6.2 Estimated dissociation constants.

Sample	K_d [a] (μM)
^{15}N UBA + Ub	83 ± 9 [110]
^{15}N Lys48-linked Ub_2-D + UBA	64 ± 22 [b]
^{15}N Lys48-linked Ub_2-P + UBA	88 ± 58 [e]
^{15}N UBA + Lys48-linked Ub_2	N/A
^{15}N Lys63-linked Ub_2-P + UBA	55 ± 19 [c]
^{15}N Lys63-linked Ub_2-D + UBA	48 ± 13 [d]
^{15}N UBA + Lys63-linked Ub_2	41 ± 21 [f]

[a] The numbers reported represent mean ± standard deviation over several residues specified below.
[b] Residues included: 5,6,11,13,14,32,41,42,44-47,51,54,62,67,68,70,73; using Eq. 4 (2 UBA bound model).
[c] Residues included: 6,13,14,32, 44-47, 67-70,73; using Eq. 4 (2 UBA bound model).
[d] Residues included: 6,9,11,13,14,29,32, 41,43,44,46,47,49,51,62,67-70,73; using Eq. 3 (1 UBA bound model).
[e] Residues included: 6,7,9,10,29,43,44,45,47,48,49,51,67,69,70,72,73; using Eq. 3 (1 UBA bound model).
[f] The apparent K_d for binding of Lys63-Ub_2 to Ede1 UBA, not the microscopic K_d for binding to individual Ub domains; using Eq. 2 (1 UBA bound model).

6.4 Exploring the Ub_2:UBA complexes using paramagnetic spin labeling

Site-specific spin labeling was used to gain structural insights into and model the UBA:Ub_2 complexes. A paramagnetic spin label (SL) was linked to UBA's sole natural cysteine (Cys1366), and the paramagnetic relaxation rate enhancement (PRE) was measured for Ub domains at saturation ($[Ub_x]:[UBA] \geq 3$) (described in Section 3.4). Attenuations in Ub's signal intensities observed in the presence of SL independently confirmed the formation of Ub_x/UBA complexes and identified residues in close proximity to SL.

As a control, we performed PRE measurements on monoUb in complex with spin-labeled UBA; the observed attenuations agreed well with the NMR structure of the complex [110] (Fig. 6.8a). The PRE patterns in the distal domains of both Lys48- and Lys63-linked Ub_2s are in good agreement with the control, indicating that UBA binds to each of these Ub moieties in the same orientation as it does to monoUb (Fig. 6.8b,c,d). Interestingly, however, the PREs in the proximal domain of Lys63-linked Ub_2 revealed that in addition to the sites expected to show signal attenuations as in the control, signals of some residues located on the Ub surface near Lys63 (the site of the isopeptide linkage) were also attenuated (Fig. 6.8b). Our model of the complex of two Ede1 UBA domains bound to Lys63-linked Ub_2 shows that these residues lie in close proximity to the SL on the UBA bound to the distal domain. As a result, areas on the proximal domain of Lys63-linked Ub_2 are also affected by this SL. A similar effect was observed previously in Lys63-linked Ub_2 bound to two UBA-2 domains of hHR23A [161].

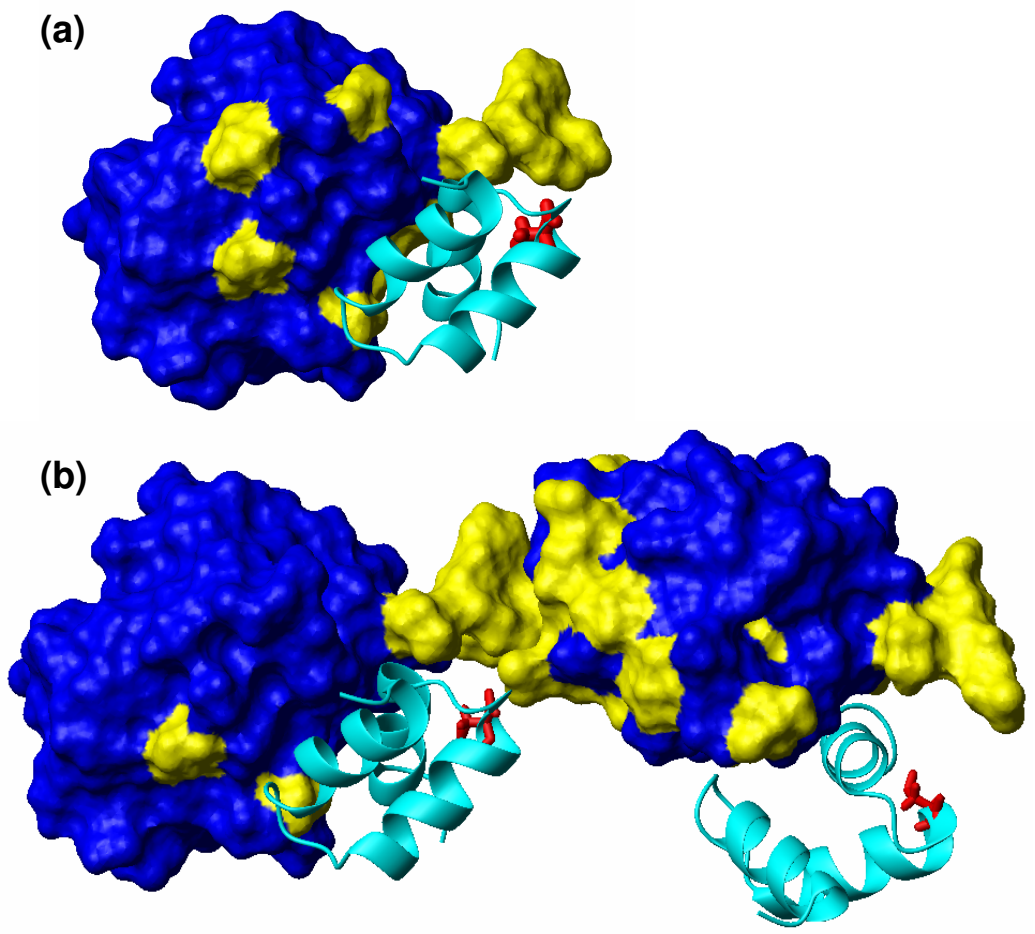

Figure 6.8 Structural insights from spin labeling experiments into UBA-Ub$_x$ interactions. The paramagnetic spin label MTSL was attached to Cys1366 on UBA (represented by red sticks). Residues reporting PRE >50% on Ub moieties in (a) monoUb, (b) Lys63-linked Ub$_2$, and (c,d) Lys48-linked Ub$_2$ are shown in yellow, while residues colored blue are not significantly affected. These structures were obtained assuming that each UBA binds to the corresponding Ub unit in the chain in the same way/orientation as to monoUb (PDB code 2G3Q) [110] and using the structure of free Lys63-linked Ub$_2$ [161] and of Lys48-linked Ub$_2$ in its complex with UBA-2 (PDB code 1ZO6) [117] as structural models of the open conformations of the chains. The resulting structures were obtained by direct superimposition of ubiquitin atoms in the UBA:Ub complex. It should be mentioned that, based on the NMR analysis of the equilibrium dynamics in Lys48-linked Ub$_2$, the relative orientation of the two Ub domains in the open state of free Ub$_2$ at pH6.8 is similar to that in the Ub$_2$:UBA-2 complex [82, 162], therefore we used this structure as a model for the open state of K48-Ub$_2$. Models of UBA superimposed facing the (c) distal and (d) proximal Ub of Lys48-linked Ub$_2$ are shown. (e) Model of Lys48-linked Ub$_2$ in "fully open" conformation bound to two UBAs.

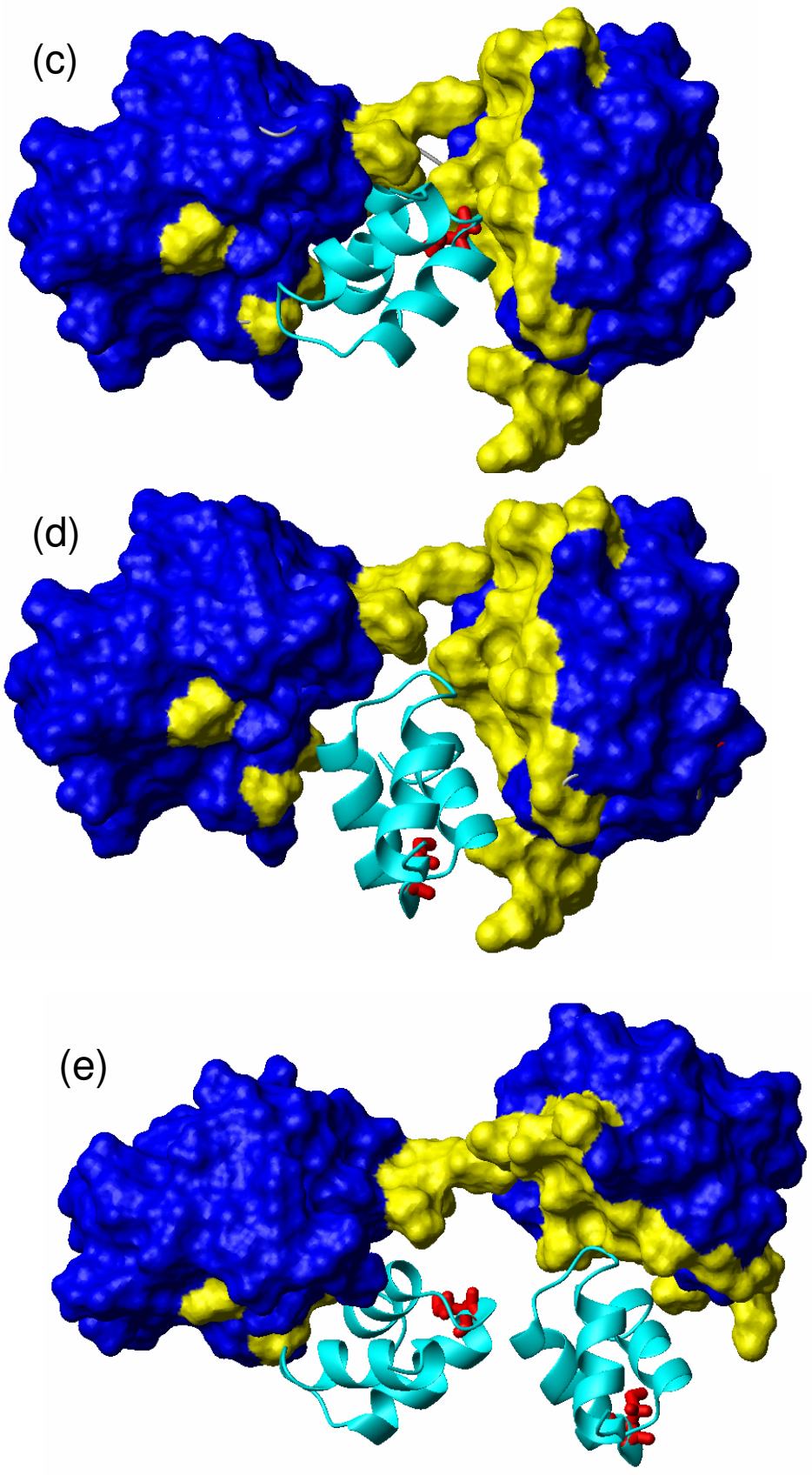
(c)
(d)
(e)

A different PRE pattern was observed in the proximal Ub of Lys48-linked Ub_2, where almost half of the residues showed strong signal attenuations (Fig. 6.9). Mapping these PREs on the proximal Ub in the Ub_2 structure showed that its entire hydrophobic surface facing the distal Ub was affected.

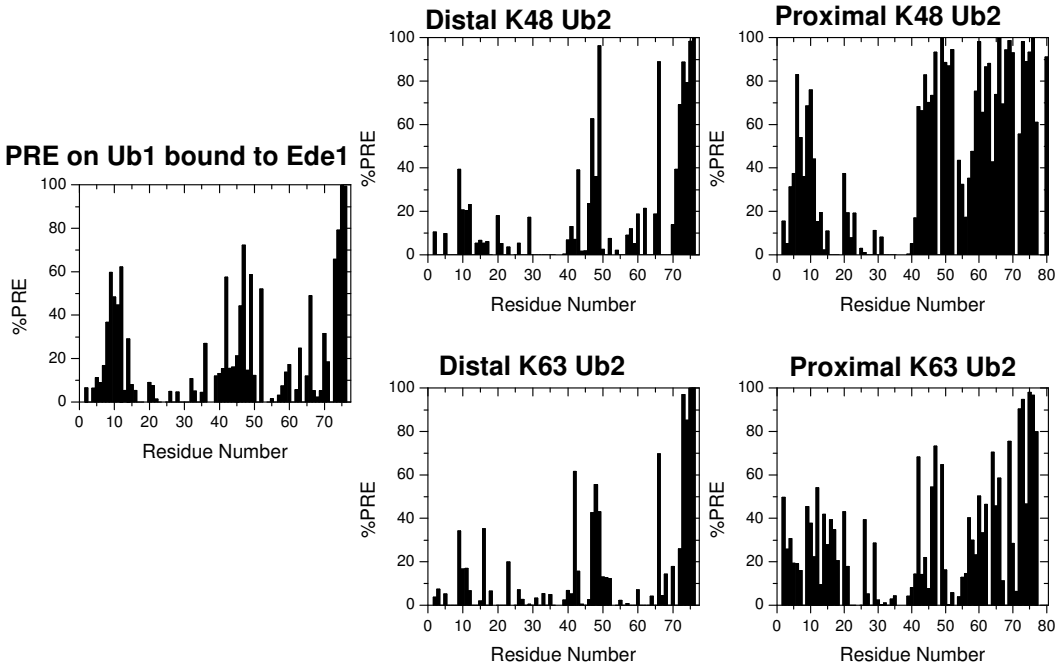

Figure 6.9 PREs in Ub due to the presence of SL on Ede1 UBA. The plot shows percent of signal attenuation $(1-I_{ox}/I_{red})*100\%$. Residues Leu8, Lys48, and Leu71 were attenuated due to the binding interaction, thus it was not possible to accurately measure their PRE effects in these experiments.

Since our T_1 relaxation data suggest that one UBA was bound to Lys48-linked Ub_2 in the experiments performed at lower concentrations and two UBAs were bound at higher concentrations, we propose structural models to describe the observed PREs in the context of a single UBA (Fig. 6.8c,d) and two UBAs (Fig. 6.8e) bound per chain, respectively. The structure models shown in Fig. 6.8c,d. illustrate how a single Ede1 UBA could be accommodated in two different orientations hydrophobic pocket in the

"partially open" conformation of Lys48-linked Ub_2. Mapping the PRE data for the proximal Ub of Lys48-linked Ub_2 shows that the entire hydrophobic surface of Ub is attenuated. In the sandwich-like Ub_2:UBA complex, if UBA is docked on the distal domain in the same orientation that it binds monoUb [110], the hydrophobic surface of the proximal Ub would be very close in space to the C-terminus of α2 where Cys1366-(SL) is located (Fig. 6.8c). This would explain both the PRE pattern in the distal Ub (similar to that in monoUb, Fig.6.8a, or the distal Ub in Lys63-Ub_2, Fig. 6.8b) and a wide affected area in the proximal Ub, including its flexible C-terminus, as well as the ε-amine of Lys48, involved in the isopeptide linker. Alternatively, if the UBA is bound to the proximal Ub in the same orientation that it binds to monoUb, the SL is oriented towards the C-terminal region of the proximal domain (Fig. 6.8d). This could explain the strong signal attenuations in the C-terminus, but not the strong PREs in the part of the proximal Ub close to the linker region, as well as the PREs in the distal Ub. Therefore, the structure shown in Fig. 6.8c appears as a plausible model of how a single Ede1 UBA could bind Lys48-linked Ub_2, although a less likely possibility shown in Fig. 6.8d cannot be fully excluded at this stage and could represent a minor conformation (perhaps in dynamic equilibrium with that in Fig. 6.8c). It should be mentioned here that while using UBA:monoUb structure to model the UBA's contacts with the distal Ub (Fig. 6.8c) can be justified by the similarity in the CSP patterns (as discussed above), there is less certainty whether the same applies to modeling UBA's contacts with the proximal Ub (Fig. 6.8c), given the differences in the CSP patterns.

The conformation of Lys48-Ub_2 observed in the Ub_2/hHR23A-UBA-2 complex (further referred as the "partially open" conformation) cannot accommodate two UBAs,

each bound to the hydrophobic patch on the corresponding Ub (Fig. 6.10). Thus, further opening of the Ub_2 conformation is required. An additional 70° rotation of one of the domains (as shown in Fig. 6.8e, 6.10b) appears sufficient for this purpose. When two UBAs are bound to a "fully open" conformation of Lys48-linked Ub_2 (Fig. 6.8e, 6.10b), our (hypothetical) model predicts that in addition to the PREs on each Ub caused by the SL on the UBA domain bound to it, one could also expect strong PREs in the proximal Ub near the Ub/Ub linker, which are caused by the SL on the UBA bound to the distal Ub. Our PRE data generally agree with such a model of the "fully open" Ub_2 conformation with two UBAs bound.

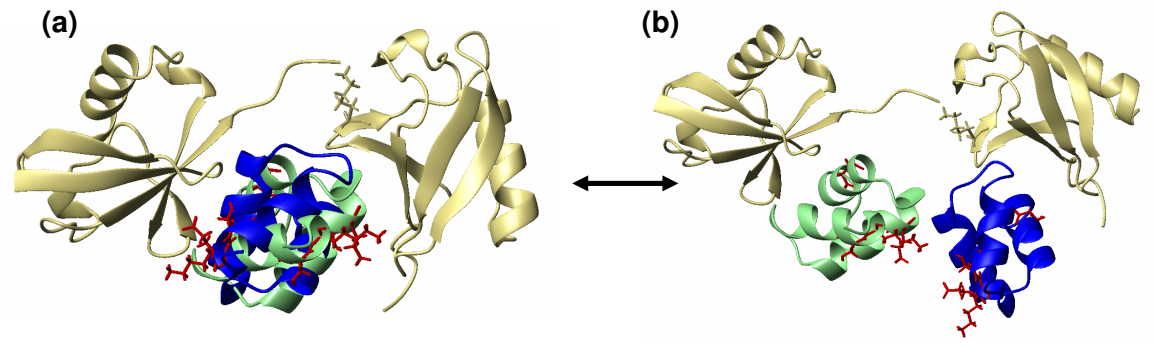

Figure 6.10 Lys48-linked Ub_2 has to open to accommodate 2 UBAs. Superimposition of 2 Ede1 UBAs onto (a) Lys48-linked Ub_2 bound to UBA-2 (PDB code 1ZO6) shows that 2 UBAs cannot be accommodated in the "partially open" conformation (b) Lys48-linked Ub_2 in a hypothetical "fully open" conformation can accommodate 2 UBAs. An additional 70° rotation of the proximal domain, and its bound UBA, was used to produce the conformation shown in (b). Ubiquitins are colored tan, UBAs are green and blue and the residues implicated in UBA aggregation are represented by red sticks (see below).

Additional experiments were performed to test the models proposed above for UBA's binding to Lys48-linked Ub_2. In this case, SL was attached to a cysteine introduced at position 12 (T12C) on the proximal Ub of Lys48-linked Ub_2 (Fig. 6.11), and PREs in Ede1 UBA were measured. Since these experiments were performed at

lower UBA concentrations (~100 μM), we expected PREs congruent with the single UBA-bound model (proposed in Fig. 6.8c,d). The PREs observed in UBA are clustered on one side of the molecule, which is facing Thr12 of the proximal Ub in the orientation shown in Fig. 6.11c. However, the alternative orientation in Fig. 6.11bc cannot be completely excluded, as in this orientation the attenuated side of UBA is also not far away from Thr12. Assuming a single UBA-bound model at low concentrations, these results suggest that the UBA could alternate between binding to the proximal and the distal Ub of Ub_2 in an orientation similar to UBA binding to monoUb.

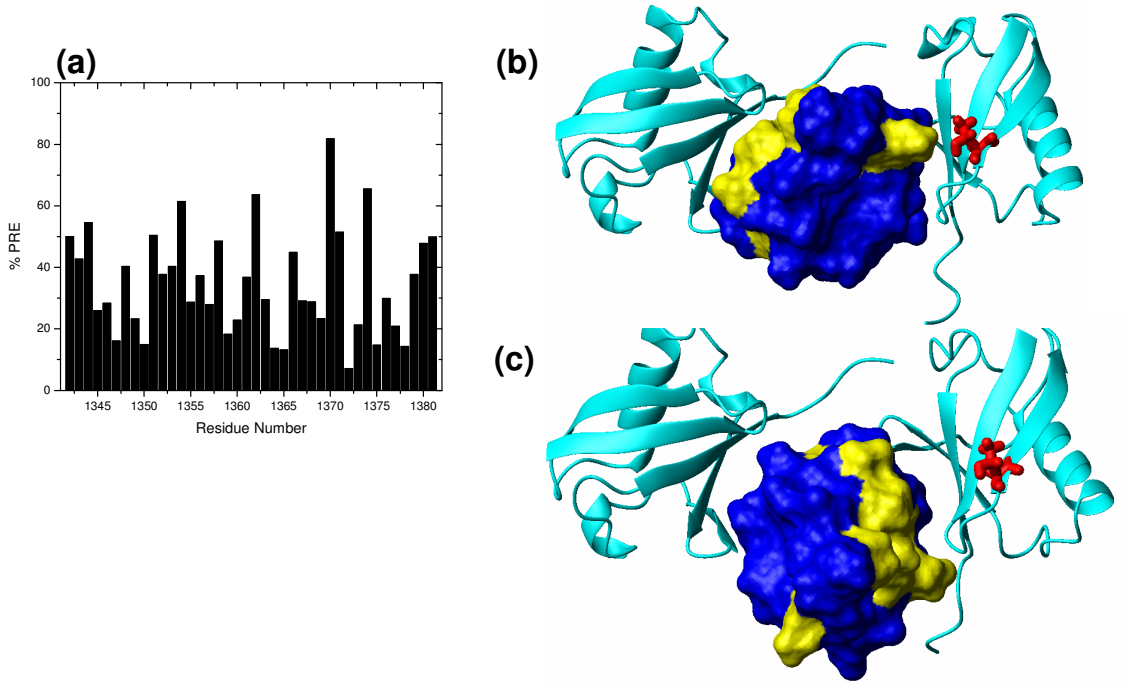

Figure 6.11 Results of spin labeling studies of UBA/Lys48-Ub_2 interactions. MTSL was attached to Cys12 on Ub (represented by red sticks). Residues sensing PRE >50% on UBA in complex with Lys48-linked Ub_2 are shown in yellow, while residues colored blue are not significantly affected. Structures in panels (b) and (c) correspond to UBA facing the distal and proximal Ub, respectively. These structures were obtained assuming that UBA binds to the corresponding Ub unit in the chain in the same way/orientation as to monoUb (PDB code 2G3Q) [110] and using the structure of Lys48-linked Ub2 in its complex with UBA-2 (PDB code 1ZO6) [117] as a structural model of the open conformation. The resulting structures were obtained by direct superimposition of ubiquitin atoms in the UBA:Ub complex. The plot shows percent of signal attenuation $(1-I_{ox}/I_{red})*100\%$.

6.5 Ede1 UBA self-associates in solution

A native gel mobility assay of Ede1 UBA at concentrations ranging from 0.07 to 0.45 mM is shown in Figure 6.12a. The gel indicates that UBA exists in the monomeric state at concentrations up to 0.14 mM and forms larger aggregates with increasing concentration. To independently validate this observation, longitudinal ^{15}N relaxation of free Ede1 UBA in solution was measured at increasing concentrations (Table 6.3). At 0.6 mM UBA, the ^{15}N T_1 averaged over residues belonging to the UBA core was 553 ± 27 ms, corresponding to a molecular weight range of 11.8-13.8 kDa, suggesting the presence of a mixture of UBA monomers (7.5 kDa) and dimers (15 kDa). At 1.6 mM the average ^{15}N T_1 was 585 ± 17 ms, corresponding to a molecular weight range of 13.4-14.7 kDa indicating the presence of UBA dimers as the predominant species, and in a 2.8 mM sample, the average ^{15}N T_1 was 728 ± 21 ms, corresponding to a molecular weight range of 18.1-19.5 kDa, suggesting a mixture of UBA dimers and trimers. The results of these independent measurements indicate that UBA has a tendency to self-associate in solution at near neutral pH. The surfaces involved in the aggregation were identified by comparing HSQC spectra at high and low UBA concentrations (Fig. 6.12b). Mapping the perturbed sites (CSP> 0.04 ppm) onto the surface of UBA revealed that two sets of polar, mostly charged residues (Lys1342, Ser1343, Glu1364, Asp1379) located on opposite faces of the UBA are affected by aggregation (Fig. 6.12c), an indication of electrostatic interactions between the UBAs.

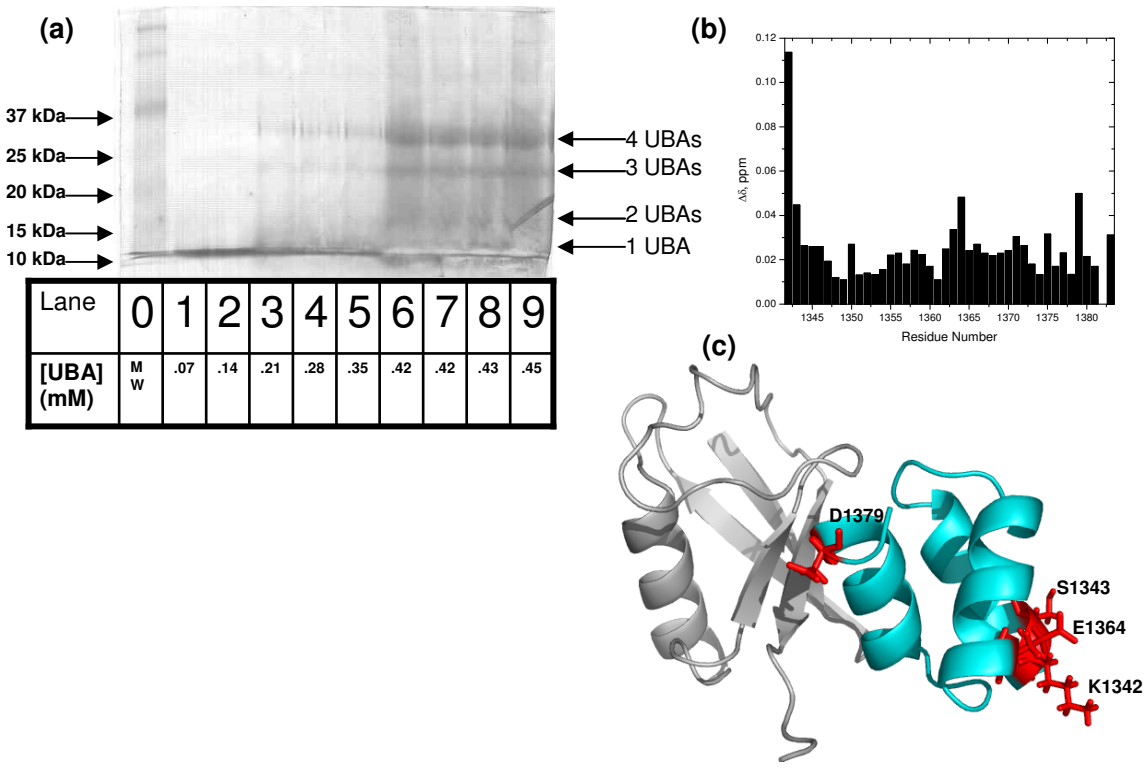

Figure 6.12 UBA of Ede1 has a tendency to self-associate. (a) Gel mobility assay of UBA at different concentrations. A nonreducing, nondenaturing polyacrylamide gel was loaded with increasing amounts of UBA, as indicated. (b) CSP plot of the difference in chemical shift positions between UBA at low concentration (0.4 mM) and high concentration (2.8 mM) (c) NMR mapping of the sites affected by aggregation on the structure of the monoUb:UBA complex is shown (Protein Data Bank code 2G3Q) [110]. UBA is colored cyan and residues perturbed by changes in UBA concentration are represented by red sticks ($\Delta\delta > 0.04$ ppm).

To further verify the electrostatic nature of the aggregation, we repeated the ^{15}N T_1 measurements at increasing salt concentrations. With only 20mM sodium phosphate, the observed average T_1 of Ede1 UBA at 1.62 mM was 585 ± 17 ms. Upon addition of 100mM NaCl, (dilution to 1.56 mM) the T_1 dropped to 521 ± 16 ms. At 200 mM NaCl (dilution to 1.50mM) the T_1 was 506 ± 15 ms, and reached 496 ± 16 ms at 300mM NaCl (1.45mM). The dilution effect did not play a major role here since at much lower concentration, 0.6mM, in the absence of NaCl the T_1 was 553 ± 27 ms. Comparing

chemical shift positions, there was a mostly uniform shift in most residues of about 0.02-0.025ppm. However, residues Ser1343, Leu1378, Asp1379 shifted more significantly (~0.04-0.045 ppm). Ser1343 and Asp1379 were implicated in aggregation by noticeable chemical shift differences between diluted and concentrated Ede1 UBA samples.

Table 6.3: Ede1 UBA self-association assay: ^{15}N T_1 values and the estimated apparent MW of Ede1 UBA at various protein and salt concentrations.

Sample	^{15}N T_1 (ms)	Molecular mass range (kDa) corresponding to the ^{15}N T_1 value
2.8mM UBA	728 ± 21	18.1-19.5
1.62mM UBA	585 ± 17	13.4-14.7
0.6mM UBA	553 ± 27	11.8-13.8
1.56mM UBA + 100mM NaCl	521 ± 16	11.0-12.3
1.50mM UBA + 200mM NaCl	506 ± 15	10.4-11.6
1.450mM UBA + 300mM NaCl	496 ± 16	9.9-11.3

6.6 Discussion

The CSPs and signal attenuations exhibited by both Ubs in Lys63-linked Ub_2 and the distal Ub of Lys48-linked Ub_2 closely resemble those observed in monoUb upon addition of Ede1 UBA. The overall level of CSPs in the proximal Ub of Lys48-linked Ub_2 is roughly 50% of the CSPs in the other Ub domains in Lys48- and Lys63-linked Ub_2s when bound to the UBA. While V70 shows no significant CSP or attenuation in monoUb, either Ub in Lys63-linked Ub_2 or the distal Ub of Lys48-linked Ub_2, it is significantly perturbed in the proximal Ub of Lys48-linked Ub_2. Smaller CSPs and increased slow and intermediate exchange behavior in the proximal Ub have been observed in complexes of UBA-2 of hHR23A [117] and UIM-2 of S5a [77] with Lys48-linked Ub_2. Thus, the differences between Ub units observed here are not unexpected, however they may signal a somewhat different mode of binding to this domain which

may be dictated by the conformation of Lys48-linked Ub_2 or may be affected by the involvement of Lys48 in the interdomain linker.

The similar signal attenuation and CSP patterns observed in monoUb, both Ubs of Lys63-linked Ub_2 and the distal Ub of Lys48-linked Ub_2 upon binding to Ede1 UBA suggest a similar mode of binding in all these events. This is further supported by our spin-labeling experiments. Since the SL's attachment site was located on α2 of UBA, which does not face Ub in the monoUb:UBA complex, the SL was a reliable, unperturbing probe for the orientation of UBA on Ub moieties because it only affects a specific subset of residues rather than attenuating the entire binding surface (if the SL were located on α1 or α3). Furthermore, since the presence of SL on the UBA bound to one Ub moiety may be within effective range of the other Ub in Ub_2 (e.g. UBA bound to distal domain affecting proximal domain), these studies provided useful information about UBA's orientation and binding to Ub_2. The similarity of PRE patterns observed in the distal domains of both Lys48- and Lys63-linked Ub_2 further confirms the conclusion that Ede1 UBA's binding to these domains is in a mode similar to its binding to monoUb. Meanwhile, the smaller magnitude of CSPs and contrasting profile of CSPs and signal attenuations on the proximal domain in Lys48-Ub_2, combined with the significantly stronger SL-induced PREs affecting a larger surface (indicative of much closer SL distance to this domain) provide strong evidence for a different mode of binding. However, the available data do not provide an unambiguous structural picture of this interaction. In fact, in our model of the "partially open" conformation of Lys48-linked Ub_2 the proximal Ub is close in space to the α2/α3 loop and the C-terminus of α2 of UBA where the SL is attached. However, the observed PREs are also satisfied by the

model of 2 UBAs bound to a Lys48-linked Ub_2 in a "fully open" conformation (Fig. 6.8e). Residues near the Ub/Ub linker in the proximal Ub are still within effective range of the SL on UBA bound to the distal Ub. Both structural scenarios could be possible, depending on the concentration of Ub_2 and UBA in solution, as evidenced by our ^{15}N T_1 relaxation data (Table 6.1).

Although the UBA domain of Ede1 shares high structural similarity with the UBA domains of hHR23A (rmsd ~ 0.8 Å) [110], the sequence homology is low. Helix α2 of Ede1 UBA is comprised of many charged and hydrophilic residues, with the side chains of Glu1357, Glu1358, His1360, Asn1361, Glu1364 and Lys1365 as well as α1 residues Lys1342, Ser1343 constituting the "back" surface of the UBA. Conversely, α2 of both hHR23A UBA domains is comprised of mostly hydrophobic residues.

Sequence alignment of the α2 helix segment:

Ede1 UBA	EEEAHNALEKCN
hHR23A UBA-2	ESLVIQAYFACE
hHR23A UBA-1	RERVVAALRASY

A comparison of the perturbations observed in UBA-1 (Fig. 6.13) and UBA-2 (see ref. [117]) of hHR23A when bound to monoUb versus Lys48-linked Ub_2, reveals that these UBAs were significantly perturbed on the "backside" (helix α2 and α2/α3 loop) in the presence of Lys48-linked Ub_2. In contrast, in the case of Ede1 UBA, a similar comparison of the CSPs (Fig. 6.1b vs. Fig. 6.4a) does not show significant differences, suggesting that the "backside" of Ede1 UBA is not involved in binding to Lys48-linked Ub_2. We did however detect an increase in the CSPs in α2's residues

Glu1364 and Lys1365 when UBA was bound to Lys63-linked Ub_2 (Fig. 6.7a). These observations are also supported by a comparison of the spectra of UBA bound to monoUb, Lys48-, and Lys63-linked Ub_2 (Fig. 6.14).

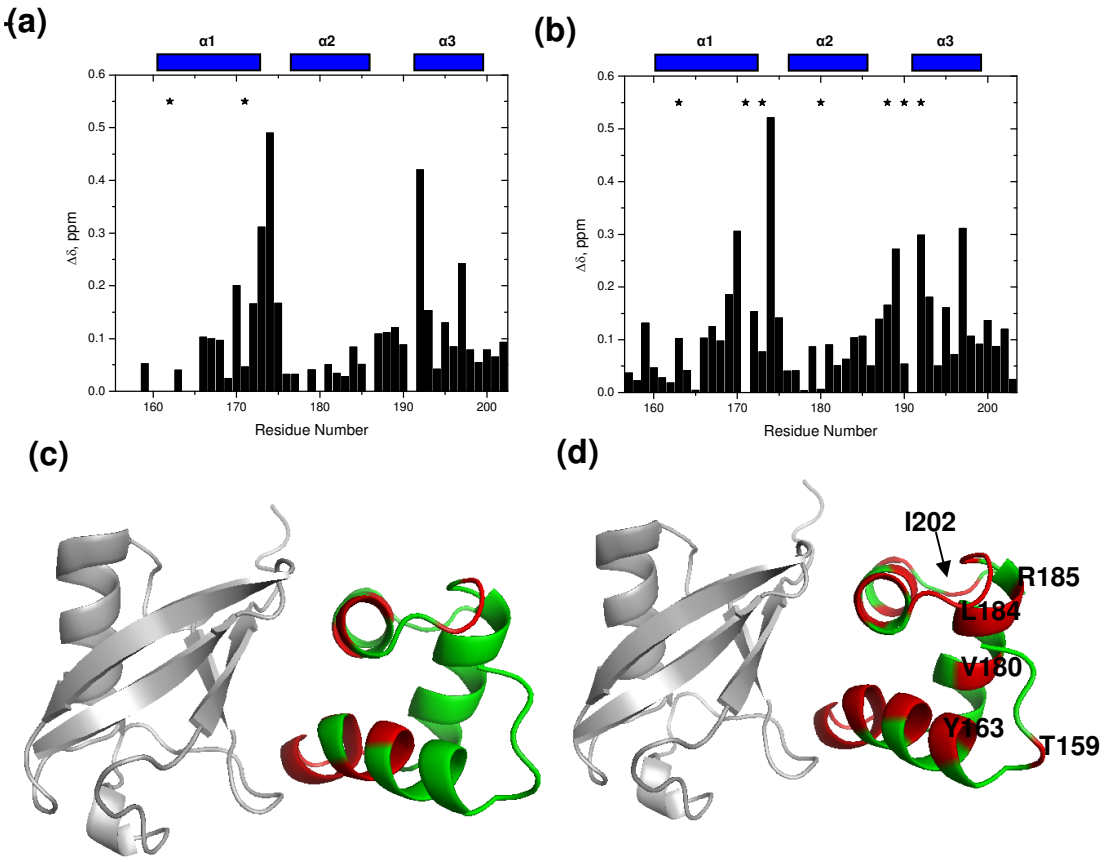

Figure 6.13 NMR mapping of residues of UBA-1 of hHR23A affected by binding to monoUb and Lys48-linked Ub_2. CSPs in UBA-1 at saturation with (a) monoUb and (b) Lys48-linked Ub_2, as a function of the residue number. Sites showing significant signal attenuation (>60%) due to intermediate or slow exchange are marked by asterisks. Horizontal bars at the top of (a) indicate elements of secondary structure. The CSPs and attenuations are mapped on the surface of UBA-1 when bound to (c) monoUb and (d) Ub_2. Residues with significant signal attenuation or $\Delta\delta > 0.1$ ppm are colored red. The structure of the monoUb:hHR23A UBA-1 complex shown is from [76]. The spectra were recorded by Bryan Dickinson.

The evidence presented in this study suggests that unlike hHR23A UBA-2 that binds to Lys48-linked Ub_2 in a different conformation than to monoUb, which allows it

to simultaneously interact with both Ub domains and with the Ub-Ub linker [117], the UBA domain of Ede1 has only one binding surface for Ub_2 regardless of linkage. While the additional interactions explain preferential binding of hHR23A UBA-2 to Lys48-linked Ub_2, there is no analogous basis for Ede1 UBA binding to Lys63-linked Ub_2 with higher affinity than Lys48-linked Ub_2. Direct involvement of Lys48 in the Ub-Ub linkage could also be a contributing factor that weakens UBA binding to the proximal Ub, and thus to Lys48-Ub_2. Since Leu1378 of UBA forms close contacts with Lys48 and Gln49 of monoUb [110], it is possible that the presence of the Gly76-Lys48 linkage interferes with them and thus weakens the UBA binding.

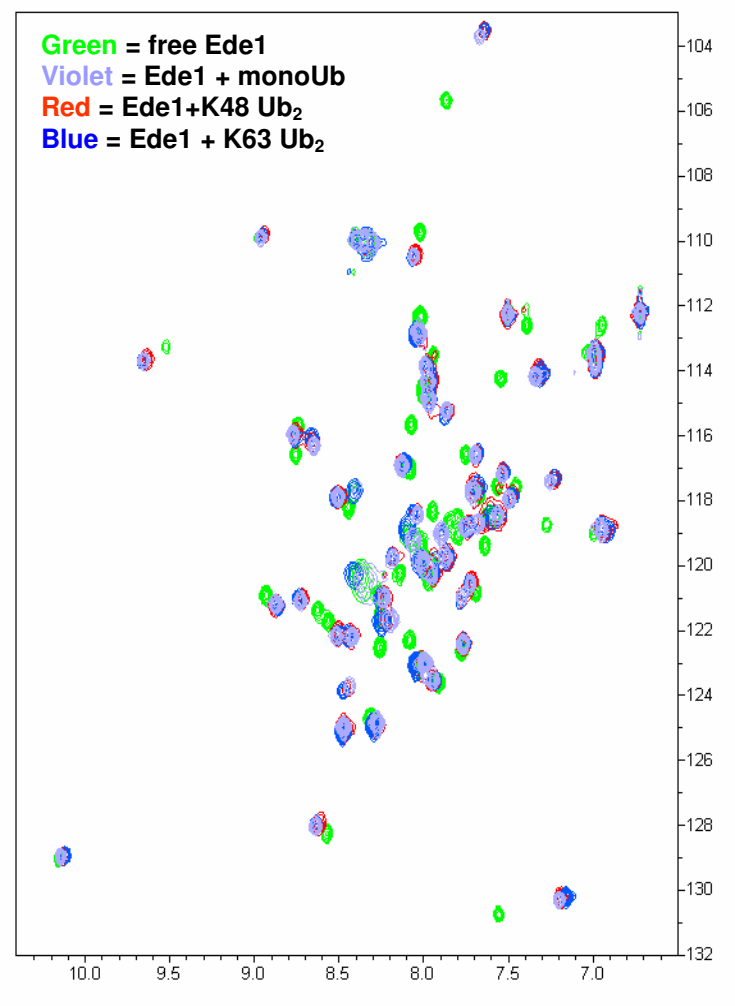

Figure 6.14 Direct experimental demonstration of the similarity of the perturbations in UBA caused by the binding to monoUb and to Lys48- and Lys63-linked Ub_2. Shown is an overlay of ^{1}H-^{15}N HSQC spectra of UBA (green), UBA:monoUb complex (violet), UBA:Lys48-linked Ub_2 complex (red), and UBA:Lys63-linked Ub_2 complex (blue).

To test our hypothesis that modification of Lys48 as a result of the Ub/Ub linkage in Lys48-linked Ub_2 reduces UBA binding, we explored other modifications at this site. The formation of the Gly76-Lys48 isopeptide bond is expected to affect the side chain of Lys48 of the proximal Ub in two ways: (1) it extends the length (hence alters the conformational properties) of the side chain and (2) neutralizes it. To test the effect of removing the positive charge at this position, we used a K48C mutant of monoUb

(referred to as Ub K48C); 10mM DTT was maintained throughout the experiment to inhibit formation of disulfide bonds (lack of disulfide-linked dimers was confirmed by non-reducing SDS-PAGE). Unlabeled K48C was added to UBA and CSPs in UBA were monitored up to a molar ratio of 1:1.5 (UBA:K48C). When compared with CSPs in UBA at the same molar ratio with K48R Ub, somewhat smaller CSPs are observed (Fig. 6.15), indicating that binding may be weakened, but not abolished. Thus, it appears that mutation at position 48 to a neutral residue does not significantly reduce binding to UBA. Note that the Lys48-to-Arg48 mutation preserves the charge and has no effect on ligand binding as inferred from the similarity in CSP and PRE patterns observed on the distal Ub of Lys48-linked Ub_2, which is a K48R mutant, and Lys63-linked Ub_2 where Lys48 is not mutated.

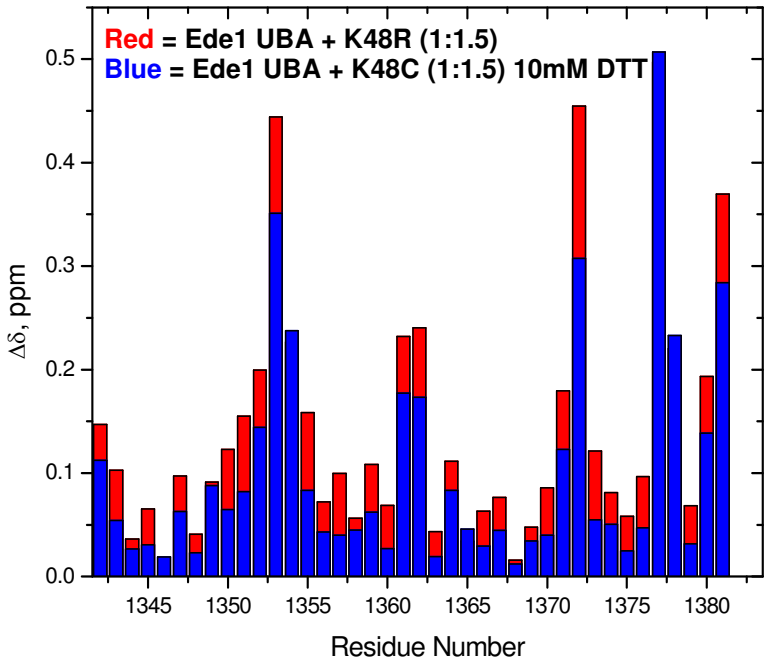

Figure 6.15 Comparison of CSPs in Ede1 UBA bound to K48R Ub and K48C Ub. Shown is an overlay of CSPs of UBA bound to K48R monoUb (red), and K48C monoUb. Both experiments were performed at a molar ratio of 1:1.5 UBA:monoUb. Disulfide bond formation between K48C monomers was prevented by incubation with 10mM DTT and verified with non-reducing SDS-PAGE (not shown).

While charge modification may not be critical, reduced binding to Lys48-linked Ub_2, especially on the proximal Ub may be a result of steric factors caused by linkage at this site. To mimic the effect of Ub/Ub linkage, K48C monoUb was allowed to form disulfides with another monoUb in the absence of any reducing agents, thereby creating a covalently linked Ub_2 connected by position Cys48 on both Ubs (the presence of disulfide linked Ub_2 confirmed by non-reducing gel, Fig. 6.16a). Practically no CSPs were observed in the HSQC spectrum of ^{15}N labeled UBA when K48C was added at a 3:1 ratio (Fig. 6.16b), thus indicating a lack of binding. To break the disulfide bonds, the sample was incubated with 20mM DTT for 20 hours (absence of disulfide bonded K48C in the NMR sample confirmed by non-reducing SDS-PAGE, Fig 6.16c). Thusly, CSPs are observed in residues Gly1353, Phe1354, Ala1372, Leu1378, and Ala1381 involved in binding to Ub (in the same direction as observed upon Ub-binding).

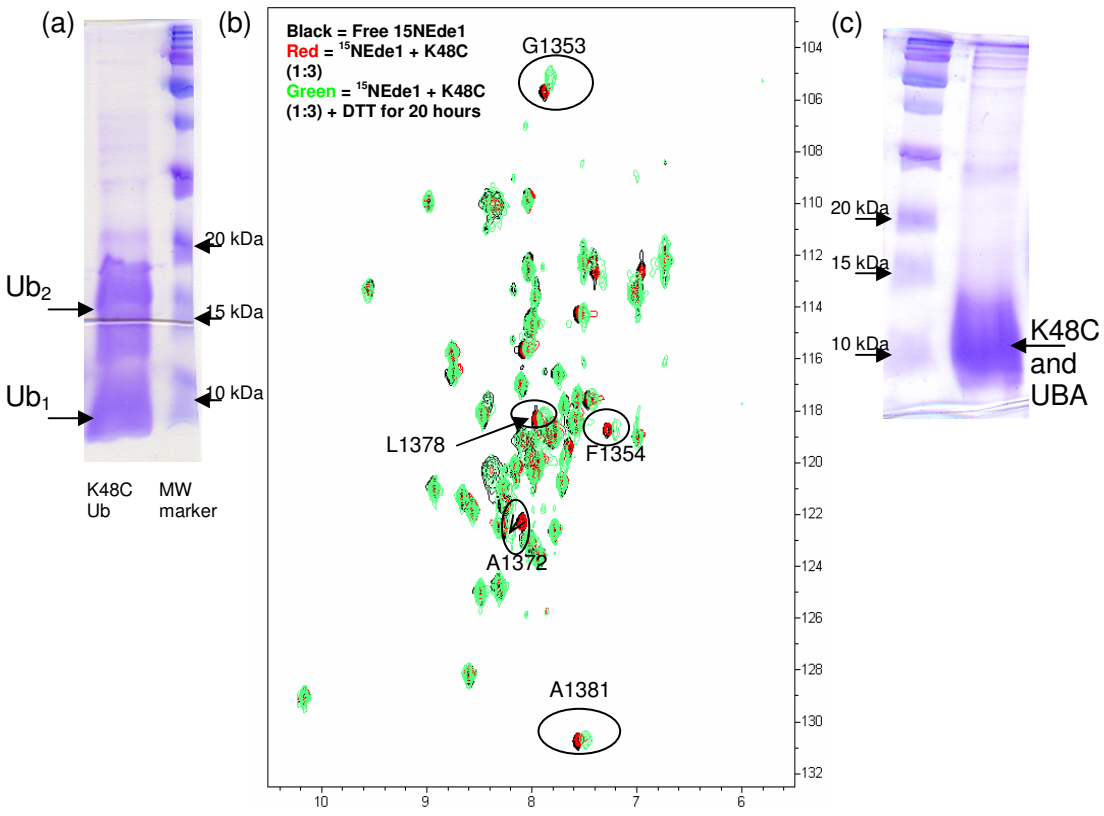

Figure 6.16 Disulfide bonds in K48C Ub inhibit binding to Ede1 UBA and binding is recovered after reduction of disulfide bonds. (a) Non-reducing SDS-PAGE of K48C stock solution showing the presence of disulfide bonded K48C Ubs in the absence of DTT. (b) Shown is an overlay of ^{1}H-^{15}N HSQC spectra of free Ede1 UBA (black), UBA + K48C Ub (3x molar excess of Ub) (red), and K48C Ub + UBA incubated with 20mM DTT for 20 hours (green). (c) Non-reducing SDS-PAGE of NMR sample used in (b) after incubation with DTT (green spectrum) confirming monomeric state of K48C Ubs.

Similarly, we performed the experiment with Lys48-linked Ub_2 carrying the K48C mutation on the distal Ub. In this experiment, both the distal Ub and UBA were ^{15}N-labeled in order to observe their resonances concurrently. In agreement with the previous result, peak positions for UBA were nearly identical to those of unbound UBA (Fig. 6.17a), indicating practically no binding. It is worth emphasizing that all side chains in position 48 in this Ub_2 were modified, either via the disulfide bond (distal Ub) or via the regular isopeptide bond (proximal Ub). This sample was then incubated with

24 mM DTT for 16 hours to reduce the disulfide bonds (confirmed by non-reducing SDS-PAGE, Fig. 6.17c), and binding was restored (Fig. 6.17b). The data suggest that linkage to another Ub via position 48 hinders UBA binding to Ub, and this may explain reduced binding to Lys48-linked Ub_2.

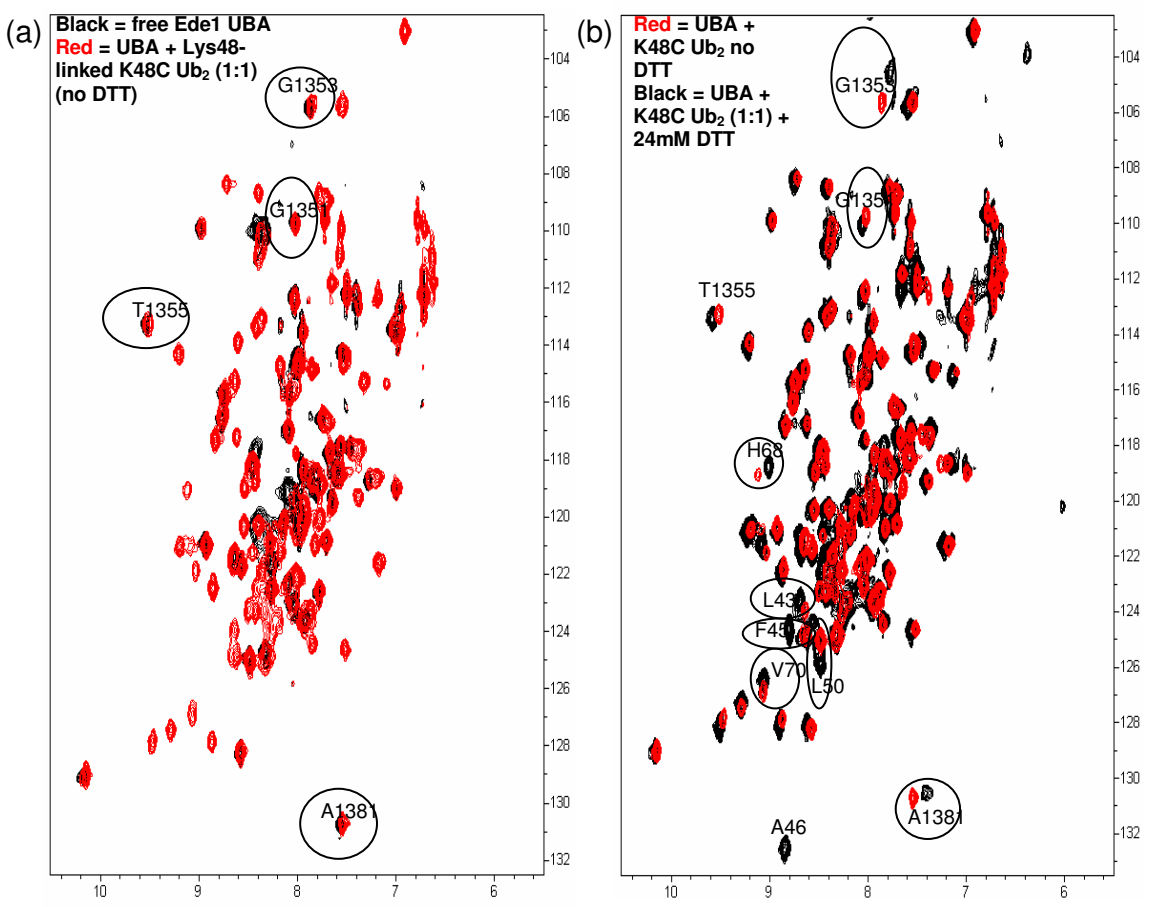

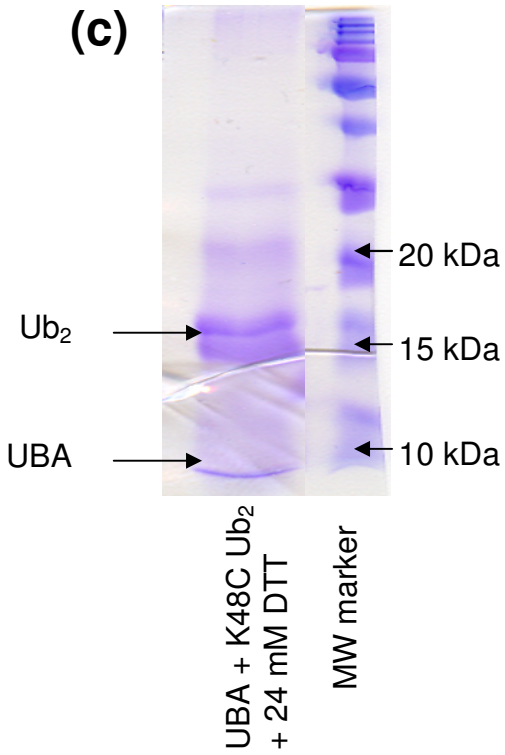

Figure 6.17 Disulfide bonds in K48C (distal) Lys48-linked Ub_2 inhibit binding to Ede1 UBA and binding is recovered after reduction of disulfide bonds. (a) Shown is an overlay of ^{1}H-^{15}N HSQC spectra of ^{15}N Ede1 UBA (black), ^{15}N Ede1 UBA + disulfide bonded K48C(distal) ^{15}N-labeled Ub_2s (equimolar ratio) (red), (b) overlay of sample in (a) (red) incubated with 24mM DTT for 16 hours (black). (c) non-reducing SDS-PAGE of sample (c) confirming that disulfide bonds between Ub_2s were reduced.

Binding of Ede1 UBA to polyUb linked via Lys48 may also be complicated by the intramolecular interaction between Ub monomers in the chain [81]. The predominantly closed conformation (85% populated) of Lys48-linked Ub_2 in solution at neutral pH effectively buries the functionally important hydrophobic patch residues Leu8-Ile44-Val70 at the Ub/Ub interface. Thus, UBA must compete for binding to each Ub surface with the other Ub moiety in a Lys48-linked Ub_2. There is no such complication in Lys63-linked Ub_2 since the two Ub moieties do not form an interface [161]. In fact, both UBA-binding sites in Ub_2 are solvent exposed in the context of a

Lys63-linked chain. Thus, burial of these hydrophobic surfaces on Ub units, as well as those on UBA, would be highly favorable.

An additional complication in our experiments may be a result of Ede1 UBA's tendency to aggregate in solution. Therefore, not only is there a competition for Ub binding between UBA and the other Ub in a Lys48-linked Ub_2, there is also competition between each Ub in the chain and other UBAs that try to form UBA_n aggregates. This may explain the complicated titration curve observed when titrating Lys48-linked Ub_2 into a 0.6mM stock of Ede1 UBA (Fig. 6.4c).

While the difference in binding affinity of the UBA domain of Ede1 for alternatively linked di-ubiquitins appears small, the effect could be more significant in longer chains. Since Lys48-linked Ub_4 behaves as a dimer of Ub_2's at neutral pH in solution [91], while Lys63-linked chains adopt extended conformations [88, 161], it is certainly plausible that the mechanisms of binding proposed in this study are applicable to longer chains.

6.7 Summary

Ede1 UBA appears to have some preference toward Lys63-linked Ub_2 and binds to Lys48-linked Ub_2 in a mode distinct from the sandwich-like binding mode observed in the Ub_2:hHR23A UBA-2 complex, where UBA interacted with both Ubs simultaneously. Based on our CSP mapping data, the binding preference Ede1 UBA could be attributed to its weaker binding to the proximal Ub in Lys48-linked Ub_2 and, similarly, those Ub units in longer chains that have their K48 modified by the isopeptide linkage. The role of the chain conformation cannot be excluded, too. While no additional contacts are afforded by binding to Lys48-linked Ub_2, UBA binding disrupts the close hydrophobic contacts

between the Ub moieties in this conformation. Conversely, UBA binding to Lys63-linked Ub_2 does not have to compete with Ub/Ub hydrophobic patch interactions, and instead buries the otherwise exposed hydrophobic surfaces. This is in contrast with hHR23A UBAs whose binding is enhanced by the linkage. Perhaps since Ede1 is involved in trafficking and endocytosis, it might have evolved this preference to be able to distinguish monoUb or Lys63-linked chains (and other non-Lys48 linkages in which Lys48 is not modified), from Lys48-linked chains that signal for proteasomal degradation.

Chapter 7: Characterization of the interaction of K6W Ub with UBAs

7.1 Background

While studies in the past have identified residues Leu8, Ile44, and Val70, located on Ubs hydrophobic patch, as essential for Ub function [79, 117, 139, 163], evidence suggests that Lys6 also plays a pivotal role in many Ub-mediated cellular processes. In fact, mutation or biotinylation of Lys6 has been shown to inhibit proteasomal degradation [62, 79, 124] and enhance susceptibility to oxidative stress [62], and mutation to alanine also inhibits endocytosis [79]. While K6A Ub is not lethal in yeast [79], yeast expressing K6R Ub grow significantly slower than yeast expressing WT Ub [62]. Interestingly, polyUb chains linked via Lys6 have been reported to protect substrates from proteasomal degradation [61, 62]. While mutation of Lys6 would preclude formation of chains via this lysine, Lys6-modified Ub is incorporated into high molecular mass ubiquitin conjugates as efficiently as unmodified ubiquitin [62]. However, high molecular weight Ub-conjugates accumulate in cells overexpressing K6A, K6R, or K6W Ub mutants confirming that modifications at position 6 inhibit Ub-mediated protein degradation and protect substrates from polyUb-dependent proteolysis [62]. Conjugates formed with K6W were reported to bind the "intrinsic" proteasomal receptor, S5a, ~60% less than those formed with WT Ub [62], however, S5a is not the only proteasomal receptor for Ub, and is not essential for polyUb-mediated degradation [105]. Therefore, reduced

binding to S5a does not fully account for the observed inhibition of proteasomal degradation of Ub conjugates formed with K6W.

Ub-dependent proteolysis is required for numerous cellular processes, including ocular lens cell cycle progression. While these cells continuously proliferate and differentiate in healthy eyes, cataract surgery patients often suffer enhanced proliferation of lens epithelial cells causing posterior capsule opacification (PCO) [164-166]. Expression of K6W in human lens epithelial cells inhibits cell proliferation, therefore, it has been suggested as a therapeutic target for PCO [63].

Because Lys6 is located on the surface of Ub critical for recognition by effector proteins (Fig. 7.1c), it is likely that modification of this residue, whether by mutation, acetylation, biotinylation, or isopeptide linkage to other Ubs, disrupts its recognition by cellular machinery in various pathways. A detailed structural characterization of K6W Ub and its interaction with proteasomal and endocytic effector proteins will provide clues to the role of Lys6 in these pathways.

7.2 Spectral comparison of K6W with WT Ub

The ^{1}H-^{15}N HSQC spectrum of K6W Ub is similar to that of WT Ub (Fig. 7.1a) and shows well-dispersed signals indicative of a well-defined tertiary fold with significant β-sheet content, characteristic of Ub. A particularly large resonance shift was observed in Trp6 and Thr7 (located in β1) as expected due to the mutation (Fig. 7.1b). Additionally, large CSPs were observed in residues Thr12, Ile13 located in β2, and Leu67, His68, Leu69, Val70, and Leu71 located in β5. These strands flank β1 on both sides and in WT Ub, Lys6 makes hydrogen bonds with Leu67 and Leu69, while its sidechain makes contacts with the sidechains of Thr12 and His68 (Fig. 7.1c). Less

expected are strong CSPs in Leu8, Thr9, Gly10, Lys11, located in the β1-β2 loop. The observed CSPs are larger than typically expected for a surface residue (c.f. Fig. 7.2) and may indicate a disruption in the interaction of Lys6 with His68 and Thr12 and/or some local rearrangement in β1 and β5.

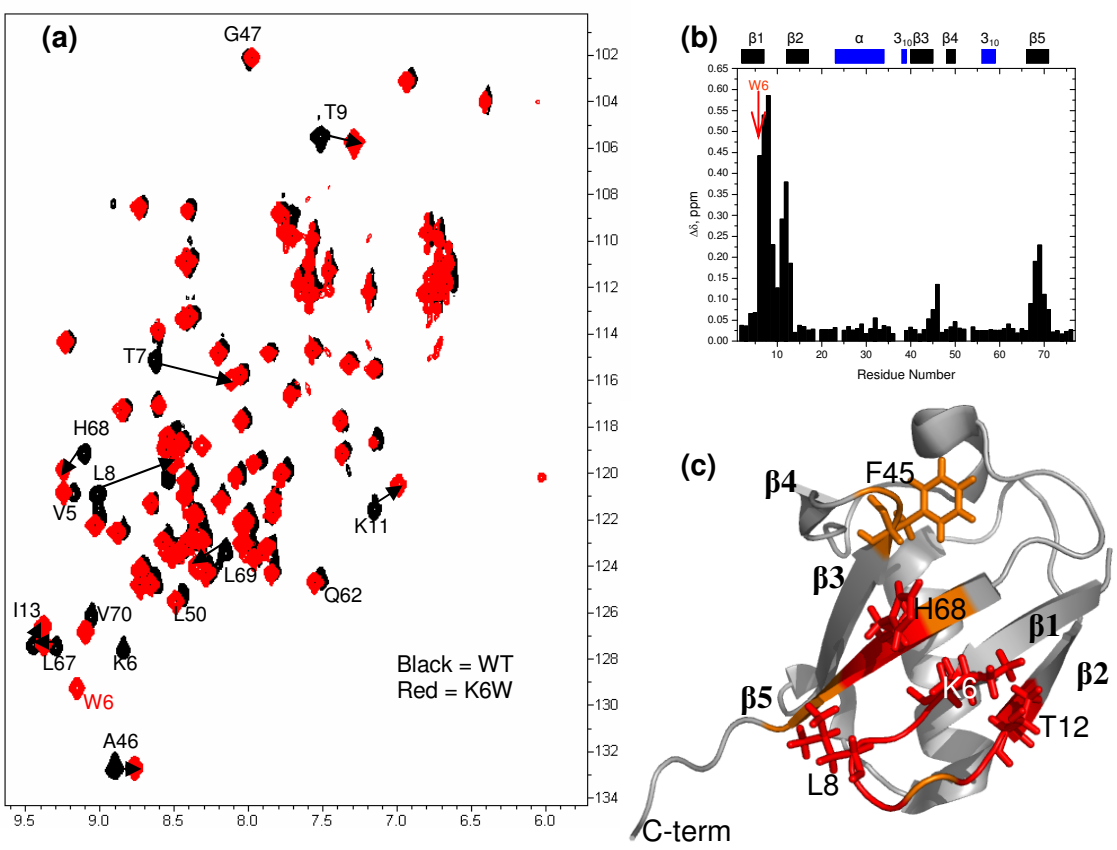

Figure 7.1 Spectral differences between K6W and WT Ub. (a) Overlay of the ^{1}H-^{15}N HSQC spectra of wild type ubiquitin (black) with K6W (red). (b) Amide chemical shift differences between the two proteins as a function of residue number. The site of mutation is indicated by the arrow. (c) Cartoon representation of the 3D structure of WT Ub with the residues showing the biggest CSPs colored (from orange to red, in increasing Δδ).

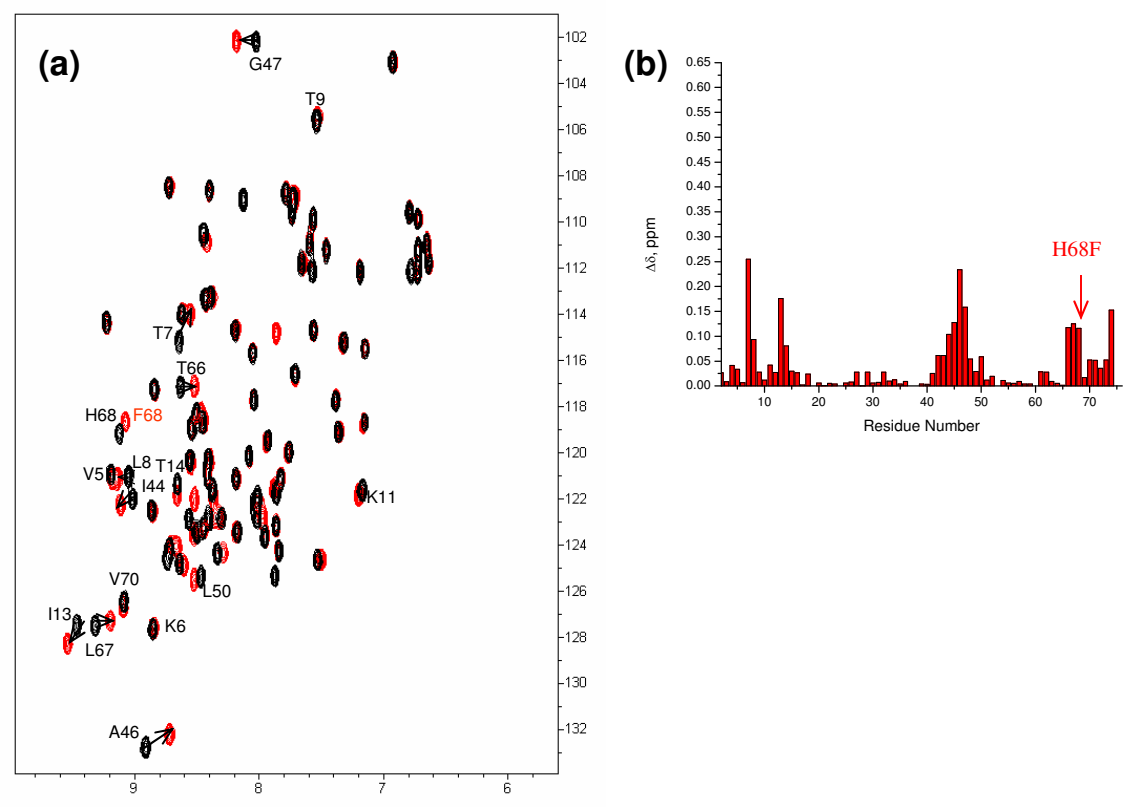

Figure 7.2 Spectral differences between H68F and WT Ub. (a) Overlay of the ^{1}H-^{15}N HSQC spectra of wild type ubiquitin (black) with H68F (red). (b) Amide chemical shift differences between the two proteins as a function of residue number.

Chemical shifts can also be perturbed by additional magnetic fields that arise from aromatic rings, referred to as ring current effects [137]. Therefore, the introduction of an additional aromatic ring (Trp6) may result in CSPs in residues close in space to it. Intriguingly, significant changes in amide resonances are also observed in Phe45, Ala46 located in the β3-β4 loop. In WT Ub, the amide of Phe45 is far from Lys6 (>10 Å), however the benzene ring of Phe45 contacts the imidazole ring of His68, thus large CSPs in His68 may suggest a change in its orientation which is felt by Phe45 and Ala46.

The sidechains of Trp6, Thr12, Phe45, and His68 are all exposed to solvent, and the large spectral changes far from the site of mutation suggest that there may be some

rearrangement of residues on the hydrophobic patch of Ub. This propagation of perturbations across the β-sheet surface of Ub is indeed interesting. Replacement of Lys with Trp introduces a bulky hydrophobic sidechain on the surface of Ub involved in ligand binding. Increased hydrophobicity and possible rearrangements of this surface may affect binding to effector proteins or other ubiquitins (i.e. in Lys48-linked chains).

7.3 Recognition by UBAs

In order to understand the effects of this mutation on Ub's function, we used NMR to study the interaction of K6W with the UBAs of a proteasomal receptor, hHR23A, and an endocytic receptor, Ede1.

7.3.1 Binding surface on UBA-2 of hHR23A in complex with K6W

Titration with K6W resulted in strong perturbations in the ^{1}H-^{15}N HSQC spectra of the UBA-2 domain of hHR23A (Fig. 7.3a). The largest CSPs were observed in residues Leu327, Leu330, G331, and Glu348. In addition, several amides (most notably, Glu348, Asn349, Leu350, and Leu356) showed strong signal attenuations indicative of an intermediate or slow exchange (on the NMR time scale) between the free and bound states of UBA-2. Surprisingly, in addition to the perturbed surface observed in UBA-2 bound to WT Ub [76, 117], CSPs are also observed on the backside surface of UBA-2 (Fig 7.3b). These additional perturbations are somewhat reminiscent of the perturbations in UBA-2/Lys48-Ub_2 complex [117] and may be indicative of an additional Ub binding to this surface. Note that these CSPs may also result from some rearrangement in UBA's core, but seems unlikely since they are not observed in complex with WT Ub. The ^{1}H T_2 measured for the UBA-2:K6W complex was 22 ms corresponding to a molecular weight

~20 kDa, suggesting a mixture of 1:1 and 1:2 stoichiometry (expected MWs are 14.0 and 22.7 kDa, respectively). In good agreement with the previous result, the ^{15}N T_1 for the complex at the end of titration (4 molar equivalents of K6W Ub per UBA) was 725 ± 33 ms, corresponding to a MW of 18-20 kDa, thus confirming that up to two K6W Ubs can bind to UBA-2 of hHR23A. Titration curves were fit to different models to consider possible scenarios where UBA-2 binds to either a single K6W Ub or to two K6W Ubs. In the scenario that UBA-2 only binds to a single Ub, a single-site 1:1 binding model was used to determine an average dissociation constant of 543 ± 86 μM (Fig. 7.3c). Using a two-site 2:1 (Ub:UBA) binding model, yielded an average microscopic K_d of 147 ± 86 μM. Using either model fit the data points well, although the accuracy of these numbers could be affected by the fact that CSPs have not reached saturation. Compared with the K_d reported for UBA-2 binding to WT yeast Ub (~500-600 μM [153]) or to WT human Ub (360 ± 78 μM [152], 400 ± 100μM [117]), the binding constant derived using a single-site 1:1 model is more similar to the literature data for WT Ub, however since the backside of UBA-2 is hydrophobic and binds to Ub in the context of Lys48-linked Ub_2 [117], it appears that a second K6W Ub binds to the back surface explaining the larger CSPs in α2 residues (Fig. 7.3a). Since CSPs have not yet saturated, and relaxation measurements indicate that there is a mixture of 1:1 and 2:1 Ub/UBA complexes, neither model is appropriate for an accurate estimate of the K_d. Thus, although it is not clear whether the mutation increases or decreases overall binding, it appears that K6W has increased avidity for interactions with the back surface of UBA-2.

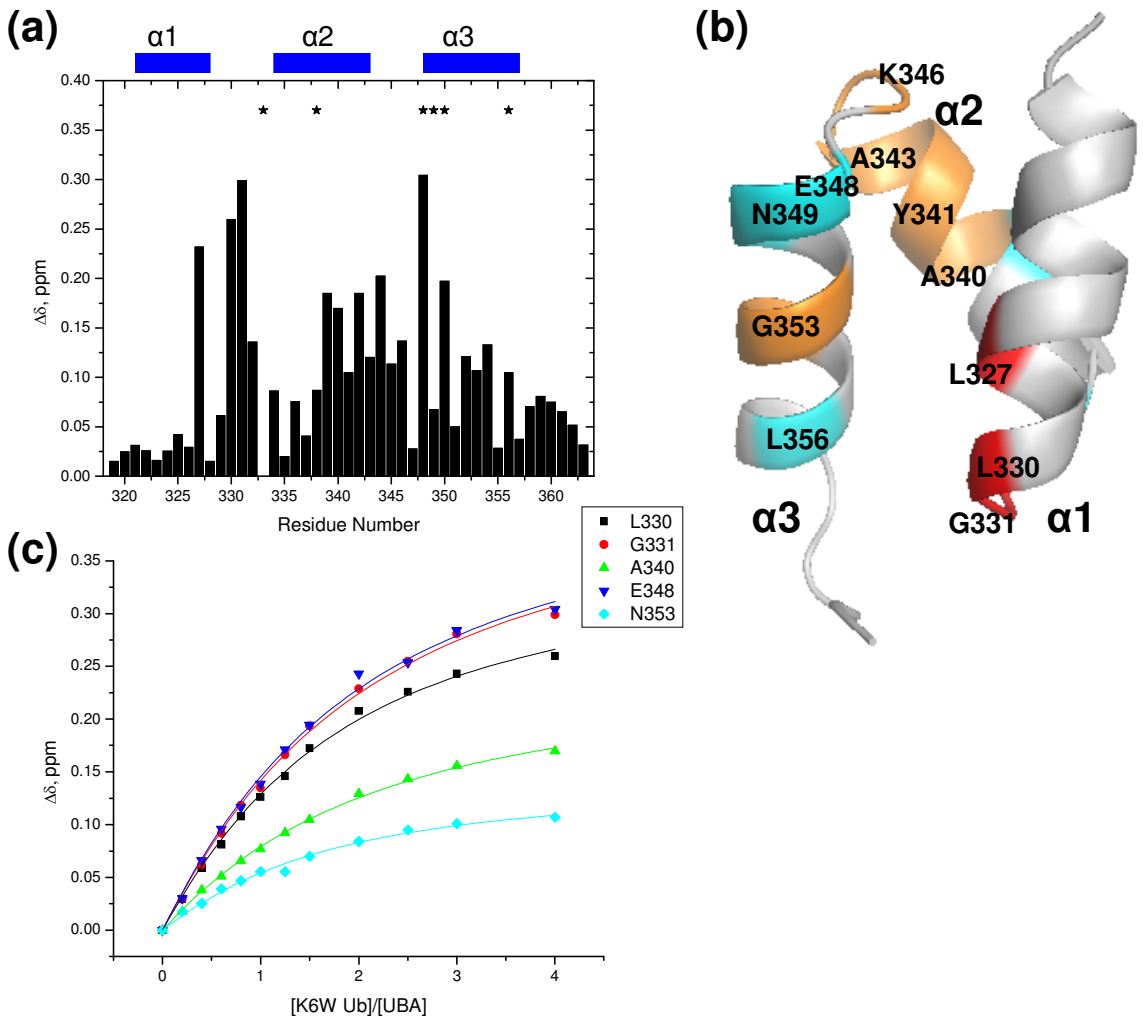

Figure 7.3 NMR titration studies of UBA-2 of hHR23A binding to K6W Ub. (a) CSPs in UBA-2 at the last titration point ([K6W Ub]/[UBA]=4:1) as a function of residue number. Asterisks in (a) indicate residues that show >70% signal attenuation in the presence of K6W Ub. (b) Ribbon representation of UBA structure color-coded by the CSP values and attenuations as follows: $\Delta\delta > 0.2$ ppm (red), $0.2 > \Delta\delta > 0.1$ ppm (orange), while residues showing significant signal attenuation (>60%) in the bound state are painted cyan. (c) Representative titration curves for several amides (as indicated). The UBA-2 concentration at the first point was 0.38 mM and 0.33 mM at the final point.

7.3.2 Binding surface on UBA of Ede1 in complex with K6W

Since K6A Ub significantly inhibits protein internalization [79], characterization of the interaction of Lys6 mutants in the context of endocytosis may provide clues to the

mechanisms of recognition of Ub by endocytic machinery. Thus, we studied binding of K6W to the UBA domain of Ede1 using NMR (Fig 7.4). The ^{15}N T_1 relaxation time for the complex at the end of titration (6 molar equivalents of K6W Ub per UBA) was 657 ± 20 ms, corresponding to a MW of 16-17 kDa, compared with 16.1 kDa expected for a 1:1 complex.

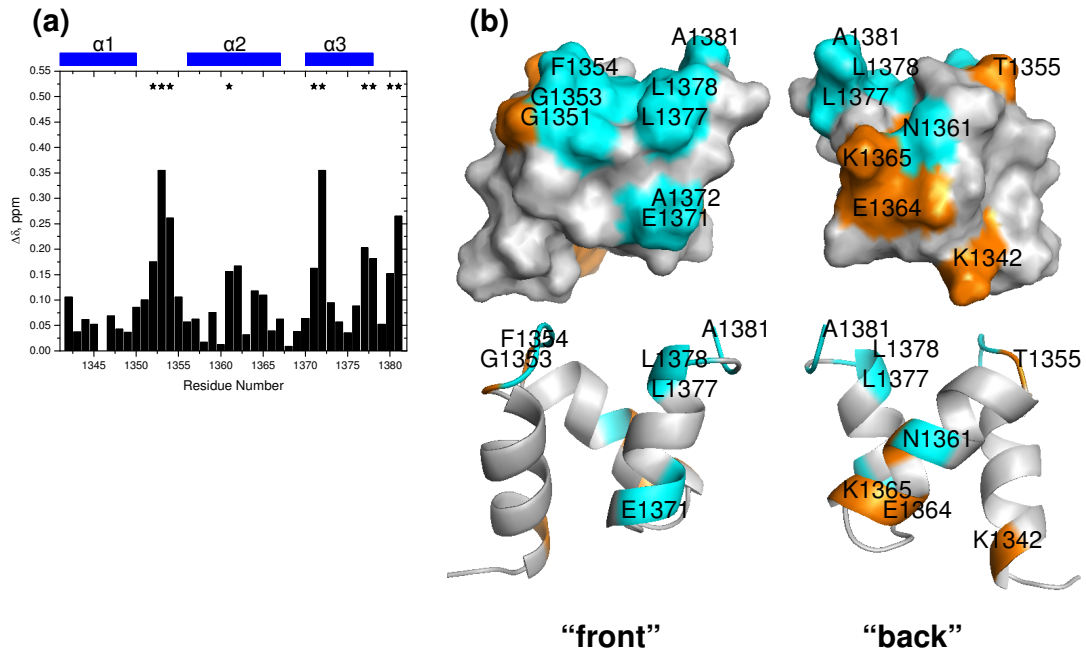

Figure 7.4 Surface mapping of the K6W Ub binding surface on Ede1 UBA. (a) Map of CSPs and attenuations on the surface of UBA bound to Lys63-linked Ub_2. Sites showing significant signal attenuation (>60%) due to intermediate or slow exchange are marked by asterisks. (b) UBA surface mapped by magnitude of CSPs. The coloring is as follows: $\Delta\delta > 0.25$ ppm (red), $0.25 \text{ ppm} > \Delta\delta > 0.10$ ppm (orange). Peaks with significant attenuation (>60%) or in slow exchange regime are painted cyan. Many residues showing CSPs >0.25ppm are also in slow exchange and are colored cyan rather than red. The denotations "front" and "back" signify the surface of UBA which faces towards (front) or away (back) from Ub in the monoUb/UBA complex (Protein Data Bank code 2G3Q).

Compared with the CSPs of UBA bound to WT Ub, the pattern of CSPs bound to K6W was similar, although smaller CSPs were observed in almost all residues, most notably in α3 (Fig 7.5a). This may be due to slow and intermediate exchange detected in

several additional residues in this region (Glu1371, Leu1377, and Ser1380) compared with WT Ub. Slow exchange was also observed in residues Gly1353 and Asn1361. CSPs did not significantly increase until 0.6 molar equivalents of K6W were added and did not fully saturate upon addition of 6 molar equivalents of K6W (see Fig. 7.5b). Thus, the resulting titration curves could not be fit reliably with our models.

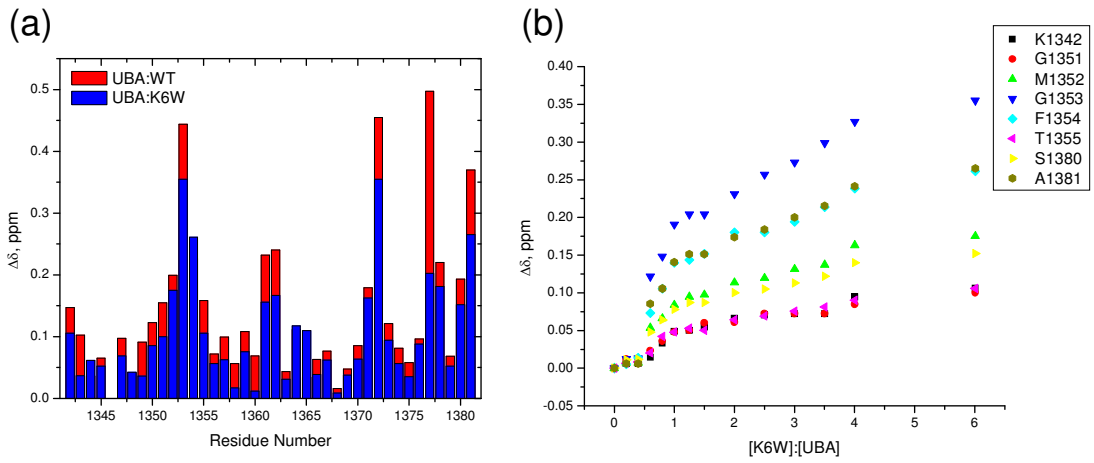

Figure 7.5 Comparison of CSPs in Ede1 UBA bound to K6W Ub and WT Ub. (a) Overlay of CSPs of UBA bound to WT Ub (red), and K6W Ub. Both experiments were performed at a molar ratio of 1:6 UBA:Ub. (b) Change in CSPs in UBA with increasing K6W Ub concentration for several residues (as indicated). The UBA concentration at the first point was 0.45 mM and 0.18 mM at the final point.

However for several residues, slowly exchanging peaks (free and bound states) were observed in the same spectra at molar ratios of 1:0.8 and 1:1 (UBA:K6W) (Fig. 7.6). In order to determine dissociation constants for binding interactions in the slow exchange regime on the NMR timescale, the ratio (R) of the peak volumes representing free (Vol_F) and bound states (Vol_B) was used and the K_d was calculated using the equation:

$$K_d = ([L_t] - [P_t].(1+R)^{-1}).R$$

where R = Vol_F / Vol_B, [P_t] is the total protein concentration, and [L_t] is the total ligand concentration. Using this analysis, the K_d values averaged over residues Met1352, Gly1353, Glu1371, Leu1377, Ser1380, and Ala1381 were determined to be 76 ± 26 and 90 ± 30 μM (mean ± standard deviation) at 1:0.8 and 1:1 molar equivalents, respectively (Table 7.1).

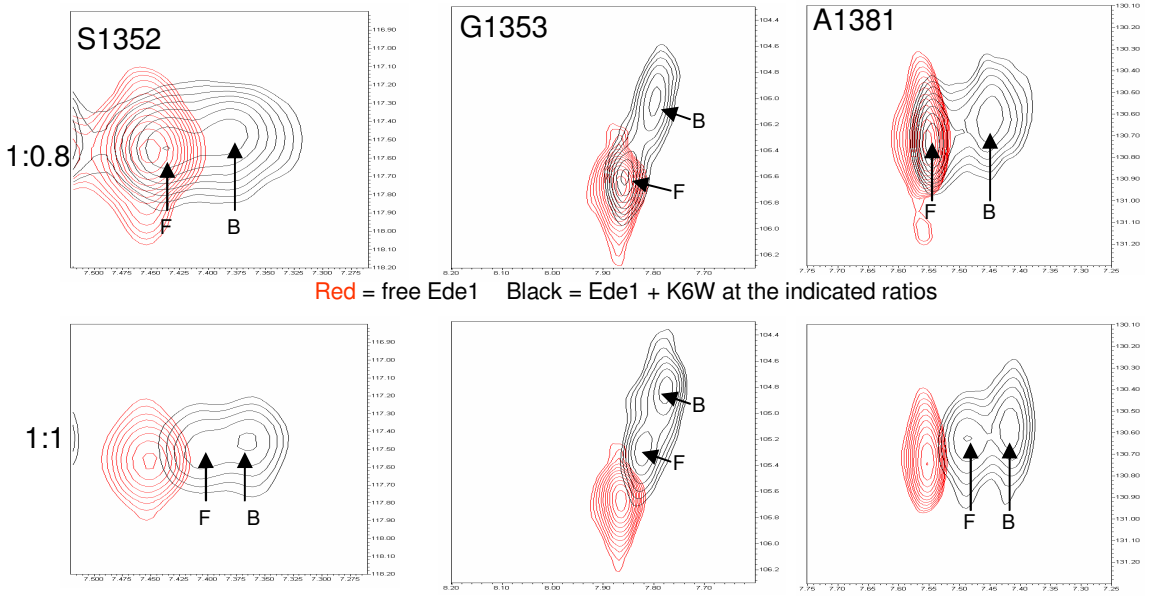

Figure 7.6 Slowly exchanging peaks (free and bound state) observed for UBA upon addition of K6W Ub. Shown are overlays of the ^{1}H-^{15}N HSQC spectra corresponding to free UBA with no Ub added (red) and peaks representing free (F) and bound (B) states of selected UBA peaks at the titration points indicated on the left.

Table 7.1 The dissociation constants for Ede1 UBA/Ub(K6W) binding, derived from peak volume integration.

residue	K_d determined at 1:08 (μM)	K_d determined at 1:1 (μM)
M1352	99	116
G1353	96	100
E1371	84	88
L1377	40	59
S1380	44	50
A1381	90	126
Average	**76 ± 26**	**90 ± 30**

Interestingly, the dissociation constants determined from this analysis agree very well with the K_d reported for WT Ub binding to Ede1 UBA from using NMR titrations (83 ± 9 μM) [110]. The difference in exchange regimes detected in this titration suggests that the mode of binding may have changed compared to UBA binding to WT Ub and may be a result of the perturbation of the hydrophobic surface of Ub caused by the mutation. Perturbations in the structural arrangement of Ub's β-sheet surface have been shown to affect ligand recognition (see Chapter 5). Since slowly exchanging peaks reflect a kinetic process dictated by on- and off-rates, it is possible that these structural changes have altered how K6W is recognized by UBA, without drastically affecting the equilibrium constants.

The Ede1 UBA/WT Ub complex involves electrostatic contacts between Glu1348 and Lys6 and His68 (Fig 7.7). In K6W, this interaction is disrupted since the bulky hydrophobic sidechain of Trp replaces lysine. Conceivably, abrogating this interaction alters the mode of recognition by UBA.

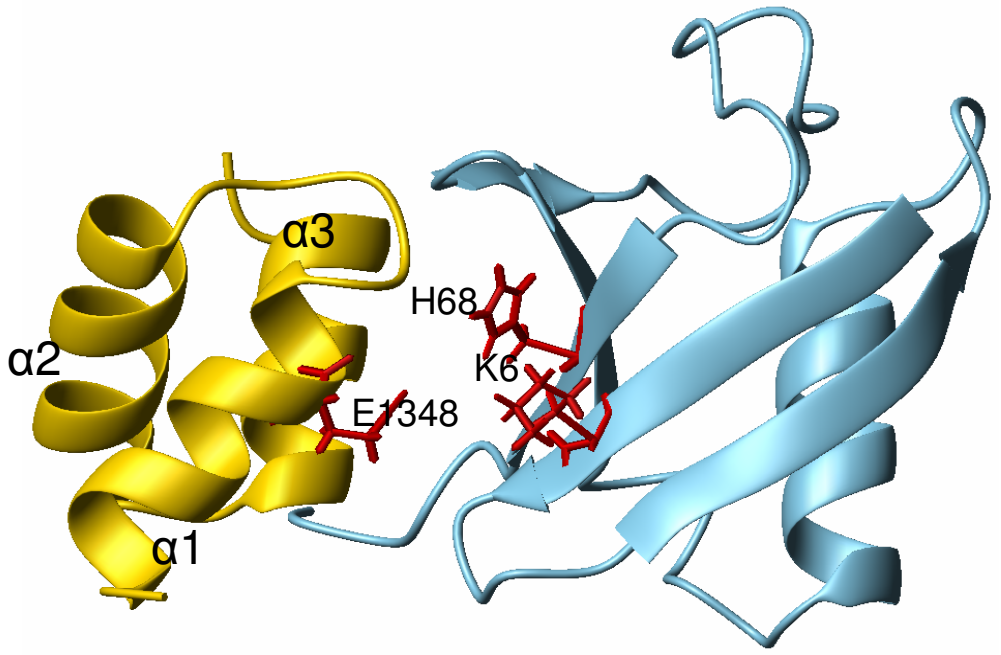

Figure 7.7 Solution structure of Ub/UBA reveals electrostatic interaction with Lys6. Shown is the cartoon representation of Ede1 UBA (gold) in complex with Ub (blue). Sidechains of Lys6, His68 of Ub and Glu1348 of UBA are shown as red sticks. (PDB ID: 2G3Q) [110]

7.4 K6W Ub aggregates in solution

Interestingly, the ^{1}H T_2 of a 2.4mM free K6W sample was 17 ms (vs. 50ms for WT Ub) corresponding to a molecular weight of ~26 kDa, thus suggesting that K6W has a tendency to aggregate. This tendency was also observed by SDS-PAGE, whereby samples taken from frozen stock solutions of K6W formed aggregates of various sizes. To better understand the formation of these apparent aggregates, we compared the migration pattern of K6W immediately after purification, after being frozen in concentrated stocks, and after incubation with 8 M urea for ~20 hours. Although monomeric and quite pure immediately after purification (Fig. 7.8, lane 1), K6W migrates as a ladder of Ub aggregates reminiscent of enzymatic Ub chain elongation

when electrophoresed from stock solutions (Fig. 7.8, lane 2). However without any enzymes, ATP, and/or other chain promoting factors present in solution to make covalent bonds, the observation of these aggregates on polyacrylamide gels containing SDS and BME is unexpected. While incubation with 8 M urea did reduce the larger aggregates, aggregates with MW corresponding to aggregates of 2 and 3 Ubs are still observed (Fig 7.8, lane 3).

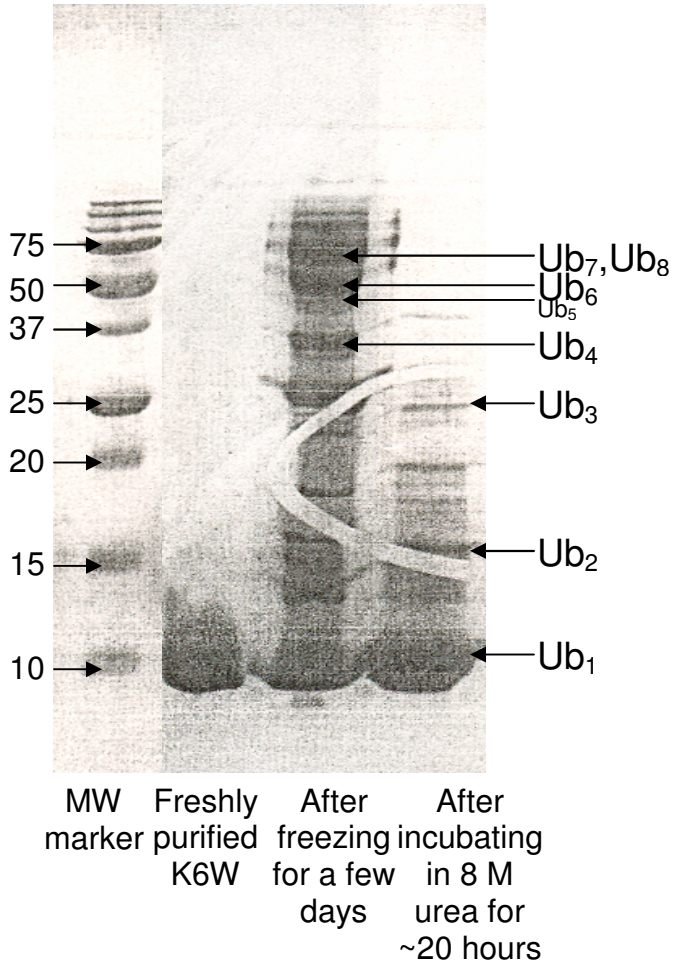

Figure 7.8 SDS-PAGE reveals high tendency for K6W aggregation. From left to right, lane (1) contains the MW standard as indicated, lane (2) is K6W ~1-2 hours after elution from cation exchange column as described in Section 3.1.2, lane (3) shows migration pattern of K6W sample from frozen cell stock. (Please note: this is observed in all cell stocks from many different preparations), lane (4) sample from lane (3) after incubating with 8M urea for ~20 hours. Expected MW for Ub_x of different sizes indicated on the right.

Analytical ultracentrifugation experiments, as well as, ^{15}N T_1 relaxation experiments at various concentrations, buffer, pH, and denaturant conditions should be used to test these properties. In addition, CD may be used to compare the stability of the mutant to WT and perhaps provide insight into the apparent resistance to SDS denaturation.

7.5 Scope for future studies

The apparently substantial tendency to self-associate suggests that some of the observed CSPs in K6W compared to WT Ub could perhaps also be explained by Ub/Ub contacts. Strong Ub/Ub interaction may have implications for ligand binding in the context of Ub chains. In Lys48-linked Ub_2, the equilibrium between open and closed conformations is critical for ligand binding. Indeed, locking the chain in the closed conformation inhibits ligand binding [84]. If the Ub/Ub interaction is in fact amplified by the mutation, it is possible that polyUb chains comprised of K6W Ubs would be less likely to open resulting in weaker ligand binding. Structural studies using polyUb chains comprised of K6W Ub are required to further explore this phenomenon.

Chapter 8: Summary and Concluding Remarks

8.1 Summary of results

Using several NMR methods, the interactions of Ub and polyUb with the tandem UIM-1/UIM-2 S5a, the isolated UIM-2 of S5a, and the UBA of Ede1 were studied. The structure, dynamics and ligand binding of Ub mutants were also characterized.

As the intrinsic polyUb receptor of mammalian proteasomes, S5a plays an important role in the degradation of unwanted cellular proteins. The results of the binding studies detailed above showed that up to two UIM-2 molecules bound to Ub_2 linked via Lys48 or Lys63. The binding interface between the UIMs and Ubs was essentially the same for both chains. Based on this data, putative structural models of the complexes were shown, and models of Lys48-linked Ub_2 bound to the tandem UIM-1/UIM-2 S5a were proposed. Although atomic-resolution characterization of the interactions of S5a with Ub_2s was hampered by signal attenuation in many residues upon binding, the data showed that when compared with S5a binding to monoUb or Lys63-linked Ub_2, additional surfaces on the Ub-Ub linker in Lys48-linked Ub_2 and a region N-terminal to UIM-2 in S5a appear to be involved in the interaction.

In agreement with *in vivo* experiments reporting that Lys63-linked conjugates are targeted for endocytosis [42], and substrates tagged with Lys48-linked polyUb are not, our NMR titration data showed that the UBA domain of Ede1 preferentially binds to Lys63-linked Ub_2. Interaction surface mapping indicated a difference in UBA binding to the proximal Ub in Lys48-linked Ub_2. Lys48 is one of the main sites of interaction at the Ede1 UBA/monoUb interface [110]. Our results showed that its modification (in the

proximal Ub) via isopeptide linkage hindered binding. Additionally, binding of UBA to Lys48-linked Ub_2 required disruption of Ub/Ub interactions [81, 85], however, unlike UBA-2 of hHR23A [117] and UBA of Mud1 [119] bound to Lys48-linked Ub_2, the disruption of the Ub/Ub interface was not compensated with favorable interactions with the back surface of Ede1 UBA. In contrast, Lys63-linked Ub_2 adopts an open, extended conformation [87] and the site of Ub-Ub linkage (Lys63) is not located near the UBA binding site [110], therefore both Lys48s are unmodified and both Ub surfaces are exposed and available for UBA binding. Thus, in the proposed structural model of 2 UBAs bound to Lys63-linked Ub_2, the interaction buried the hydrophobic surfaces of both Ubs and UBAs, while the hydrophilic back surface of the UBAs remained solvent exposed.

Characterization of the structure, dynamics, and rigidity of a Ub core mutant (L69S) revealed that although the mutation had relatively little effect on Ub's overall structure, structural rigidity was reduced and the terminal β-sheet was displaced. These changes had surprisingly potent and specific effects on molecular recognition. L69S and L67S could bind to UBAs of Rad23 and hHR23A, but failed to bind the UIMs in the intrinsic proteasomal receptors Rpn10 and S5a. Moreover, chains assembled on target substrates with these mutant Ubs were unable to support substrate degradation by the proteasome *in vitro*, or sustain viability of yeast cells. Many cellular pathways mediated by ubiquitination of substrates involve proteins that contain UBAs and UIMs. Comparison with known Ub/UIM and Ub/UBA complexes suggested that the effects of these mutations on Ub's binding surface, stability, and rigidity compromise association with other UIMs, but not UBAs.

The structure of Ub bound to several UBAs and UIMs reveals electrostatic interactions with Lys6 of Ub. Interestingly, such electrostatic contacts are present in the Ede1 UBA/Ub [110] and UIM-1/Ub [74] complexes. Since polyUb comprised of K6W has been shown to bind S5a ~60% weaker compared with WT [62], disruption of these interactions may explain reduced binding. To explore the interaction of this mutant with endocytic and proteasomal receptors, binding of K6W to the UBA of Ede1 was characterized. The results showed that the UBA of Ede1 bound to K6W in a different mode compared with WT Ub, suggesting a different mode of recognition which may play a role in reduced endocytic efficiency when Lys6 is mutated [79]. Interestingly, since there is no such electrostatic contact between Lys6 of Ub and UBA-2 of hHR23A [76], one would expect that the binding would not be weakened. Our results show that while the binding surface of UBA which contacts WT Ub was nearly identical, a second K6W Ub appeared to bind to the back surface of UBA reminiscent of the 'sandwich' model in Lys48-linked Ub_2 with UBA-2. Mutation of Lys6 has been shown to inhibit proteasomal degradation [62]. Based on the results of this study and the binding study with S5a [62], it is possible that increased binding of K6W to UBA-2 of hHR23A, the "extrinsic" proteasomal receptor, coupled with reduced binding by S5a, the "intrinsic" proteasomal receptor, may result in polyUb chains comprised of these mutants being sequestered on hHR23A rather than being recognized and transferred to the 19S subunit of the proteasome. On the other hand, the aggregation of K6W Ubs in polyUb chains may lock the Ubs in a self-associated state, thereby inhibiting interactions with both UBAs and UIMs.

8.2 Scope for future studies

Although Ub is highly promiscuous with regard to binding partners and therefore signals for many diverse cellular outcomes, it is highly conserved and stable suggesting strong evolutionary pressure to maintain its fold and binding surface. Additional insights into the basis for Ub's interactions with effector proteins may be attained from studies of other Ub core mutants, as well as polyUb chains comprised of these mutants. Furthermore, deconstructing the role of the various receptor proteins involved in proteasomal degradation is vital to understanding the basis for its disfunction and the associated pathologies. The ability of L69S and L67S Ubs to distinguish between UIM- and UBA-containing receptor proteins may prove to be an invaluable tool in this endeavor. Finally, while WT Ub has some tendency to self-associate, the dramatically increased tendency of K6W Ub to aggregate may be important in the context of cellular homeostasis. It is possible that strong self-association of Ubs modified at Lys6 may impede recognition of substrates tagged with these chains by their intended targets leading to accumulation of unwanted proteins, effectively grinding cellular transport and waste disposal to a halt. Structural and functional studies of polyUb comprised of K6W with Ub binding domains may provide valuable insights into the breakdown of cellular machinery.

Bibliography

1. Pickart, C.M., *Ubiquitin enters the new millennium.* Mol Cell, 2001. **8**(3): p. 499-504.
2. Pickart, C.M. and D. Fushman, *Polyubiquitin chains: polymeric protein signals.* Curr Opin Chem Biol, 2004. **8**(6): p. 610-6.
3. Hershko, A. and A. Ciechanover, *The ubiquitin system.* Annual Review of Biochemistry, 1998. **67**: p. 425-479.
4. Cook, W.J., et al., *Structure of a Diubiquitin Conjugate and a Model for Interaction with Ubiquitin Conjugating Enzyme (E2).* Journal of Biological Chemistry, 1992. **267**(23): p. 16467-16471.
5. Haldeman, M.T., et al., *Structure and function of ubiquitin conjugating enzyme E2-25K: The tail is a core-dependent activity element.* Biochemistry, 1997. **36**(34): p. 10526-10537.
6. Jiang, F. and R. Basavappa, *Crystal structure of the cyclin-specific ubiquitin-conjugating enzyme from clam, E2-C, at 2.0 A resolution.* Biochemistry, 1999. **38**(20): p. 6471-8.
7. Hamilton, K.S., et al., *Structure of a conjugating enzyme-ubiquitin thiolester intermediate reveals a novel role for the ubiquitin tail.* Structure, 2001. **9**(10): p. 897-904.
8. Eddins, M.J., et al., *Mms2-Ubc13 covalently bound to ubiquitin reveals the structural basis of linkage-specific polyubiquitin chain formation.* Nat Struct Mol Biol, 2006. **13**(10): p. 915-20.
9. Chen, Z. and C.M. Pickart, *A 25-kilodalton ubiquitin carrier protein (E2) catalyzes multi-ubiquitin chain synthesis via lysine 48 of ubiquitin.* J Biol Chem, 1990. **265**(35): p. 21835-42.
10. Hofmann, R.M. and C.M. Pickart, *In vitro assembly and recognition of Lys-63 polyubiquitin chains.* J Biol Chem, 2001. **276**(30): p. 27936-43.
11. Hershko, A., *Ubiquitin: roles in protein modification and breakdown.* Cell, 1983. **34**(1): p. 11-2.
12. Hershko, A., *The ATP-ubiquitin proteolytic pathway.* Prog Clin Biol Res, 1985. **180**: p. 11-6.
13. Fang, S. and A.M. Weissman, *A field guide to ubiquitylation.* Cell Mol Life Sci, 2004. **61**(13): p. 1546-61.
14. Pickart, C.M., *Ubiquitin in chains.* TIBS, 2000. **11**: p. 544-48.
15. Taylor, J.P., J. Hardy, and K.H. Fischbeck, *Toxic Proteins in Neurodegenerative Disease.* Science, 2002. **296**(5575): p. 1991-1995.
16. Michalik, A. and C. Van Broeckhoven, *Pathogenesis of polyglutamine disorders: aggregation revisited.* Human Molecular Genetics, 2003. **12**: p. R173-R186.
17. Liu, Y.C., et al., *The UCH-L1 gene encodes two opposing enzymatic activities that affect alpha-synuclein degradation and Parkinson's disease susceptibility.* Cell, 2002. **111**(2): p. 209-218.
18. Ward, C.L., S. Omura, and R.R. Kopito, *Degradation of CFTR by the ubiquitin-proteasome pathway.* Cell, 1995. **83**(1): p. 121-7.

19. Hershko, A. and A. Ciechanover, *The ubiquitin system.* Annu Rev Biochem, 1998. **67**: p. 425-480.
20. Arrigo, A.P., et al., *Identity of the 19S 'prosome' particle with the large multifunctional protease complex of mammalian cells (the proteasome).* Nature, 1988. **331**(6152): p. 192-4.
21. Brooks, P., et al., *Subcellular localization of proteasomes and their regulatory complexes in mammalian cells.* Biochem J, 2000. **346 Pt 1**: p. 155-61.
22. McGuire, M.J., et al., *An enzyme related to the high molecular weight multicatalytic proteinase, macropain, participates in a ubiquitin-mediated, ATP-stimulated proteolytic pathway in soluble extracts of BHK 21/C13 fibroblasts.* Biochim Biophys Acta, 1988. **967**(2): p. 195-203.
23. Ciechanover, A., *The ubiquitin-proteasome pathway: on protein death and cell life.* EMBO J., 1998. **17**(24): p. 7151-7160.
24. Smith, D.M., et al., *ATP binding to PAN or the 26S ATPases causes association with the 20S proteasome, gate opening, and translocation of unfolded proteins.* Mol Cell, 2005. **20**(5): p. 687-98.
25. Unno, M., et al., *The structure of the mammalian 20S proteasome at 2.75 A resolution.* Structure, 2002. **10**(5): p. 609-18.
26. Walz, J., et al., *26S proteasome structure revealed by three-dimensional electron microscopy.* J Struct Biol, 1998. **121**(1): p. 19-29.
27. Matthews, W., et al., *Involvement of the proteasome in various degradative processes in mammalian cells.* Proc Natl Acad Sci U S A, 1989. **86**(8): p. 2597-601.
28. Berger, F., et al., *Subcellular compartmentation and differential catalytic properties of the three human nicotinamide mononucleotide adenylyltransferase isoforms.* J Biol Chem, 2005. **280**(43): p. 36334-41.
29. Koradi, R., M. Billeter, and K. Wuthrich, *MOLMOL: a program for display and analysis of macromolecular structures.* J. Mol. Graph., 1996. **14**: p. 51-55.
30. DeLano, W.L., *The PyMOL Molecular Graphics System*. 2002, San Carlos: DeLano Scientific.
31. Elsasser, S., et al., *Rad23 and Rpn10 serve as alternative ubiquitin receptors for the proteasome.* J Biol Chem, 2004. **279**(26): p. 26817-22.
32. Chen, L. and K. Madura, *Rad23 promotes the targeting of proteolytic substrates to the proteasome.* Molecular and Cellular Biology, 2002. **22**(13): p. 4902-4913.
33. Schauber, C., et al., *Rad23 links DNA repair to the ubiquitin/proteasome pathway.* Nature, 1998. **391**(6668): p. 715-8.
34. Saeki, Y., et al., *Identification of ubiquitin-like protein-binding subunits of the 26S proteasome.* Biochemical and Biophysical Research Communications, 2002. **296**(4): p. 813-819.
35. Elsasser, S., et al., *Proteasome subunit Rpn1 binds ubiquitin-like protein domains.* Nat Cell Biol, 2002. **4**(9): p. 725-30.
36. Saeki, Y., et al., *Identification of ubiquitin-like protein-binding subunits of the 26S proteasome.* Biochem Biophys Res Commun, 2002. **296**(4): p. 813-9.
37. Wilkinson, C.R., et al., *Proteins containing the UBA domain are able to bind to multi-ubiquitin chains.* Nat Cell Biol, 2001. **3**(10): p. 939-43.

38. Aguilar, R.C. and B. Wendland, *Ubiquitin: not just for proteasomes anymore.* Current Opinion in Cell Biology, 2003. **15**(2): p. 184-190.
39. Roth, A.F., D.M. Sullivan, and N.G. Davis, *A large PEST-like sequence directs the ubiquitination, endocytosis, and vacuolar degradation of the yeast a-factor receptor.* J Cell Biol, 1998. **142**(4): p. 949-61.
40. de Melker, A.A., et al., *c-Cbl ubiquitinates the EGF receptor at the plasma membrane and remains receptor associated throughout the endocytic route.* J Cell Sci, 2001. **114**(Pt 11): p. 2167-78.
41. Rotin, D., O. Staub, and R. Haguenauer-Tsapis, *Ubiquitination and endocytosis of plasma membrane proteins: role of Nedd4/Rsp5p family of ubiquitin-protein ligases.* J Membr Biol, 2000. **176**(1): p. 1-17.
42. Galan, J.-M. and R. Haguenauer-Tsapis, *Ubiquitin Lys63 is involved in ubiquitination of a yeast plasma membrane protein.* EMBO J., 1997. **16**(19): p. 5847-5854.
43. Strack, B., et al., *A role for ubiquitin ligase recruitment in retrovirus release.* Proc Natl Acad Sci U S A, 2000. **97**(24): p. 13063-8.
44. Patnaik, A., V. Chau, and J.W. Wills, *Ubiquitin is part of the retrovirus budding machinery.* PNAS, 2000. **97**(24): p. 13069-13074.
45. Katzmann, D.J., G. Odorizzi, and S.D. Emr, *Receptor downregulation and multivesicular-body sorting.* Nat Rev Mol Cell Biol, 2002. **3**(12): p. 893-905.
46. Garrus, J.E., et al., *Tsg101 and the vacuolar protein sorting pathway are essential for HIV-1 budding.* Cell, 2001. **107**(1): p. 55-65.
47. Li, M., et al., *Mono- versus polyubiquitination: differential control of p53 fate by Mdm2.* Science, 2003. **302**(5652): p. 1972-5.
48. Baptiste, N. and C. Prives, *p53 in the cytoplasm: a question of overkill?* Cell, 2004. **116**(4): p. 487-9.
49. Hicke, L., *Protein regulation by monoubiquitin.* Nature Reviews Molecular Cell Biology, 2001. **2**(3): p. 195-201.
50. Sun, Z.W. and C.D. Allis, *Ubiquitination of histone H2B regulates H3 methylation and gene silencing in yeast.* Nature, 2002. **418**(6893): p. 104-8.
51. Pham, A.D. and F. Sauer, *Ubiquitin-activating/conjugating activity of TAFII250, a mediator of activation of gene expression in Drosophila.* Science, 2000. **289**(5488): p. 2357-60.
52. Hofmann, R.M. and C.M. Pickart, *Noncanonical MMS2-encoded ubiquitin-conjugating enzyme functions in assembly of novel polyubiquitin chains for DNA repair.* Cell, 1999. **96**(5): p. 645-53.
53. Stelter, P. and H.D. Ulrich, *Control of spontaneous and damage-induced mutagenesis by SUMO and ubiquitin conjugation.* Nature, 2003. **425**(6954): p. 188-91.
54. Ulrich, H.D., *Natural substrates of the proteasome and their recognition by the ubiquitin system.* Proteasome-Ubiquitin Protein Degradation Pathway, 2002. **268**: p. 137-174.
55. Spence, J., et al., *A ubiquitin mutant with specific defects in DNA repair and multiubiquitination.* Mol.Cell.Biol., 1995. **15**: p. 1265-73.
56. Sun, L. and Z.J. Chen, *The novel functions of ubiquitination in signaling.* Curr Opin Cell Biol, 2004. **16**(2): p. 119-26.

57. Baltimore, D., N. Rosenberg, and O.N. Witte, *Transformation of immature lymphoid cells by Abelson murine leukemia virus.* Immunol Rev, 1979. **48**: p. 3-22.
58. Rothwarf, D.M. and M. Karin, *The NF-kappa B activation pathway: a paradigm in information transfer from membrane to nucleus.* Sci STKE, 1999. **1999**(5): p. RE1.
59. Deng, L., et al., *Activation of the IkappaB kinase complex by TRAF6 requires a dimeric ubiquitin-conjugating enzyme complex and a unique polyubiquitin chain.* Cell, 2000. **103**(2): p. 351-61.
60. Nishikawa, H., et al., *Mass spectrometric and mutational analyses reveal Lys-6-linked polyubiquitin chains catalyzed by BRCA1-BARD1 ubiquitin ligase.* J Biol Chem, 2004. **279**(6): p. 3916-24.
61. Morris, J.R. and E. Solomon, *BRCA1 : BARD1 induces the formation of conjugated ubiquitin structures, dependent on K6 of ubiquitin, in cells during DNA replication and repair.* Hum Mol Genet, 2004. **13**(8): p. 807-17.
62. Shang, F., et al., *Lys6-modified ubiquitin inhibits ubiquitin-dependent protein degradation.* J Biol Chem, 2005. **280**(21): p. 20365-74.
63. Liu, Q., et al., *Expression of K6W-ubiquitin inhibits proliferation of human lens epithelial cells.* Mol Vis, 2006. **12**: p. 931-6.
64. Narasimhan, J., J.L. Potter, and A.L. Haas, *Conjugation of the 15-kDa interferon-induced ubiquitin homolog is distinct from that of ubiquitin.* J Biol Chem, 1996. **271**(1): p. 324-30.
65. Pan, Z.Q., et al., *Nedd8 on cullin: building an expressway to protein destruction.* Oncogene, 2004. **23**(11): p. 1985-97.
66. Johnson, E.S., *Protein modification by SUMO.* Annu Rev Biochem, 2004. **73**: p. 355-82.
67. Dye, B.T. and B.A. Schulman, *Structural mechanisms underlying posttranslational modification by ubiquitin-like proteins.* Annu Rev Biophys Biomol Struct, 2007. **36**: p. 131-50.
68. Ibarra-Molero, B., et al., *Thermal versus guanidine-induced unfolding of ubiquitin. An analysis in terms of the contributions from charge-charge interactions to protein stability.* Biochemistry, 1999. **38**(25): p. 8138-49.
69. Johnson, E., et al., *Solution structure and dynamics of a designed hydrophobic core variant of ubiquitin.* Structure Fold Des, 1999. **7**: p. 967-76.
70. Haas, A.L. and P.M. Bright, *The immunochemical detection and quantitation of intracellular ubiquitin-protein conjugates.* J Biol Chem, 1985. **260**(23): p. 12464-73.
71. Vijay-Kumar, S., C. Bugg, and W. Cook, *Structure of ubiquitin refined at 1.8 A resolution.* J Mol Biol, 1987. **194**: p. 531-44.
72. Vijay-Kumar, S., et al., *Comparison of the three-dimensional structures of human, yeast, and oat ubiquitin.* J Biol Chem, 1987. **262**(13): p. 6396-9.
73. Hamilton, K.S., M.J. Ellison, and G.S. Shaw, *Identification of the ubiquitin interfacial residues in a ubiquitin-E2 covalent complex.* J Biomol NMR, 2000. **18**(4): p. 319-27.

74. Wang, Q., P. Young, and K.J. Walters, *Structure of S5a bound to monoubiquitin provides a model for polyubiquitin recognition.* J Mol Biol, 2005. **348**(3): p. 727-39.
75. Ryu, K.S., et al., *Binding surface mapping of intra- and interdomain interactions among hHR23B, ubiquitin, and polyubiquitin binding site 2 of S5a.* Journal of Biological Chemistry, 2003. **278**(38): p. 36621-36627.
76. Mueller, T.D., M. Kamionka, and J. Feigon, *Specificity of the interaction between UBA domains and ubiquitin.* J. Biol. Chem., 2004: p. M312865200.
77. Haririnia, A., M. D'Onofrio, and D. Fushman, *Mapping the interactions between Lys48 and Lys63-linked di-ubiquitins and a ubiquitin-interacting motif of S5a.* J Mol Biol, 2007. **368**(3): p. 753-66.
78. Cornilescu, G., et al., *Validation of Protein Structure from Anisotropic Carbonyl Chemical Shifts in a Dilute Liquid Crystalline Phase.* J. Amer. Chem. Soc., 1998. **120**(27): p. 6836-6837.
79. Sloper-Mould, K.E., et al., *Distinct functional surface regions on ubiquitin.* J Biol Chem, 2001. **276**(32): p. 30483-9.
80. Peng, J., et al., *A proteomics approach to understanding protein ubiquitination.* Nat Biotechnol, 2003. **21**(8): p. 921-926.
81. Varadan, R., et al., *Structural properties of polyubiquitin chains in solution.* Journal of Molecular Biology, 2002. **324**(4): p. 637-647.
82. Ryabov, Y. and D. Fushman, *Interdomain mobility in di-ubiquitin revealed by NMR.* Proteins, 2006. **63**(4): p. 787-96.
83. Fujiwara, K., et al., *Structure of the ubiquitin-interacting motif of S5a bound to the ubiquitin-like domain of HR23B.* Journal of Biological Chemistry, 2004. **279**(6): p. 4760-4767.
84. Dickinson, B.C., R. Varadan, and D. Fushman, *Effects of cyclization on conformational dynamics and binding properties of Lys48-linked di-ubiquitin.* Protein Sci, 2007. **16**(3): p. 369-78.
85. Cook, W.J., et al., *Structure of a diubiquitin conjugate and a model for interaction with ubiquitin conjugating enzyme (E2).* J Biol Chem., 1992. **267**: p. 16467-71.
86. Pickart, C.M., *Ubiquitin in chains.* Trends in Biochemical Sciences, 2000. **25**(11): p. 544-548.
87. Varadan, R., et al., *Solution conformation of Lys63-linked di-ubiqutin chain provides clues to functional diversity of polyubiquitin signaling.* J Biol Chem, 2004. **279**: p. 7055-7063.
88. Tenno, T., et al., *Structural basis for distinct roles of Lys63- and Lys48-linked polyubiquitin chains.* Genes Cells, 2004. **9**(10): p. 865-75.
89. Cook, W.J., et al., *Structure of Tetraubiquitin Shows How Multiubiquitin Chains Can Be Formed.* Journal of Molecular Biology, 1994. **236**(2): p. 601-609.
90. Phillips, C.L., et al., *Structure of a new crystal form of tetraubiquitin.* Acta Cryst D, 2000. **57**: p. 341-4.
91. Eddins, M.J., et al., *Crystal Structure and Solution NMR Studies of Lys48-linked Tetraubiquitin at Neutral pH.* J Mol Biol, 2007. **367**(1): p. 204-11.
92. Cook, W.J., et al., *Structure of tetraubiquitin shows how multiubiquitin chains can be formed.* J.Mol.Biol., 1994. **236**: p. 601-609.

93. Phillips, C.L., et al., *Structure of a new crystal form of tetraubiquitin.* Acta Crystallographica Section D-Biological Crystallography, 2001. **57**: p. 341-344.
94. Hurley, J.H., S. Lee, and G. Prag, *Ubiquitin-binding domains.* Biochem J, 2006. **399**(3): p. 361-72.
95. Hofmann, K. and L. Falquet, *A ubiquitin-interacting motif conserved in components of the proteasomal and lysosomal protein degradation systems.* Trends in Biochemical Sciences, 2001. **26**(6): p. 347-350.
96. Raiborg, C., et al., *Hrs sorts ubiquitinated proteins into clathrin-coated microdomains of early endosomes.* Nature Cell Biology, 2002. **4**(5): p. 394-398.
97. Glickman, M.H., et al., *A subcomplex of the proteasome regulatory particle required for ubiquitin-conjugate degradation and related to the COP9-signalosome and eIF3.* Cell, 1998. **94**(5): p. 615-23.
98. Young, P., et al., *Characterization of two polyubiquitin binding sites in the 26 S protease subunit 5a.* J.Biol.Chem., 1998. **273**: p. 5461-7.
99. van Nocker, S., et al., *Arabidopsis MBP1 gene encodes a conserved ubiquitin recognition component of the 26S proteasome.* PNAS, 1996. **93**(2): p. 856-860.
100. Fisher, R.D., et al., *Structure and ubiquitin binding of the ubiquitin-interacting motif.* J Biol Chem, 2003. **278**(31): p. 28976-84.
101. Shekhtman, A. and D. Cowburn, *A ubiquitin-interacting motif from Hrs binds to and occludes the ubiquitin surface necessary for polyubiquitination in monoubiquitinated proteins.* Biochemical and Biophysical Research Communications, 2002. **296**(5): p. 1222-1227.
102. Swanson, K.A., et al., *Solution structure of Vps27 UIM-ubiquitin complex important for endosomal sorting and receptor downregulation.* Embo Journal, 2003. **22**(18): p. 4597-4606.
103. Mueller, T.D. and J. Feigon, *Structural determinants for the binding of ubiquitin-like domains to the proteasome.* Embo Journal, 2003. **22**(18): p. 4634-4645.
104. Sadler, J.E., *von Willebrand factor.* J Biol Chem, 1991. **266**(34): p. 22777-80.
105. Verma, R., et al., *Multiubiquitin chain receptors define a layer of substrate selectivity in the ubiquitin-proteasome system.* Cell, 2004. **118**(1): p. 99-110.
106. Hawryluk, M.J., et al., *Epsin 1 is a polyubiquitin-selective clathrin-associated sorting protein.* Traffic, 2006. **7**(3): p. 262-81.
107. Hofmann, K. and P. Bucher, *The UBA domain: a sequence motif present in multiple enzyme classes of the ubiquitination pathway.* Trends Biochem Sci, 1996. **21**(5): p. 172-3.
108. Dieckmann, T., et al., *Structure of a human DNA repair protein UBA domain that interacts with HIV-1 Vpr.* Nat Struct Biol, 1998. **5**(12): p. 1042-7.
109. Mueller, T.D. and J. Feigon, *Solution structures of UBA domains reveal a conserved hydrophobic surface for protein-protein interactions.* J Mol Biol, 2002. **319**(5): p. 1243-55.
110. Swanson, K.A., L. Hicke, and I. Radhakrishnan, *Structural basis for monoubiquitin recognition by the Ede1 UBA domain.* J Mol Biol, 2006. **358**(3): p. 713-24.
111. Chim, N., et al., *Solution structure of the ubiquitin-binding domain in Swa2p from Saccharomyces cerevisiae.* Proteins, 2004. **54**(4): p. 784-93.

112. Ciani, B., et al., *Structure of the ubiquitin-associated domain of p62 (SQSTM1) and implications for mutations that cause Paget's disease of bone.* J Biol Chem, 2003. **278**(39): p. 37409-12.
113. Mueller, T.D. and J. Feigon, *Solution structures of UBA domains reveal a conserved hydrophobic surface for protein-protein interactions.* Journal of Molecular Biology, 2002. **319**(5): p. 1243-1255.
114. Ohno, A., et al., *Structure of the UBA Domain of Dsk2p in Complex with Ubiquitin Molecular Determinants for Ubiquitin Recognition.* Structure (Camb), 2005. **13**(4): p. 521-32.
115. Raasi, S., et al., *Diverse polyubiquitin interaction properties of ubiquitin-associated domains.* Nat Struct Mol Biol, 2005. **12**(8): p. 708-14.
116. French, M., et al., *Identification and characterization of modular domains that bind ubiquitin.* Methods Enzymol, 2005. **399**: p. 135-57.
117. Varadan, R., et al., *Structural Determinants for Selective Recognition of a Lys48-Linked Polyubiquitin Chain by a UBA Domain.* Mol. Cell, 2005. **18**(6): p. 687-698.
118. Kang, R.S., et al., *Solution structure of a CUE-ubiquitin complex reveals a conserved mode of ubiquitin binding.* Cell, 2003. **113**(5): p. 621-630.
119. Trempe, J.F., et al., *Mechanism of Lys48-linked polyubiquitin chain recognition by the Mud1 UBA domain.* Embo J, 2005. **24**(18): p. 3178-89.
120. Varadan, R., et al., *Structural Determinants for Selective Recognition of a Lys48-Linked Polyubiquitin Chain by a UBA Domain.* Mol Cell, 2005. **18**(6): p. 687-98.
121. Prag, G., et al., *Mechanism of ubiquitin recognition by the CUE domain of Vps9p.* Cell, 2003. **113**(5): p. 609-620.
122. Shih, S.C., et al., *A ubiquitin-binding motif required for intramolecular monoubiquitylation, the CUE domain.* Embo Journal, 2003. **22**(6): p. 1273-1281.
123. Beal, R.E., et al., *The Hydrophobic Effect Contributes to Polyubiquitin Chain Recognition.* Biochemistry, 1998. **37**: p. 2925-2934.
124. Thrower, J.S., et al., *Recognition of the polyubiquitin proteolytic signal.* EMBO J., 2000. **19**: p. 94-102.
125. Studier, F.W., *Protein production by auto-induction in high density shaking cultures.* Protein Expr Purif, 2005. **41**(1): p. 207-34.
126. Piotrowski, J., et al., *Inhibition of the 26S proteasome by polyubiquitin chains synthesized to have defined lengths.* J.Biol.Chem., 1997. **272**: p. 23712-21.
127. Schanda, P., E. Kupce, and B. Brutscher, *SOFAST-HMQC experiments for recording two-dimensional heteronuclear correlation spectra of proteins within a few seconds.* J Biomol NMR, 2005. **33**(4): p. 199-211.
128. Hall, J.B. and D. Fushman, *Characterization of the overall and local dynamics of a protein with intermediate rotational anisotropy: Differentiating between conformational exchange and anisotropic diffusion in the B3 domain of protein G.* J Biomol NMR, 2003. **27**: p. 261-275.
129. Kay, L.E. and A. Bax, *New methods for the measurement of NH-CalphaH coupling constants in ^{15}N-labeled proteins.* J Magn Reson, 1990. **86**: p. 110-126.
130. Vuister, G.W. and A. Bax, *Quantitative J Correlations: A new approach for measuring homonuclear three-bond J(HnHa) coupling constants in 15N-enriched proteins.* J. A. C. S., 1993. **115**(1): p. 7772-7777.

131. Cornilescu, G., F. Delaglio, and A. Bax, *Protein backbone angle restraints from searching a database for chemical shift and sequence homology.* J Biomol NMR, 1999. **13**(3): p. 289-302.
132. Guntert, P., C. Mumenthaler, and K. Wuthrich, *Torsion angle dynamics for NMR structure calculation with the new program DYANA.* J.Molec.Biol., 1997. **273**: p. 283-98.
133. Ruckert, M. and G. Otting, *Alignment of biological macromoleculse in novel nonionic liquid crystalline media for NMR experiments.* J. Amer. Chem. Soc., 2000. **122**: p. 7793-7797.
134. Ottiger, M., F. Delaglio, and A. Bax, *Measurement of J and dipolar couplings from simplified two-dimensional NMR spectra.* J Magn Reson, 1998. **131**(2): p. 373-8.
135. Brunger, A. and e. al., *Crystallography & NMR System: A new software suite for macromolecular structure determination.* Acta Cryst., 1998. **D54**: p. 905-21.
136. Linge, J.P., S.I. O'Donoghue, and M. Nilges, *Automated assignment of ambiguous nuclear overhauser effects with ARIA.* Methods Enzymol, 2001. **339**: p. 71-90.
137. Rule, G.S. and K.T. Hitchens, *Fundamentals of Protein NMR Spectroscopy*, ed. R. Kaptein. Vol. 5. 2006, Dordrecht: Springer. 517.
138. Walker, O., R. Varadan, and D. Fushman, *Efficient and accurate determination of the overall rotational diffusion tensor of a molecule from 15N relaxation data using computer program ROTDIF.* J. Magn. Reson., 2004. **168**: p. 336-345.
139. Beal, R., et al., *Surface hydrophobic residues of multiubiquitin chains essential for proteolytic targeting.* PNAS, 1996. **93**(2): p. 861-866.
140. Young, P., et al., *Characterization of two polyubiquitin binding sites in the 26 S protease subunit 5a.* Journal of Biological Chemistry, 1998. **273**(10): p. 5461-5467.
141. Wang, Q.H., P. Young, and K.J. Walters, *Structure of S5a Bound to Monoubiquitin Provides a Model for Polyubiquitin Recognition.* J. Mol. Biol., 2005. **348**(3): p. 727-739.
142. Zuiderweg, E.R., *Mapping protein-protein interactions in solution by NMR spectroscopy.* Biochemistry, 2002. **41**(1): p. 1-7.
143. Deveraux, Q., et al., *A 26 S protease subunit that binds ubiquitin conjugates.* J. Biol. Chem., 1994. **269**: p. 7059-7061.
144. Hirano, S., et al., *Double-sided ubiquitin binding of Hrs-UIM in endosomal protein sorting.* Nat Struct Mol Biol, 2006. **13**(3): p. 272-7.
145. Baboshina, O.V. and A.L. Haas, *Novel multiubiquitin chain linkages catalyzed by the conjugating enzymes E2(EPF) and RAD6 are recognized by 26 S proteasome subunit 5.* Journal of Biological Chemistry, 1996. **271**(5): p. 2823-2831.
146. Raasi, S., et al., *Binding of polyubiquitin chains to ubiuitin associated (UBA) domains of HHR23A.* J. Mol. Bio., 2004. **341**(5): p. 1367-1379.
147. Kang, Y., et al., *Defining how Ubiquitin Receptors hHR23a and S5a Bind Polyubiquitin.* J Mol Biol, 2007. **369**(1): p. 168-76.
148. Kumar, S., C.J. Tsai, and R. Nussinov, *Thermodynamic differences among homologous thermophilic and mesophilic proteins.* Biochemistry, 2001. **40**(47): p. 14152-65.

149. Verma, R., R.M. Feldman, and R.J. Deshaies, *SIC1 is ubiquitinated in vitro by a pathway that requires CDC4, CDC34, and cyclin/CDK activities.* Mol Biol Cell, 1997. **8**(8): p. 1427-37.
150. Petroski, M.D. and R.J. Deshaies, *Function and regulation of cullin-RING ubiquitin ligases.* Nat Rev Mol Cell Biol, 2005. **6**(1): p. 9-20.
151. Hoppe, T., et al., *Activation of a membrane-bound transcription factor by regulated ubiquitin/proteasome-dependent processing.* Cell, 2000. **102**(5): p. 577-86.
152. Ryu, K.S., et al., *Binding surface mapping of intra and inter domain interactions among hHR23B, ubiquitin and poly ubiquitin binding site 2 of S5a.* J Biol Chem, 2003. **278**(38): p. 36621-7.
153. Mueller, T.D., M. Kamionka, and J. Feigon, *Specificity of the interaction between ubiquitin-associated domains and ubiquitin.* J Biol Chem, 2004. **279**(12): p. 11926-36.
154. Clore, G.M. and D.S. Garrett, *R-factor, free R, and complete cross-validation for dipolar coupling refinement of NMR structures.* J.Am.Chem.Soc., 1999. **121**(39): p. 9008-12.
155. Hicke, L., H.L. Schubert, and C.P. Hill, *Ubiquitin-binding domains.* Nat Rev Mol Cell Biol, 2005. **6**(8): p. 610-21.
156. Beal, R.E., et al., *The hydrophobic effect contributes to polyubiquitin chain recognition.* Biochemistry, 1998. **37**(9): p. 2925-34.
157. Zuckerkandl, E., *Evolutionary processes and evolutionary noise at the molecular level. I. Functional density in proteins.* J Mol Evol, 1976. **7**(3): p. 167-83.
158. Hicke, L. and R. Dunn, *Regulation of membrane protein transport by ubiquitin and ubiquitin-binding proteins.* Annual Review of Cell and Developmental Biology, 2003. **19**: p. 141-172.
159. Verma, R., et al., *Ubistatins inhibit proteasome-dependent degradation by binding the ubiquitin chain.* Science, 2004. **306**(5693): p. 117-20.
160. Gagny, B., et al., *A novel EH domain protein of Saccharomyces cerevisiae, Ede1p, involved in endocytosis.* J Cell Sci, 2000. **113 (Pt 18)**: p. 3309-19.
161. Varadan, R., et al., *Solution conformation of Lys(63)-linked di-ubiquitin chain provides clues to functional diversity of polyubiquitin signaling.* Journal of Biological Chemistry, 2004. **279**(8): p. 7055-7063.
162. Ryabov, Y. and D. Fushman, *A Model of Interdomain Mobility in a Multi-Domain Protein.* J Am Chem Soc, 2007. **129**(11): p. 3315-27.
163. Lam, Y.A., et al., *Specificity of the ubiquitin isopeptidase in the PA700 regulatory complex of 26 S proteasomes.* J.Biol.Chem., 1997. **272**: p. 28438-46.
164. Wormstone, I.M., et al., *Human lens epithelial cell proliferation in a protein-free medium.* Invest Ophthalmol Vis Sci, 1997. **38**(2): p. 396-404.
165. Davidson, M.G., D.K. Morgan, and M.C. McGahan, *Effect of surgical technique on in vitro posterior capsule opacification.* J Cataract Refract Surg, 2000. **26**(10): p. 1550-4.
166. Marcantonio, J.M., et al., *Epithelial transdifferentiation and cataract in the human lens.* Exp Eye Res, 2003. **77**(3): p. 339-46.